

LIQUID-LIQUID FLOWS AND SEPARATION

MARK JOHN HARRY SIMMONS M.Eng.

Thesis submitted to the University of Nottingham for the degree of Doctor of Philosophy

December 1998

Dedicated to my family and friends

When in doubt tell the truth.

--Mark Twain

I disapprove of what you say, but I will defend to death your right to say it

--Voltaire

I know I am intelligent, because I know that I know nothing.

-- Socrates

The beginning is the most important part of the work.

--Plato

The time to repair the roof is when the sun is shining.

-- John F. Kennedy

Abstract

The transport and separation of oil and water is a vital process to the oil and chemical industries. Fluids exiting from oil wells usually consist of gas, oil and water and these three phases need to be transported and separated before they can be processed further.

Operation of the primary separators has often proved to be problematic due to the change in composition of the fluids as the well matures, often accompanied by the build up of sand or asphaltenes. These vessels are very expensive to install so there is motivation to improve their design and performance.

One major factor affecting separator performance is the phase distribution of the inlet flow, as reflected in the flow pattern and droplet size. In this work, flow pattern boundaries and drop sizes of liquid-liquid dispersions were measured for vertical and horizontal flow of a kerosene and water mixture in a 0.063m tube. Drop size was investigated by using two different laser optical techniques. A laser backscatter technique was employed for concentrated dispersions and a diffraction technique was used at low concentrations.

In order to develop a greater understanding of separator performance, a 1/5th-scale model was constructed of diameter 0.6m and length 2.5m. Residence Time Distributions were obtained for a range of different internal configurations and flow rates using a colorimetric tracer technique. Flow rates of 1.5-4 kg/s oil and 1-4 kg/s water were used and the vessel was equipped with a perforated flow-spreading baffle at the inlet and an overflow weir. Experiments were performed with no internals and

with dip or side baffles. The side baffles acted to create quiescent zones within the vessel while the dip baffle caused a local acceleration of both phases. These situations are similar to those that can be caused by blocked internals or existing baffling or structured packing within field separators.

A Residence Time Distribution model of a primary separator, the Alternative Path Model, was developed using transfer functions. This model has the ability to reproduce features of the experimental data by representing the flow as a series of continuous stirred tanks in series or in parallel. The model was used to develop parameters that could be used to obtain information about the performance of the separator. This model was also applied to Residence Time Distribution data obtained from field separators by BP Exploration, to relate features of the pilot scale separator to the field vessels.

ACKNOWLEDGEMENTS

I would like to take this opportunity to thank both of my supervisors Prof. B.J. Azzopardi and Dr J.H Hills for their unfailing help, support and patience. I would also like to acknowledge Dr Douglas Dick of BP Exploration for his support of this project. I would also like to thank the technical staff, in particular Phil Bennett, Reg Briggs, Mick Fletcher, Marion Smith, Fred Anderton, John Travis and Derek Wood for their invaluable expertise and good humour when working on all my “5 minute jobs”. I would like to acknowledge my gratitude to Ekaterina Ponomareva and Dr J.A. Wilson for their help with the mechanics of the separator model and Dr Adam Burbidge and Dr Paul Langston for their mathematical knowledge.

I would also like to acknowledge the support of my colleagues past and present in the Postgraduate Office, who have always offered sound advice, in particular, Pols, JonEM, Sue, John (x2), Luca, Ian, Liz, Fabio, Wayne, Ayse, Basel, Chibuike, Sam, Diego, Jose, Anca and Tunde, apologies to anyone I have forgotten.

I would also like to thank everyone in Lincoln Hall for a very happy time there, particularly members of the SCR, past and present. Particular thanks go to Dorte, Adam, Gertrud, Karen, Giuseppe and Dave for their support over the last few mad months. Thanks also to Joanne Wright and family and Vicki and Steve for letting me sleep on their sofa beds while I was doing my final corrections. Finally and most importantly I would like to thank Mum, Dad and all my family and friends for their constant love and support during my time at University.

TABLE OF CONTENTS

ABSTRACT

ACKNOWLEDGEMENTS

1. INTRODUCTION

1

2. REVIEW OF THE LITERATURE

2.1	INTRODUCTION.....	6
2.2	FLOW PATTERNS AND DROPLET SIZE MEASUREMENTS IN LIQUID-LIQUID SYSTEMS.....	7
2.2.1	STRATIFIED FLOW.....	8
2.2.2	FLOW PATTERN TRANSITIONS.....	11
2.2.3	DROP SIZE MEASUREMENTS.....	15
2.2.4	DROPLET SIZE CORRELATIONS.....	20
2.3	PHASE SEPARATION OF DISPERSIONS.....	25
2.3.1	CONFIGURATION OF A PRIMARY SEPARATOR.....	26
2.3.2	SETTLING OF PARTICLES THROUGH A CONTINUOUS MEDIUM.....	28
2.3.3	COALESCENCE OF DROPLETS AT THE LIQUID-LIQUID INTERFACE.....	32
2.4	PERFORMANCE ENHANCEMENT OF PRIMARY SEPARATORS.....	34
2.4.1	PLATE SEPARATOR PACKS.....	35
2.4.2	STRUCTURED PACKINGS.....	36
2.4.3	PERFORATED BAFFLES.....	37
2.4.4	INDUSTRIAL EXPERIENCE OF PERFORMANCE ENHANCING INTERNALS.....	37
2.5	IN-SITU PERFORMANCE MEASUREMENT AND PROBLEM IDENTIFICATION.....	39
2.5.1	BACKGROUND TO RESIDENCE TIME MEASUREMENT.....	39
2.5.2	NUCLEONIC RESIDENCE TIME DISTRIBUTION MEASUREMENT.....	42
2.5.3	INTERFACE LEVEL MEASUREMENT BY NEUTRON BACK-SCATTER.....	43
2.5.4	INTERFACE LEVEL MEASUREMENT USING GAMMA RAYS.....	44
2.6	POSSIBLE MODELLING TECHNIQUES.....	45
2.6.1	TRANSFER FUNCTIONS.....	45
2.6.2	COMPUTATIONAL FLUID DYNAMICS.....	53
2.8	SUMMARY.....	63

3. EXPERIMENTAL EQUIPMENT

3.1	INTRODUCTION.....	65
3.2	LIQUID-LIQUID FLOW FACILITY.....	65
3.2.1	PIPE TEST SECTIONS.....	68
3.2.2	PILOT SCALE SEPARATOR VESSEL.....	70
3.3	RESIDENCE TIME DISTRIBUTION TRACER TECHNIQUE.....	73
3.4	TEST CELL FOR SIMULTANEOUS DROP SIZE MEASUREMENT.....	76

4. DROP SIZES AND FLOW PATTERNS IN LIQUID-LIQUID PIPE FLOW

4.1	INTRODUCTION.....	78
4.2	EXPERIMENTAL DETAILS.....	79
4.2.1	CONVERTING CHORD DISTRIBUTIONS TO DIAMETER DISTRIBUTIONS.....	79
4.2.2	TESTS ON GLASS BEADS.....	83
4.2.3	EXPERIMENTS PERFORMED AND TEST CONDITIONS ON PIPE FLOW RIG	84
4.2.4	EXPERIMENTAL ERROR.....	85
4.3	RESULTS.....	86
4.4	DISCUSSION.....	88
4.4.1	DROP SIZE COMPARISONS.....	88
4.4.2	FLOW PATTERNS.....	97
4.5	CONCLUSIONS.....	100

5. MATHEMATICAL MODELS OF LIQUID-LIQUID SEPARATORS AND THEIR APPLICATION TO FIELD DATA

5.1	INTRODUCTION.....	102
5.2	DEVELOPMENT OF THE MODEL.....	102
5.2.1	TEST MODEL.....	103
5.2.2	NSTIS MODEL.....	104
5.2.3	“ALTERNATIVE PATH” MODEL (APM).....	105
5.3	CALCULATION OF FREQUENCY RESPONSE FROM RESIDENCE TIME DISTRIBUTION....	107
5.4	ANALYSIS OF RESIDENCE TIME DISTRIBUTION FROM BP SEPARATORS.....	108
5.4.1	MODELLING PERFORMED ON FIELD DATA.....	108
5.4.2	RESULTS.....	112
5.5	CONCLUSIONS.....	129

6. MEASUREMENT OF RESIDENCE TIME DISTRIBUTIONS IN A PILOT SCALE LIQUID-LIQUID SEPARATOR

6.1 INTRODUCTION..... 134

6.2 EXPERIMENTAL..... 135

 6.2.1 FLOW MEASUREMENT..... 135

 6.2.2 RESIDENCE TIME DISTRIBUTION MEASUREMENT TECHNIQUE..... 135

 6.2.3 TEST CONDITIONS..... 139

 6.2.4 EXPERIMENTAL ERROR..... 142

6.3 RESULTS AND DISCUSSION..... 143

6.4 CONCLUSIONS..... 160

7. PERFORMANCE CHARACTERISATION AND MATHEMATICAL MODELLING OF A PILOT SCALE SEPARATOR

7.1 INTRODUCTION..... 167

7.2 INTERPRETATION OF DATA FROM PILOT SCALE SEPARATOR..... 168

 7.2.1 FLOW OBSTRUCTION CAUSED BY SIDE BAFFLES..... 168

 7.2.2 COALESCING ZONES..... 169

 7.2.3 NOMINAL RESIDENCE TIMES..... 173

7.3 DISCUSSION OF RESULTS..... 174

 7.3.1 EFFECT OF CHANGING WEIR HEIGHT..... 174

 7.3.2 EFFECT OF SIDE BAFFLES..... 180

 7.3.3 EFFECT OF DIP BAFFLE..... 185

 7.3.4 COMPARISONS WITH FIELD DATA..... 189

7.4 CONCLUSIONS..... 192

8. CONCLUSIONS AND FUTURE WORK

8.1 DROP SIZES AND FLOW PATTERNS IN LIQUID-LIQUID PIPE FLOWS..... 194

8.2 MATHEMATICAL MODEL OF A PRIMARY SEPARATOR..... 196

8.3 RESIDENCE TIME MEASUREMENT AND MODELLING OF A PILOT SCALE SEPARATOR 197

8.4 FUTURE WORK..... 199

NOMENCLATURE

BIBLIOGRAPHY

APPENDIX A1 CALCULATION OF LIQUID PHYSICAL PROPERTIES

**APPENDIX A2 TECHNIQUES FOR CONVERTING CHORD DISTRIBUTIONS TO
DIAMETER DISTRIBUTIONS**

(Accepted for publication in Powder Technology, in Print)

APPENDIX A3 IMAGE ANALYSIS OF VIDEO FOOTAGE

APPENDIX A4 DROP SIZE DISTRIBUTIONS

APPENDIX A5 FLOW PATTERN MAPS

APPENDIX A6 PROGRAM LISTINGS

APPENDIX A7 MODELLING OF PILOT-SCALE SEPARATOR-TABLES OF RESULTS

Chapter 1

INTRODUCTION

The operation of many pieces of equipment in the chemical, oil and power generation industries is characterised by the simultaneous flows of more than one phase. This is termed multiphase flow and can cover several combinations of phases.

Multiphase flows are extremely complex because of the interactions occurring between the phases. It is difficult enough for gas-solid flows where the effect of the gas on the particles is obviously important. However, the particles can also influence the gas flow. When one of the phases is a liquid the interactions are even more complicated because the interface between the phases is deformable.

Research into multiphase flows has been prompted by industrial problems. An example of gas-solid flow is pneumatic conveying of powders where it is necessary to predict the pressure of air required in the equipment. The boiling of water in tubes is an illustration of gas-liquid flow and was rigorously studied by the nuclear industry in order to be able to prevent over-heating of the reactor core in Pressurised Water Reactors. This is even more complicated because the composition is constantly changing along the pipe as the water boils.

Another study of multiphase flows occurs in pipelines from oil wells. Hydrocarbon production from oil wells almost inevitably contains natural gas and water as well as oil. This mixture is extracted at a large range of orientations due to the complexity of

modern well drilling. The well itself may be undersea or on land and the liquids once extracted have to be either transported or separated depending on their location. The design of a multiphase pipeline is complicated by the fact that the interactions between the phases have significant effects on the pumping power required. This means that it is not possible to design the system by considering the mixture as a single phase and so a thorough understanding of the fluid dynamics is required. Visual observation and pressure measurements of the mixtures flowing through transparent pipes revealed that the behaviour of the flow could be classified into a number of different regimes or flow patterns.

The flow pattern boundaries observed in pipes are dependent on the characteristics of the fluids, the diameter and orientation of the pipe and the velocities of each phase. If horizontal flow is taken as an example, at low flow rates the heavier phases tended to travel as a separate layer in the pipeline, with the lighter phase travelling on top. At higher flow rates, slug flow was seen to develop, where the majority of the volume of the pipe is alternately filled with gas or liquid. This unstable flow pattern can cause problems as the packets of gas and liquid can become very long if the pipeline is long and the momentum of the large liquid slugs can be very destructive at bends in the pipeline, or outlets into other pieces of equipment. At higher rates still, an annular flow pattern may be observed, or dispersions of one phase in another. The sizes of droplets in these dispersions can have important effects on downstream equipment such as phase separators or reactors. Similar flow patterns exist at vertical or inclined orientations and the pipeline has to be designed to try to avoid flow patterns which might be detrimental to the performance of downstream equipment or expensive in terms of pumping power.

Although transport of multiphase mixtures is often necessary because of the location of the wellhead, it is usually beneficial to separate out the phases as soon as possible in order to reduce cost and avoid the problems described above. Onshore or offshore processing facilities are therefore required to perform this task.

As the volumes of gas and liquid emerging from oil wells are very large, the primary separation of the gas-oil-water mixture has traditionally been performed by gravity in large horizontal cylindrical vessels. These vessels are typically about 3m in diameter and 10m long although vessels as large as 4m diameter and 25m in length have been built. The horizontal configuration of these separators is necessary due to the high volume fraction of liquid. The bulk of these vessels mean that they are costly both to manufacture and to install. A carbon steel vessel will typically cost £5000 per tonne of weight while a stainless steel vessel will cost twice this value. If it is to be used on an offshore platform, the support structure costs approximately £20 000 per tonne of vessel weight.

The high construction costs have led to a considerable amount of motivation to develop methods which will enable reduction in size of these vessels. Partial separation, by use of the maldistribution of phases at T-junctions, (Azzopardi and Hervieu, 1994) is a possible option, although currently interest appears to focus on improvement of the design of the vessels themselves, Hafskjold and Dodge (1989) and Hansen *et al.* (1991, 1994, 1995). Recent advances in the design and manufacture of structured packings and flow smoothing internals all claim to improve the performance of existing separators, while new separators can be made smaller to capitalise on the design improvements.

Improvement of the performance of primary separators has proved problematic due to a number of factors. The change in composition of the fluids as the well matures, together with the build-up of sand or heavy asphaltenes all are detrimental to the performance and make design optimisation a difficult process. The phases are often dirty and settle out slowly so accurate interface level control is also very difficult. Unwelcome flow patterns at the separator inlet, such as slug flow, also create control difficulties. Wash systems have been developed to clean the inside of the vessels in-situ but there is still a need to be able to determine problems on-line. A nucleonic technique was developed to measure the Residence Time Distribution (RTD) of the separators, together with some sealed source scans which can identify the position of gas-oil and oil-water interfaces within the vessel.

There is therefore a need to examine more closely the relationships between the properties of the liquids and the tank configurations upon the performance of the separator. Once a greater understanding of the processes taking place is found then it will be possible to suggest ways of improving design and performance, with the ultimate goal of saving capital at a time of ever tightening environmental regulations.

The purpose of this dissertation is to increase the understanding of liquid-liquid pipe flows and separations. Measurements were made of drop size and flow patterns in pipe flow and residence time experiments were performed on a pilot scale primary separator for which a mathematical model was developed. This work has been chosen on the basis of a review of the literature which is presented in Chapter 2 and the equipment used is described in Chapter 3. The details of the drop size and flow

pattern measurements are shown in Chapter 4. The mathematical model of the separator was developed and tested against field data from BP Exploration and is described in Chapter 5. The residence time measurements performed on the pilot scale separator are detailed in Chapter 6 and are modelled and analysed in Chapter 7. The conclusions from this work are then presented in Chapter 8.

Chapter 2

REVIEW OF THE LITERATURE

2.1 INTRODUCTION

In order to determine what will affect the performance of an oil-water primary separator, it is necessary to consider several factors. The physical properties of the phases, the flow pattern and drop sizes present in the inlet pipe are parameters which are likely to affect the separation. It is therefore of interest to examine ways in which these parameters can be obtained experimentally and whether any modelling work has been performed. Within the separator itself, understanding of the physics of the phase disengagement is required to be able to predict the separation efficiency. This forms the basis of current published design methods and it is necessary to review the adequacy of these and whether there are other modelling tools which could be applied to these vessels.

As the vessels have to handle a wide range of flow conditions, new internals have been developed to enhance the separation process and some vessels have been modified by the inclusion of either baffles or packings, which it is hoped will improve the performance. The different types of internals employed and configurations used are therefore of interest to this review.

Industrial performance measurement techniques have focussed on obtaining information on Residence Time Distribution (RTD) and the position of phase interfaces. As disruption to an operating flow facility has to be kept to a minimum, application of these techniques to a range of different vessel configurations and

throughputs is not possible. Any types of measurement made in research facilities do not suffer from this limitation, but published work on these vessels is scarce.

In light of the above information, this literature review focuses on three distinct but linked areas. The characteristics of liquid-liquid pipe flow, which could be expected at the inlet to a primary separator, will be examined. The physics of the phase separation will be discussed and existing design techniques, together with possible new modelling techniques will be critically reviewed. Finally, the measurements made in either research facilities or industry on such vessels will be presented. A programme of work will be proposed from this information which will be able to expand upon the database of existing information and will lead to an increased understanding of the nature of primary separators.

2.2 FLOW PATTERNS AND DROPLET SIZE MEASUREMENTS IN LIQUID-LIQUID SYSTEMS.

Several studies of drop sizes and flow patterns have been made for two fluid systems, in particular for air-water systems in the annular flow regime. Such systems can be considered as two fluid systems, characterised by low gas-liquid density and viscosity ratios. The density difference between the fluids is much less in a liquid-liquid system, but the viscosity of the organic phase can vary widely from high viscosity, heavy crude oils to light petroleum fractions. Oil-water mixtures entering a primary separator have typically travelled through pipelines which can sometimes run for several miles over varying terrain. Flow patterns in a horizontal geometry can be broadly categorised into four basic types:

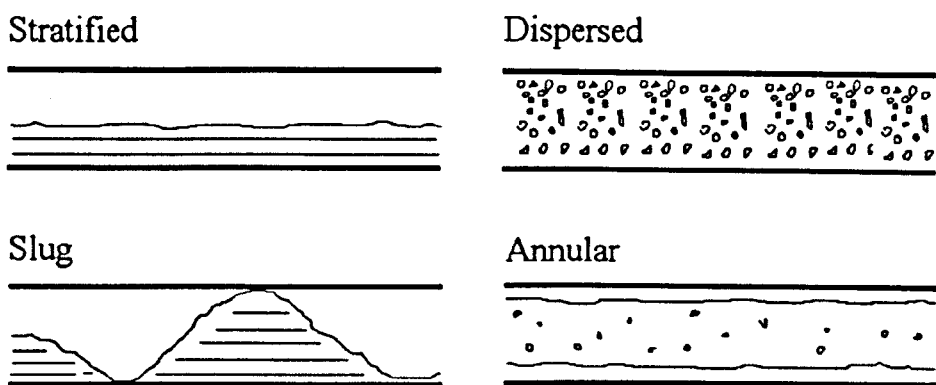


Figure 2.1: Basic Horizontal Flow Patterns

- 1) Stratified, or separated flow
- 2) Slug or plug flow
- 3) Dispersed flow of one liquid in the other
- 4) Annular flow

These can be further subdivided, depending on the degrees of inter-dispersion between the liquid layers and whether waves occur on the liquid-liquid interface. These flow patterns have been mathematically modelled and of particular interest is the location of flow pattern transitions. This allows prediction of flow patterns in different flow situations. This is useful, as it is often beneficial to avoid certain flow patterns in some cases. The momentum of liquid slugs in plug/slug flow for example, can have a disastrous effect on pipework, particularly at bends.

2.2.1 Stratified Flow

Prediction of the properties of stratified or separated flow was first developed as a plane interface two-fluid model by Taitel and Dukler (1976). The analysis was

further extended to include transients and curved interfaces by Brauner and Moalem Maron (1992a,1992b). The dominant flow patterns and shape of the interface were classified according to the Eotvos number in Equation 2.1 below

$$Eo_D = \frac{\Delta\rho g D^2}{8\sigma} \quad (2.1)$$

Where D is the tube diameter, $\Delta\rho$ is the difference in density between phases, g is the acceleration due to gravity and σ is the surface tension. For systems where the value of $Eo_D \gg 1$, annular flow is unlikely as surface tension and wall adhesion forces are insufficient to hold the liquid onto the tube walls. The interface can be assumed to be planar in stratified flow. When $Eo_D \ll 1$ the interface is curved and annular flow becomes the dominating flow pattern. For the systems of interest in the studies to be performed, $Eo_D \gg 1$ and the schematic of the plane interface two-fluid model is shown below in Figure 2.2. In this diagram, u_1 and u_2 are the phase velocities, P_1 , P_2 , and P_i are the wetted perimeters and S_1 and S_2 are the cross sectional areas.

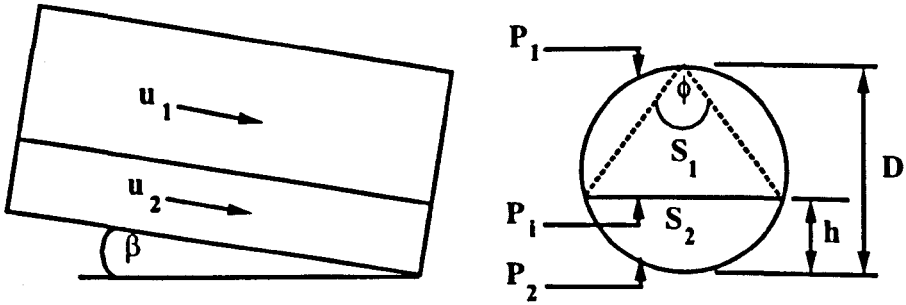


Figure 2.2: Diagram and parameters of two-fluid model with plane interface

The basis of the model is one dimensional momentum equations derived separately for each fluid.

$$-S_i \left(\frac{dp}{dz} \right) - T_i P_i - T_i P_i + \rho_i S_i g \sin \beta = 0 \quad (2.2)$$

$$-S_2 \left(\frac{dp}{dz} \right) - T_2 P_2 + T_i P_i + \rho_2 S_2 g \sin \beta = 0 \quad (2.3)$$

Where z is axial length and T is the shear stress. The pressure gradient in both phases must be equal, therefore eliminating this term between Equations 2.2 and 2.3 gives:

$$\Delta F_{12} = T_1 \frac{P_1}{S_1} - T_2 \frac{P_2}{S_2} + T_i P_i \left(\frac{1}{S_1} + \frac{1}{S_2} \right) + (\rho_2 - \rho_1) g \sin \beta = 0 \quad (2.4)$$

To close the equations it is necessary to solve the shear stresses. The shear stresses are defined as

$$T_1 = \frac{f_1 \rho_1 u_1^2}{2}; \quad T_2 = \frac{f_2 \rho_2 u_2^2}{2} \quad (2.5)$$

For systems where the density ratios are close to unity, the interface is considered as free and the interfacial stress T_i , can be set to zero. The friction factors, f , are defined as

$$f_1 = C_1 \left[\frac{\rho_1 u_1 D_1}{\eta_1} \right]^{-m_1}; \quad f_2 = C_2 \left[\frac{\rho_2 u_2 D_2}{\eta_2} \right]^{-m_2} \quad (2.6)$$

Where D_1 and D_2 are the equivalent hydraulic diameters, ρ is the density and η is the dynamic viscosity. If the velocities of the phases are of the same magnitude, as usually occurs in systems with density ratios close to unity then D_1 and D_2 can be defined as

$$D_1 = \frac{4S_1}{P_1}; \quad D_2 = \frac{4S_2}{P_2} \quad (2.7)$$

For turbulent flow, $C_1 = C_2 = 0.046$ and $m_1 = m_2 = 0.2$. For laminar flow the values are set to 16 and 1 respectively.

Values for wetted perimeters, interface height and flow areas can all be obtained directly from the flow geometry. By setting the superficial velocities of both phases and knowing the physical properties of the flowing fluids, the interface height and phase velocities can be calculated by satisfying Equation 2.4. The system of equations can be further enhanced by non-dimensionalising if required. The Martinelli (1949) parameter, X^2 , can be derived from this analysis.

$$X^2 = \frac{\left(\frac{dp_f}{dz} \right)_{2s}}{\left(\frac{dp_f}{dz} \right)_{1s}} = \frac{u_{2s}^2 \rho_2 f_{2s}}{u_{1s}^2 \rho_1 f_{1s}} \quad (2.8)$$

Where the subscript s refers to superficial values, i.e. values calculated due to one phase travelling through the pipe alone.

2.2.2 Flow Pattern Transitions

As stated previously, the ability to predict flow patterns in a given situation is a valuable commodity. Brauner and Moalem Maron (1992a, 1992b) stated that a unified approach to flow pattern mapping was unlikely to be possible due to the wide variety of liquid-liquid flows, in terms of both the physical properties of the liquids and the different flow geometries. However, some general guidelines can be made and these lead to the flow pattern map shown in Figure 2.3 below. The key to Figure 2.3 also lists the abbreviations used to describe each flow pattern.

The boundaries of interest to this literature review are those between stratified flow and dispersed flow. Preliminary experiments on the liquid-liquid facility to be used in the experimental studies had generated stratified and dispersed flow patterns and the boundaries presented by Brauner and Moalem Maron are discussed below.

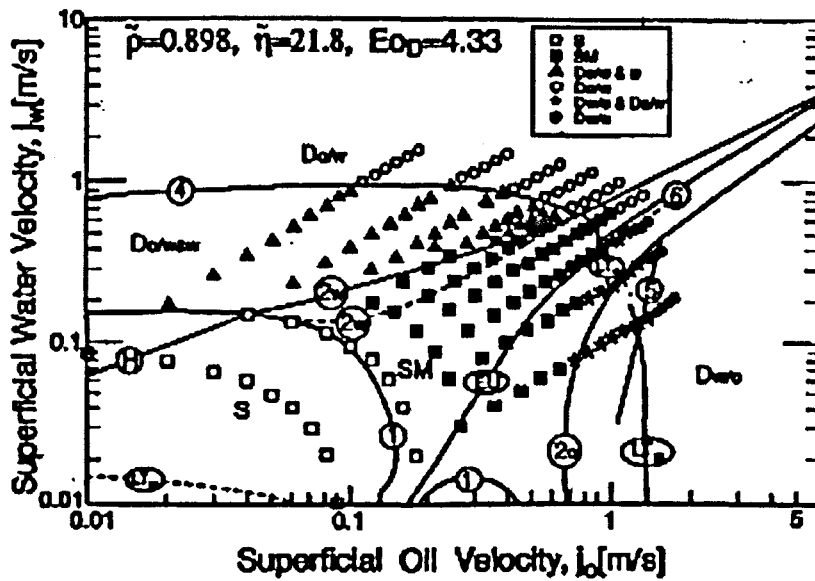


Figure 2.3: Flow Pattern Map of Brauner and Moalem Maron (1992) compared with experimental data of Guzhov (1973)

Key to Figure 2.3

S	Stratified flow with smooth or wavy interface
SM	Stratified flow with interface mixing
Do/w+w	Dispersion of oil in water plus a water layer
Do/w	Dispersion of oil in water
Dw/o+Do/w	Two interdispersed layers, of oil in water and water in oil
Dw/o	Dispersion of water in oil

2.2.2.1 Stratified Smooth to Stratified Wavy Boundary

The criteria to develop this boundary arise from linear stability analysis on the two-fluid model. The boundary considered is the long wave neutral stability boundary, which includes Kelvin-Helmholtz instability (growth of infinitesimally small waves on the interface) as well as a wave sheltering mechanism, which introduces a coefficient to allow for the damping effect due to the presence of the upper phase.

An extreme case of stratified-wavy flow is slug flow, where the wave grows to such a height that the gas-liquid interface reaches the top of the pipe. When waves are present, it is possible for the interface to break up and droplets can appear. The criterion for the onset of interfacial waves is given below

$$J_1 + J_2 + J_h = 1 \quad (2.9)$$

$$J_1 = \frac{\rho_1}{\Delta\rho} \frac{j_1^2}{Dg \cos \beta} \frac{\dot{\varepsilon}_2}{(1 - \varepsilon_2)^3} \left[\left(\frac{C_m}{u_1} - 1 \right)^2 + (\gamma_1 - 1) \left(1 - 2 \frac{C_m}{u_1} \right) \right] \quad (2.10)$$

$$J_2 = \frac{\rho_2}{\Delta\rho} \frac{j_2^2}{Dg \cos \beta} \frac{\dot{\varepsilon}_2}{\varepsilon_2^3} \left[\left(\frac{C_m}{u_2} - 1 \right)^2 + (\gamma_2 - 1) \left(1 - 2 \frac{C_m}{u_2} \right) \right] \quad (2.11)$$

$$J_h = C_h \frac{\rho}{\Delta\rho} \frac{(u_1 - u_2)^2}{Dg \cos \beta} \frac{4P_i}{\pi \varepsilon_2 (1 - \varepsilon_2) D} \quad (2.12)$$

where

$$C_m = \frac{\frac{u_2}{\varepsilon_2} \frac{\partial \Delta F_{12}}{\partial u_2} - \frac{u_1}{(1 - \varepsilon_2)} \frac{\partial \Delta F_{12}}{\partial u_1} - \frac{\partial \Delta F_{12}}{\partial \varepsilon_2}}{\left[\frac{1}{\varepsilon_2} \frac{\partial \Delta F_{12}}{\partial u_2} - \frac{1}{(1 - \varepsilon_2)} \frac{\partial \Delta F_{12}}{\partial u_1} \right]} \quad (2.13)$$

$$\varepsilon_2 = \frac{S_2}{S}; \dot{\varepsilon}_2 = \frac{d\varepsilon_2}{d(h/D)} \quad (2.14)$$

All the variables in the above equations are solved initially for steady state stratified flow as described in 2.2.1. The subset of variables that satisfy Equation 2.9 then define the boundary. In these equations, C_m is the wave propagation velocity and γ_1 and γ_2 are shape functions, for which constant values of 1.1 and 1.0 respectively are suggested. ΔF_{12} is defined in Equation 2.4. Values of C_h , the interfacial shear coefficient are currently unknown for liquid-liquid systems. However, as the

velocities of both phases are of the same order, interfacial shear is low and hence the value is set to zero. This assumption cannot be made for gas-liquid systems where the differential velocity is large and interfacial shear becomes significant. This transition is indicated by Boundary 1 on Figure 2.3.

2.2.2.2 Upper Bound on Stratified Flow Patterns

Stratified flow patterns exist outside the boundary predicted from 2.2.2.1, albeit with some degree of dispersion or other forms of mixing at the interface. This stratified flow pattern exists until the two fluid model becomes ill-posed. This condition is given by:

$$\begin{aligned} & \tilde{\rho}_2 u_2^2 \gamma_2 (\gamma_2 - 1) + \tilde{\rho}_1 u_1^2 \gamma_1 (\gamma_1 - 1) - (\gamma_2 u_2 - \gamma_1 u_1)^2 + \\ & \frac{D}{\rho_{12}} [(\rho_2 - \rho_1) g \cos \beta - C_h \rho (u_1 - u_2)^2 P_i (S_1^{-1} + S_2^{-1})] \geq 0 \end{aligned} \quad (2.15)$$

$$\tilde{\rho}_2 = 1 + \frac{\rho_2 S_1}{\rho_1 S_2}; \quad \tilde{\rho}_1 = 1 + \frac{\rho_1 S_2}{\rho_2 S_1}; \quad \rho_{12} = \frac{D \left(\frac{dS_2}{dh} \right) \rho_1 \rho_2}{S_2 \left[\rho_1 + \rho_2 \frac{S_1}{S_2} \right]} \quad (2.16)$$

This boundary can be constructed in two parts, depending on which phase travels at a higher velocity. In Figure 2.3, for a faster water layer, the boundary 2w marks the transition from SM to Do/w +w transition. The boundary 2o, for a faster oil layer, gives the transition between SM and Do/w and Dw/o. Additionally, constructing the line EU, where the actual phase velocities are equal ($u_1 = u_2$), it is shown on Figure 2.3 that patterns which involve a layer of w/o dispersion lie to the right of this line.

2.2.2.3 Transition to w/o Dispersion

If turbulence in the oil layer is sufficiently high, the water phase can be dispersed into stable small droplets. Applying Hinze's theory, the following criterion can be derived.

$$\left[\frac{0.4\sigma}{\Delta\rho g D^2} \right]^{1/2} \left(\frac{\rho_o D j^2}{\sigma} \right)^{0.6} \left(\frac{v_o}{D j} \right)^{0.08} = 1.88 \left[1 + a \left(\frac{j_w}{j} \right)^{1/2} \right] \quad (2.17)$$

This condition applies as long as the oil phase is turbulent. Calderbank (1958) suggested that $a=5.72$. This transition is indicated by boundary S on Figure 2.3.

2.2.3 Drop Size Measurements.

Dispersion of one phase in the other can occur at the interface in stratified flow and is a common phenomenon in several flow patterns, specifically dispersed and annular flow. A significant body of work has been published measuring drop sizes for liquid-liquid systems, but little attempt has been made to compare measurement techniques or results between workers. A variety of measurement and analysis techniques have been performed and a summary of this research can be found in Table 2.1. It can be seen that the pipe diameter tended to be no greater than 0.05 m, which is significantly lower than those of interest to the oil industry.

Table 2.1: Summary of Previous Work

Author	d_i (m)	σ (N/m)	μ_o (kg/ms)	ρ_o (kg/m ³)	Dispersion	Measurement Technique
El-Hamouz and Stewart (1996)	0.025	0.038	0.00096	800	o/w	Malvern 2600 and Par-Tec M300
Karabelas (1978) (w/to)	0.05	0.033	0.018	890	w/o	Photography of encapsulated sampled drops
Karabelas (1978) (w/k)	0.05	0.03	0.00186	808		
Kubie & Gardner (1977) (water/alcohol)	0.017	0.0049	0.0048	828	w/o and o/w	Photography of drops inside pipe
Kubie & Gardner (1977) (water/acetate)	0.017	0.0145	0.0007	884		
Kurban <i>et al</i> (1995)	0.025	0.017	0.0016	800	w/o	Photography using borescope plus conductivity probe

Measurement techniques used are generally either optically or electrically based. There is a potential problem with physical measurement of drop size as any intrusion may alter the size distribution, possibly by causing local changes in the condition of the continuous phase, which may cause break-up or coalescence. A selection of the measurement techniques used is reported below, together with some reported correlations for drop size.

2.2.3.1 Laser Diffraction

A mathematical method, based on the theory of Fraunhofer diffraction, was developed by Swithenbank *et al.* (1976) to obtain droplet size distributions and concentration from laser diffraction patterns. A low power He-Ne laser illuminates the flow, and the interception of the laser beam by a spherical particle creates a far-field diffraction pattern. This scattered light passes through a Fourier transform lens, and then falls onto a series of concentric photoelectric detectors. The size of the particles dictates the angle of scatter, (Figure 2.4) and a least-squares analysis is used to fit a diffraction pattern from a generated size distribution to the experimentally obtained data. This technique is limited to low dispersed phase concentrations because the Fraunhofer theory is dependent upon the detected light being only scattered by individual particles. If the light is scattered by multiple particles due to high concentration, then the theory of measurement is no longer valid.

This technique was adopted by Malvern Instruments Ltd and has been used extensively for drop size measurements in gas-liquid flow as reviewed by Azzopardi (1997). It has also been applied successfully by El-Hamouz and Stewart (1996) to measure drop sizes of an oil-water mixture through various pipe fittings.

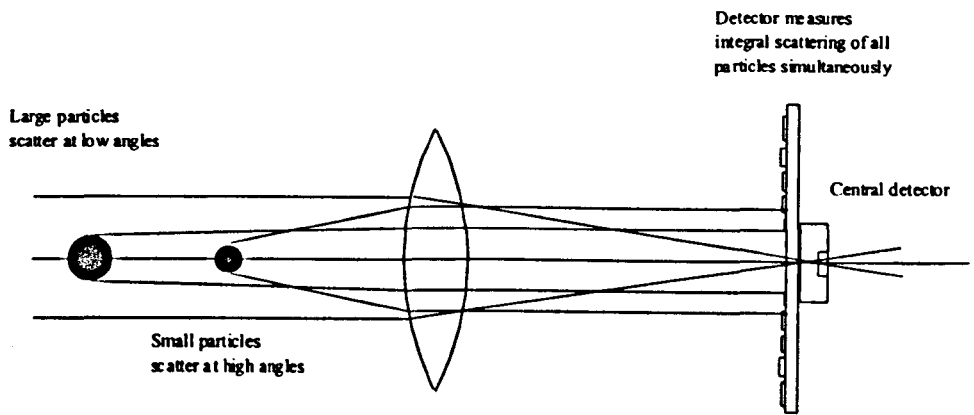


Figure 2.4: Operation of Malvern 2600 instrument

2.2.3.2 Laser Back-Scatter

A method of obtaining particle chord distributions from back-scattered laser light was developed by Lasentec and utilised in their Par-Tec and FBRM range of instruments. A beam from a laser diode is focussed to a very small spot, which produces a high light density at the focal point. This beam is passed through an eccentric spinning lens that produces a circular rotating beam, normal to the motion of the fluid (Figure 2.5). When the spot intercepts the particle, enough light is back scattered to be detected by a photodiode. The detected light is converted into electrical pulses, classified by time, which are recorded by computer. As the time of detection and angular velocity of the spinning beam are known, dividing these two quantities yields the chord size of each particle detected.

This chord data is not directly useful for comparison as most techniques measure droplet diameter. It is therefore necessary to convert this chord distribution to compare results with data obtained from other sources. A similar problem arises for the analysis of data from needle conductance probes and Herringe and Davis (1976), and Clark and Turton (1988) have examined this. The operation of the Par-Tec, as described above, is somewhat different and hence a method of converting the chords

to diameters needs to be developed. A probabilistic technique is described by Hobbel *et al.* (1991) but it is reported that the cumulative error at the small diameter sizes is high.

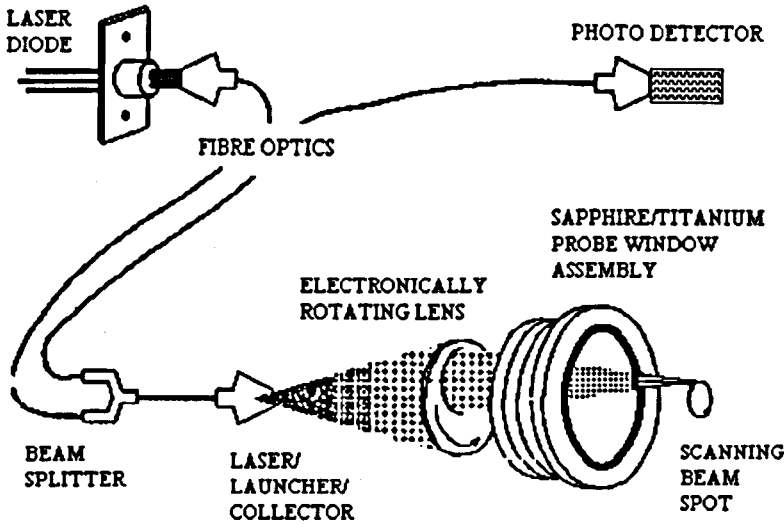


Figure 2.5: Principle of operation of the Par-Tec instrument.

2.2.3.3 Photographic Techniques

Several photography-based methods have been developed in order to size droplets. Karabelas (1978) photographed water droplets dispersed in two different hydrocarbons flowing in a 0.05m pipe. The droplets were collected in a sampling vessel with an optical quality glass bottom. This allowed photographs to be taken of the settled drops, which could be magnified to allow the droplets to be sized by ruler or travelling microscope. This technique was used in conjunction with droplet encapsulation to maintain the drop size distribution and prevent coalescence.

Kurban *et al.* (1995) used a borescope in conjunction with a video camera to examine droplets within oil-water dispersions in 0.0254m horizontal pipe. This had the added advantage of visualisation of the processes of droplet break-up and coalescence.

Photographic techniques in general are slow because of the time required to process and size a representative sample of drops. Karabelas (1978) sized more than 300 drops to obtain a representative size distribution. The techniques are also limited to low concentrations of the dispersed phase so that each droplet can be detected individually during measurement.

2.2.3.4 Droplet Encapsulation

This technique prevents coalescence of droplets and hence the droplet size distribution remains constant for sampling and measurement. A small quantity of monomer is introduced into the dispersed phase, and this reacts on the surface of the droplet to form a polymer when it comes into contact with another reacting monomer introduced into the continuous phase. This polymer layer then stops the droplets from sticking together or coalescing during analysis procedures.

Karabelas (1978) used this technique in conjunction with photography as described above. The monomers used were piperazine in the aqueous phase and terephthalic acid chloride in the organic phase.

2.2.3.5 Electrical Conductivity or Capacitance

Wicks and Dukler (1966) first reported this technique. It is possible to detect water droplets dispersed in an organic phase by placing 2 needles in line separated by a known distance. An electrical potential difference is imposed across the two needles and current flows when a conducting drop touches both. This can be counted electronically for a number of different needle spacings, and converted to a diameter distribution. Alternatively, the capacitance of the two electrodes can be used to

determine the droplet sizes in a similar way. Obviously the separation of the probes is critical for determining the size range of droplets which can be detected.

The technique is only useful for oil continuous systems and has been applied by Kurban *et al.* (1995). For water continuous systems, an oil droplet touching one probe only can interrupt the flow of current and thus the technique becomes size independent and no longer useful. Another limitation is that drops can become stuck to the needles if the flow is slow or the interfacial tension is high.

2.2.4 Droplet Size Correlations

Once drop size has been measured experimentally, it is useful to be able to predict droplet sizes for a particular system if this is an important parameter. Several correlations have been published that attempt to predict either the entire droplet size distribution or a characteristic of the distribution for liquid-liquid dispersions.

2.2.4.1 Prediction of Droplet Distribution

Karabelas (1978) measured the size of water droplets in oil by an encapsulation technique discussed above and suggested that a Rosin-Rammler type equation was appropriate to predict the drop size distribution.

$$f(d) = 1 - \exp\left[-2.996 \frac{d}{d_{95}}\right]^n \quad (2.18)$$

Where d is the drop diameter. The diameter at which 95% of the sample population are less than this size is represented by d_{95} . Similarly, d_{10} , d_{50} and maximum drop diameter d_{max} , can be defined. Karabelas found that an equally good, and sometimes better fit was obtained by use of an upper-limit log-normal distribution.

$$f(d) = 1 - \frac{1}{2} [1 - \operatorname{erf}(\delta Z)] \quad (2.19)$$

Where

$$Z = \ln \left[\frac{ad}{d_{\max} - d} \right] \quad (2.20)$$

and a , δ and d_{\max} are parameters determined from the experimental data as follows

$$\frac{d_{\max}}{d_{50}} = \frac{d_{50}(d_{90} + d_{10}) - 2d_{90}d_{10}}{d_{50}^2 - d_{90}d_{10}} \quad (2.21)$$

$$a = \frac{d_{\max} - d_{50}}{d_{50}} \quad (2.22)$$

and

$$\delta = \frac{0.394}{\log_{10} \left[\frac{v_{90}}{v_{10}} \right]} \quad (2.23)$$

where

$$v_{90} = \frac{d_{90}}{d_{\max} - d_{90}} \quad (2.24)$$

and a similar expression can be written for v_{10} . Values of $a=1.2$ and $\delta = 0.9$ were determined by Karabelas for water-kerosene dispersions.

Pacek and Nienow (1997) proposed a more general approach where by normalising the distributions by dividing by the Sauter mean diameter, all distributions should fall onto one line, which can be described by a cumulative normal distribution.

$$f(d) = 0.5 \left[1 + \operatorname{erf} \left(\frac{X - \mu}{\sigma_v \sqrt{2}} \right) \right] \quad (2.25)$$

where $X=d/d_{32}$, μ is the population mean and σ_v is the standard deviation. Values of $\mu=1.03$ and $\sigma_v = 0.37$ were obtained for a Kenics type mixer used in these studies.

Sauter Mean Diameter is a commonly referenced parameter defined as:

$$d_{32} = \frac{\sum_{i=1}^N n_i d_i^3}{\sum_{i=1}^N n_i d_i^2} \quad (2.26)$$

Where n_i is the number of droplets of diameter d_i . A disadvantage of the use of a normal distribution is that this distribution assumes a finite number of drops of size zero and infinity, which is obviously not physically reasonable. Application of the normalising technique to an upper-limit log-normal distribution may prove to be more realistic.

2.2.4.2 Prediction of Maximum Drop Size

In order to utilise the models described above, values of maximum drop size are required. Hinze (1955) and Hesketh *et al.* (1987) have presented 2 different equations which claim to predict this. Hinze developed a theoretically derived model based on a dilute flow field (Equation 2.27) while Hesketh *et al.* proposed a different equation, which included the dispersed phase density, ρ_d , as well as the continuous phase density, ρ_c (Equation 2.28).

$$d_{max}^{\frac{5}{3}} \left(\frac{\rho_c u^2}{\sigma} \right) \left[\frac{f}{D} \right]^{\frac{2}{3}} = 0.369 \quad (2.27)$$

$$d_{max} = 1.38 \left(\frac{\sigma^{0.6}}{(\rho_c^2 \rho_d)^{0.2} \eta_c^{0.1}} \right) \left(\frac{D^{0.5}}{u_c^{1.1}} \right) \quad (2.28)$$

In the above equations, u is the mixture velocity, D is the pipe diameter and η is the dynamic viscosity. f is the friction factor that can be obtained from the Blasius Equation which is based on the Reynolds number, Re .

$$f = \frac{0.079}{Re^{0.25}} \quad (2.29)$$

Where

$$Re = \frac{Du\rho}{\eta} \quad (2.30)$$

Most experimental data is quoted in the form of Sauter Mean Diameter so it is necessary to apply a relationship between Sauter mean diameter, d_{32} and maximum drop size, d_{max} . If we assume the upper-limit log-normal distribution, the following relationship can be derived.

$$d_{32} = \frac{d_{max}}{1 + a \exp\left(\frac{1}{4\delta^2}\right)} \quad (2.31)$$

The above equations can be used to predict Sauter Mean Diameter for a particular flow system if physical properties and geometry for the system are known, and values of a , d_{max} and δ can be assumed or calculated. If drop size distribution data are available, an attempt can be made to fit the experimental data to the theoretical distributions described above.

The prediction of maximum stable drop diameter is dependent upon the assumption of a fully developed and stable flow regime. For flowing dilute systems, a static steady state can occur if the rate of coalescence is negligible and this results in the formation of a stable emulsion. At higher concentrations, where the assumption of minimal coalescence cannot be made, a dynamic steady state exists where the

processes of breakage and coalescence balance. Kostoglou and Karabelas (1998) reported a significant discrepancy between the size distributions measured by different workers for dilute liquid-liquid dispersions (for concentrations below 1.3 % by volume) and those calculated from theoretical steady state predictions using models for drop breakage as shown by Kostoglou *et al.* (1997). The attainment of steady state was found to be a negative exponential function of time, so the final value of maximum drop diameter is attained very slowly. This conclusion questions the practical significance of the maximum drop diameter, as any measured values are dependent on the level of development of the flow. However, for systems of a higher concentration where there is significant coalescence still need to be characterised and there are no other predictive methods available at this time. It is important to be aware of the development of the flow when formulating any conclusions from measured distributions.

2.2.4.3 Effects of Drop Concentration

The equations of Hinze (1955) and Hesketh *et al.* (1987) are based on a dilute flow field. As the concentration of the dispersed phase increases, it has been observed that coalescence effects cause the mean drop size to increase. This effect is obviously strongest in concentrated systems but recent work by Pacek and Nienow (1997) has shown a dependence at volume concentrations as low as 0.5% by volume in a “Kenics Mixer”. Some empirical equations have been presented which relate Sauter Mean Diameter to volume concentration in gas-liquid flow and liquid-liquid mixers and are of a similar form. Azzopardi *et al.* (1980) proposed the following equation for gas-liquid flow.

$$\frac{d_{32}}{D} = 1.91 \frac{Re_g^{0.1}}{We^{0.6}} \left(\frac{\rho_g}{\rho_l} \right)^{0.6} + 0.4 \frac{\dot{m}_{IE}}{\rho_l u_g} \quad (2.32)$$

where

$$We = \frac{\rho_g u_{gs}^2 D}{\sigma}$$

and

$$Re_g = \frac{\rho_g u_{gs} D}{\eta_g}$$

In this equation, \dot{m}_{lE} is the mass flux of entrained liquid and the subscripts g and l refer to the gas and liquid phase respectively.

Many correlations have been proposed for liquid-liquid mixtures agitated in vessels by Godfrey *et al.* (1987, 1989) and Davies (1992) but the most recent are of the form

$$\frac{d_{32}}{D} = K_1 (1 + K_2 \phi) We^{-0.6} \quad (2.33)$$

Here ϕ is the volume fraction of the dispersed phase and the Weber Number, We , can be defined as above.

2.3 PHASE SEPARATION OF DISPERSIONS

The most difficult separation of a three-phase mixture of gas, oil and water as obtained from an oil well is usually the disengagement of the two liquid phases. The gas can usually be separated easily by gravity due to the large density difference between the gas and the liquids. Separation of a dispersion of two immiscible liquid phases is achieved by the coalescence of the particles to form a second continuous phase. There are several different methods which can be used to achieve this. If there is a significant density difference between the liquid phases, gravity can again be employed, either by

settling in a large tank as in the case of a primary separator or by use of centrifugal force as in a cyclone. Coalescence can also be promoted by use of the inertia of the drops as in flat or corrugated plates, Rowley and Davies (1988). In this type of separation, the inertia of the entrained drops causes them to collide with the plates. The impacted drops form a film on the coalescing surface which can then be collected. Differences in the conductivities of the phases can also be utilised. Coalescence can be initiated in water-in-oil dispersions by an electrostatic technique. Bailes and Larkai (1981, 1982) investigated the use of a pulsed DC electrical field to separate aqueous solutions of cyclohexanol or sulphuric acid dispersed in kerosene and proposed mechanisms for coalescence. A model for electrostatic coalescers was proposed by Bailes (1995).

Due to the large volume of liquids to be processed, the primary separation of the three-phase mixture is performed by gravity in large cylindrical horizontal vessels. It is essential to know the physics of phase disengagement in order to design a primary separator and indeed this knowledge forms the basis of published design methods. Recent developments of internal packings have meant that these design methods are now somewhat conservative, as the performance enhancements offered by these packings mean that smaller vessels can be specified.

2.3.1 Configuration of a Primary Separator

A three phase primary separator traditionally has a three phase inlet mounted at the top of the vessel. The liquids plunge to the bottom of the vessel and most of the gas disengages and exits through the top of the vessel at the opposite end. The separation of the organic and aqueous phases is achieved along the length of the vessel and a weir is

used to split the phases to their separate outlets. A perforated baffle may be installed to smooth the flow past the inlet region.

Control of the vessel is performed by use of level controllers on both oil and water exit lines. Overall pressure is maintained by the action of a control valve on the gas outlet. The efficiencies of the level controllers are dependent on the stability of the inlet flow and also the quality of the phase interfaces, which can be subject to foaming or dirt in some cases. The levels reported by the controllers are therefore subject to error. This means that the separator may not be working at the optimum conditions and this can create inefficiencies that may affect the separation performance.

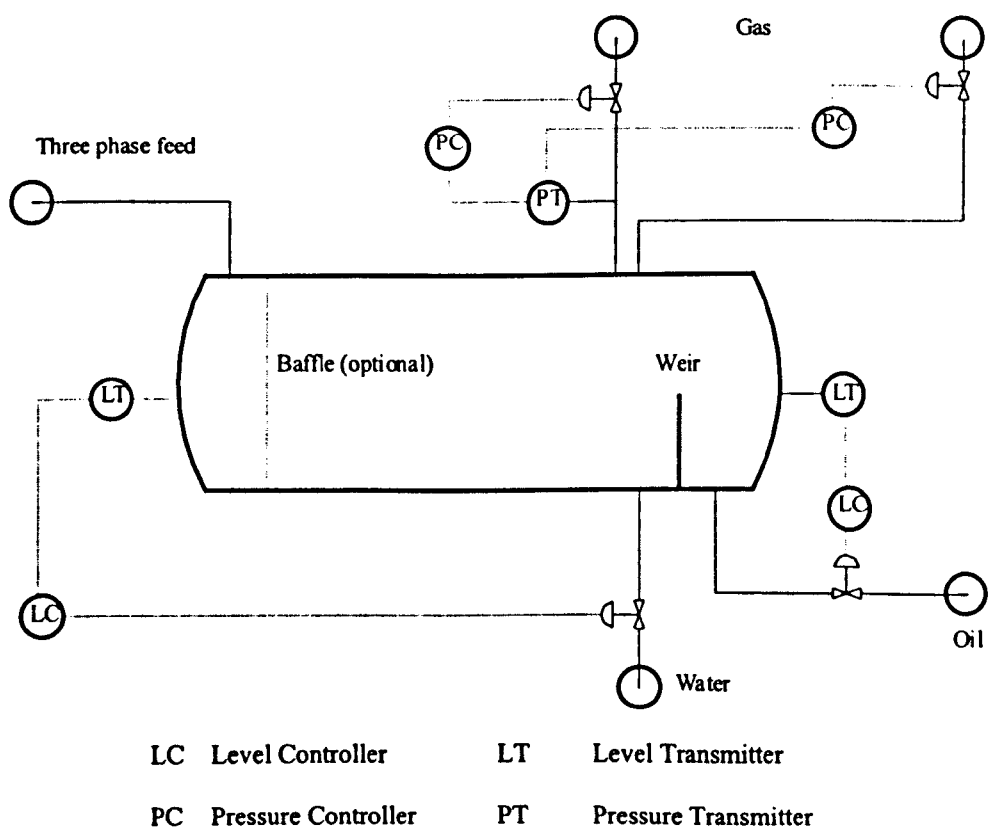


Figure 2.6: Traditional separator control scheme

2.3.2 Settling of Particles Through a Continuous Medium

To understand the physics of gravity phase separation, it is necessary to study the forces acting on a droplet as it settles through a fluid medium. As a particle or droplet settles through a fluid, there are several forces acting on it. When these forces are in balance, the droplet travels at a steady velocity, known as the terminal velocity. This analysis is applicable to any particle of one phase dispersed in another, as long as the particles can be considered spherical. This effect is illustrated in Figure 2.7 below.

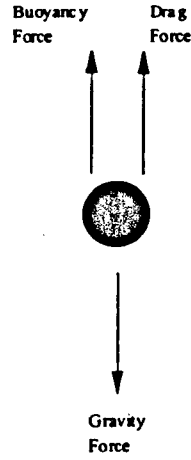


Figure 2.7 Forces acting on a settling droplet.

The gravity and buoyancy forces can be expressed respectively as

$$F_g = m_d \cdot a = \frac{\pi d^3}{6} \rho_d g \quad (2.34)$$

$$F_b = m_c \cdot a = \frac{\pi d^3}{6} \rho_c g \quad (2.35)$$

Where m_c refers to the mass of continuous phase displaced by the particle. The drag force acting on the particle is proportional to its projected area.

$$F_d = \frac{\pi}{4} d^2 \left[\frac{1}{2} \rho_d u^2 \right] C_d \quad (2.36)$$

By performing a force balance on the droplet, we can derive the terminal velocity of the droplet.

$$F_g = F_b + F_d \quad (2.37)$$

Whence

$$u_t = \left(\frac{4gd(\rho_d - \rho_c)}{3\rho_c C_d} \right)^{1/2} \quad (2.38)$$

These expressions can be simplified in the Stokes' law region ($Re < 1$) which is applicable for the droplets of liquids dispersed in gases. This analysis is extended to liquid-liquid systems by use of a different equation for drag coefficient, C_d , later in this Chapter. Within the Stokes Law region the drag coefficient can be expressed as:

$$C_d = \frac{24}{Re} \quad (2.39)$$

Substituting this expression into Equation 2.38 gives a much simpler result.

$$u_t = \frac{g d^2 (\rho_d - \rho_c)}{18\eta_c} \quad (2.40)$$

This theory was first used to examine the carry up of drops by vapour between the trays of distillation columns, but is also applies to phase separators. When designing such equipment, in most cases the drop diameter, d , is not known, so the following empirical disengagement equation was proposed by Souders and Brown (1951).

$$u_t = K \left[\frac{(\rho_d - \rho_c)}{\rho_c} \right]^{1/2} \quad (2.41)$$

K values in the range from 0.1 to 0.35 have been proposed for distillation columns, with 0.227 suggested as a typical value for most applications, including phase separators. For the design of a simple gas-liquid gravity separator without internals, the allowable vapour velocity of the separator, u_s should be taken as a fraction of the terminal velocity

and 15% was suggested by Gerunda (1981) as a sensible value. Use of a mist eliminator pad in either horizontal or vertical separators eliminates the need for this safety factor and so the relative sizes of the vessels are greatly reduced.

Once the gas velocity is determined, the cross sectional area of a vertical vessel can then be calculated directly by dividing the volume flow rate by the allowable velocity. The diameter can then be found from geometry. The height of the liquid in the sump can be calculated from the required liquid residence time, which is usually a function of the conditions of the downstream plant. Dimensions for the other sections of the separator are usually dictated by the mechanical design.

Horizontal vessels require a trial and error procedure to solve. Gerunda assumed a limiting case where a droplet settles just before the gas outlet (Figure 2.8). The settling distance for droplets falling at u_t is now the fraction of the vessel diameter occupied by the gas. This is described by setting two variables, f_{av} , the fraction of area taken up by the vapour space and f_{hv} , the height taken up by the vapour space. Similar variables, f_{al} and f_{hl} can be defined for the liquid phase. The same value of allowable vapour velocity is taken ($0.15u_t$) and basic geometry then yields the separator diameter (Equation 2.42).

$$D = \left[\frac{f_{hv} V}{\frac{L}{D} \cdot \frac{\pi}{4} \cdot u_t f_{av}} \right]^{1/2} \quad (2.42)$$

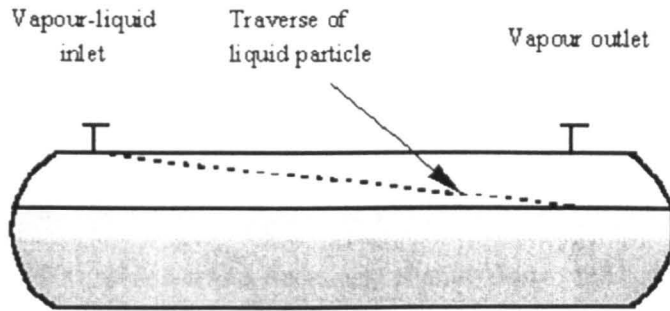


Figure 2.8: Traverse of a liquid particle in a horizontal separator.

Obviously, values are required for the ratio of length to diameter and liquid level. Economic L/D ratios were suggested by Gerunda for different pressure ranges and a half full drum typically taken as a starting point. These values are highly arbitrary.

Table 2.2: Values of L/D suggested by Gerunda

Operating Pressure, psig	L/D Ratio
0-250	3.0
251-300	4.0
501 and higher	5.0

Within horizontal separators the liquid residence time can be an important design consideration as it affects the separation efficiency. The liquid residence time can be calculated from geometry using where Q_l is the liquid volumetric flow.

$$t_{liq} = \frac{\pi D^2 f_{al} L}{4 Q_l} \quad (2.43)$$

This adds further to the trial and error procedure and so there has to be a compromise in the design depending on whether the oil or water quality is the more important condition in each case.

This settling theory can be extended to liquid liquid systems by choice of a different equation for the drag coefficient. Wu (1984) postulated that the range of Reynolds number was $1 < Re < 1000$, which was a necessary change due to the presence of another dense phase. In this situation a different expression can be derived for the drag coefficient.

$$C_d = \frac{18}{Re^{0.6}} \quad (2.44)$$

Equation 2.44 can now be utilised in a similar way to Equation 2.39 and an expression can again be written for the allowable velocity. Wu also suggests a reduction in the safety factor to 0.7- 0.9 u_a for vessels without mist eliminators. This will result in much smaller vessels.

2.3.3 Coalescence of Droplets at the Liquid-Liquid Interface

Disengagement of the oil and water phases is a very important design consideration as liquid product quality usually needs to be specified. A settling droplet of liquid upon reaching the interface will either pass through or bounce and stay on the surface for a time. The critical condition is whether the droplet has sufficient impact momentum to break the interfacial film. By equating these two forces we obtain Equation 2.45. If the condition specified is met, then the droplet will coalesce with the interface. If not, the

droplet will stay on the surface of the interface, coalesce with other droplets and finally break through once it has reached a sufficient size.

$$\frac{\pi d^2 \rho_d u_i^2}{4g} \geq \pi d \sigma_i \quad (2.45)$$

Depending on the value of Reynolds number and hence the flow region in question, u_i and C_d can be substituted using an appropriate correlation. It was suggested by Wu that the region is transition flow where $1 < Re < 1000$ and hence Equation 2.44 above is valid. The minimum droplet size that can break through the interface is therefore easily calculated, together with the corresponding terminal velocity, for any case in question. The liquid residence time can then be set so that the droplets have enough time to coalesce and settle. This is simply calculated from the separator geometry and liquid flow rate although, as will be seen later, the theoretical residence time is rarely attained.

All the methods presented so far are based on calculation of terminal velocity. Arnold and Koszela (1990) questioned the validity of these methods. Due to the wide variation of physical properties of crude oils, it was proposed that batch settling tests gave more information about the nature of the oil liquid separation. To design a separator using this method, oil and water samples are mixed and then allowed to separate. The time required for the separation is then recorded, and together with the L/D ratio set by process economics, the separator can be designed. However, it is stated that there is insufficient data to prove which method is the most appropriate and that a pooling of data from operators would greatly simplify this process.

Hafskjold and Morrow (1994) analysed the performance of both a field separator and a laboratory model in an attempt to relate separator performance to convenient laboratory

measurements. A computer code was developed to relate separator performance to data obtained from batch settling tests. It was discovered that both droplet coalescence and separation rate were non-linear functions of time, and hence oil-water separators were found to be highly sensitive to flow rates. The critical parameter was found, unsurprisingly, to be the liquid residence time, while the weir overflow rate was found to be of little importance.

The quality of the published design methods has obviously increased with time. The equations and safety factors proposed by Gerunda would produce a very conservative design. The later modifications as proposed by Wu would produce a more efficient design but local conditions within the separator are not taken into account. Three-phase separators are often the largest installed items on an offshore platform. Great savings can therefore be made by reducing the size and increasing the efficiency of these vessels. This implies that detailed and accurate design methods are needed. More advanced modelling techniques should therefore be used to design these vessels and estimate their performance.

2.4 PERFORMANCE ENHANCEMENT OF PRIMARY SEPARATORS

The need to minimise the size and maximise the performance and flexibility of primary separators has led to the development of several internal devices that are claimed to improve the operation of these vessels. These internals can be used not only to reduce the size of new separators, but also to debottleneck existing plant. The effects of such operations and the type of internals that are commonly fitted are presented below.

2.4.1 Plate Separator Packs.

It is possible to greatly improve the liquid/liquid separation performance of 3 phase separators by installation of a series of flat or corrugated plates (vane packs) in the liquid pool as illustrated by Rowley and Davies (1988) and Rommel *et al.* (1992). These plates act as flow guides and produce near uniform flow both across and along the vessel and reduce the settling distance between the entry of a drop and the phase boundary.

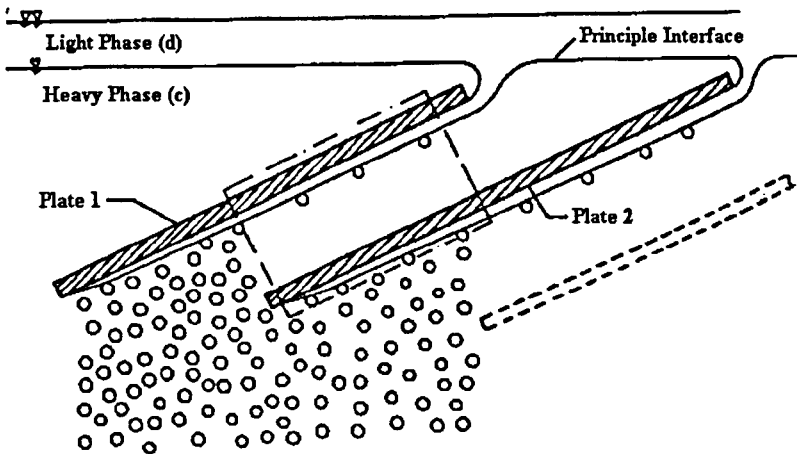


Figure 2.9: Principal Physical Processes in a Plate Settler.

The plates act as a set of parallel channels through which the phases travel. The lighter phase (oil) rises and coalesces on the underside of the upper plate while the heavy phase (water) settles to the topside of the plate below. The plates are installed so that the dispersed phase exits near to its outlet and there are different ways of achieving this.

For a cross flow arrangement, the plates are arranged parallel to the axis of the vessel and inclined at an angle θ , say 45° . The coalesced phase therefore travels perpendicularly to the bulk phase.

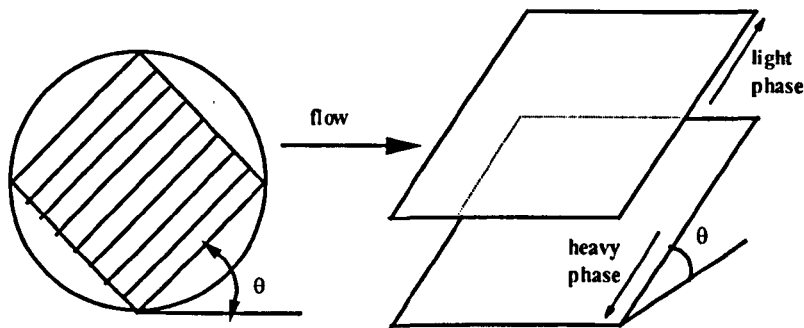


Figure 2.10:Cross Flow Plate Arrangement

For co/counter-current flow, the plates are inclined in the direction of the flow. The flow is either co or counter current depending on which phase is dispersed and the angle of the plates above or below the horizontal.

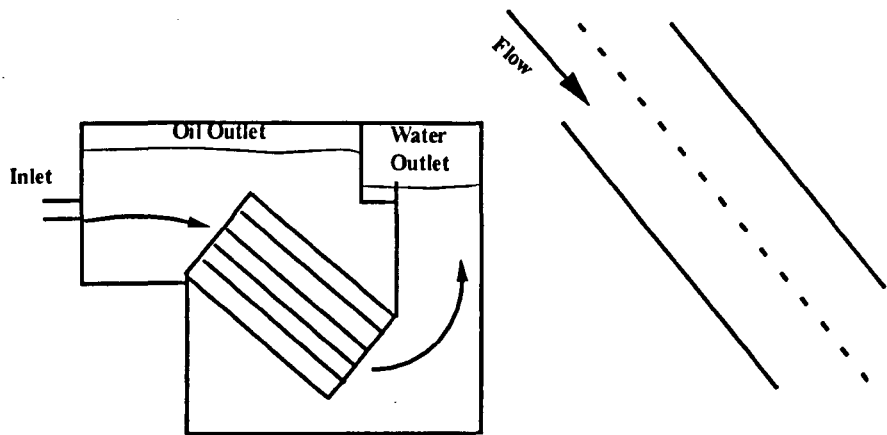


Figure 2.11: Co/Counter Current Flow Plate Arrangement.

2.4.2 Structured Packings

Several types of structured packings have been developed which claim to produce improvements in the liquid-liquid coalescence. Typical trade names of these packings are Sulzer Mellapak and Natco Performax and the details are proprietary.

The packings provide a large surface area for droplet coalescence but the location of the packings within the separator vessel is very important to avoid blockage by sand or dirt.

2.4.3 Perforated baffles

Perforated baffles may be installed close to the inlet of a primary separator to act as flow spreading devices to minimise dead zones within the vessels. The inlet of the separator usually causes some turbulence so these baffles are beneficial to smooth out the flow which aids the settling of the drops by gravity. Momentum breakers are also often installed on the vessel inlets for the same purpose.

2.4.4 Industrial Experience of Performance Enhancing Internals.

Internals of the types described above have been utilised in existing vessels in an attempt to improve their performance in terms of both efficiency and capacity. Broussard and Meldrum (1992) discussed the retrofit of two separators found to be performing below standard in the S.W. Fateh oil field. Increasing production rates led to these problems so it was decided to retrofit these separators in order to improve their performance.

The first vessel tackled, was a 3m by 13 m over 3m by 20m 'piggy back' style of vessel. It was used as the primary two-phase gas/liquid separator on the field up to 1985 and it was purchased for its high gas and slug handling abilities. The performance was found to be substandard due to the design of the inlet diverter which created foaming problems and resulted in severe liquid carryover into the gas phase at high flow rates. This created severe flow restrictions. Upon dismantling the separator, the inlet diverter was found to be lying in pieces on the vessel bottom due to failure of the bolts. The inlet diverter was replaced and new structured packing internals were added to assist in

the oil-water separation and hence convert the vessel to three-phase operation. The retrofit was a success and the maximum operating capacity increased threefold.

The second vessel tackled, was a 4.8m by 21m vessel designed to handle three-phase flow. However, it under-performed on three-phase separation significantly due to an insufficient liquid residence time which caused slugging of the outlet flows. Radioactive tracer techniques, which will be discussed later, showed that the inlet diverter directed flow down the side of the vessel, which resulted in excessive turbulence. Additionally, the packing inside the vessel did not extend to the bottom of the liquid phase which caused channelling. To combat these problems new internal packing was fitted and the inlet diverter was replaced by a new dished head model which included a shroud containing a basket of pall rings to act as a momentum breaker. After the retrofit, the capacity again increased greatly.

These results illustrate the great importance of the internal design upon the performance of these vessels. Of particular concern are the arrangement of the inlet momentum breaker and the position of packing and baffling within the vessel. Increasing knowledge of the nature of the oil-water separation and the effect of different internal configurations could lead to smaller vessels and better separations than were previously possible. It is especially beneficial to identify when internals are actually a hindrance rather than helpful.

2.5 IN-SITU PERFORMANCE MEASUREMENT AND PROBLEM IDENTIFICATION.

Shutdown of a primary separator usually proves very costly, as in the absence of relief vessels, this also involves shutdown of downstream plant. It is therefore highly beneficial, indeed necessary, to be able to identify any problems of the types described above in-situ. Nucleonic techniques have been developed to give information on phase interface positions and Residence Time Distributions (RTD). The results of these tests can be used to gain information about the effectiveness and flow characteristics of the vessel, although interpretation requires careful thought as there are several factors which can affect the Residence Time Distribution which will be discussed later.

2.5.1 Background to Residence Time Measurement

In order to describe the nucleonic techniques used on primary separators, it is necessary to review the theory of Residence Time Distribution measurement first. The Residence Time Distribution of a particular system is a measure of how long a packet of fluid resides within the system before it exits. It is possible for packets of fluid entering a system at the same time to have different residence times, perhaps due to mixing, backflow or chemical reaction. The residence time of the fluid within the vessel is an important design parameter, as it defines the length of time the phases have to disengage. To measure the residence times, chemical tracers can be added to the feed lines. The concentration of tracer at the outlets is monitored with time and hence the Residence Time Distribution of the system can be found. The tracer can be injected in 3 ways, either as an instantaneous pulse, continuously after an elapsed time (step change) or intermittently, as either pulses or sinusoidally.

The concentration of tracer leaving the outlet(s) is then measured and this data can be used to find the Residence Time Distribution. The Residence Time Distribution, $E(t)$, can be defined as the fraction of elements leaving with ages between t and $t+dt$. If the tracer is an instantaneous pulse, modelled as a Dirac Delta function.

$$E(t) = \frac{c}{m/Q} \quad (2.46)$$

Where m is the mass of tracer injected and Q is the volumetric flow rate. Here c is the outlet concentration at time t . Since, by definition:

$$\int_0^{\infty} E(t) dt = 1 \quad (2.47)$$

It follows that

$$\frac{m}{Q} = \int_0^{\infty} c dt \quad (2.48)$$

This obviates the need to know m , although if it is known, the mass balance can be checked. Now by definition,

$$t_m = \int_0^{\infty} t E(t) dt \quad (2.49)$$

Using

$$E(t) = \frac{c(t)}{\int_0^{\infty} c dt} \quad (2.50)$$

We obtain

$$t_m = \frac{\int_0^{\infty} t c(t) dt}{\int_0^{\infty} c dt} \quad (2.51)$$

The upper limit can be replaced by some time, T , beyond which no more tracer can be detected.

The variance σ^2 can also be calculated as

$$\sigma^2 = \int_0^{\infty} (t - t_m)^2 E(t) dt \quad (2.52)$$

Hence similarly,

$$\sigma^2 = \frac{\int_0^{\infty} (t - t_m)^2 c(t) dt}{\int_0^{\infty} c dt} \quad (2.53)$$

Further analysis is required to obtain the Residence Time Distribution from a step change. We can define the cumulative age distribution, $F(t)$, where F is the fraction of elements leaving younger than t . Hence

$$F(t) = \int_0^t E(t_1) dt_1 \quad (2.54)$$

The tracer is injected to give a steady concentration c_0 in the feed from $t=0$. The outlet concentration c is measured from this moment. Fluid elements that entered before $t=0$ have $c=0$ and elements which entered after have $c=c_0$. $c(t)$ is then given as

$$c(t) = c_0 F(t) \quad (2.55)$$

Hence

$$F(t) = \frac{c(t)}{c_0} \quad (2.56)$$

Then

$$E(t) = \frac{dF}{dt} \quad (2.57)$$

If the tracer is injected sinusoidally or intermittently at a known frequency, by measuring the outlet concentration we can calculate the magnitude and phase difference of the resulting signal. The magnitude is the ratio between the output and input amplitudes of the signals and the phase difference is the phase shift between outlet and inlet. $E(t)$ can be obtained from this information, as shown by Luyben (2nd Ed. 1990)

2.5.2 Nucleonic Residence Time Distribution Measurement.

Residence Time Distribution of both organic and aqueous phases in industrial separators is obtained by use of radioactive tracers. A compatible “radiotracer” is injected into the appropriate feed line and then its progress is monitored by strategically located radiation detectors. This technique has been widely used in industry to obtain in-house data of the operation of separators. BP Exploration (BPX) has applied this procedure to four of its production units, Magnus in Scotland, Ula in Norway, Milne Point in Alaska and Kinneil, Grangemouth UK.

The tracer used in these tests was Bromine 82, a strong gamma emitter with a half-life of 36 hours. The water-soluble form of the tracer is potassium bromide and the oil soluble form is 4,4-dibromo-biphenol. The sensitive scintillation detectors used are installed just downstream of the injection point in the feed line and at each outlet. A separate shielded detector is also installed at each outlet to measure background radiation and hence eliminate any external effects.

The salient features of the Residence Time Distribution curves produced can yield important information about the operation of the separators. Significant differences between the theoretical and measured residence times can be due to excessive

turbulence due to poor design, blockage due to sand or equipment internal failure. Clearly the information produced in these reports is substantial but difficult to analyse without an experimental facility to provide comparative data. Construction of a test separator upon which tracer tests can be performed would provide a control environment under which the features of the Residence Time Distribution curves can be investigated further. An example set of these Residence Time Distribution curves is shown below.

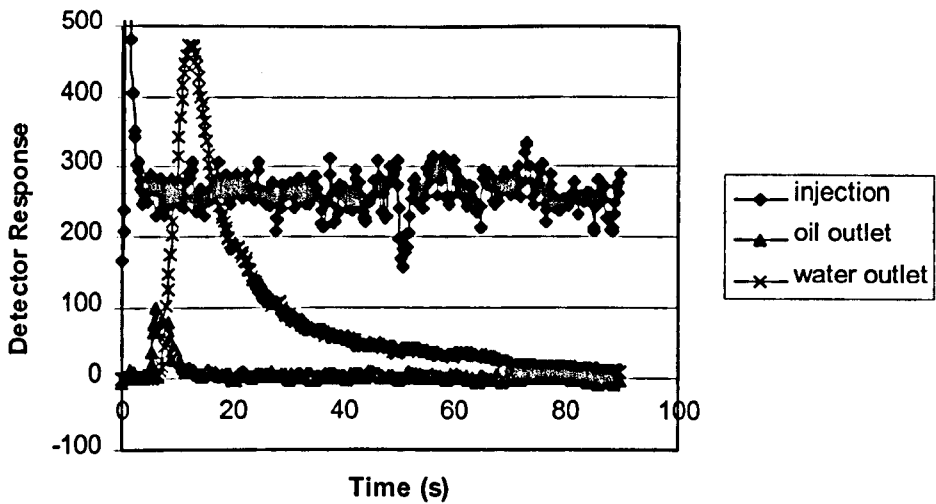


Figure 2.12: Typical Residence Time Distribution output from the Milne Point Separator

2.5.3 Interface Level Measurement by Neutron Back-Scatter

Neutron back scatter can be used to monitor the level of the oil-water interface within the separator. This allows comparison within instrument readings and also monitors for the presence of excessive foaming or other problems due to the nature of the liquids.

The measuring device is installed near to or on the vessel walls. An Americium/Beryllium source emits fast neutrons which are absorbed essentially exclusively by hydrogen atoms which then re-emit slow neutrons. By measuring the

slow neutrons scattered back to a detector, the hydrogen concentration within a short range of the detector head is measured. The hydrogen concentration within water differs significantly from that of oil or gas so this permits the location of the oil-water interface to be measured. Presence of sand within the vessel will result in a lower back-scatter reading, so this technique can also be used to locate any clogging within the vessel. The technique only has a very short range, however, so any measurements taken are indicative of the flow conditions close to the vessel walls.

This technique can also reveal a lack of distinction of the oil-water interface. This is indicative of blockage or excessive turbulence, due usually to poor design of the inlet flow diverter. This problem was detected on the BPX Ula platform, Norway.

2.5.4 Interface Level Measurement Using Gamma Rays

Gamma ray scanning can be performed on the separators to monitor the position and condition of the gas/oil interface. A gamma source is mounted on the wall of the vessel and the detector is placed on the opposite side. The intensity of radiation detected is dependent on the density of the medium it passes through so a drop in radiation count is detected as the beam passes through the gas/oil interface. The drop is not perfectly sharp, however, due to the necessity of using a wide scanning beam as a narrow beam requires too much heavy shielding. The vessel walls have some effect on the count, so the beam is passed through the vessel when it is empty in order to provide a control scan.

Nucleonic gamma scans are beneficial for the detection of foaming within vessels. This can occur for light crudes and in situations where the vessels are running at high throughputs.

2.6 POSSIBLE MODELLING TECHNIQUES

The existing design methods described above all make use of settling theory. However, the complexity of these vessels has been shown to increase as new internals have been developed. This calls into question the effectiveness of these methods, particularly in light of industrial experience. Measurements performed on these vessels yield data on Residence Time Distribution and interface height, which are variables that cannot be derived from settling theory. It is therefore of interest to examine modelling techniques which could be used to develop a Residence Time Distribution model of the system. This could prove useful for determining vessel performance.

2.6.1 Transfer Functions

This mature technique is based on control theory and gives the Residence Time Distribution of the system directly. The system to be modelled is split into a series of zones, and then a type of flow is assigned to each zone. The types of zone that can be used are related to the degree of turbulence and mixing which occur and are described below.

Stirred Tank Zone.

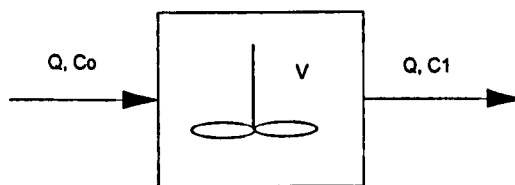


Figure 2.13: Diagram of a Stirred Tank Zone

This type of zone is analogous to a Continuously Stirred Tank Reactor (CSTR). Within a stirred tank there is complete mixing. This means that the concentration of any substance in the outlet is identical to the concentration throughout the zone. This can be defined by a differential mass balance.

$$c_0 = c_1 + \tau \frac{\partial c_1}{\partial t} \quad \tau = \frac{V}{Q} \quad (2.58)$$

Here τ is the mean residence time of the zone. If there is chemical reaction then an extra term, $r\tau$, is added to the equation, where r is the reaction rate.

PFR Zone.

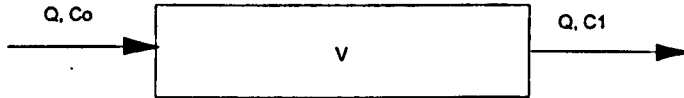


Figure 2.14: Diagram of a PFR Zone.

As its name implies, this type of zone can be compared to a Plug Flow Reactor. This is almost the direct opposite of a stirred tank as no mixing occurs at all and there is complete segregation. If there is no chemical reaction then a PFR zone is equivalent to a delay or dead time equal to the residence time of the zone, i.e:

$$c_1(t) = c_0(t - \tau) \quad (2.59)$$

If there is chemical reaction then an incremental mass balance yields

$$\tau = \int_{c_{inlet}} \frac{dc_A}{r_A} \quad (2.60)$$

Reality, of course, deviates from these two ideals. Several more complex models have been proposed in order to describe partial mixing situations, for example, the Dispersed Plug Flow Model which can be found in Levenspiel (1962). These zones can be combined in many possible ways and a visual representation of this is the Signal Flow Block Diagram. This is shown below for a simple Stirred Tank with Bypass system. Once the system has been described in this way, a Residence Time Distribution model can be derived mathematically as described by Luyben (1990) and Levenspiel (1962).

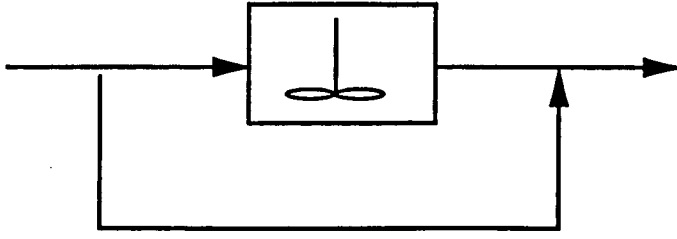


Figure 2.15: Example of a Signal Flow Block Diagram for a Simple Stirred Tank with Bypass.

As models increase in complexity, the differential equations describing the system obviously become more difficult to solve. A useful technique which can be applied to solve such a system of equations is Laplace Transforms. This approach converts the differential equations to algebraic ones, which can then be simply manipulated to give a time-domain solution using look-up tables. The Laplace transformation from the time domain to the Laplace domain is

$$F(s) = \int_0^{\infty} f(t)e^{-st} dt \tag{2.61}$$

Here $f(t)$ is the measured concentration and s is a complex parameter. Alternatives to Laplace transforms are proprietary computer programs such as ACSL or numerical techniques.

A Residence Time Distribution model can be developed entirely from theory, but many researchers have used experimental data to build models. A transfer function model of the process can be developed by looking at the frequency response of the system. By performing a Fast Fourier transform analysis on the experimental data described by Luyben (1990), the magnitude and phase can be plotted on a Bode Plot from which the order of the system and dead time can be derived. This procedure can either be performed manually or by computer.

2.6.1.1 Applications of Transfer Function Models

Transfer Function models are mostly used for the purposes of process control or reactor design but this often involves multiphase systems. Some examples of the multiphase equipment modelled using transfer functions are described below.

2.6.1.1.1 PWR.

In the event of a loss of cooling accident in a PWR, water is injected into the reactor. Some of this cooling water evaporates to form steam and different flow motions and regimes can be identified. Boddem and Mewes (1995) developed a model to predict these regimes by taking transfer functions from Residence Time Distribution profiles. Residence Time Distribution profiles were obtained by injection of a pulse of sodium chloride tracer into the inlet. A diagram of the constructed test rig is shown in Figure 2.16 below. The outlet concentrations at the top and bottom of the rigs were measured by conductance probes from which the concentration can be calculated directly. A Bode plot was drawn for the system and it was determined to be proportional 4th order, as shown in the Signal Flow block diagram and Equation 2.62 below

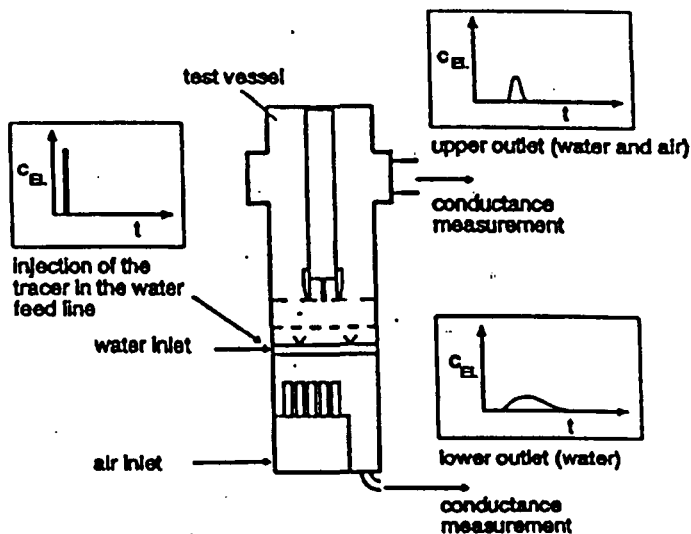


Figure 2.16: Diagram of PWR Rig and Tracer Technique

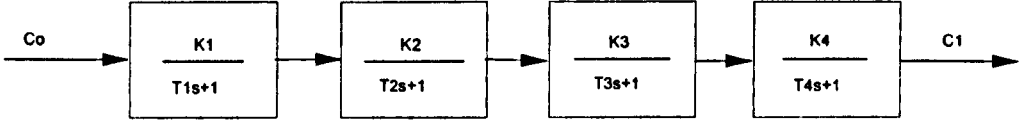


Figure 2.17: Signal Flow Block Diagram of a PWR.

$$\frac{c_o(s)}{c_i(s)} = \frac{K_1 K_2 K_3 K_4}{(\tau_1 s + 1)(\tau_2 s + 1)(\tau_3 s + 1)(\tau_4 s + 1)} \quad (2.62)$$

In Equation 2.62, the values K_i are the constant gain factors and τ_i are the time constants. This transfer function model was then parameter fitted to the experimental data and the resulting curve fit was found to be in good agreement. Future work suggested was examination of the effects of different flow conditions upon the Residence Time Distribution and fitted parameters, for both verification purposes and in order to obtain a more exact model.

2.6.1.1.2 Spray Drier.

Spray driers are commonly used for drying of particulate slurries by spraying through suitable nozzles into a hot air stream. Ade-John and Jeffries (1978) studied the flows within a PVC model by smoke injection. Turbulent zones were identified at the spray nozzles and air entry ports and the volume of these were seen to vary with air flow rate. In between these zones a cylindrical plug flow zone existed and a bypass zone was found to exist near the tower walls. Tracer experiments were performed on the air using carbon dioxide pulses to examine the shape of the Residence Time Distribution.

A zone model of the tower was then established (Figure 2.5) then transfer functions for these zones were postulated. To model the turbulent zones at the air inlet and

nozzles the Gamma distribution model was applied. This model considers dead time within the system and non-ideal mixing.

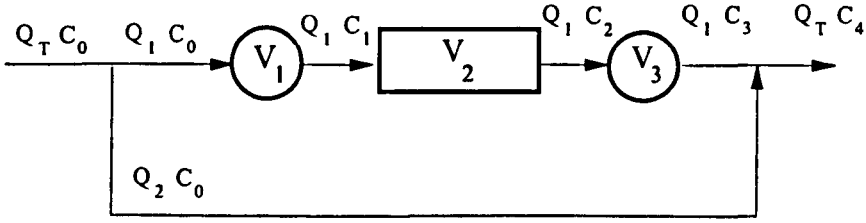


Figure 2.18: Air Residence Time Distribution Model.

$$E(t) = \frac{1}{\tau^p \Gamma(p)} (t - d)^{p-1} \exp\left(-\frac{t-d}{\tau}\right) \quad (2.63)$$

Here d is the dead time in the system, τ is the mean residence time and p is a mixing parameter. For the plug flow zone the standard form for plug flow was postulated. This form was also used to take into account the delay as the pulse passed through the inlet and outlet tubing outside the reactor.

$$E(t) = E(t + t_1) \quad (2.64)$$

Where t_1 = residence time from zone inlet to zone outlet. A mass balance was performed to calculate the concentration after the by-pass.

$$Q_1 C_3 + Q_2 C_0 = Q_T C_4 \quad (2.65)$$

By taking Laplace transforms of the above equations and combining them the system is described in the Laplace domain. Re-inverting into the time domain then yielded the transient response of the system. This was then fitted to the experimental tracer curves. The volume of each zone was obtained from this fit and found to be in good agreement with the zone volumes estimated from the smoke injection experiments.

2.6.1.1.3 Multistage Agitated Contactor.

A Multistage Agitated Contactor is used for gas/liquid reactions and consists of chambers in series each with its own stirrer. This causes minimal axial mixing which

is beneficial for several reactions. Due to a scarcity of data available a rig was built to obtain Residence Time Distribution and a mathematical model was fitted. The experimental Residence Time Distribution data was obtained by tracer pulse injection.

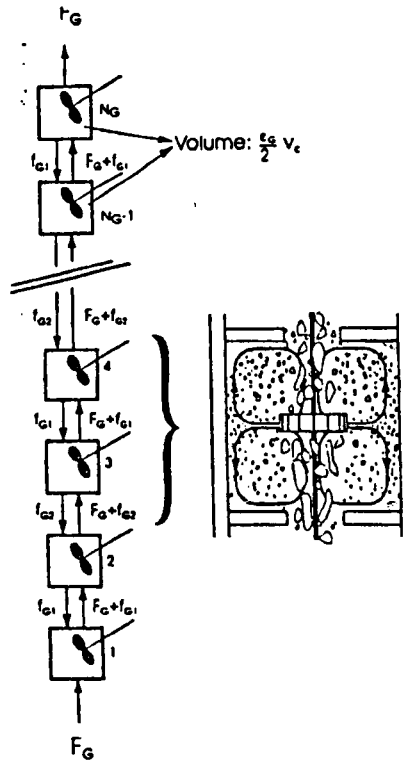


Figure 2.19: Diagram of the CTAB Model.

Within such a contactor Bremen *et al.* (1995) reported that there were 4 distinct flow regimes and it was hoped that each could be identified by the shape of the Residence Time Distribution. The model chosen for the simulation of the Multistage Agitated Contactor was the Cascade of equal ideally mixed Tanks in series with Alternating Backflow (CTAB) model. The model was parameter fitted to Residence Time Distributions obtained by pulse injection into the inlet of an experimental rig. The parameters of the model were found to vary consistently with the parameters of the

experiments and hence the CTAB model described the system quite accurately. A flow map was developed from the experimental data for the various flow regimes in the contactor. Similar work has taken place to model a finite packed bed chemical reactor using the axial dispersion model.

2.6.1.1.4 Monolith Reactor.

A monolith is a catalyst support which contains an array of parallel, uniform and non-connecting channels. An application is the catalytic converter in car exhausts, although the high surface area to volume ratio of these supports means that they are suitable for many catalytic three-phase reactions. In order to increase the understanding of the effects of flow upon reaction rate, the construction of a Residence Time Distribution model of the monolith was described by Patrick *et al.* (1995)

An experimental rig was constructed and the Residence Time Distribution of the liquid phase was measured using pulse tracer technique. Various flow regimes were noted in the monolith channels. It was decided to split the reactor into 4 zones. There was a significant amount of tubing at the inlet and outlet and so these were modelled as plug flow. Frothy flows existed at the inlet and the phase separator at the outlet and these were modelled as Stirred Tanks. The monolith itself was modelled as a “tanks in series” model (with no back mixing). Parameters for the model were obtained by deconvolution of the Residence Time Distribution using Fast Fourier Transforms. Comparison of the model curve with the experimental data was in good agreement.

2.6.2 Computational Fluid Dynamics

The transfer function type models discussed previously all produce good results when compared with the experimental data. This is in some cases an artefact of the parameter fitting and it is very important that the models can be verified by examining trends in the parameter values and by visualisation of the flow regimes. Transfer function type models are robust and easy to construct, but they do assume a “black box” type operation in each flow zone.

A technique which considers the action of the fluid at every point throughout the system in question is Computational Fluid Dynamics (CFD). CFD uses powerful computers to solve numerically the non-linear differential equations which describe the flow of a fluid within a particular system. The complexity of the CFD codes which have been developed and the flow systems to which they have been applied have increased over passing years due to the great advances in computer speed and efficiency. CFD is therefore a rapidly expanding field of increasing diversity. It is beyond the scope of this literature review to provide an in depth description of the subject, this has already been performed by Peyret (1996) and Wendt (1992) amongst many other authors. This section is therefore limited to an overview of CFD and its application to multiphase flow situations. A review of the scope of CFD to the petrochemical industry is given by Colenbrander (1991).

2.6.2.1 The Navier-Stokes Equations

All CFD models are developed from and solve the Navier-Stokes equations of fluid flow which completely describe any flow field. The equations are named after the mathematicians who first derived the equations independently of each other at the end of the 19th century. These equations are general and can be written for any co-

ordinate system but for illustrative purposes they are written here in general form in Cartesian co-ordinates (conservative form). Most multiphase systems considered use Newtonian fluids.

$$\frac{\partial}{\partial t} \rho u_i + \frac{\partial}{\partial x_j} \rho u_i u_j = \frac{\partial}{\partial x_j} \sigma_{ij} + \rho F_i \quad (2.66)$$

$$\frac{\partial \rho}{\partial t} + \frac{\partial}{\partial x_j} \rho u_j = 0 \quad (2.67)$$

$$i=1,2,3 \quad j=1,2,3$$

Where σ_{ij} is the stress tensor, F_i is an external force, eg gravity and Equation 2.67 is the continuity equation. u_i is the flux of the fluid in the direction x_i , where $i=1,2,3$. For Newtonian incompressible fluids we can write the stress tensor in terms of a pressure term and a shear stress term as below:

$$\sigma_{ij} = -P\delta_{ij} + \tau_{ij} \quad (2.68)$$

where

$$\delta = \begin{cases} 1 & i = j \\ 0 & i \neq j \end{cases} \quad (2.69)$$

$$\tau_{ij} = \mu \left\{ \frac{\partial u_i}{\partial x_j} + \frac{\partial u_j}{\partial x_i} \right\} \quad (2.70)$$

Boundary conditions are needed to close the equations and the system can then be solved. Boundary conditions can have a great influence on the result of the CFD simulation and therefore the choice of boundary conditions is of great importance.

Once the equations and boundary conditions governing the system are established, their highly non-linear nature requires them to be solved using numerical solution techniques. The solution domain needs to be discretised into a finite set of elemental

or control volumes formed by a computational grid. This technique is usually performed using finite difference (FD), finite volume (FV) or finite element (FE) methods that can require a great deal of computer power and time to solve. Commercially available computer packages have been developed, most notably PHOENICS, FLUENT and FLOW-3D. To reduce computer power and solve more complex systems, several models have been proposed.

2.6.2.2 Turbulence Modelling

The computation of even simple turbulent flows has difficulties. This is due to the non-linear nature of the Navier-Stokes equations which give a broad range of turbulent scales. The largest turbulent scales carry most of the turbulent kinetic energy and are responsible for most of the diffusion of the fluid. The smaller scales account for most of the dissipation of the kinetic energy within the flow. Both these effects need to be modelled in order to produce meaningful results.

Resolution of all the scales present is made possible using a Direct Numerical Simulation (DNS) approach. However, the number of grid points required to solve such a system is a rapidly growing function of Reynolds number and so the Reynolds number at which DNS can be performed is limited by computer resources.

The Reynolds number restriction can be bypassed by use of a Large Eddy Simulation approach (LES). As the name suggests, the large eddies only are directly simulated while the smaller scales are included by supplying a so-called subgrid model. There are significant computational benefits in the use of LES and it has been found that the smaller scale eddies are often simpler in nature than the larger scale motion of the

fluid and hence can be simply modelled. LES modelling retains a full three dimensional solution and time dependence of the turbulent fluctuations.

The next level of solution is to model the entire flow using suitable averaged quantities for the mean and turbulent motion. This process, known as Reynolds averaging, splits the variables into a mean plus a fluctuating component. The solution for the Reynolds averaged Navier Stokes equations can then be found, coupled with a closure model for the unknown turbulent Reynolds stress terms. Reynolds stress is defined as $\rho\tau_{ij}$. Many models have been proposed, one which is commonly used for multiphase flows is the κ - ϵ or two equation model described by Launder and Spalding (1972). A review of these turbulence models and CFD in general is given by Peyret (1996).

2.6.2.3 Flow Fields

There are two different approaches which can be used to form a computational grid for the fluid. An Eulerian approach fixes the grid in space and examines the fluid passing through each point in the grid. A Lagrangian approach tracks elements of the fluid individually, and the computational grid moves with the fluid elements through time. Multiphase flow CFD models can use combinations of the above methods.

2.6.2.4 Multiphase Flow Models.

To model dispersed flows, the Euler-Lagrange two phase flow model is often used. The Euler approach is used to model pressure and velocity properties of the continuum and a Lagrangian analysis is then performed on the particles which constitute the dispersed phase. The simplest Euler-Lagrangian models treat the two phases as an interspersed continua and the dispersed phase is not considered to affect

the properties of the continuous phase. This limits the models to low concentrations of the dispersed phase. Additional modifications have been developed to include the effect of the dispersed phase in order to increase the versatility of these models. DNS of dispersed flows have been made using this model, Elghobashi (1994) and Druzhinin and Elghobashi (1998).

These models can be developed further to model large bubbles of gas in liquid by interface tracking. They are characterised by a Lagrangian description of the gas bubbles and an Eulerian description of the continuous liquid phase. At each time interval, the co-ordinates of the gas bubble are recalculated and the system is modelled by the mass and momentum equations. The phases are linked by volumetric fraction. The interfacial forces define the interface position and the computational grid is either chosen to fit round the interface, or the cells in the grid are selected to contain either gas or liquid, depending on the relative interface position. The main problems with these models, as with all two phase CFD models, is that the types of equation used for each phase are optimised for single phase flow. Additionally, interface tracking models require very powerful computers and a large CPU time. Taylor bubbles and slugs in pipe flow have been simulated using this approach by Clarke & Issa (1997).

Two-fluid or “Eulerian-Eulerian” models consider the phases as interspersed continua and each phase is treated separately. The system of equations is solved by introducing the interfacial friction.

The location of the interface between each phase is a problem that needs to be solved and this is discussed in greater detail by Hirt and Nichols (1981). The Volume of Fluid model (VOF) defines a variable F that is assigned a value between 0 and 1 depending on the phase. Computational cells that have values between 0 and 1 are said to contain the interface. This obviously smears the interface but is computationally inexpensive as only 1 variable needs to be stored for each cell to describe the phase present.

2.6.2.5 Application of CFD to Phase Separators.

CFD models for 3 phase separators have been proposed by two workers, Hansen *et al.* (1994) and Wilkinson and Waldie (1994). Experimental work was performed in conjunction with these models for verification purposes. Both methods were developed to provide data which can be applied in two ways, to either improve internal configurations of existing separators or to improve the accuracy of design procedures for new separators.

The experimental rig by Hansen *et al.* was a small scale rectangular section model of length 1.83 m and height 0.46 m (Figure 2.20). It was equipped with an inlet breaker and an internal baffle plate in an attempt to emulate larger scale separators. 3 phase flows of oil, water and gas were used on all runs. Residence time of the liquid phases were obtained by injection of a pulse of chemical tracer. The velocity profile was obtained by a laser Doppler method for two-phase gas/water flow only. Attempts were also made to measure the profile for oil/water flow but the cloudiness of the entrained droplets in the liquid made this impossible. Pressure measurements were made on the inlet zone using a specially devised baffle plate. Additionally, batch

settling tests were performed on oil in water and water in oil dispersions in order to provide the model with data on settling times.

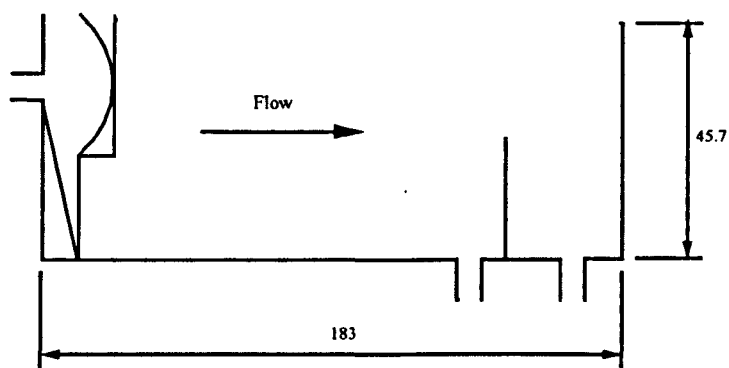


Figure 2.20: Experimental Apparatus of Hansen *et al.*

The flow patterns within the phases were seen from the rig to be complex, so the separator was split into various zones (Figure 2.21). and the CFD model was applied to the inlet zone (2) and bulk liquid zone (3). The flows around the inlet, where all the phases are present, are modelled as a 2 phase gas liquid zone using the KAMELEON CFD code. This gas/liquid jet is modelled to flow against a cup shaped momentum breaker. The resulting data also gives required details of the distributed velocity field down to the liquid pool.

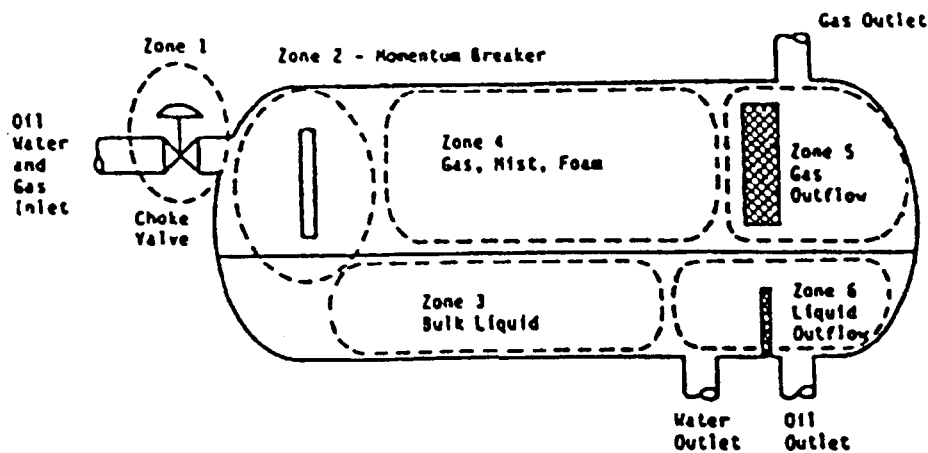


Figure 2.21: Flow Zones for the Model of Hansen *et al.*

The liquid flow inside the bulk liquid zone was considered to be homogeneous, i.e. the oil and water phases travel at the same velocity. This is considered to be acceptable as the liquid velocities are quite low. Due consideration is given to the internals within the separator. The modelling code used for this zone is the HYD-3D package.

This model was named FLOSS (FLOW Simulator for Separators) and the simulation may be performed in 2 or 3 dimensions. Comparison of the experimental data (Figure 2.22) with the theoretical is said to yield "fair to good" agreement although visual inspection shows poor agreement for residence times.

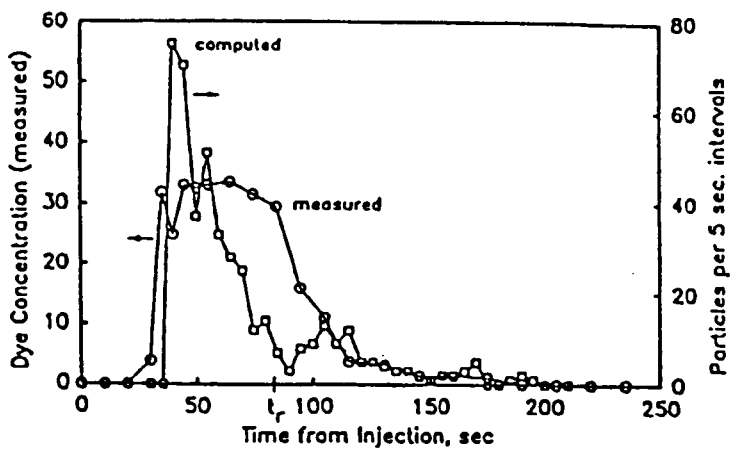


Figure 2.22: Model Prediction of Residence Time Distribution and Experimental Data.

The model was then applied to an actual separator, namely a primary separator from the Gullfaks A oil field. This 3.5m diameter, 16m long vessel had experienced operational difficulties due to changes in the oil field. The difficulties are listed below:

- i) Increased liquid flow rate through separator.
- ii) Water level control failed when amount of water in process fluid increased.
- iii) Formation of emulsions within separator.
- iv) Sand accumulation.
- v) Rising water cut in oil out of separator.

The model was run to simulate the separator at a range of liquid flow rates. At high liquid flows, it was seen that the magnitude of the velocity of the eddy currents increased around the vapour flowstreamers and it was this excessive turbulence which was reducing separator efficiency.

A retrofit was performed on the separator following the modelling. The sand removal system and liquid level control was redesigned and the vapour flowstreamers were cut so that they did not extend into the liquid pool. This removed the problem of eddies and the separator's performance improved greatly.

Two rigs were built by Wilkinson and Waldie (1994) in order to assist development of the CFD model. The first model was a two dimensional rectangular acrylic section measuring 0.875 m long by 0.23 m wide with a fill depth of 0.25 m. The model was run at 3 different flows of water and oil was added at a T junction upstream of the inlet up to a concentration of 0.1% vol. The velocity profile was obtained by Phase Doppler Anemometry (PDA) and it was the restriction of this method that prevented the use of higher concentrations of oil in the model. The analysis provided vertical and horizontal velocity components and individual drop diameters.

The second rig was a three dimensional cylindrical model of 3.77 m length and 1 m diameter. Liquid fill depth was about 50% and the separator was run at 2 different liquid flow rates each for 3 outlet flow ratios of oil (overflow) and water (underflow). Laser Doppler Anemometry (LDA) was used to calculate the horizontal vertical component at six different points to give six horizontal profiles at six distances along the separator.

The model of Wilkinson and Waldie was based on the FLUENT CFD package and the flow of the liquid phases was modelled along the entire length of the separator. The computational grid was set to be finer at the inlet and outlet zones due to the rapid changes in these areas.

Comparison with the experimental data obtained from the two rigs showed good agreement for the smaller two dimensional separator. Both showed a pronounced recirculation loop, presumably promoted by the downward facing slot used for injection of the feed. However, there is considerable discrepancy for the larger model. Reynolds number analysis showed the flow to be in the transition region so the difference could be due to the inability of FLUENT to model unstable flows, too large a computational grid or a poor representation of weir plate. Improvements suggested were use of body fitted co-ordinates within the package or more computational cells.

The problems with CFD were due to limitations of the packages and the experimental difficulties with the laser techniques due to the cloudiness of the

oil/water emulsions. The number of assumptions is high. It is has not been possible to obtain data at realistic cuts of oil and water. A simpler transfer function approach which involves tracer experiments for residence time would give data which could be applied more realistically to field separators.

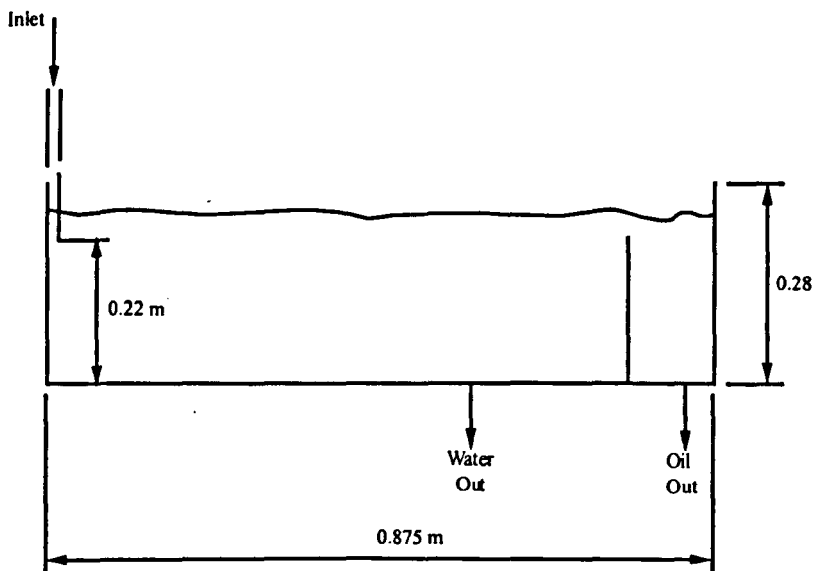


Figure 2.23: Side View of Rectangular Separator

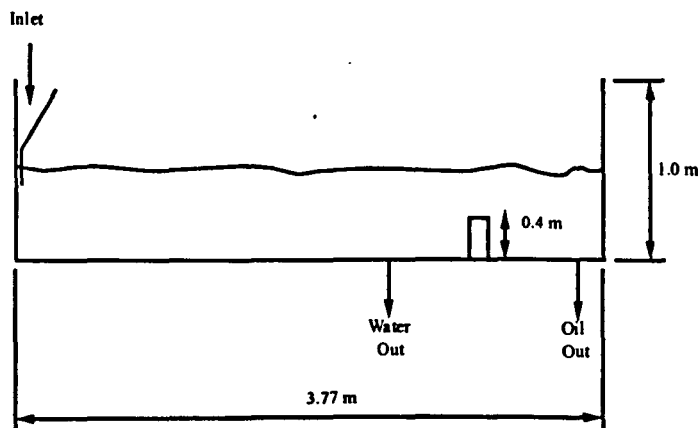


Figure 2.24: Side View of Cylindrical Separator.

2.7 SUMMARY

This literature review has shown that existing design methods are somewhat simplistic and produce conservative designs, particularly with the emergence of new

performance enhancing internals. Industrial measurements of Residence Time Distribution and interface height are restricted to limited process conditions and there is scope to measure these parameters in an experimental facility which will give greater flexibility for changing flow rates and internal configurations. Parameters from an Residence Time Distribution model could then be correlated with separation efficiency.

The choice of modelling technique is between Laplace Transforms and CFD. CFD has been found to be a useful tool for the modelling of simple multiphase flows but the modelling of complex and heterogeneous systems, such as a primary separator, is at a very early stage. Most of the methods that exist are limited to low concentrations of the dispersed phase, or require very detailed information of interfacial characteristics. The modelling which has been performed to date for test separators has several limitations and some discrepancies have arisen. The available information about the fluid dynamics inside the vessel is insufficient in order to check the validity of the assumptions of the two-phase CFD model. In order to develop a better understanding, the best procedure is to produce simple models using transfer functions which can be modified and improved as knowledge of the processes occurring within the separator increases. Eventually, once a knowledge base has been developed, CFD modelling could be applied in the future.

Chapter 3

EXPERIMENTAL EQUIPMENT

3.1 INTRODUCTION

A liquid-liquid flow facility was used for the experimental work described in this study. This had been used previously by Azzopardi *et al.* (1999) and James *et al.* (1999) to measure drop size distributions upstream and downstream of fittings such as bends and a ball valve. Three different test sections were used on this rig. Vertical and horizontal pipe sections were used for the measurement of flow pattern and drop sizes in dispersed pipe flow. A pilot scale liquid-liquid separator vessel was also installed and Residence Time Distributions were obtained. This vessel was designed so that it could be equipped easily with different types of internal baffle plates.

The other major piece of equipment used in this study was a small test cell. This was devised to allow simultaneous measurement of glass beads suspended in water by the instrumentation employed in this study and other techniques which were deployed to test the instrumentation.

3.2 LIQUID-LIQUID FLOW FACILITY

The purpose of this facility was to provide a supply of an organic phase and an aqueous phase. These were mixed in the test sections. For the drop size measurements, the liquids used were odourless kerosene and aqueous potassium carbonate solution. For the pilot scale separator experiments, the potassium carbonate solution was replaced by deionised water. A clean aqueous phase was

required for the Residence Time Distribution measurement technique used. The physical properties of the liquids used are listed in Table 3.1 below and the determination of these variables are described in Appendix A1.

Table 3.1: Physical Properties of Liquids

	Kerosene	Potassium Carbonate Solution	Deionised Water
Density, @ 22°C (kg/s)	797	1166	998
Viscosity @ 22°C (kg/ms)	0.0018	0.0016	0.001
Interfacial Tension @ 22°C (N/m)		0.01	0.01

The liquid-liquid flow facility is shown schematically on Figure 3.1. The liquids are stored in separate storage tanks. The kerosene is stored in two tanks of volume 4.5 m³ each while the aqueous phase has only one tank of the same volume. The total inventory of liquid in the system is of the order of 7500 litres of kerosene and 5500 litres of aqueous phase.

The two liquids were pumped separately from their respective storage tanks and their flow rates are metered by orifice plates. The pressure drop across the plates is measured by electronic pressure transducers which are calibrated to convert the voltage generated directly into a pressure drop in mbar. The pressure drops are displayed by digital meters attached to the test section inlet. The orifice meters were designed to the BS 1042 standard and calibrated by use of another orifice plate located at the maximum distance downstream from the liquid inlets. This test was performed because the length of the inlet piping before the flow meters was shorter

than was required by the British Standard. However this was found not to pose a problem.

After passing through the test section, the liquids enter a large separator vessel. This vertical cylindrical vessel of height 2.5m and diameter 2.4m, was equipped with 38 Knitmesh™ coalescer cartridges. These cartridges are filled with very fine fibreglass wool that acts as a coalescing medium for the tiny droplets of dispersed phase. After passing through the separator, the liquids return by gravity to the storage tanks. The separator allows continuous operation of the rig and it was reasonably effective in separating the phases. However, with extended operation, there was a build up of haze but this settled out when operation was stopped.

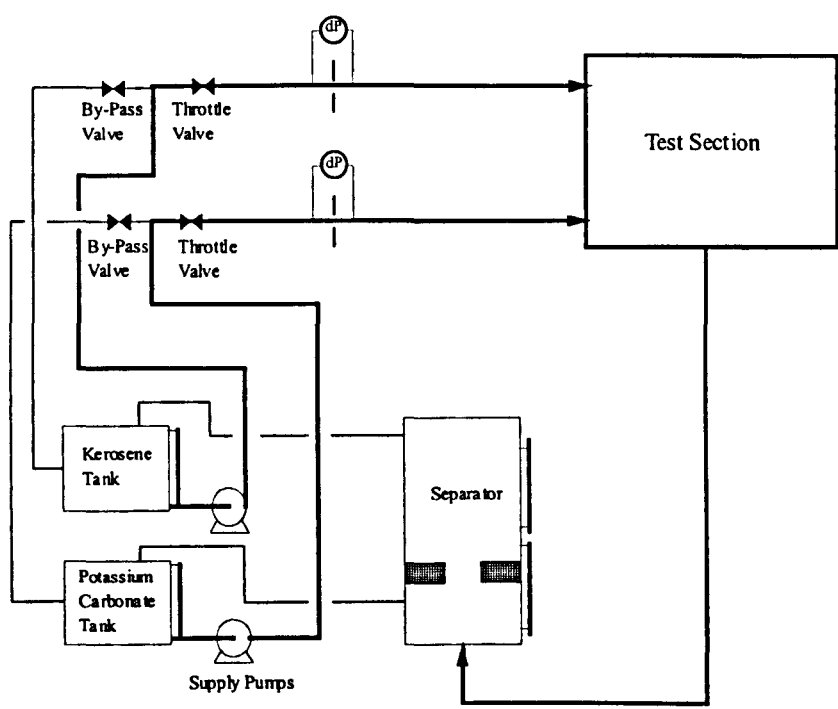


Figure 3.1: Schematic of Liquid-Liquid Pipe Flow Rig

3.2.1 Pipe Test Sections

Vertical and horizontal pipe flow sections of diameter 0.063m were used for drop size and flow pattern measurement. At the inlet of the test sections a specially designed mixer was used to combine the phases. The aqueous phase was introduced onto the wall of the pipe and the kerosene phase entered through the centre. This arrangement was chosen to ensure that any dispersion created was caused by the hydrodynamics of the flow rather than any mixing effects.

Measurement of drop size or flow pattern was made 4m downstream of the test section for vertical flow and 4.5m for horizontal. The total length of the test sections was limited by the dimensions of the laboratory. Flow patterns were observed by high speed videography through a clear acrylic resin section of pipe. Specific test sections for the drop size instrumentation were designed and manufactured from clear acrylic resin or PVC.

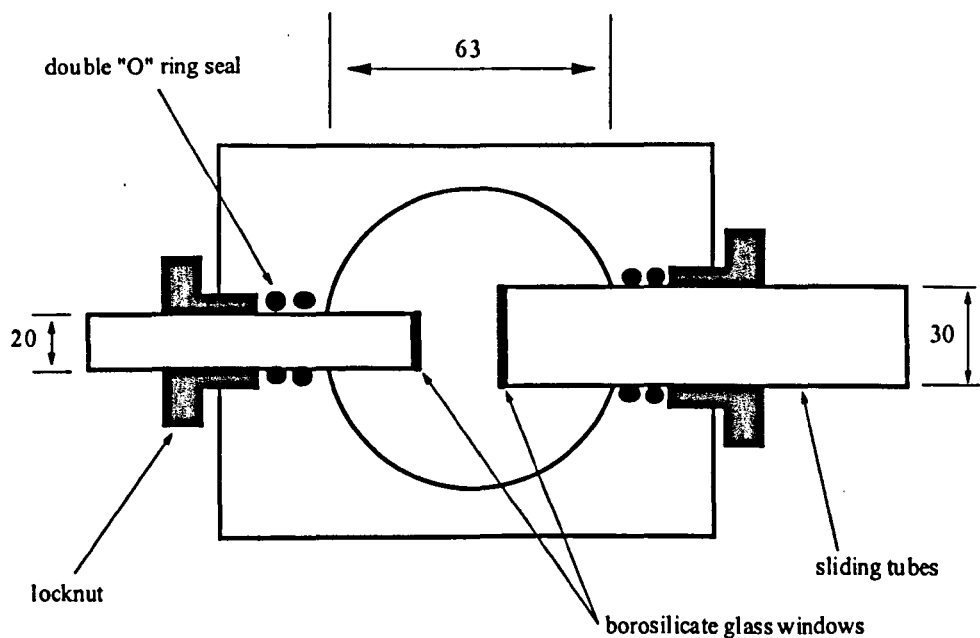


Figure 3.2: Cross section of Malvern pipe test section.

The test section for the laser diffraction technique (Malvern 2600 instrument) consisted of 2 sliding tubes with optical quality glass discs inserted in the ends as shown in Figure 3.2. All dimensions on all the Figures are in millimetres. This allowed the path of the Malvern laser through the two-phase mixture to be shortened, and hence the obscuration of the laser beam by the liquid droplets could be reduced.

The test section for the laser backscatter technique (Par-Tec 300C), was designed to allow the insertion of the Par-Tec probe at 45° to the flow, which was necessary in order to minimise eddies near to the probe window which could cause the particles to streamline past the window without being detected (Figure 3.3). This configuration was also designed to minimise breakage at the point of measurement. Any disturbance to the flow was downstream of the probe. The distance at which the probe was inserted into the pipe was maintained by a series of plastic spacers. Both sections utilised o-ring seals to prevent leakage of the fluids.

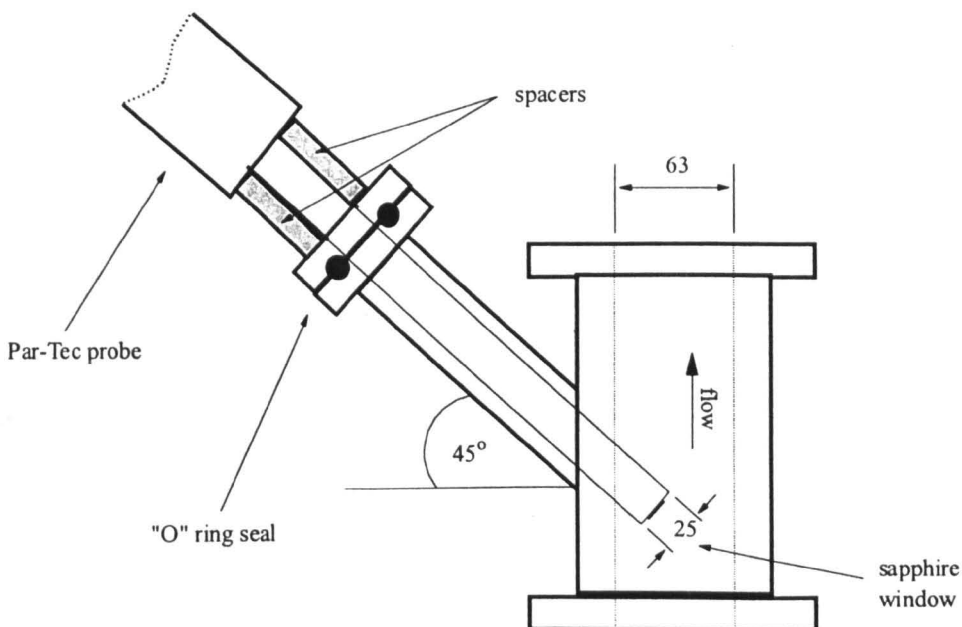


Figure 3.3: Cross section of Par-Tec pipe test section.

3.2.2 Pilot Scale Separator Vessel

The separator vessel was designed as a 1/5th scale model of a 3 phase separator used on the Ula production platform in the North Sea by British Petroleum and installed in the liquid-liquid facility described above. In view of the investigations on the disengagement of the phases, the vessel was made slightly longer ($L/D=4$). The vessel was manufactured from clear uPVC and a perforated baffle, as used on some field separators, was installed at the inlet to attempt to smooth the flow through the vessel. Two sizes of perforated baffle were used, either 20mm perforations on a 30mm pitch or 50 mm perforations on a 75mm triangular pitch. The use of a constant ratio of pitch divided by diameter, means that the open area is kept constant at 40%. A nitrogen purge was installed at the top of the vessel to expel any kerosene vapour present and hence reduce any flammability risk. Two different weirs of height 0.22m and 0.3m were used in order to investigate the effects of changing interface position and weir height.

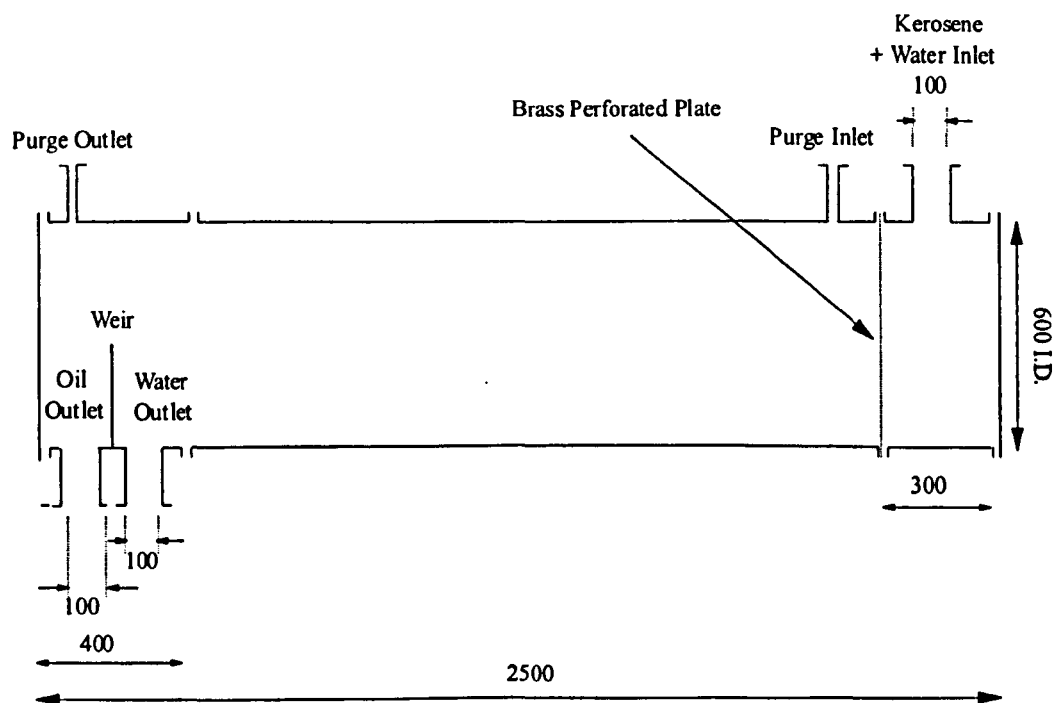


Figure 3.4: Diagram of Separator Vessel

Control of the liquid-liquid interface was accomplished by a 0.1m butterfly valve on the water outlet with fine adjustment of the interface being achieved by a 0.025m bypass line equipped with a ball valve. A similar arrangement was employed on the organic outlet line.

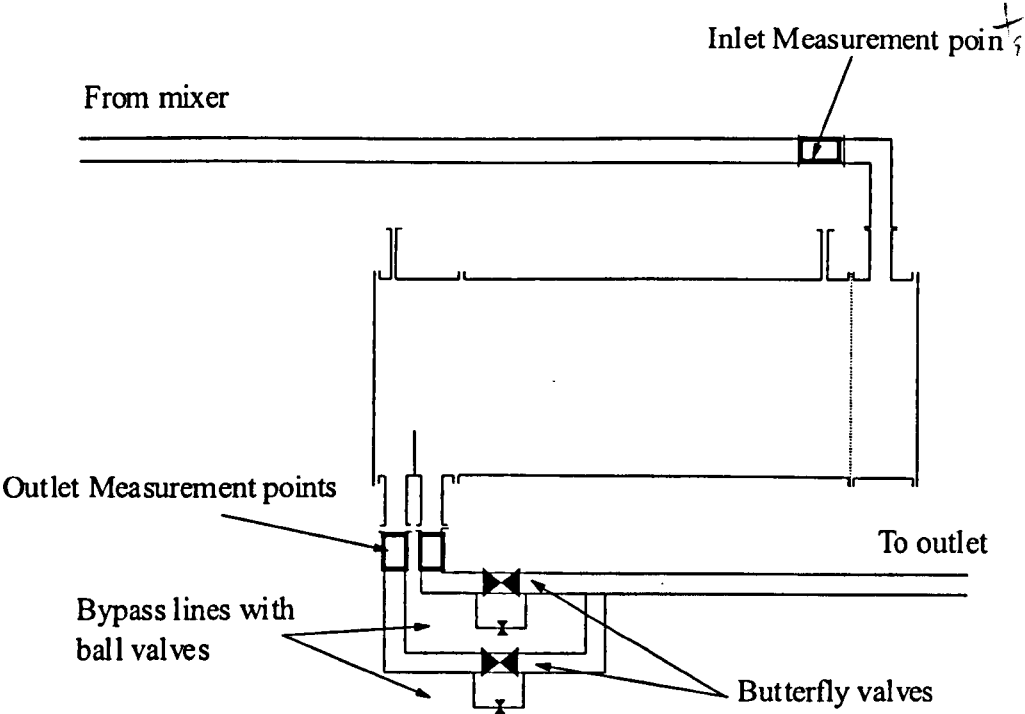


Figure 3.5: Control Scheme.

Sampling points were provided as close to the inlet and outlets as possible in order to minimise the effects of sample tubing on the true Residence Time Distribution of the vessel. A colorimetric tracer technique described in 3.3 below was used in order to obtain the results.

To investigate the effect of baffling within the vessel, two different styles of baffles were constructed. Side baffles, as shown in Figure 3.6, were employed to simulate

dead or quiescent zones within the separator. A dip baffle, which extended to 0.2m from the bottom of the vessel (Figure 3.7), was also constructed to simulate the effect of internals designed for the gas phase interfering with the liquid. This problem can occur quite often on real separator vessels and these baffles act to reduce the flow area available to the liquid phase. The liquid is therefore forced under the baffle and accelerates.

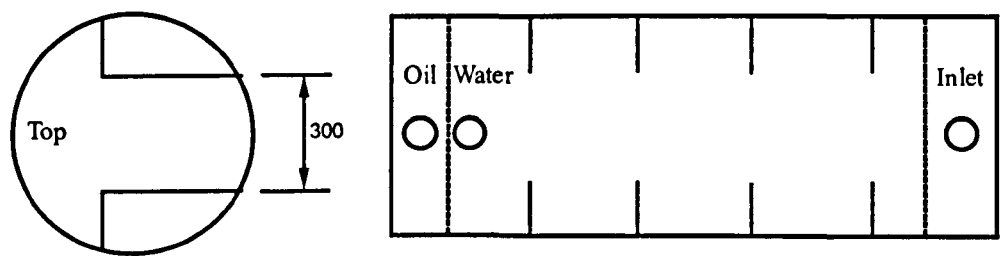


Figure 3.6: Plan View of Side Baffles

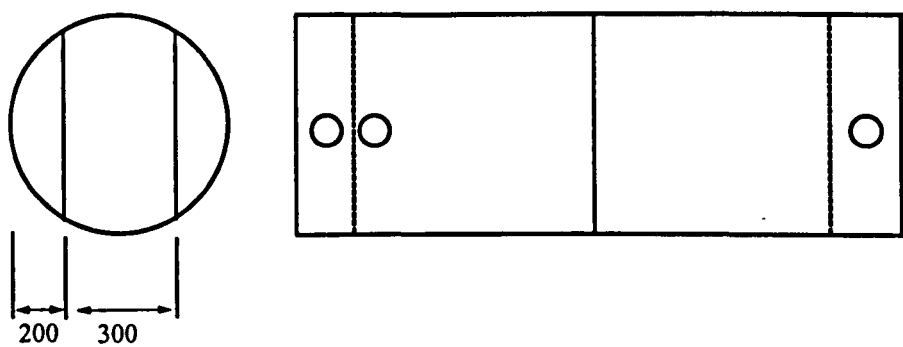


Figure 3.7: Plan View of Dip Baffle

3.3 RESIDENCE TIME DISTRIBUTION TRACER TECHNIQUE.

In order to obtain Residence Time Distribution profiles of both organic and aqueous phases within the separator, a concentrated dye soluble in either the oil or water phase was injected by compressed air into the inlet line from a small 250 ml vessel mounted just upstream of the inlet measurement point. The outlet concentration of the dye was monitored on line by a Jenway 6300 spectrophotometer. This piece of equipment was fitted with an RS-232 interface which allowed connection to a standard IBM compatible PC. The outlet concentration was recorded every second by the PC and the data were then imported into a spreadsheet for interpretation.

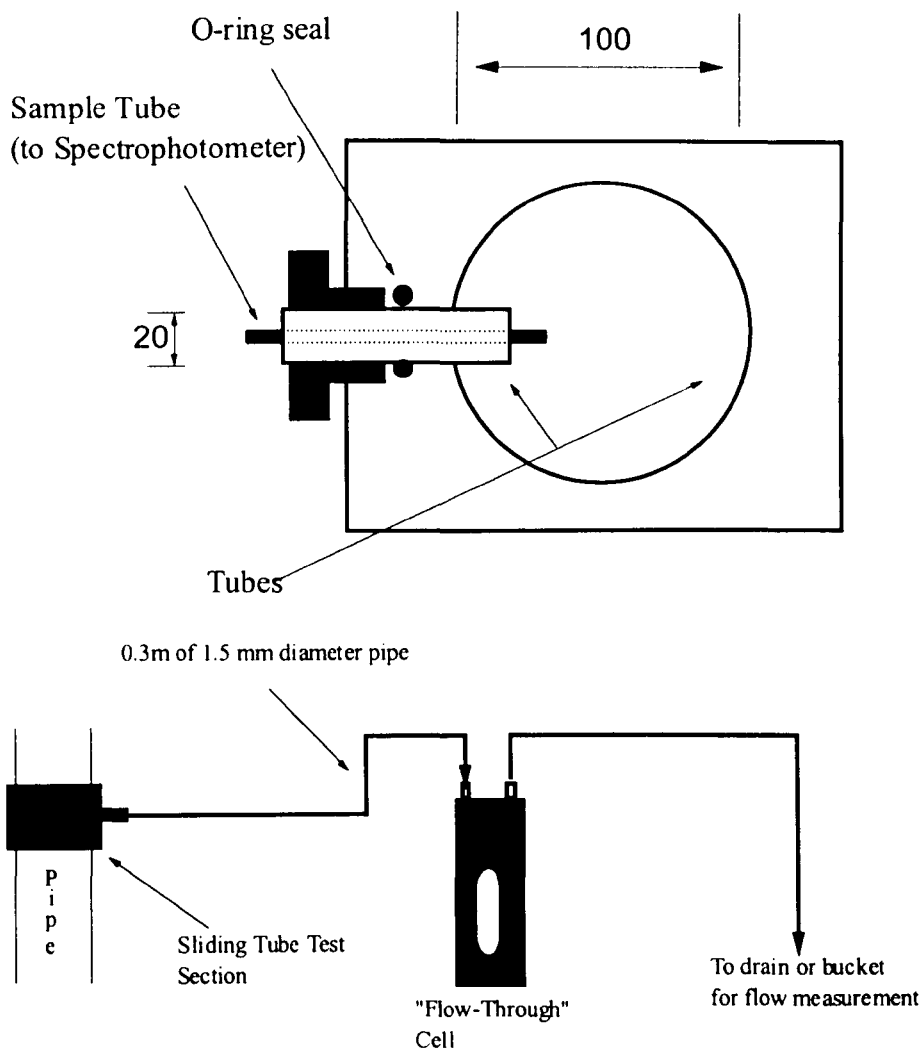


Figure 3.8: Schematic of Sampling System and Sliding Tube Test Section

The sampling system itself is shown on Figure 3.8 and comprised a test section equipped with sliding tubes through which sample tubes of different configurations could be easily attached. The length of tubing between the test section and the measurement point within the spectrophotometer was kept to a minimum in order to keep the instrument as responsive as possible and to minimise any Taylor type dispersion which may have occurred in the piping. The piping was of 1.6 mm bore and was connected in the instrument to a “flow-through” cell of volume 0.5 cm^3 and path length of 10mm. Two separate flow cells were used, one for each phase, in order to minimise any contamination effects. Any liquid exiting the sampling system was collected in a bucket and either returned to the flow loop or disposed of.

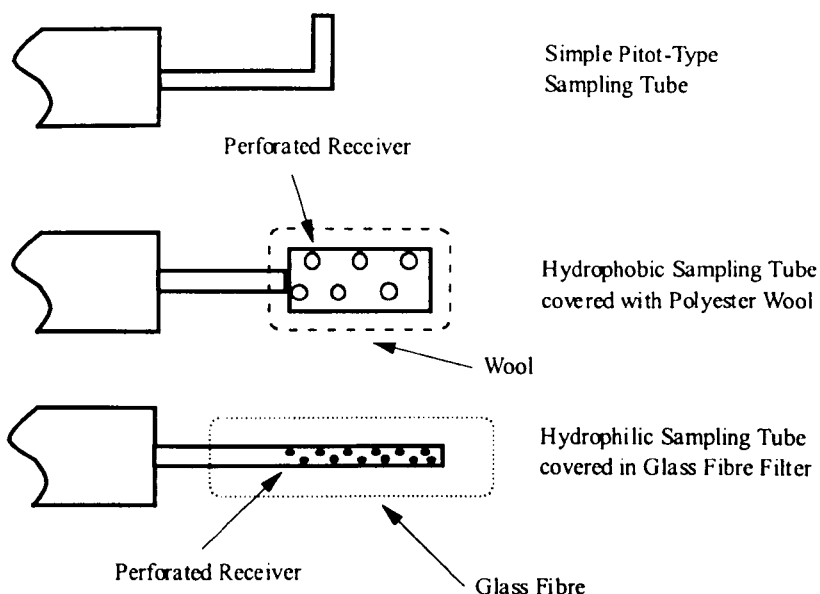


Figure 3.9: Diagram of Sample Tubes used.

A problem found with the colorimetric technique on initial trials was that it was impossible to obtain samples of water or oil from the outlets which were not contaminated with small amounts of the other phase, if a simple pitot-type sampling

tube was used. These droplets tended to settle in the flow cells and upset the measurements. To try to overcome this problem, two different types of sampling tube were developed which were wrapped in either hydrophilic or hydrophobic material as shown in Figure 3.9. The hydrophilic material used was glass-fibre filter paper and the hydrophobic material was polyester wool. These modified sample tubes successfully reduced the problem, although they were unable to filter out the haze caused by very fine particles that can occur in liquid-liquid systems. The tubes were designed to have as low a pressure drop as possible by use of perforated tube underneath the materials, but nevertheless the flow rate through the cells was monitored very carefully in order to ensure that it was kept above $0.5 \text{ cm}^3/\text{s}$. This flow rate would refresh the cell sufficiently to allow readings to be taken every second.

In general, the performance of the sample tubes was satisfactory, although it was found that a greater thickness of hydrophilic material was required than for hydrophobic. For this reason the diameters of the perforated receivers were different in order to keep the total diameter of the tube below 20mm. If this dimension were exceeded, the tube would no longer fit in the test section.

The visible light frequency responses of the dyes used were obtained using a scanning spectrophotometer in order to choose a wavelength which would give greatest sensitivity when performing measurements. This information was then used to set the scanning frequency of the Jenway instrument. The bandwidth of the instrument was 10 nm so resolution the scanning frequency was very good. Several

different dyes were tested as possible tracers, the selection criteria being solubility in one phase only and not to be staining to any of the materials of construction present in the rig. Fluorescein Sodium was chosen as the dye for the aqueous phase and Biebrich Scarlet R was chosen for the oil phase. Optimum absorption frequencies were found to be 450nm and 515nm respectively. Details of the testing and calibration procedures may be found in Section 6.2.2.

3.4 TEST CELL FOR SIMULTANEOUS DROP SIZE MEASUREMENT

This test cell was employed to obtain simultaneous measurement of a sample of particles by two particle sizing instruments. The cell was constructed from clear acrylic resin, with glass windows inserted on two opposite sides.

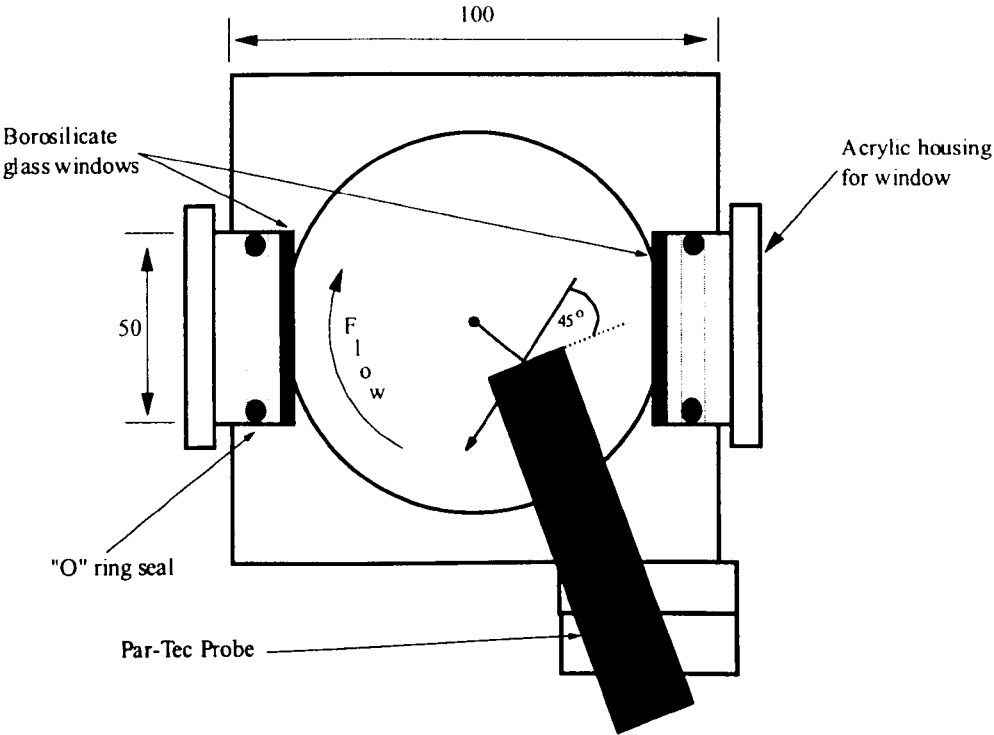


Figure 3.10: Plan view of Test Cell

Both the Malvern instrument and a Phase Doppler Anemometer could be used with the cell by aligning the laser beams through these windows. An angled hole was

drilled through a third side to allow insertion of the Par-Tec probe. The angle of the hole was chosen so the radial component of the flow within the cell intercepts the centre of the probe window at 45° . This is necessary to prevent particles streamlining around the probe and not being detected. The cell was used with a sieve cut of glass beads suspended in water by use of a magnetic stirrer. The cell was sealed during measurement to prevent air bubbles being introduced into the liquid and affecting the results obtained.

Chapter 4

DROP SIZES AND FLOW PATTERNS IN LIQUID-LIQUID PIPE FLOW

4.1 INTRODUCTION

Liquid-liquid two-phase flows occur widely in the chemical, oil and food industries. As well as being useful for studying the effects of phase separation as described in Chapter 2, the drop size distribution has important effects upon reaction rate in continuous or stirred batch reactions. There are also significant implications for pressure drop and design of industrial equipment, such as processing facilities downstream of pipelines from oil wells. The effects on pressure drop are particularly important because the interaction between the two liquid phases in a pipeline can create a dispersion of one phase in the other. This dispersion can have a viscosity higher than either liquid. Hence more pumping power is required than would be necessary for a single phase. In order to pump and process these mixtures efficiently, knowledge of drop formation and the nature of dispersions is required.

Both Malvern 2600 and Par-Tec 300C instruments have been used to obtain drop size distributions for liquid-liquid mixtures on the pipe test sections described in Section 3.2.1. Measurements have been performed for both horizontal flow and vertical upflow. Video footage of the flows was obtained for both geometries and these images were used for determination of flow patterns. An attempt was also made to determine drop size distributions from these video images.

It is known that there can be significant discrepancy between results obtained from different drop size measurement techniques. Kurban *et al.* (1995) reported Sauter mean diameters of 678 μm for a photographic technique and 206 μm for a conductivity technique at the same flow conditions. In order to determine comparability between instruments and to be able to interpret features of the results which may be artefacts of the measurement techniques, both Par-Tec and Malvern instruments were used to measure simultaneously samples of glass beads suspended in water. The test cell used to perform this task is described in Section 3.4. Drop sizes in the liquid-liquid pipe flow facility were then determined by the same instruments, and also by high speed photography.

This chapter presents, compares and contrasts the results obtained from each technique and attempts to provide a greater understanding of the nature of immiscible liquid-liquid flow.

4.2 EXPERIMENTAL DETAILS

4.2.1 Converting Chord Distributions to Diameter Distributions

The Par-Tec 300C instrument actually measures a distribution of chords made by the laser beam crossing the drops. These must be converted to a diameter size distribution. Before presenting the data obtained, a method which was devised to make this conversion is discussed. Herringe and Davis (1976) and Clark and Turton (1988) have presented probabilistic techniques to solve a similar problem which arises with the use of needle conductance probes, but the output is very dependent upon the shape of the particles and can suffer problems with very irregular distributions. Hobbel *et al.* (1991) described a method of calculating diameter

distributions from chord distributions assuming random sphere cuts. This is basically a “peeling” method where the largest chord size is assumed to be the largest diameter, and the chord distribution from this diameter is subtracted from the total chord size distribution. This is repeated for successively smaller diameters. As noted by Hobbel *et al.* this method is sensitive to “noise” in the population of the largest sizes. Most recently, Liu *et al.* (1998) have considered the probability relationships in obtaining representative overall bubble size distributions from local bubble chord measurements in heterogeneous bubbling systems, such as fluidised beds.

The total sample size is an important parameter to ensure that what is measured is representative of the entire system. It is important to have a statistically significant sample size when determining the size distribution and this in turn depends upon the breadth of droplet size in the distribution. Data have been presented from photographic measurement techniques where the sample size is of the order of 250-500 particles, Karabelas (1978). This is due to the rather tedious analysis procedures of such techniques but this is a very small sample when compared to samples of the order of thousands that can be obtained very quickly from the Malvern and the Par-Tec instrument.

To create an ideal chord size distribution from a known particle diameter distribution it is necessary to make some assumptions. For spherical particles in a dilute system, where there are no interactions between particles, there is an even probability of taking a cut through any part of the projected area of the sphere. In this case, if we

consider a chord at eccentricity y , of thickness dy (Figure 4.1) then the probability, $P\{y, y + dy\}$, of cutting a sphere in the band of thickness dy is

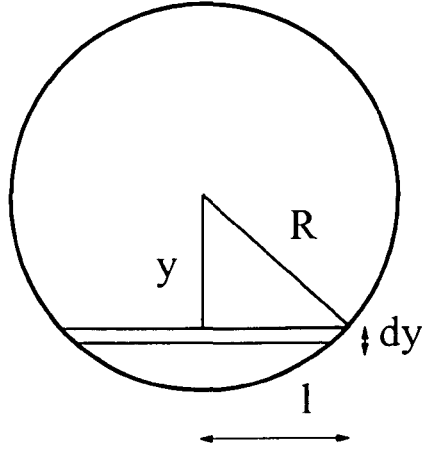


Figure 4.1: Nomenclature for cutting a sphere

$$P\{y, y + dy\} = \frac{2dy}{2R} = \frac{dy}{R} \quad (4.1)$$

Also, from Pythagoras:

$$y = \sqrt{R^2 - l^2} \quad (4.2)$$

Differentiating the above with respect to l yields (dropping the negative sign since a negative probability is meaningless):

$$dy = \frac{l dl}{\sqrt{R^2 - l^2}} \quad (4.3)$$

Hence, substituting equation 4.3 in Equation 4.1 we obtain:

$$P\{l, l + dl\} = \frac{l dl}{R \sqrt{R^2 - l^2}} \quad (4.4)$$

The probability, $P\{l_1, l_2\}$ of a detected chord being between sizes l_1 and l_2 is therefore

$$P\{l_1, l_2\} = \int_{l_1}^{l_2} \frac{l dl}{R \sqrt{R^2 - l^2}} \quad (4.5)$$

Integrating the above expression gives the discrete probability as:

$$P\{l_1, l_2\} = \frac{\sqrt{R^2 - l_1^2} - \sqrt{R^2 - l_2^2}}{R} \quad (4.6)$$

This equation can be rearranged to give a discretised distribution for a sphere of diameter D with chord lengths, x .

Now $x = 2l$ and $D = 2R$, Hence

$$P\{x_1, x_2\} = \frac{\sqrt{D^2 - x_1^2} - \sqrt{D^2 - x_2^2}}{D} \quad (4.7)$$

Where $P\{x_1, x_2\}$ is the probability of obtaining a chord size between x_1 and x_2 .

Hence for a known diameter distribution, we can calculate a range of chord lengths for each diameter band using Equation 4.7. Since this is a linear transform, the total probability distribution of a polydisperse system is the number weighted sum of the probability distributions of the component diameters. A Galerkin finite element method, Zienkiewicz and Taylor (1997), has been used to solve simultaneously the system of equations developed from Equation 4.7, which relates the chord data to the diameter distribution. This method also addresses cumulative error problems associated with the “peeling off” method of Hobbel *et al.* The full details of this method are discussed in Appendix A2, together with comparisons to a different conversion method and some “pseudo-experimental” data. It was found that the finite element method was suitable for conversion of the chord data to diameter data, but that caution was necessary if discontinuities in the distributions were present. These cause instabilities in the solution. This method was applied to all the Par-Tec results.

4.2.2 Tests on Glass Beads

Both Par-Tec and Malvern instruments were installed on a test cell and used to measure simultaneously the size distribution of samples of glass beads. The glass beads were also sized independently by image analysis of photographs as described in Appendix A3.

It was found that there was reasonable agreement for the instruments used with the tests performed. As can be seen in Figure 4.2 for a nominal 90-106 μm sample, the laser based techniques both produce similar results. However, the drop diameter distribution from the Par-Tec, as converted by the method shown in Section 4.2.2 below is noticeably wider, particularly for larger particles. This can be explained by the large size bands at the large end of the measurement scale of the instrument. The mean of the distribution obtained from image analysis is slightly larger, but the width is less. The smaller width is most likely due to the smaller sample size of beads measured using this technique. However, it should be noted that this sample of glass beads contains a much narrower distribution of sizes than was observed in the pipe flow.

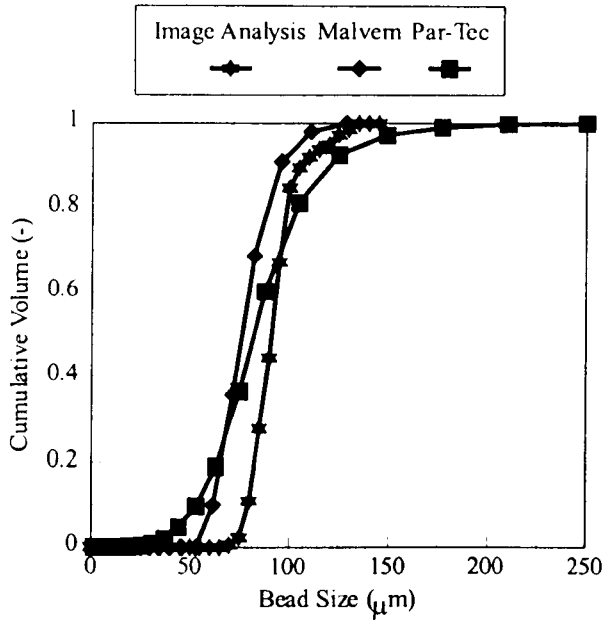


Figure 4.2: Instrument comparisons nominal 90-106 μm beads

4.2.3 Experiments Performed and Test Conditions on Pipe Flow Rig

The Malvern 2600 and Par-Tec 300C instruments were used on the liquid liquid pipe flow facility for the flow rates given in Table 4.1. It proved necessary to choose 2 different flow ranges because use of the Malvern is restricted to low concentrations of the dispersed phase. This is due to errors caused by further scattering of the light already scattered by the drops. Measurements were made at the central axis of the pipe and also 7mm either side. In the case of horizontal flow, the measurements were made 7mm above and below the axis.

The Malvern 2600 instrument gives drop diameter directly and to allow comparisons, the chord data from the Par-Tec instrument was converted to a diameter distribution by the mathematical technique in Section 4.2.1 above. Video footage of the flows was obtained using a Kodak EKTAPRO camera, and drop size was measured for the

vertical geometry at the low concentration flow rates using the method discussed in Appendix A3.

The flow patterns obtained from the video footage were classified according to the work of Brauner and Moalem Maron (1992a, 1992b)

Table 4.1: Flow conditions

Flow conditions for back-scatter technique (Set 1)			Flow conditions for all techniques upflow only (Set 2)		
Kerosene superficial velocity v_{so} (m/s)	Aqueous phase superficial velocity v_{sw} (m/s)	Mixture superficial velocity v_m (m/s)	Kerosene superficial velocity v_{so} (m/s)	Aqueous phase superficial velocity v_{sw} (m/s)	Mixture superficial velocity v_m (m/s)
0.837	0.158	0.995			
0.837	0.317	1.154			
0.837	0.488	1.325			
0.837	0.614	1.451			
1.49	0.158	1.648	0.837	0.029	0.866
1.49	0.317	1.807	1.49	0.029	1.519
1.49	0.488	1.978	1.837	0.029	1.902
1.49	0.614	2.104	2.393	0.029	2.422
2.393	0.158	2.551			
2.393	0.317	2.710			
2.393	0.488	2.881			
2.393	0.614	3.007			

4.2.4 Experimental Error

The errors in the drop size measurements are difficult to measure quantitatively but are discussed qualitatively in Section 4.3.1 below. Errors in the flow rate measurements can be obtained from the accuracy of the measurement of the transducers and the results are tabulated below.

Table 4.2: Error in Flow Rate Measurements

Kerosene Flow (kg/s)	Uncertainty (%)	Aqueous Solution Flow (kg/s)	Uncertainty (%)
2.11	17	0.105	33
3.76	5.2	0.6	33
4.73	3.3	1.17	12.5
6.04	2.0	1.80	5.3
		2.27	3.3

The errors in the orifice plate readings at the low flow rates are large but because the steps in flow rate are also large there is no overlap. The orifice plate size was changed in the later work to improve the accuracy of the flow readings.

4.3 RESULTS

The tables below present the Sauter Mean Diameter values obtained by the different measurement techniques on the pipe flow test sections.

Table 4.3: Sauter Mean Diameter values from Par-Tec on vertical section

u_{mix} (m/s)	Position. 1 (μm)	Pos. 2 (centre) (μm)	Position 3 (μm)
0.995	590.4	490.0	570.3
1.154	550.2	485.1	584.6
1.325	509.5	496.7	511.2
1.451	491.5	465.6	426.2
1.648	462.6	447.8	445.1
1.807	441.4	410.5	440.7
1.978	406.0	385.6	450.4
2.104	404.6	404.7	428.1
2.551	399.2	426.2	407.9
2.710	423.0	428.1	424.2
2.881	414.6	421.4	410.9
3.007	417.2	418.4	395.1

Table 4.4: Sauter Mean Diameter values from Par-Tec on horizontal section

u_{mix} (m/s)	Pos. 1 (low) (μm)	Pos. 2 (centre) (μm)	Pos. 3 (high) (μm)
0.995	364.5	308.7	57.6
1.154	473.7	247.1	75.3
1.325	446.9	399.4	141.3
1.451	172.9	430.5	268.4
1.648	505.5	371.8	275.8
1.807	403.6	396.5	351.8
1.978	394.2	382.9	332.8
2.104	369.8	373.9	400.7
2.551	305.7	328.8	355.9
2.710	309.3	319.2	311.4
2.881	325.4	318.9	303.0
3.007	315.4	319.1	303.7

Table 4.5: Sauter Mean Diameter values from Malvern 2600 on vertical section

u_{mix} (m/s)	Pos. 1 (μm)	Pos. 2 (μm)	Pos. 3 (μm)	Pos. 4 (μm)	Pos. 5 (μm)
0.866	251.6	217.6	373.2	257.8	392.7
1.519	272.4	242.1	170.5	226.0	254.6
1.902	258.6	243.0	162.0	168.9	201.0
2.422	271.2	194.5	172.8	160.1	191.3

Table 4.6: Sauter Mean Diameter values from Image Analysis on vertical section

u_{mix} (m/s)	Equivalent D_{32} (μm)
0.866	5117
1.519	4429
1.902	3939
2.422	3252

4.4 DISCUSSION

The drop size distributions obtained were characterised by the Sauter Mean Diameter as defined in Equation 2.26. This is a commonly used parameter in the literature and represents the ratio of particle volume to surface area.

The reproducibility of the backscatter technique is shown in Figure 4.3 below. The figure shows clearly that the repeatability is very good and this was observed at all the flow conditions used.

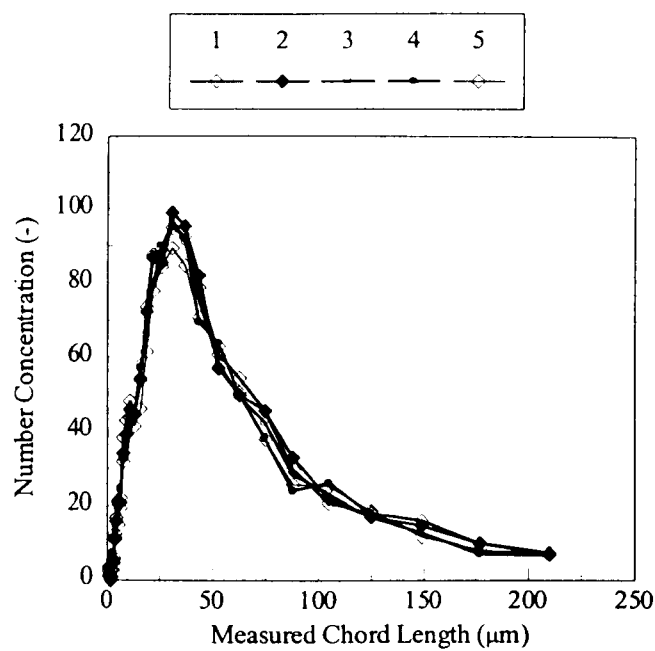


Figure 4.3: Repeatability of Par-Tec 300C instrument at a mixture velocity of 2.88 m/s

Repeatability of the Malvern instrument was also good but there was some scatter due to the dilute concentration of droplets used.

4.4.1 Drop Size Comparisons

The variation of Sauter mean diameter with different flow geometries and flow rates can be seen in Figures 4.4-4.5. The Par-Tec is seen to give a consistent trend at each

measuring position for the matrix of flow rates used and this gives confidence that the results obtained are a true representation of the system (Figure 4.4a). This figure also shows that at low flow rates, the values of Sauter mean diameter are lower away from the centre line position. This is most likely due to a sharper velocity profile within the pipe at the lowest superficial velocities. The Sauter mean diameter is seen to decrease with mixture velocity and this is to be expected as shear increases with increasing turbulence.

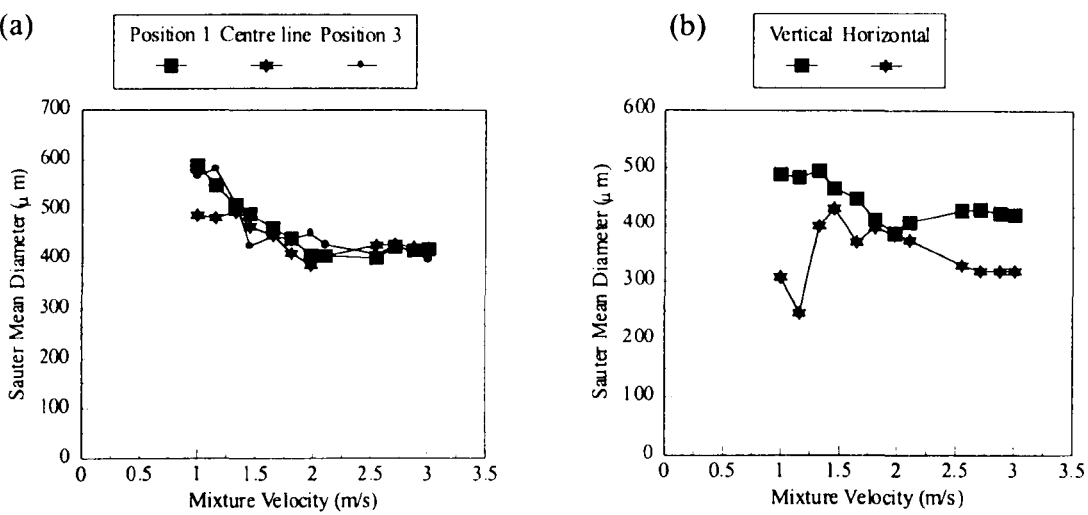


Figure 4.4 Variation of Par-Tec data with Position in Vertical Flow (a) and Geometry (b)

The full set of droplet size distributions and mean diameter values from the liquid-liquid rig experiments are shown in Appendix A4. Figures A4.1-A4.12 illustrate the drop size distributions obtained from the liquid-liquid rig vertical section using the Par-Tec 300C instrument after application of the chord-diameter conversion. It is interesting to note that there is little variation of distribution with measurement position. Where small differences do exist, they are most pronounced at low flow rates. This is in dramatic contrast to the drop size distributions obtained for

horizontal flow (Figures A4.13-A4.24). At low flow rates, the distributions obtained at the low measurement position have a much smaller mean value of particle size than for the other two positions. There is also a difference between middle and high positions. This indicates a definite gradient in particle size and concentration. This can be explained by the stratification of the phases. As the stratified flow pattern breaks down to form dispersed flow at higher flow rates, the results from each position move much closer together, giving similar results to those obtained for the vertical flow conditions.

Comparison of data obtained from the Par-Tec for both geometries shows some discrepancies (Figure 4.4b). The much lower values of Sauter mean diameter for horizontal flow at low flow rates is due to the flow being stratified rather than dispersed at these small mixture velocities. The probe data is therefore not reliable in this region. Flow development is an issue that could explain the poor agreement at higher velocities as in the short lengths of pipe used in these studies, the drop distributions produced are not fully developed.

Figure 4.5 compares the Sauter mean diameter values at the centre line measurement point for both Par-Tec and Malvern for vertical upflow. Good agreement is found at the lowest flow measured but the value from the diffraction technique drops off much more rapidly. This effect was also reported by El-Hamouz and Stewart (1996) who used a Par-Tec M300 and a Malvern 2600 to measure a dispersion of Catenex in water, 1% by volume.

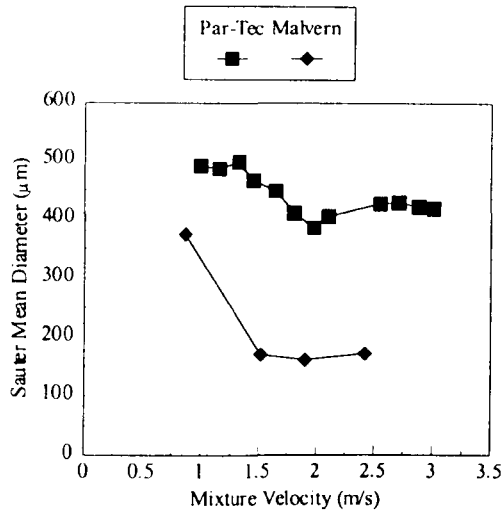


Figure 4.5: Comparing instruments on vertical section

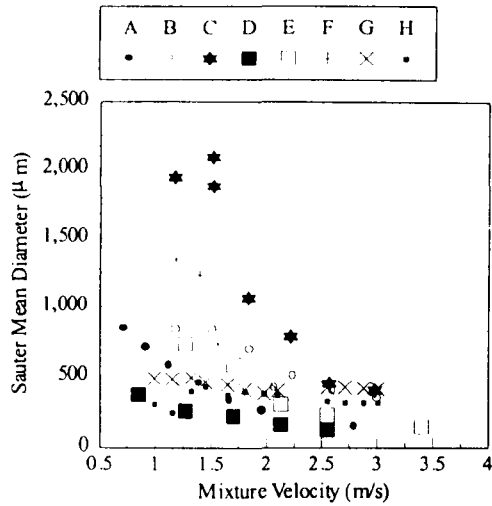


Figure 4.6: Comparing Sauter mean diameter from different workers

Table 4.7: Key to Figure 4.6

Set	Author		Dispersion	Measurement Technique
A	El-Hamouz and Stewart (1996)		o/w	Malvern 2600 and Par-Tec M300
B	Karabelas (w/to) (1978)			Photography of encapsulated sampled drops
C	Karabelas (w/k) (1978)			
D	Kubie & Gardner (water/alcohol) (1977)		w/o and o/w	
E	Kubie & Gardner (water/acetate) (1977)			
F	Kurban <i>et al</i> (1995)		w/o	Photography using borescope plus conductivity probe
G	This Work	Vertical Flow	w/o	Malvern 2600 and Par-Tec 300
H		Horizontal Flow		Image analysis of video footage
I		Vertical Flow		

A difficulty experienced was the different concentration ranges over which the laser instruments can operate. It was found that an insufficient number of drops were detected by the Par-Tec to give a statistically reliable distribution below concentrations of about 5% by volume. A similar problem was also reported by Hobbel *et al* (1991). Conversely, the Malvern can only be applied at very low concentrations (below 3% by volume) due to limitations imposed by the scattering of scattered light by drops as the drops become more closely spaced. This distorts the angular distribution of light scattering and the relationship between the size distribution and the scattered light ceases to follow. To overcome this, 2 separate flow ranges were used so that the concentration was kept in the correct region.

The concentration is an important variable in determining the drop size distribution as well as flow velocity and some correlations for dilute systems are presented in Section 2.2.4.3. The reason for the increase in mean drop size with dispersed phase concentration is that the rate of collision of drops increases greatly. In Figure 4.5, the mean drop sizes are generally less at the lower concentrations. The data were tested against Equation 2.23 using the velocity of the organic phase. The effect of concentration cannot be assessed directly as the presence of so much dispersed phase at the higher concentrations significantly alters the velocity.

Sauter mean diameters obtained from published work are compared with those from the current study on Figure 4.6. There is considerable scatter, but in all cases there is a reduction of Sauter mean diameter with velocity which is as expected. The values also tend to converge somewhat at higher velocities.

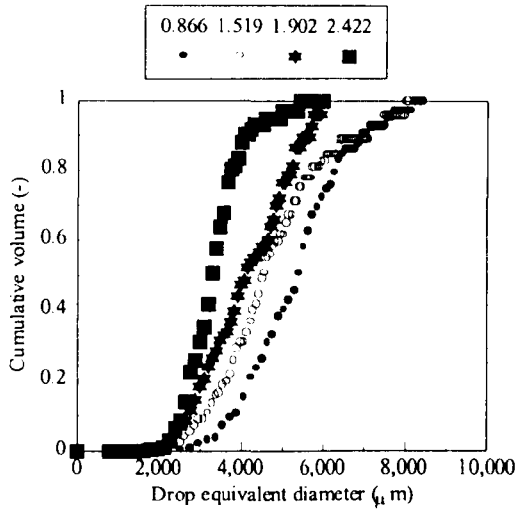


Figure 4.7: Drop size distributions obtained from image analysis at different mixture velocities

The drop sizes from image analysis are much higher than those obtained from the laser based techniques (Figure 4.7). D_{32} ranges from 3.3 to 5.1mm, a factor of 10 greater than the Malvern or Par-Tec results. This can partly be explained by the low concentration of dispersed phase which means that the processes of break-up and coalescence are less frequent, but it is also of interest to note that no droplet below 2 mm was detected. This oversizing has been noted by both Kurban *et al* and Karabelas and can be partly explained by the fact that smaller droplets are likely to have a higher velocity in the pipe and hence will appear out of focus even at high shutter speeds. Additionally the depth of field means that large drops are likely to obscure smaller ones and are more easily detected. The relatively low quality of the video footage also meant that manual tracing of the drop outlines was required, and the human eye favours tracing of the larger drops. The smaller drops are also less likely to be detected due to the low resolution of the scans. The intrusive nature of the Par-Tec and Malvern test sections may also have affected detection of larger drops.

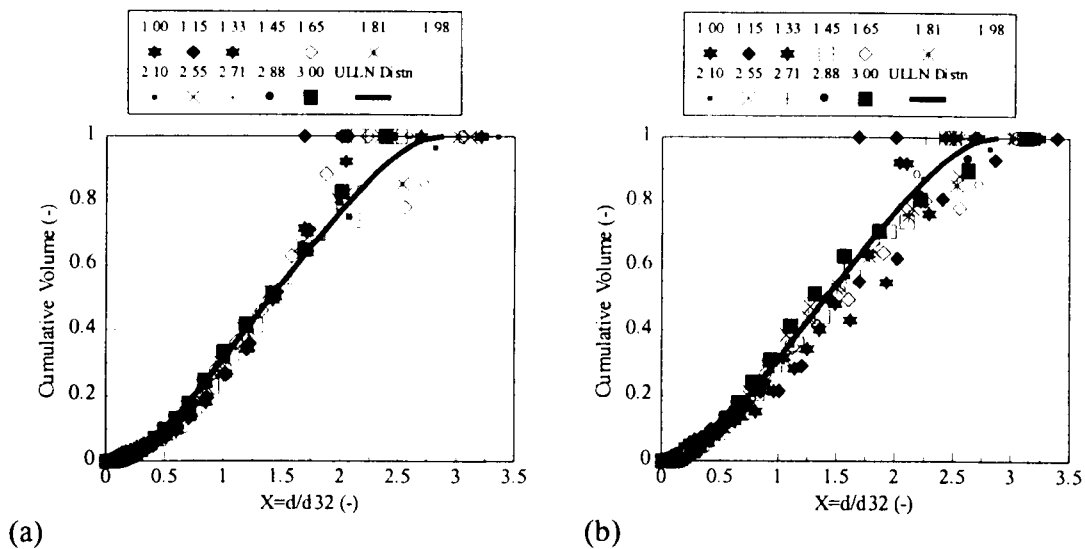


Figure 4.8 Fitting ULLN distribution to (a) vertical and (b) horizontal Par-Tec data

In order to attempt to predict the drop size distribution that would be obtained, an upper-limit log-normal (ULLN) distribution was fitted to the back-scatter data. This is illustrated on Figure 4.8. Normalising the experimental data by dividing by the Sauter mean diameter causes the data to collapse onto a single curve. The majority of the scatter present is due to data from low mixture velocities where the flow pattern was stratified rather than dispersed. The discrepancies for vertical upflow occur at high velocities and dispersed phase concentrations (15-40% vol) and it may be possible that the upper operating limit of the detector is being reached. The upper limit log-normal distribution was found to fit the data most accurately with values of $\delta=0.6$, $X_{max}=2.9$ and $X_{50}=1.41$. The value of a was calculated from these results to be 1.06. This is a noticeable deviation from the values of $a=1.2$ and $\delta=0.9$ suggested by Karabelas.

Maximum droplet diameter cannot be obtained directly from the techniques employed in this study, due to the upper size limits on both measuring instruments. Values can be proposed, however, by use of the ratio of d_{max}/d_{32} , from either equation 2.31 or by use of experimental data. Karabelas (1978) measured a ratio of 2.24 for a dispersion of water in kerosene. Plotting these results for vertical upflow, with the equation of Hinze (Equation 2.27) on Figure 4.9 shows that there is an inverse relationship between maximum diameter and velocity. The choice of ratio of d_{max} to d_{32} shifts the experimental data along the vertical axis but the trend of the data is less steep. This could be due to an effect of concentration, a parameter which Hinze does not take into consideration.

Flow development is an issue that has still not been resolved for liquid-liquid dispersions. Indeed, it is not possible to assess whether the experimental facilities are long enough to obtain fully developed flow. In the present study, the lengths from the mixer to the test section were about 5 m for both horizontal and vertical geometries. It is therefore possible that the change of size distribution with mixture velocity could also be due to the change in residence time within the pipe. If this effect is present, measurements at different positions along longer pipes of different diameter would be required to deconvolute it. The pipe lengths used in this work were as long as practicable within the confines of the laboratory. However, multiphase pipelines in the North Sea can run for hundreds of metres.

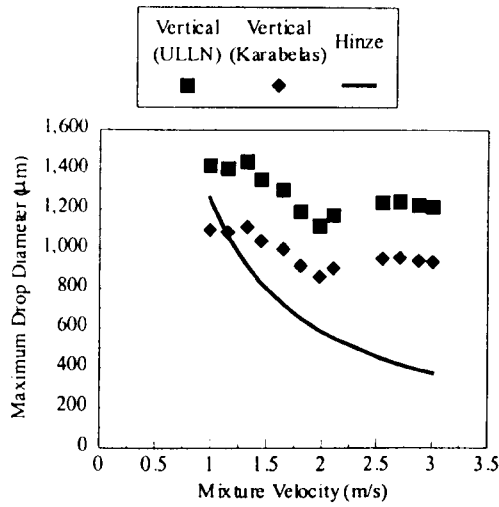


Figure 4.9: Comparing calculated values of d_{\max} with equation of Hinze

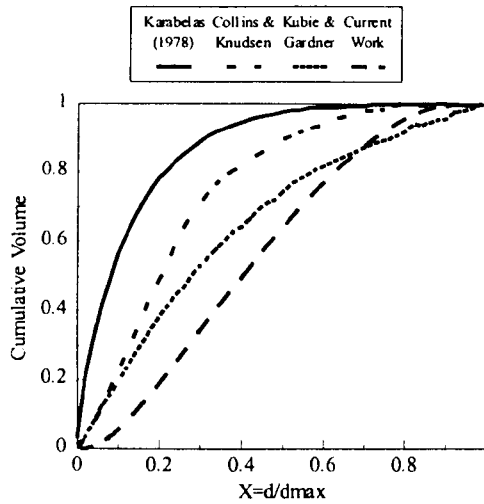


Figure 4.10: Typical measured cumulative volume distributions

As discussed in Chapter 2, a recent study by Karabelas (1998) has reported that for fully developed flow, if a plot of volume fraction distribution versus normalised particle diameter is drawn, the profile should lie to the right of the leading diagonal of the graph. Experimental data were found to lie to the left of the diagonal, and hence it was concluded that no experimental study has measured fully developed flow, and that full flow development occurs exponentially with time. This means that the final steady state is attained very slowly, and that the variations are so small

that they cannot be measured experimentally. This plot is extended to include the current work on Figure 4.10 and it can be seen that the vertical data is much closer to the diagonal. This would suggest that the flow is reasonably well developed and that the residence time effect should not be strong but may also be due to the upper limits on drop size imposed by the measurement techniques. A systematic study is required in order to study flow development, with a much longer flow loop than has been used previously. The length of flow loop may be beyond what can be reasonably installed in University facilities.

4.4.2 Flow Patterns

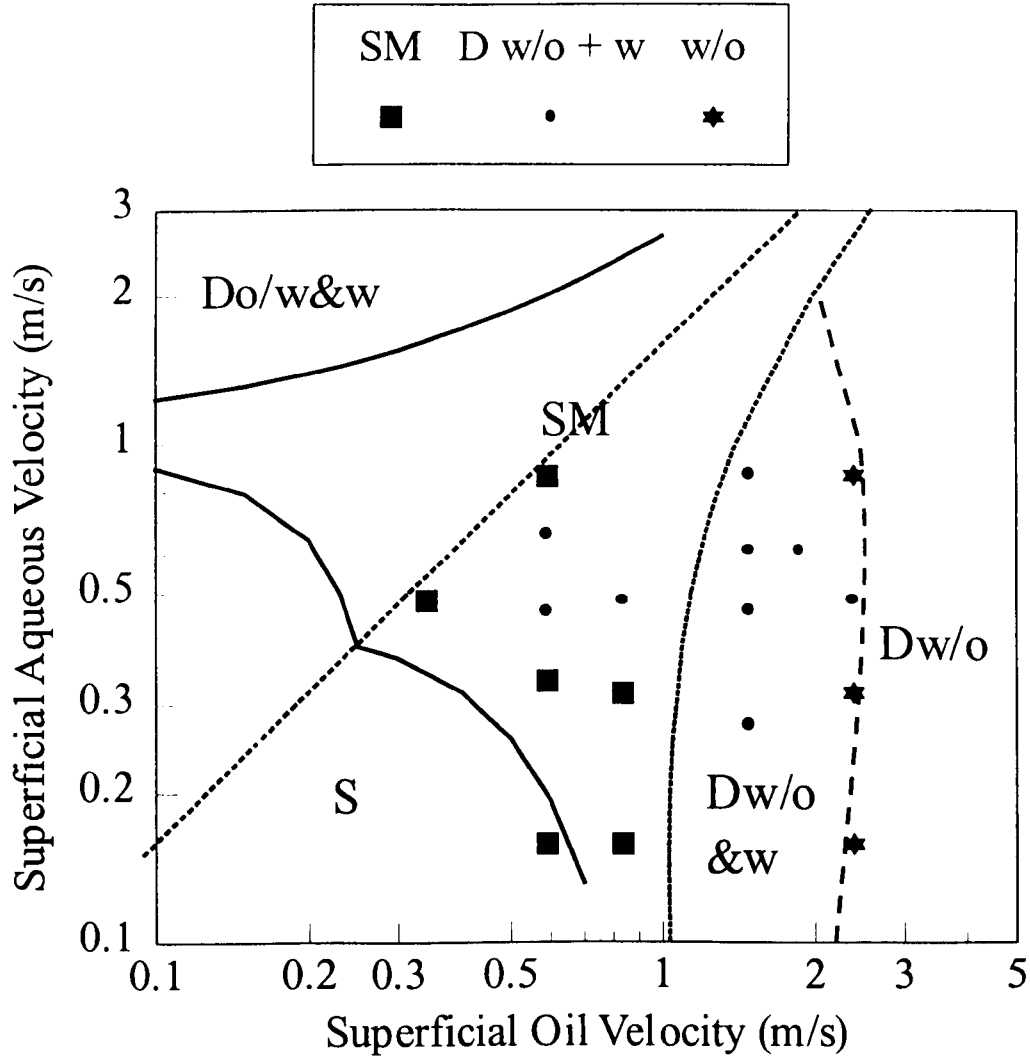


Figure 4.11: Flow pattern map for horizontal flow

Key to Figure 4.11

S	Stratified flow with smooth or wavy interface
SM	Stratified flow with interface mixing
Do/w+w	Dispersion of oil in water plus a water layer
Do/w	Dispersion of oil in water
Dw/o+w	Dispersion of water in oil plus a water layer
Dw/o	Dispersion of water in oil

Determination of flow pattern was made from visual judgement of the video footage. Dispersed flows were observed for the range of flow rates used for vertical upflow. Stratification occurred at lower flow rates for the horizontal geometry so from these observations the flow regimes were further classified according to Brauner and Moalem-Maron (1992a,1992b). The data are shown on Figure 4.11 together with the theoretical flow boundaries predicted from that work. Excellent agreement is shown at the D w/o boundary. All the measured points lie to the right of the EU boundary, where the actual velocities of each phase are equal, so for all cases the actual oil velocity is greater than that of the aqueous phase. This explains the dispersion of the aqueous phase in the oil as well as the presence of a water layer on the bottom of the pipe for most of the measurements. The boundaries 2w and 2o in Figure 4.11, which predict the change from SM to Dw/o +Do/w and Dw/o+w respectively do not correlate as well with the data. More dispersion of water in oil occurs at lower velocities than is predicted by the boundaries. This is most likely due to flow

development, as in any case the Dw/o dispersions produced are not stable and readily settle out.

Some other flow pattern maps for liquid-liquid pipe flow are shown in Appendix A5 but as can be seen, these are experimentally developed and hence are only valid in specific flow situations. Trallero *et al.* (1997) have also developed a flow pattern model which has been tested against experimental data. The flow pattern transitions were predicted using the two-fluid model and a balance between gravity and turbulent fluctuations, similar to the approach of Brauner and Moalem Maron (1992a, 1992b) as shown in Chapter 2.

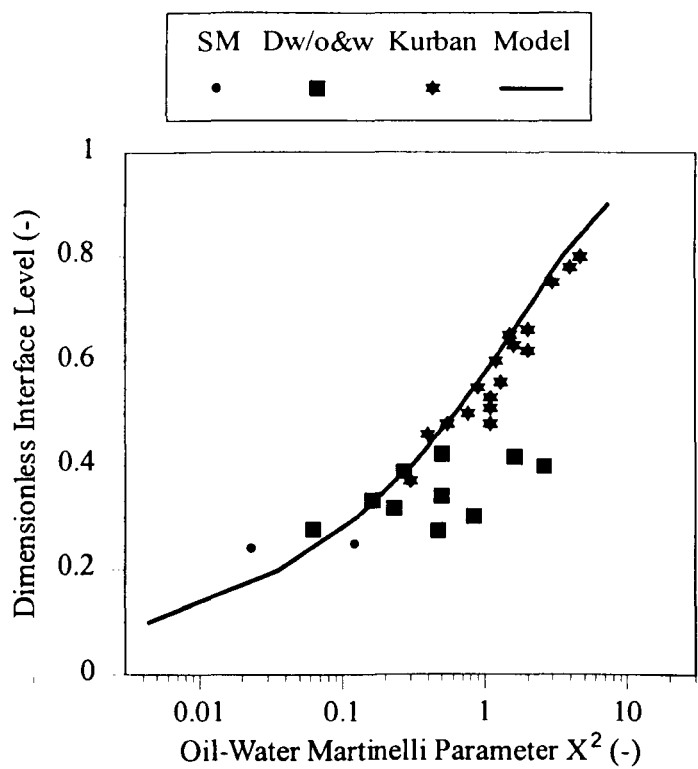


Figure 4.12: Comparing Observed Interface Height with Taitel Dukler Model (1976)

From the high speed video sequences, it was also possible to measure the position of the interface between the oil and aqueous layers. Over the range of flows examined

the interface lay between 20 and 45% of the diameter from the bottom. Kurban *et al.* (1995) have adapted the analysis of Taitel and Dukler (1976) for stratified gas/liquid flow to liquid/liquid stratified flow. Dimensionless interface level, h/D , is plotted versus the Lockhart-Martinelli parameter, X^2 (Equation 2.8) on Figure 4.14. The Figure shows that, as with their data, the present stratified flow data is well predicted by this analysis. In the case of stratified/dispersed flow, the analysis over-predicts the height of the interface. This is not surprising as part of the aqueous phase is now dispersed above the interface and so the height of the aqueous layer is less.

4.5 CONCLUSIONS

Two drop sizing instruments have been applied to pipe flows of kerosene and aqueous potassium carbonate solution for vertical and horizontal orientations. Both instruments were found to be suitable for this task but the Malvern 2600 was limited to concentrations below 3% by volume. This was necessary in order to prevent scattering of the diffraction pattern by more than one droplet, and reduce the obscuration. The Par-Tec 300C instrument was found to operate reliably at concentrations above 5% and a method of conversion of the chord distributions produced to diameter distributions has been developed (Appendix A2).

There was little variation of Sauter Mean Diameter with position in vertical upflow but there was considerable difference for horizontal flow at low flow rates due to the effects of stratification. The Malvern produced lower values of Sauter Mean Diameter. This is likely to be due to concentration effects and the fact that the size bins on the Par-Tec are very coarse at high drop sizes which will increase the values of Sauter Mean Diameter measured. The Malvern also had a different range of measurement to the Par-Tec.

Testing of the instruments on glass beads suspended in water in the test cell showed they all gave similar results for a 90-106 μm sieve cut. The distribution obtained from the Par-Tec was slightly wider. It is noted that the distribution of sizes was much narrower than those obtained from the pipe flow measurements. A systematic study of different bead sizes and distribution shapes would prove useful in the future as the work performed in this study was curtailed by malfunction of the Par-Tec probe.

The flow patterns obtained for horizontal flow agree reasonably well with the flow pattern of Brauner and Moalem Maron (1992a, 1992b). There is some scatter which is most likely due to the short length of the test section. The test section length was limited by the dimensions of the laboratory. The height of the interface in stratified flow was predicted well by the model of Taitel and Dukler (1976) until significant interface mixing and dispersion took place.

Chapter 5

MATHEMATICAL MODELS OF LIQUID-LIQUID SEPARATORS AND THEIR APPLICATION TO FIELD DATA

5.1 INTRODUCTION

Characterisation of the performance of liquid-liquid separators has traditionally been obtained from Residence Time Distribution data and interface positions from nucleonic scans. Companies operating oil production systems such as BP Exploration have used these techniques on several of their facilities. However, in the past only rudimentary information has been inferred from the data produced. Development of a mathematical model is required to provide a greater understanding of the processes occurring within the vessels. As discussed in Chapter 2, the complexity of the liquid-liquid separation due to droplet sizes, break up and coalescence, both in the bulk phases and at the interface, limits the applicability of most CFD codes at this time. Therefore a simpler method has been selected.

The mathematical model presented below is developed from a transfer function approach, Luyben (1990). The separator is split into a series of zones, using techniques as described in section 2.4. The model has been coded into FORTRAN and has been tested against data from field separators provided by BP Exploration.

5.2 DEVELOPMENT OF THE MODEL

Observations of the flow of the liquids within the test separator have shown that the inlet zone is a region of high turbulence. After the baffle, the flow settles and

becomes much smoother. In light of these characteristics, it is suggested that the separator can be split into a series of zones.

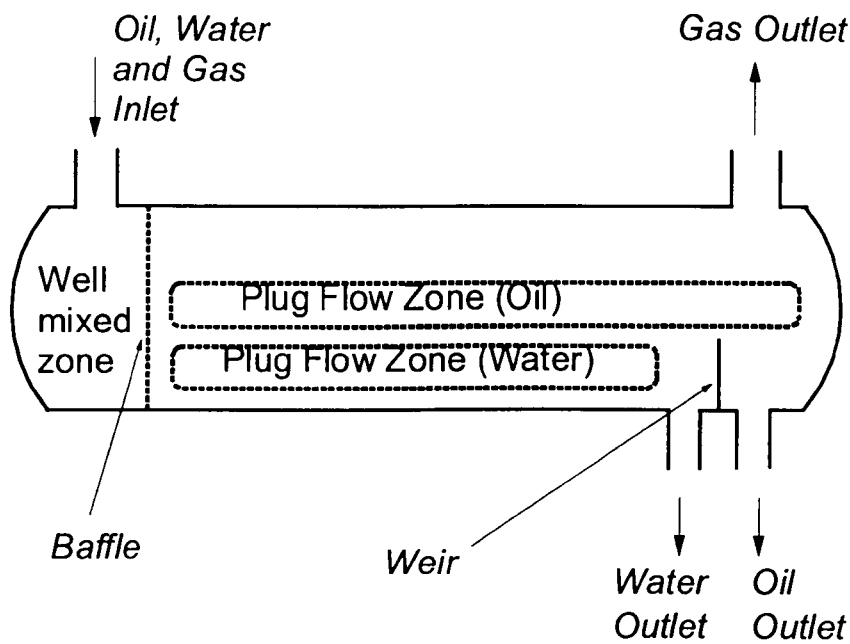


Figure 5.1: Possible Flow Zones

The separator can be modelled assuming that the inlet zone is completely mixed, followed by no mixing at all within the bulk flow (plug flow). An enhancement to this model is to allow some mixing within the bulk flow, which in reality is more likely, and also to consider two parallel streams within one phase, to allow for the presence of dead zones or internals. The advantage of using the transfer function approach is that the models can be easily modified and increased in complexity.

5.2.1 Test Model

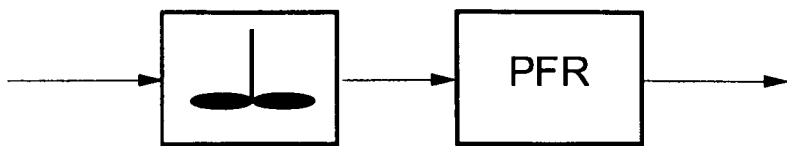


Figure 5.2: Test Model

This simple model produces a first order response. The derivation of the differential equations describing this model is trivial and is shown below.

$$E(t-\tau_2)=E(0)+\tau_1\frac{dE(t-\tau_2)}{dt}\tag{5.1}$$

Assuming that $E(0)$ is a perfect impulse, a solution to the above equation may be obtained from Laplace transforms or otherwise as

$$E(t)=\frac{1}{\tau_1}e^{-\left(\frac{t-\tau_2}{\tau_1}\right)}\tag{5.2}$$

This model is not appropriate to the separator as visual inspection of the Residence Time Distribution curves shows that they are of a higher order than one. This model was found useful however, in order to check the mathematics and FORTRAN code for errors. It served as a debugging tool.

5.2.2 NSTIS Model

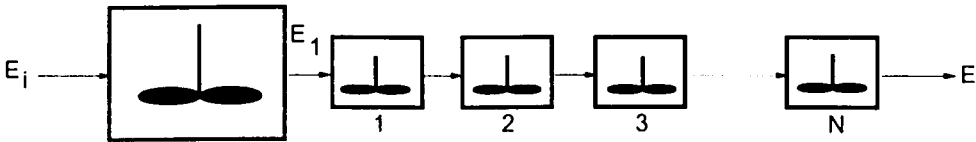


Figure 5.3: NSTIS Model

The “N Stirred Tanks in Series” (NSTIS) model allows for some mixing in the bulk phase. This is more realistic as turbulence due to the velocity of the phases and the disengagement process means that true plug flow is never approached. The mixing is introduced by modelling the main section as a series of equal sized stirred tanks. The level of mixing can be quickly and easily altered by changing the number of stirred tanks, N. If the number of tanks is equal to unity, complete mixing occurs.

Increasing the value of N to higher numbers reduces the mixing until finally at infinity, a plug flow behaviour is obtained.

The transfer function of the system is as follows

$$G(s) = \frac{1}{\tau_1 s + 1} \left[\frac{1}{\tau_2 s + 1} \right]^N \quad (5.3)$$

Where τ_2 is the residence time of one tank in the series of N tanks. The analytical solution for the above system was obtained by use of the software package MAPLE.

$$E(t) = \frac{\tau_1^{N-1}}{(\tau_1 - \tau_2)^N} e^{\left(\frac{-t}{\tau_1}\right)} - \sum_{i=1}^N \frac{\tau_1^{N-i} t^{i-1}}{(\tau_1 - \tau_2)^{N+1-i} \tau_2^{i-1} (i-1)!} e^{\left(\frac{-t}{\tau_2}\right)} \quad (5.4)$$

5.2.3 “Alternative Path” Model (APM)

The final model that was constructed considers two alternative paths in order to allow for the modelling of dead zones or bypasses. Altering the time constant through each path performs this function.

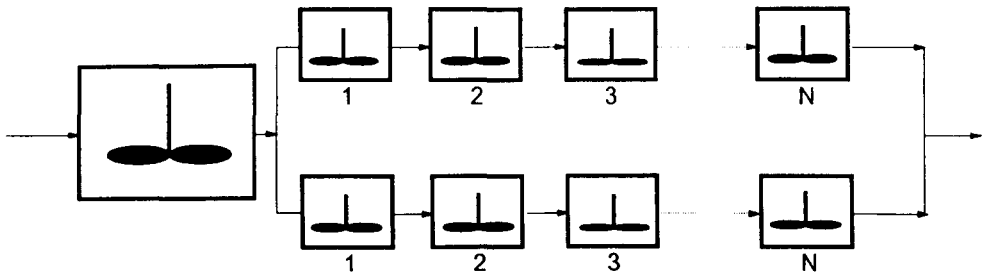


Figure 5.4: Alternative Path Model

This Alternative Path Model model therefore has 6 adjustable parameters for each phase:

- 1) Time constant in inlet mixing (CSTR) zone, τ_1
- 2) Time constant of a stirred tank in each series, τ_2, τ_3

- 3) Flow fraction through each path, f is defined as the flow fraction through path corresponding to τ_3 .
- 4) Number of stirred tanks in each path, N

The transfer function and analytical solution of this model are as follows.

$$G(s) = \frac{1}{\tau_1 s + 1} \left[(1-f) \left(\frac{1}{\tau_2 s + 1} \right)^N + f \left(\frac{1}{\tau_3 s + 1} \right)^N \right] \quad (5.5)$$

$$G(t) = \frac{(1-f)\tau_1^{N-1}}{(\tau_1 - \tau_2)^N} e^{\left(\frac{-t}{\tau_1}\right)} - (1-f) \sum_{i=1}^N \frac{\tau_1^{N-i} t^{i-1}}{(\tau_1 - \tau_2)^{N+1-i} \tau_2^{i-1} (i-1)!} e^{\left(\frac{-t}{\tau_2}\right)} \\ + \frac{f\tau_1^{N-1}}{(\tau_1 - \tau_3)^N} e^{\left(\frac{-t}{\tau_1}\right)} - f \sum_{i=1}^N \frac{\tau_1^{N-i} t^{i-1}}{(\tau_1 - \tau_3)^{N+1-i} \tau_3^{i-1} (i-1)!} e^{\left(\frac{-t}{\tau_3}\right)} \quad (5.6)$$

The Alternative Path Model assumes that there is a dead zone or similar feature within the vessel at the location of each phase. Recent studies performed by Davies (1998), show that the flow in the vessel is much faster near the oil-water interface, due to the settling of the drops. This behaviour was visualised by injection of dye into the water phase. The dye was initially carried up towards the interface and then carried down near the water outlet. After the main portion of dye had exited, diffusion effects caused some dye to be temporarily trapped in the central dead zone. This is a powerful argument supporting the physical validity of the Alternative Path Model. It is suggested that a similar effect could occur in the oil phase if the oil layer was thick.

5.3 CALCULATION OF FREQUENCY RESPONSE FROM RESIDENCE TIME

DISTRIBUTION

It is possible to calculate directly the frequency response of a particular system from the residence time distribution. If we consider a system with an input pulse $E_i(t)$ and an outlet pulse $E(t)$, then by definition, the transfer function of the process, $G(s)$ is

$$G(s) = \frac{E(s)}{E_i(s)} \quad (5.7)$$

We can relate this expression to the time domain by using the definition of Laplace Transforms. To determine the frequency response we enter the frequency domain by substituting $s=i\omega$, where i is a complex parameter and ω is the frequency.

$$G(s) = \frac{\int_0^{\infty} E(t)e^{-st} dt}{\int_0^{\infty} E_i(t)e^{-st} dt} \quad (5.8)$$

hence

$$G(i\omega) = \frac{\int_0^{\infty} E(t)e^{-i\omega t} dt}{\int_0^{\infty} E_i(t)e^{-i\omega t} dt} \quad (5.9)$$

We can now make use of the definition

$$Re^{-i\theta} = R(\cos \theta - i \sin \theta) \quad (5.10)$$

Equation 5.9 can now be written as

$$G(i\omega) = \frac{\int_0^{\infty} E(t) \cos(\omega t) dt - i \int_0^{\infty} E(t) \sin(\omega t) dt}{\int_0^{\infty} E_i(t) \cos(\omega t) dt - i \int_0^{\infty} E_i(t) \sin(\omega t) dt} \quad (5.11)$$

The numerator is the Fourier transform of the output pulse, while the denominator is the Fourier transform of the input pulse. If the input pulse can be approximated by a perfect delta function, then $E_i(s)=1$ and the frequency response becomes a function of the outlet pulse only.

The Fourier transformations of the pulses were performed by use of the MATLAB software package. The program codes used to perform this are shown in Appendix A6. It is possible to generate Bode plots of Magnitude and Phase Angle from the transformations from the following equations.

$$M(dB) = 20 \log_{10} \sqrt{Re(G(i\omega))^2 + Im(G(i\omega))^2} \quad (5.12)$$

$$\theta = arg(G(i\omega)) = \tan^{-1} \left[\frac{Re(G(i\omega))}{Im(G(i\omega))} \right] \quad (5.13)$$

5.4 ANALYSIS OF RESIDENCE TIME DISTRIBUTION FROM BP SEPARATORS

5.4.1 Modelling Performed on Field Data

BP have provided 4 sets of Residence Time Distribution data from different field separators, BP Ula, Norway, BP Kinneil, UK, BP Milne Point, Alaska and BP Magnus, UK. The Residence Time Distributions were obtained from injection of radioactive tracers and nucleonic scans provided some information on interface heights within the vessels. The following table lists the geometries of the field separators, together with the flow rates and conditions used for each run. The Ula, Magnus and Milne Point vessels were performing mainly oil-water separation while the Kinneil vessel was utilised for gas-oil separation, with only small amounts of water present.

The Residence Time Distributions were obtained for all the cases in Table 5.1 by the injection of either organic or aqueous soluble compounds of Bromine 82. Curve fitting was performed for both the NSTIS and AP models by using the least squares method. The least squares method employed was unweighted so the fit obtained was optimised over the whole Residence Time Distribution curve.

Table 5.1: Basic Information on BP Trials on Field Separators.

BP MILNE POINT	1	2	3	4	5	6
Vessel height (m)	3.6	3.6	3.6	3.6	3.6	3.6
Vessel length (m)	24.5	24.5	24.5	24.5	24.5	24.5
Flow oil (m ³ /s)	0.073	0.076	0.074	0.070	0.074	0.070
Flow water (m ³ /s)	0.033	0.033	0.033	0.037	0.037	0.032
Gas-oil int. ht (cm)	157.48	157.48	147.32	147.32	157.48	157.48
Oil-water int. ht (cm)	91.44	93.98	86.36	86.36	97.79	81.28
Sand depth (cm)	40	40	40	40	40	40

BP KINNEIL	1	2	3	4	5
Vessel height (m)	3.05	3.05	3.05	3.05	3.05
Vessel length (m)	12.28	12.28	12.28	12.28	12.28
Flow gas (Nm ³ /s)	1.57	2.36	1.79	3.06	2.18
Flow liquid (m ³ /s)	0.14	0.23	0.19	0.26	0.17
Gas-oil int. ht (cm)	1.53	1.53	1.53	1.53	1.53
Oil-water int. ht (cm)					

BP MAGNUS	1	2
Vessel height (m)	3	3
Vessel length (m)	10	10
Flow gas (Nm ³ /s)	0.479	0.479
Flow oil (m ³ /s)	0.107	0.109
Flow water (m ³ /s)	0.064	0.062
Gas-oil int. ht (cm)	115	115
Oil-water int. ht (cm)	67.5	69.5

BP ULA	HP 1	2	3	4	TEST 1
Vessel height (m)	3.3	3.3	3.3	3.3	2.64
Vessel length (m)	10	10	10	10	7.4
Flow oil (m ³ /s)	0.121	0.099	0.123	0.121	0.033
Flow water (m ³ /s)	0.101	0.043	0.143	0.010	0.060
Gas-oil int. ht (cm)	N/A	N/A	1.9	1.9	1.19
Oil-water int. ht (cm)	N/A	N/A	0.87	0.85	0.87

A feature of the Residence Time Distribution curves produced is a long “tail” which has the effect of lengthening the Mean Residence Time, t_m and is difficult to model accurately as the rate of change of $E(t)$ with time is very small. The accuracy of the experimental data is also questionable at these low rates of change so it was chosen to concentrate on the fitting of the peaks. As was shown in Chapter2,

$$t_m = \frac{\int_0^{\infty} t c(t) dt}{\int_0^{\infty} c dt} \tag{5.14}$$

The upper limit can be replaced by some time T, at which it can be assumed all tracer has exited. Choice of this value is somewhat arbitrary and can obviously have a significant effect on the value of t_m . To obtain T, the background values of radiation intensity were subtracted from the Residence Time Distribution curve and the value of T was chosen where the corrected intensity value returned to zero. This is obviously subject to error if any baseline drifting was present. However, this was adopted as a self-consistent method. If very long tails are experienced on the Residence Time Distribution curves, it is possible that the peak to peak residence time may be a more representative parameter, however, a measure of the skewness of the Residence Time Distribution curve would then be necessary.

As an additional verification, the frequency response of both the models and the experimental data was examined. Accurate measurement of the inlet pulse function was provided for both Milne Point and Kinneil data, but mass balances were not attempted due to the large amounts of noise present on the inlet signals and the absence of any concentration or calibration data for the detectors.

The time constants obtained from the AP model were used to back-calculate the volume of the tank occupied by the liquid. This was performed by multiplying the mean residence times obtained from the model (t_m) by the individual phase flow rates. The total size of the inlet mixing zone can also be estimated similarly (Equations 5.15-5.17).

$$t_{mi} = \tau_{li} + (f\tau_{2i} + (1-f)\tau_{3i}) \quad (5.15)$$

where $i=0$ or w .

$$V_{mix} = F_o\tau_{lo} + F_w\tau_{lw} \quad (5.16)$$

$$V_{Total} = t_{mo} \cdot F_o + t_{mw} \cdot F_w \quad (5.17)$$

A Fractional Mixed Volume, D , can now be defined as

$$D = \frac{V_{mix}}{V_{total}} \quad (5.18)$$

This parameter, D is a measure of the volume of the vessel occupied by turbulent mixing.

A feature noticeable on several of the Residence Time Distribution curves produced was the presence of a secondary peak. In order to characterise this effect, a “secondary peak” number, F is proposed that can be calculated from parameters in the Alternative Path Model.

$$F = f \cdot \left(\frac{\tau_3}{\tau_2} - 1 \right) \quad (5.19)$$

This definition was chosen as it includes the ratio of time constants through each path as well as the flow fraction, f . If τ_3 is close to τ_2 then the secondary peak is less noticeable and the term in brackets tends to zero.

5.4.2 Results

The parameters obtained from the curve fitting can be seen from Tables 5.2 to 5.5. It was assumed that for all runs, the inlet pulse could be considered as a perfect delta function. Inspection of the raw data indicated that duration of the inlet pulse was typically less than 1.5% of the total measurement time, so this assumption is not unreasonable. The effects of non-ideal inlet pulses are discussed in Chapter 6.

The quality of the curve fits can be seen in Figures 5.5 to 5.22. In most cases, the fit of the Alternative Path Model to the Residence Time Distribution data is excellent. A feature of most of the experimental curves is high frequency “noise”, which is most likely an artefact of the radio-tracer measurement technique. Examination of the frequency response of one of the curves, in this case Milne Point Run 3 with aqueous tracer, clearly shows noise at the high frequencies on the Magnitude plot (Figure 5.23). As expected, as the curve fit is of high quality, the experimental and model magnitude and phases agree well (Figures 5.23-5.24), until the high frequency disturbances become the dominating factors.

Although it is true to say that an infinite number of models could produce equally good fits, the validation of the model comes from the investigation of the variation of the model parameters between runs. However, it is difficult to judge any variation of

parameters for Milne Point and Ula runs due to the similarity of flow rates between runs. However, the Ula runs do show some variation of flow rate of water, while the flows for the Kinneil runs range from 0.14-0.26 m³/s. Plotting the MRT from both the Alternative Path Model and experimental curve shows an expected downward trend with flow rate (Figure 5.25). This effect is present, but understandably less noticeable for the Milne Point and Ula runs, where the differences in flow rate between runs are much less (Figures 5.26-5.27). It is interesting to note that the values of MRT do not show a trend with individual flow rates of each phase, but this is to be expected as the MRT of both phases are linked quite closely, particularly when well mixed. The interactions are very complex, and depend greatly on the physical properties of the liquids as well as the flow rates and design of the vessels. This will be studied more closely when the experimental data from the liquid-liquid rig is examined.

The values of the volume occupied by both phases in the tank from the Alternative Path Model agree well with the measured volume as shown at the bottom of Tables 5.2-5.4. This provides a useful check on the calculations and shows them to be correct.

The Ula and Magnus vessels are unbaffled, and the value of Fractional Mixed Volume is approx. 0.67. The Milne Point vessel is baffled and the value is approx 0.45. It would be expected that a baffle plate would smooth out the flow and hence a decrease in the value of the Fractional Mixed Volume would be expected. This observation is quite powerful because it means that a measure of the smoothness of

the flow in the vessel, which is related to the quality of the separation, can be easily obtained from Residence Time Distribution profiles.

The Kinneil data produces very high values of Fractional Mixed Volume of approx 0.80. This indicates a turbulent flow regime within the vessel, even though there is a baffle plate in place. It was noted from nucleonic scans that there was no distinct liquid-liquid interface within the vessel, and the water cut was very low. This indicates that at the end of the vessel there is a water-rich phase and an oil-rich phase, so there is still significant mixing taking place. In any case, the very low quantities of water present mean that it is unlikely that an oil-water interface would appear. Observations of the Milne Point facility indicated the appearance of a distinct oil-water interface about a third of the way along the vessel. This further validates the argument relating the Fractional Mixed Volume, this aspect will be discussed further in Chapter 7. There appears to be no trend of Fractional Mixed Volume with flow rate from the BP data sets, the controlling factor appears to be the internal configuration of the vessels (Figure 5.28). The limited amount of data prevents further analysis.

The values of F number from all four cases is plotted on Figures 5.29 and 5.30. There is considerable scatter but there is a very general upward trend for the organic values and a downward trend for the aqueous runs. This suggests that secondary peaks in the aqueous Residence Time Distribution are more likely to occur for low aqueous flows and that the opposite is true for organic Residence Time Distributions. It is likely that any recirculating effects in the aqueous phase would be exacerbated by low flow rates. The reason for the increase of secondary peaks at higher oil flow

rates is less clear but may be due to slower disengagement of oil from the water phase due to greater turbulence at higher oil flows.

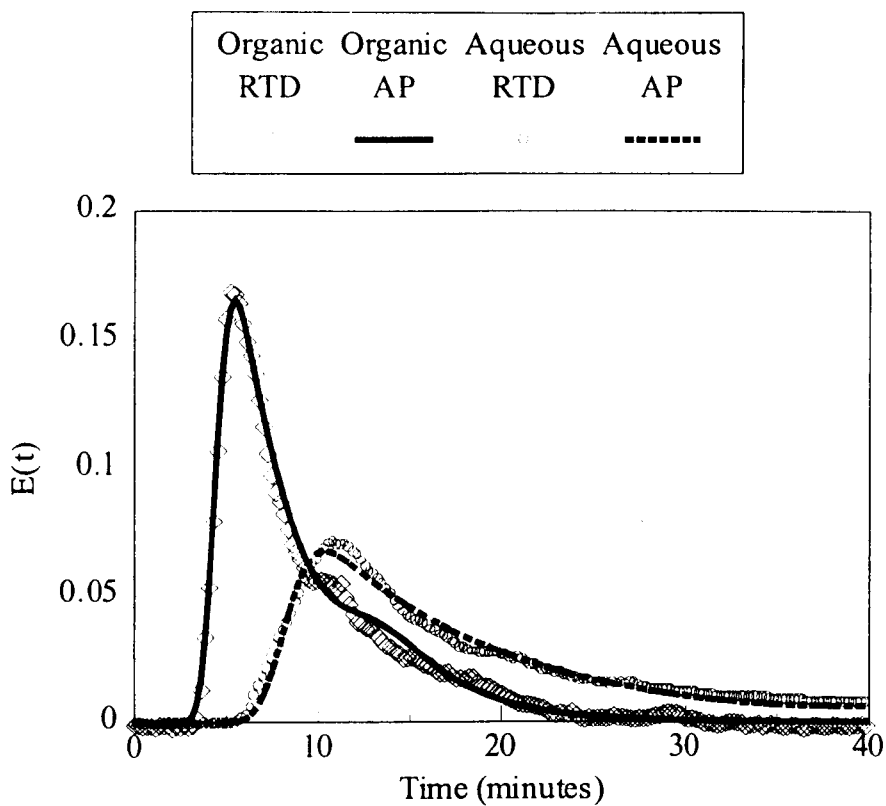


Figure 5.5: Curve fitting Alternative Path Model to Milne Run 1

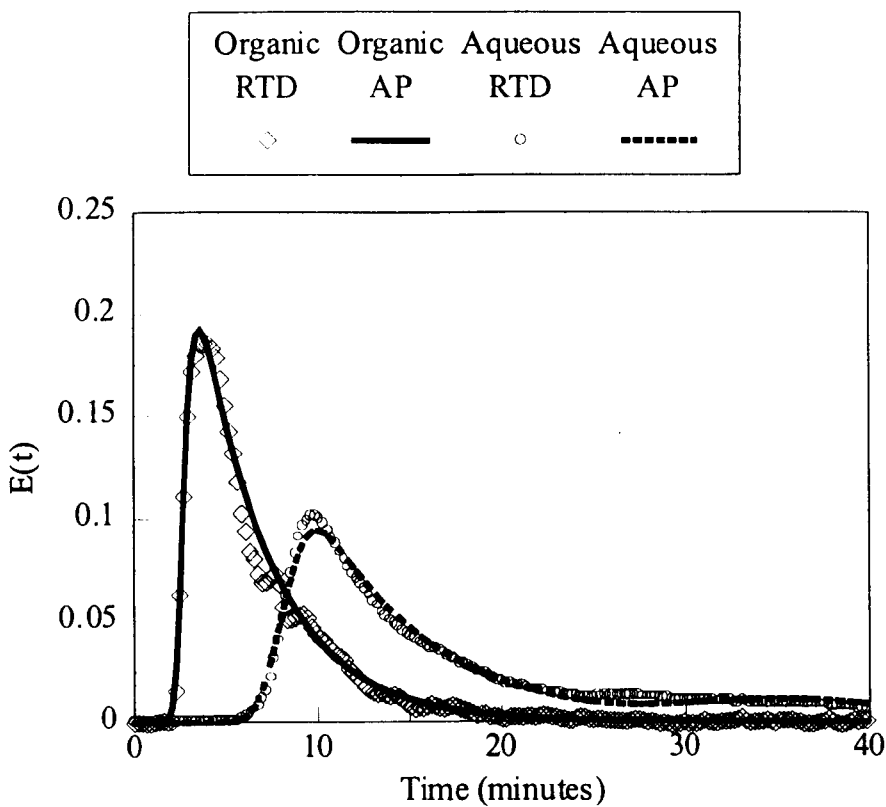


Figure 5.6: Curve fitting Alternative Path Model to Milne Run 2

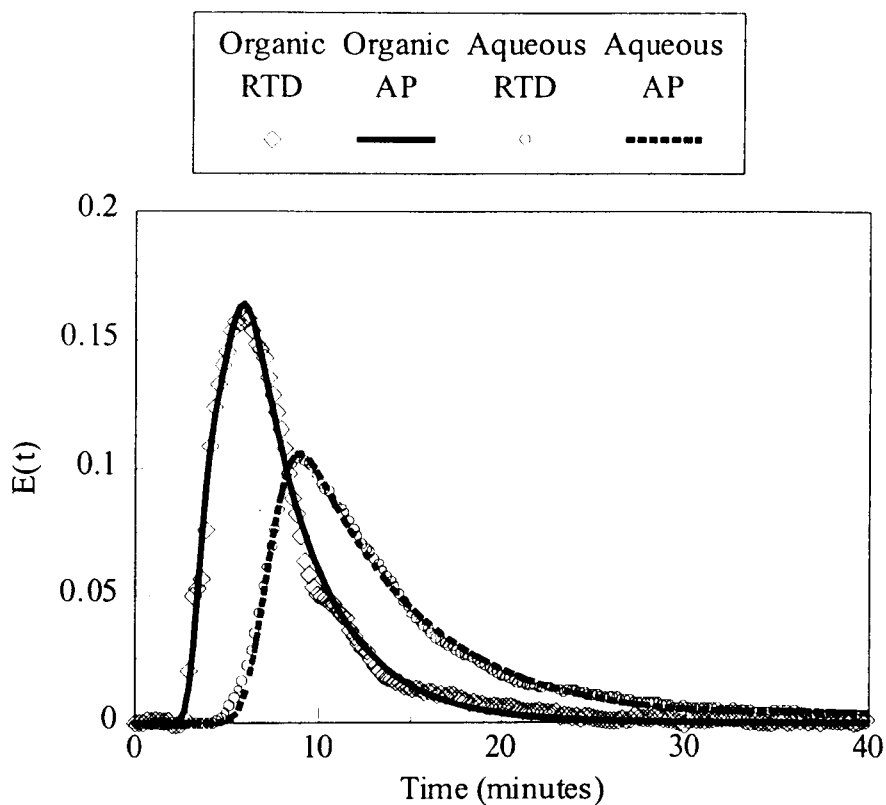


Figure 5.7: Curve fitting Alternative Path Model to Milne Run 3

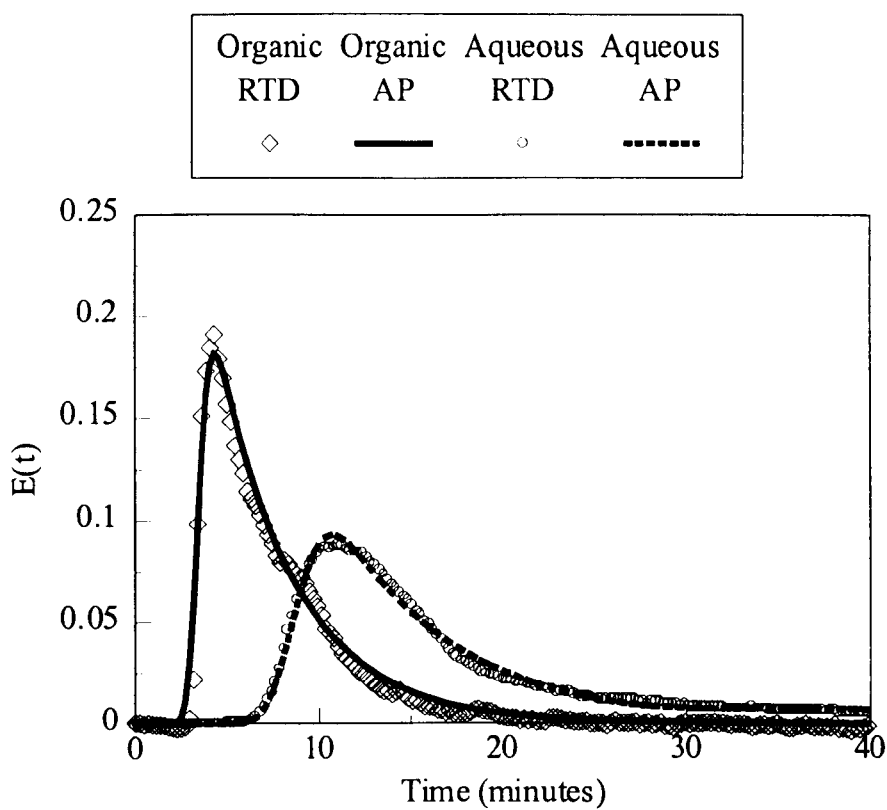


Figure 5.8: Curve fitting Alternative Path Model to Milne Run 4

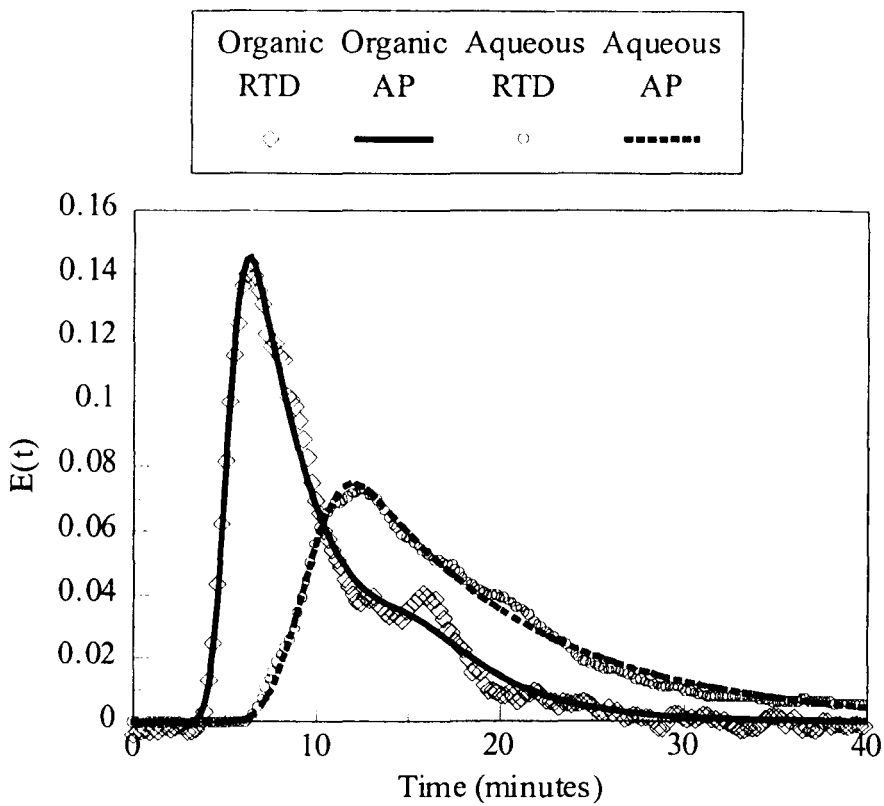


Figure 5.9: Curve fitting Alternative Path Model to Milne Run 5

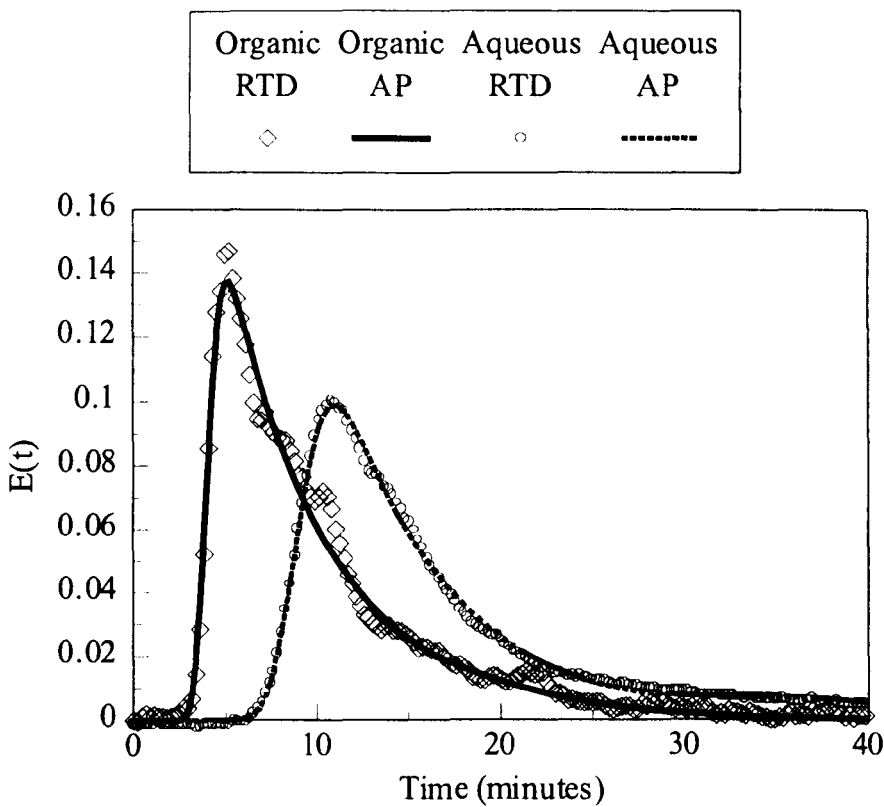


Figure 5.10: Curve fitting Alternative Path Model to Milne Run 6

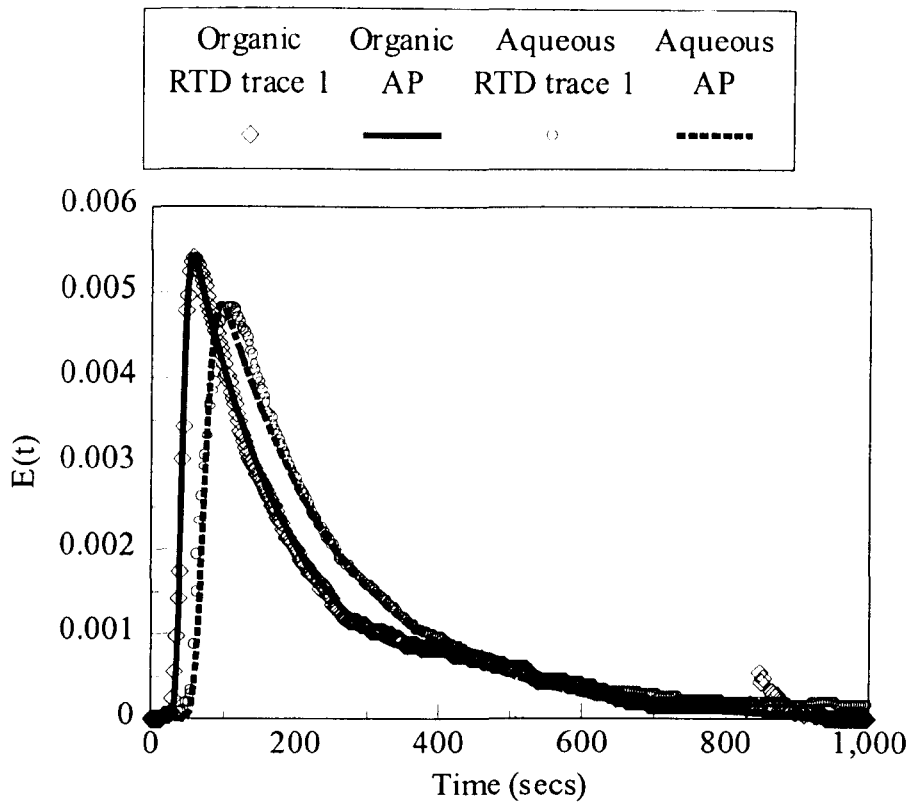


Figure 5.11: Curve fitting Alternative Path Model to Ula Run 1

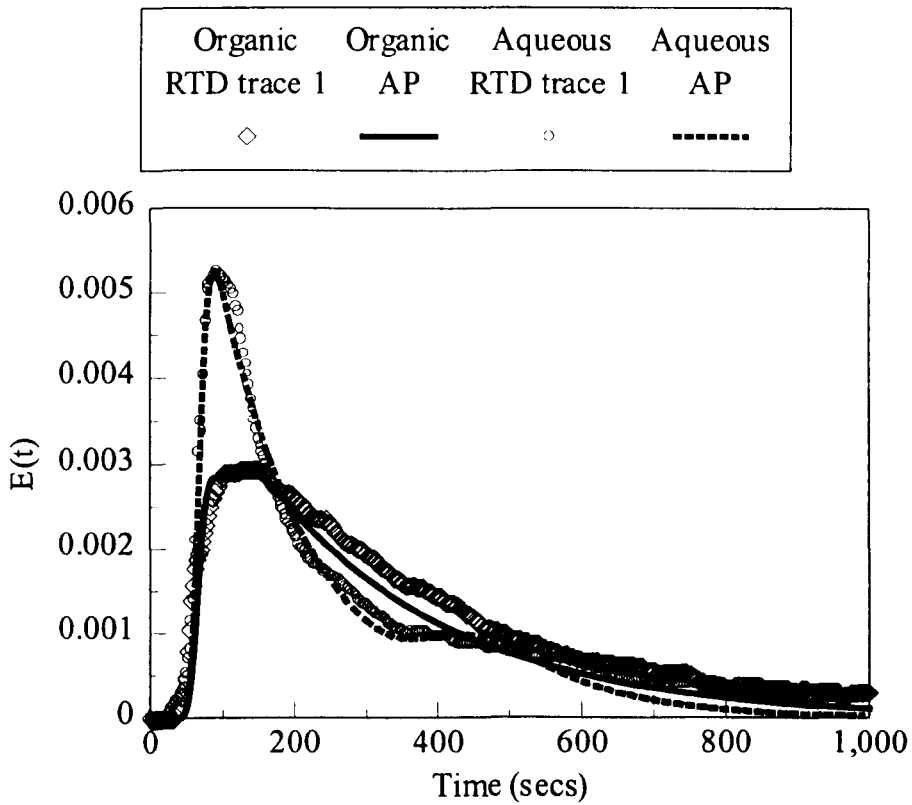


Figure 5.12: Curve fitting Alternative Path Model to Ula Run 2

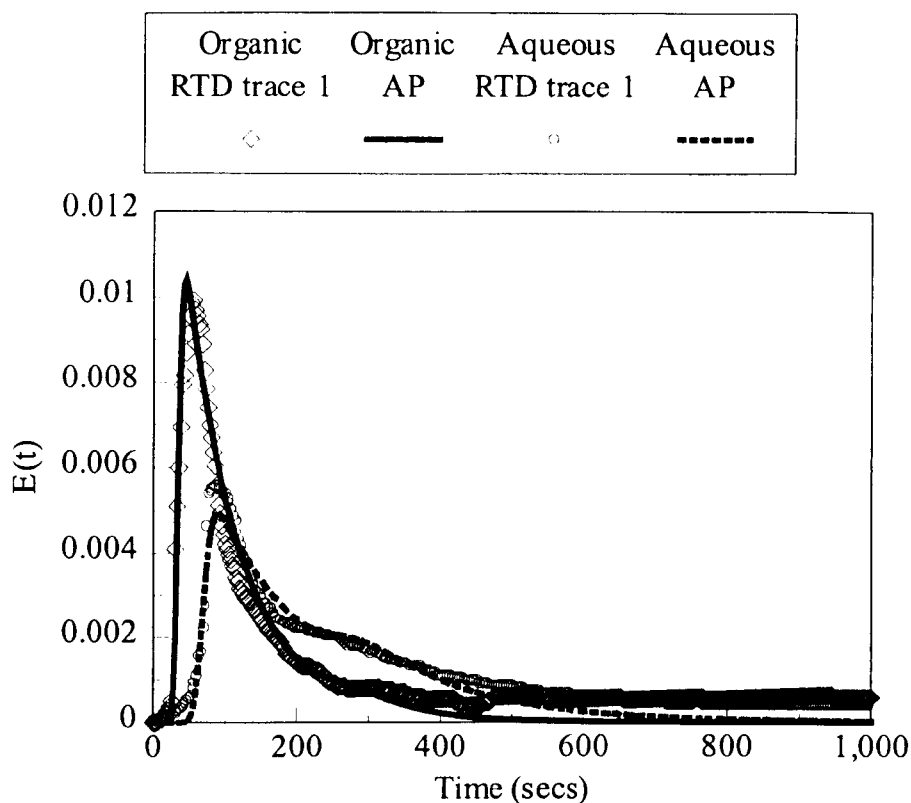


Figure 5.13: Curve fitting Alternative Path Model to Ula Run 3

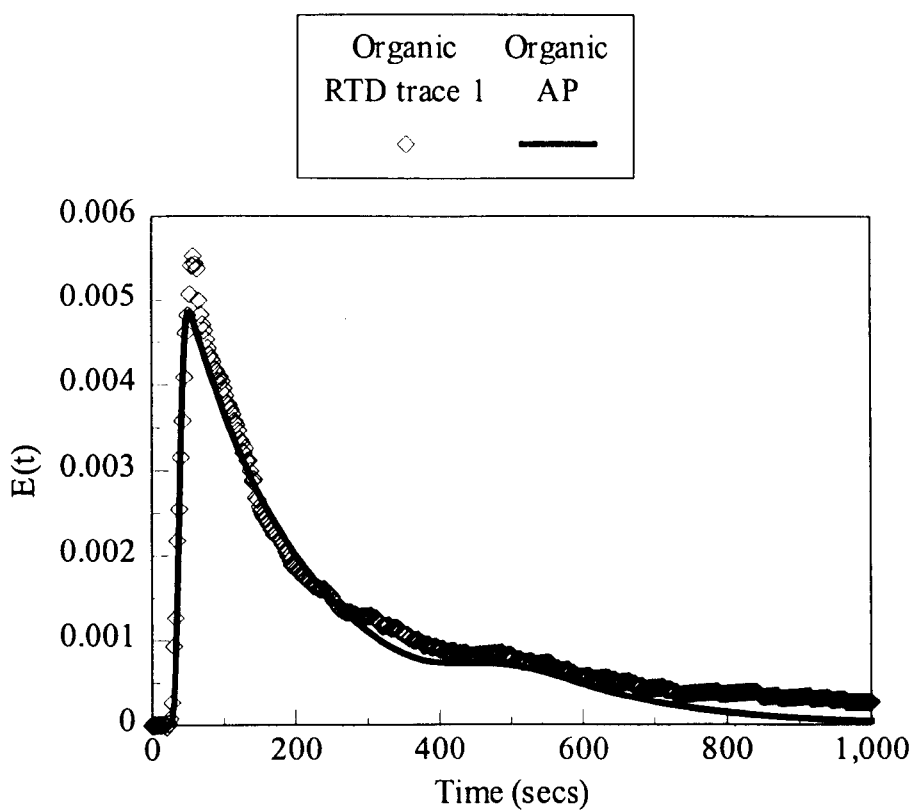


Figure 5.14: Curve fitting Alternative Path Model to Ula Run 4

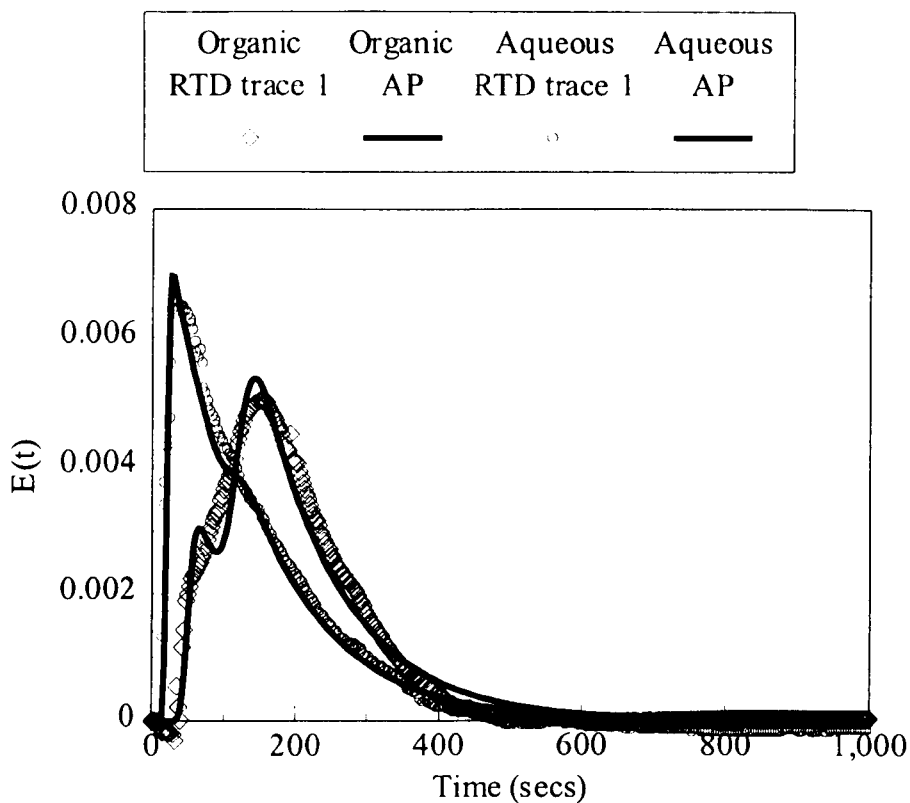


Figure 5.15: Curve fitting Alternative Path Model to Ula Run 5

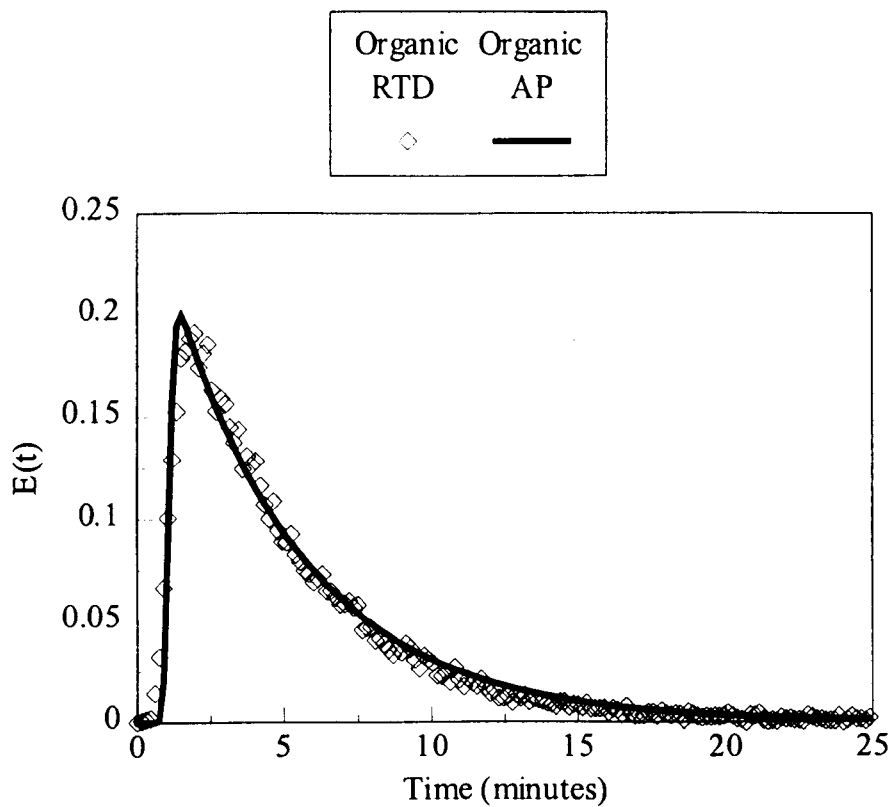


Figure 5.16: Curve fitting Alternative Path Model to Kinneil Run 1

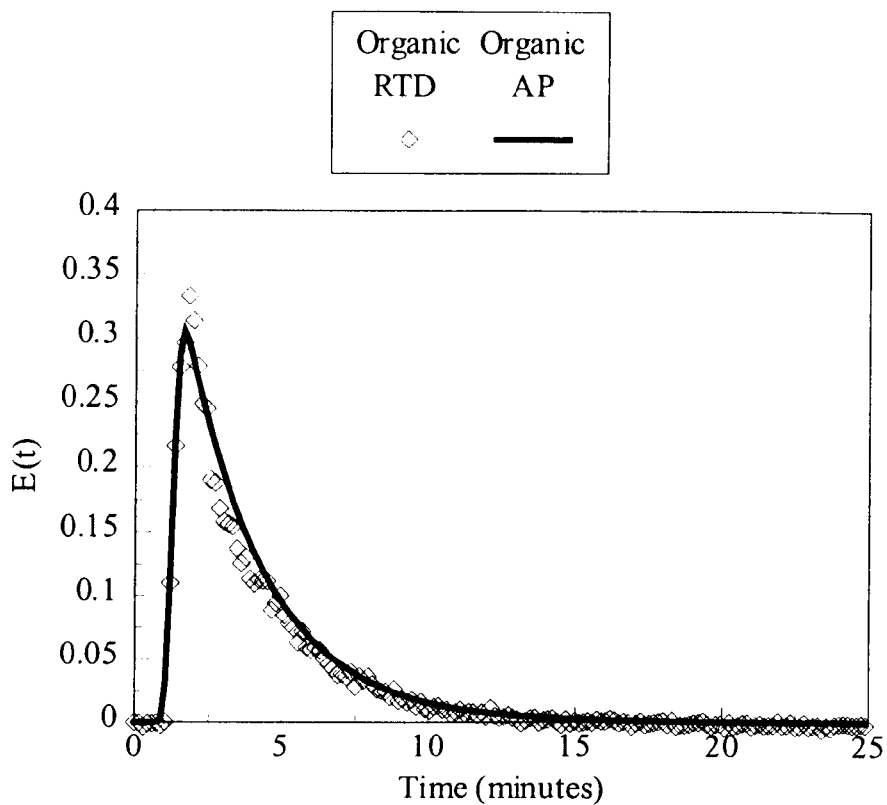


Figure 5.17: Curve fitting Alternative Path Model to Kinneil Run 2

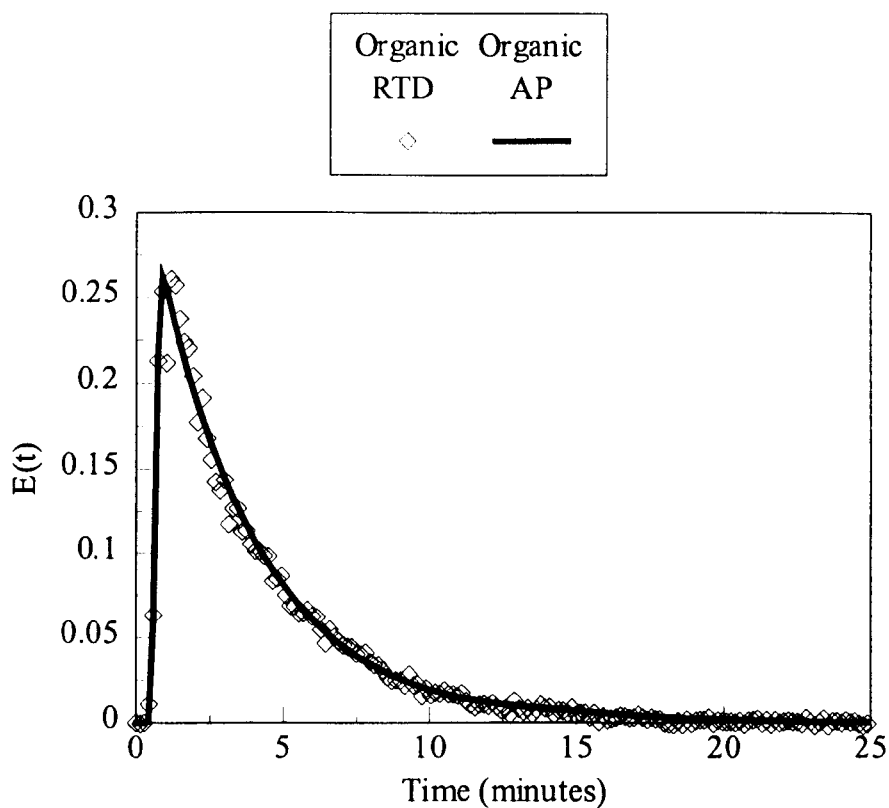


Figure 5.18: Curve fitting Alternative Path Model to Kinneil Run 3

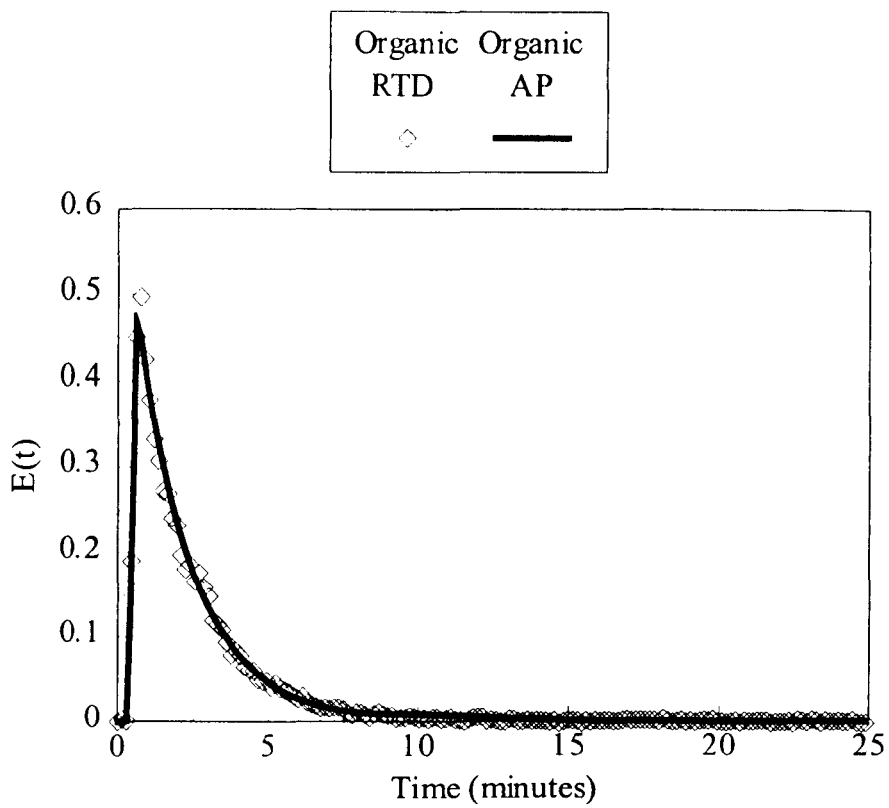


Figure 5.19: Curve fitting Alternative Path Model to Kinneil Run 4

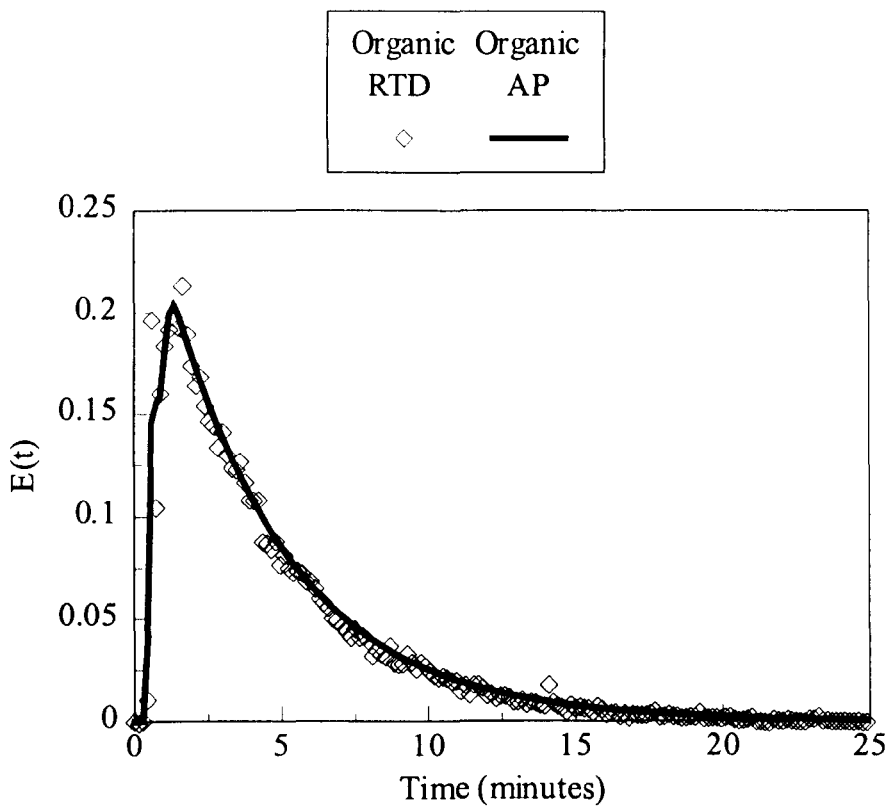


Figure 5.20: Curve fitting Alternative Path Model to Kinneil Run 5

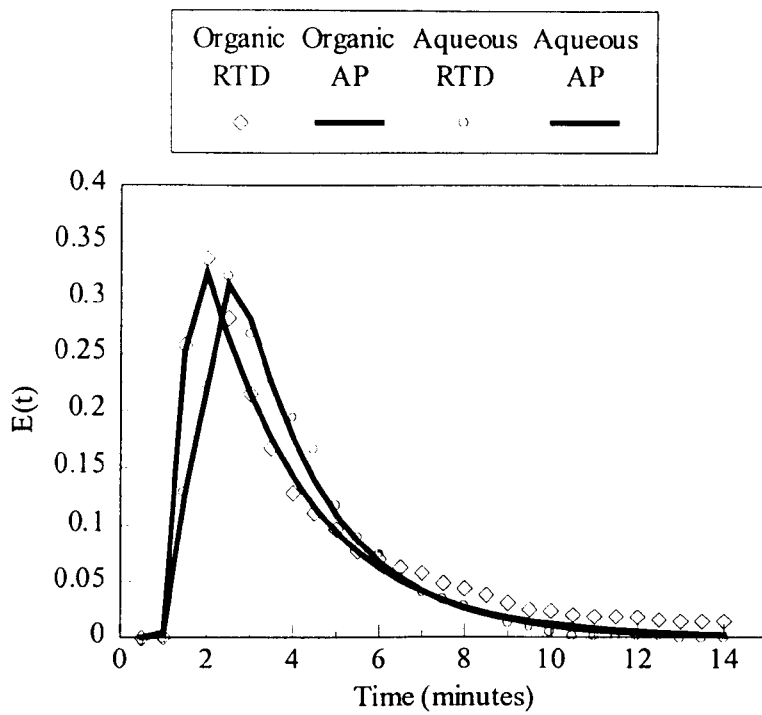


Figure 5.21: Curve Fitting Alternative Path Model to Magnus Run 1

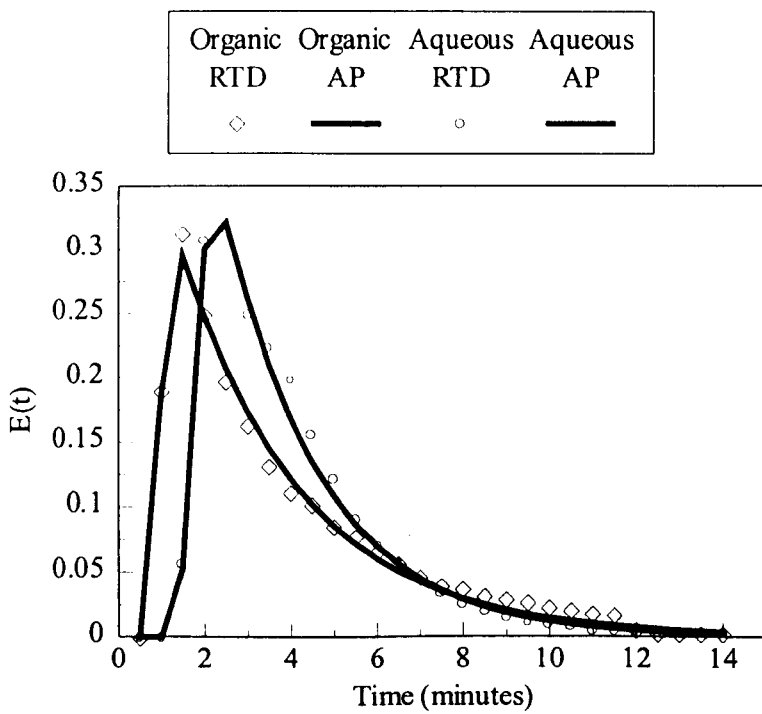


Figure 5.22: Curve Fitting Alternative Path Model to Magnus Run 2

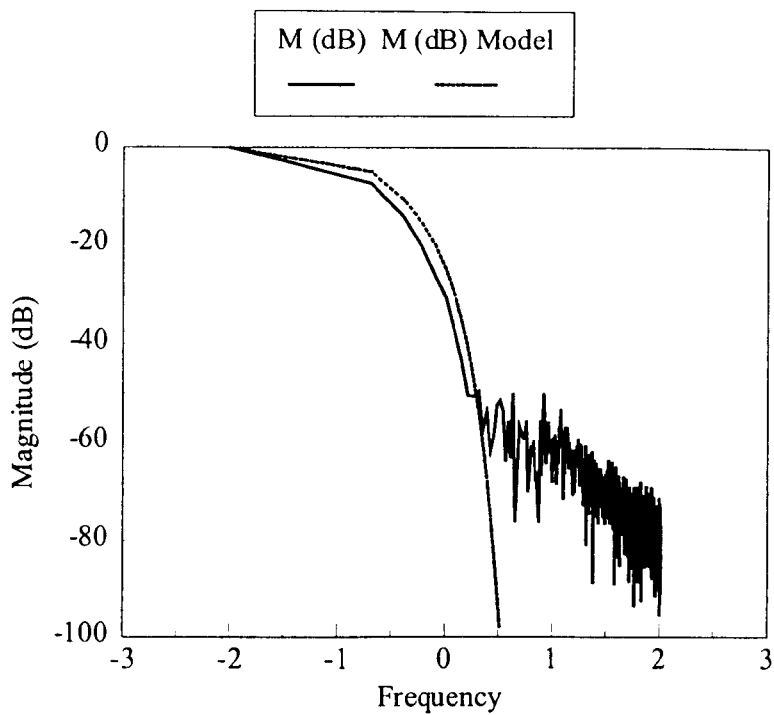


Figure 5.23: Magnitude Plot for Milne Run 3 Organic Tracer

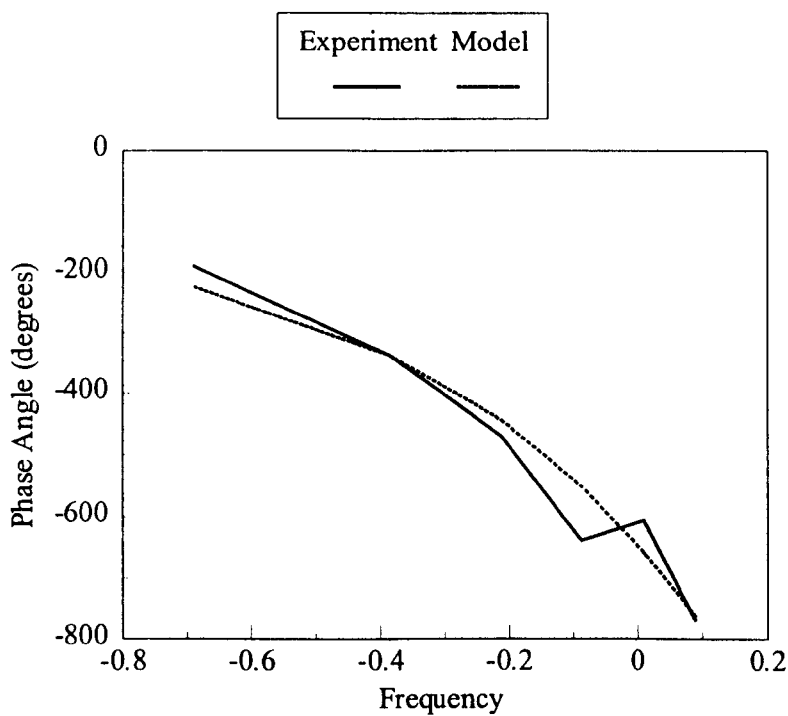


Figure 5.24: Phase Angle Plot for Milne Run 3 Aqueous Tracer

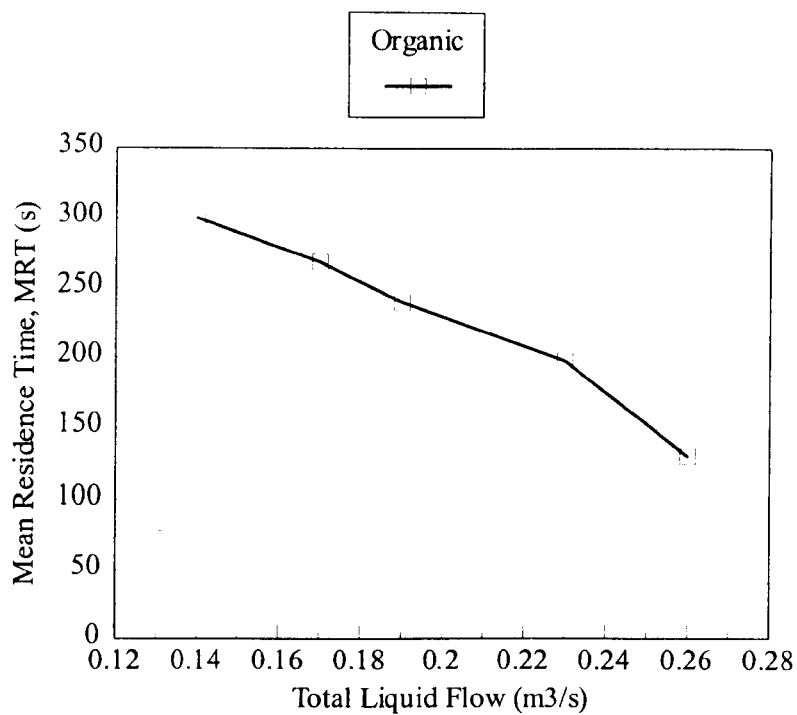


Figure 5.25: Kinneil: Variation of MRT with Liquid Flow Rate.

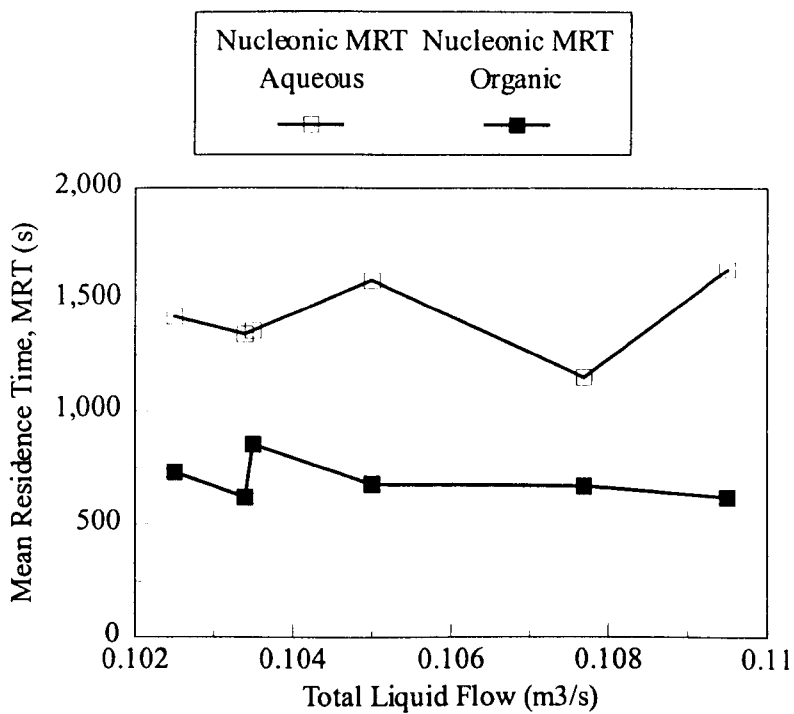


Figure 5.26: Milne Point: Variation of MRT with Liquid Flow Rate.

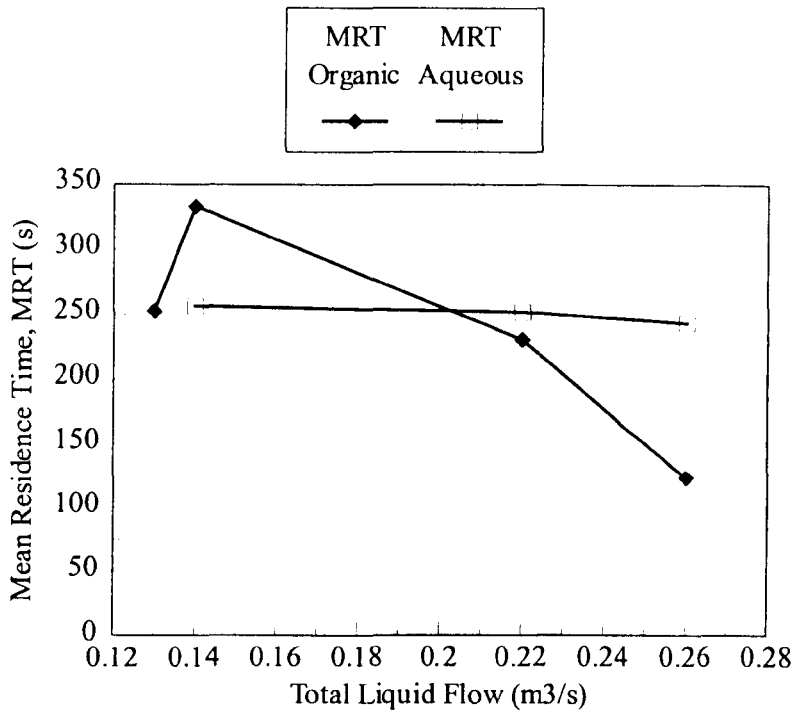


Figure 5.27: Ula: Variation of MRT with Liquid Flow Rate.

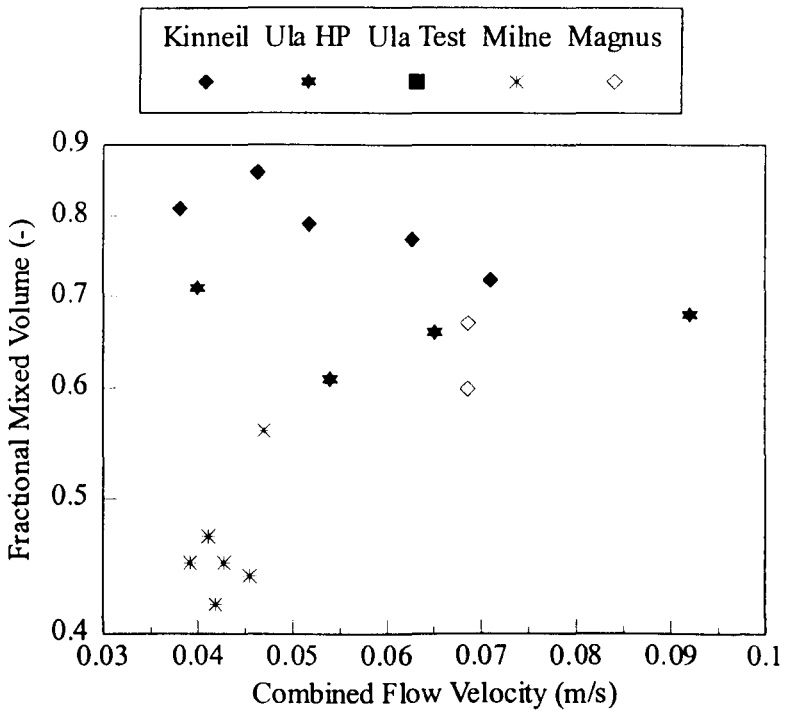


Figure 5.28: Variation of Fractional Mixed Volume

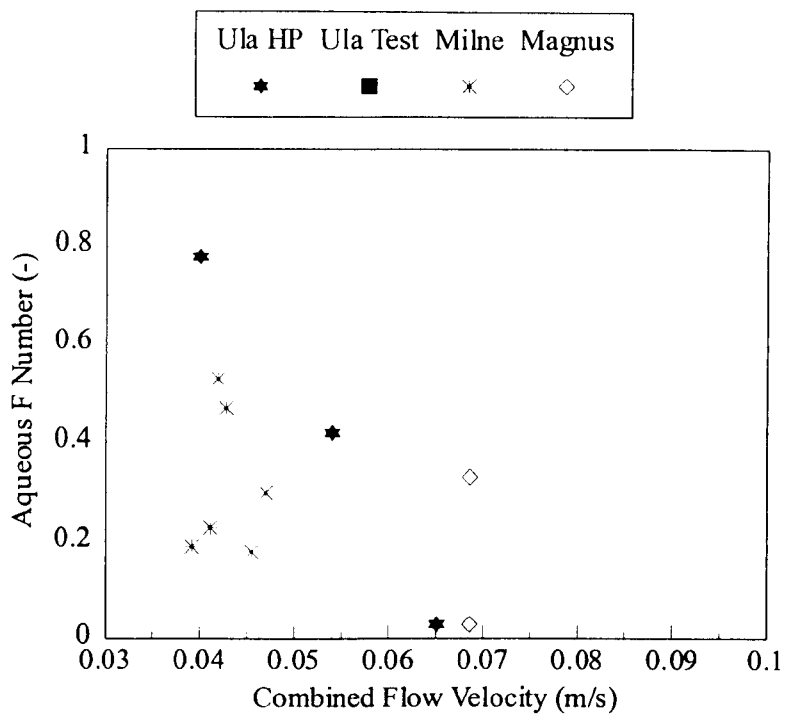


Figure 5.29: Variation of Aqueous Phase F Number with Flow

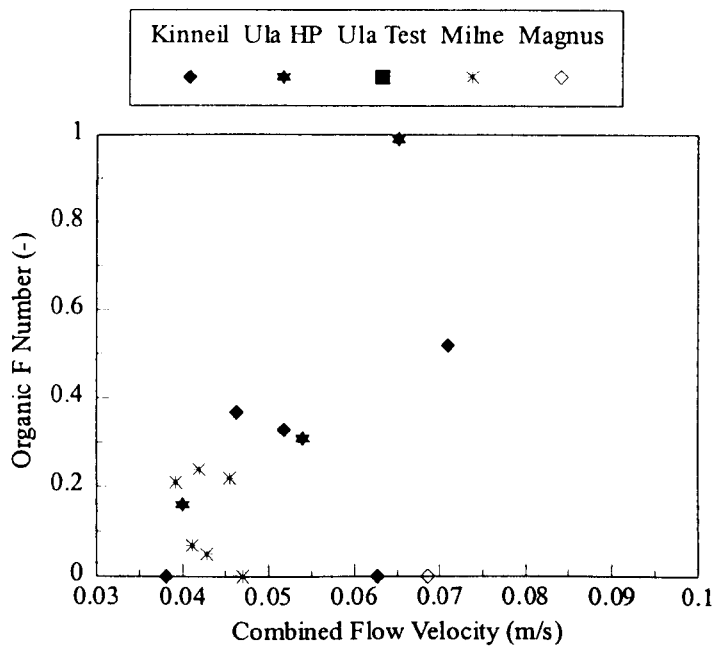


Figure 5.30: Variation of Organic Phase F Number with Flow

5.5 CONCLUSIONS

A transfer function based model of a pilot scale separator has been developed and tested against field data supplied by BP Exploration. The model chosen, the Alternative Path Model, consists of a large mixer at the inlet followed by two parallel paths. The time constant and fraction of flow through each path can be altered which allows reproduction of features of the field Residence Time Distribution curves such as secondary peaks.

The fit obtained from the Alternative Path Model has been found to be excellent. Some other parameters have been derived from the model to characterise the system. Fractional Mixed Volume is the fraction of the volume of the tank that is taken by the inlet mixing zone and can be used as a measure of overall performance. The vessels which have perforated flow spreading baffles installed have lower values of this parameter than empty ones. The F number is a measure of the prominence of any secondary peaks present on the Residence Time Distribution curve and is an indication of the presence of dead zones and recirculatory effects. F numbers have been found to be highest at low water flow rates and high oil flow rates.

TABLE 5.2: BP MILNE POINT MODELLING SUMMARY

RUN NUMBER	INJECTION TYPE	1	2	3	4	5	6
Oil Flow (m3/s)		7.25E-02	7.62E-02	7.36E-02	6.99E-02	7.38E-02	7.05E-02
Water Flow (m3/s)		3.31E-02	3.33E-02	3.35E-02	3.66E-02	3.66E-02	3.20E-02
Water cut (vol %)		31.4	30.4	31.3	34.4	33.2	31.2
Transit Time (s)	Aqueous	854	533	660	808	1036	687
Transit Time (s)	Organic	443	559	476	476	414	428
APM PARAMETERS							
INLET, τ_{1a}	Aqueous	594.21	365.84	386.62	397.37	576.63	366.15
BULK 1, N.τ_{2a}	Aqueous	499.95	497.39	440.91	533.22	477.00	550.94
BULK 2, N.τ_{3a}	Aqueous	2641.35	1962.94	2097.77	2103.69	593.88	1989.17
f	Aqueous	0.12	0.16	0.05	0.10	0.79	0.09
F	Aqueous	0.53	0.47	0.18	0.30	0.19	0.23
Alternative Path Model MRT	Aqueous	1360	1096	909	1088	1146	1043
Nucleonic MRT	Aqueous	1585	1632	1152	1343	1359	1421
INLET, τ_{1o}	Organic	219.63	234.90	213.67	255.57	254.31	338.24
BULK 1, N.τ_{2o}	Organic	268.52	161.3	215.39	209.06	308.92	244.73
BULK 2, N.τ_{3o}	Organic	733.77	203.49	312.45	0	842.70	1068.09
f	Organic	0.14	0.18	0.48	0	0.12	0.02
F	Organic	0.24	0.05	0.22	0.00	0.21	0.07
Alternative Path Model MRT	Organic	553	403	475	464	629	599
Nucleonic MRT	Organic	680	621	668	622	854	730
Nucleonic MRT/TT	Aqueous	1.96	1.91	1.76	1.96	1.31	2.67
Nucleonic MRT/TT	Organic	1.43	1.40	1.40	1.46	2.06	1.31
VOLUMES							
CSTR Vol from APM (m3)		35.61	30.08	28.68	32.42	39.88	35.56
Total Vol from APM (m3)		85.10	67.27	65.46	72.34	88.42	75.66
Actual CSTR Vol (m3)		13.86	13.86	12.68	12.68	13.86	13.86
Actual Total Vol (m3)		86.58	86.58	79.25	79.25	86.58	86.58
Fractional Mixed Volume, D	Expt	0.42	0.45	0.44	0.45	0.45	0.47
Fractional Mixed Volume, D	Calc	0.16	0.16	0.16	0.16	0.16	0.16

TABLE 5.3: BP ULA MODELLING SUMMARY						
Run Number	INJECTION TYPE	1	2	3	4	5
Oil Flow (m3/s)		0.12	0.10	0.12	0.12	0.03
Water Flow (m3/s)		0.10	0.04	0.14	0.01	0.06
Water Cut (vol %)		45.5	28.6	53.8	7.7	64.1
Transit Time (s)	Aqueous	110	190	240	N/A	140
Transit Time (s)	Organic	190	280	120	215	54
APM PARAMETERS						
INLET, τ_{1a}	Aqueous	175.50	133.79	144.09	N/A	116.41
BULK 1, $N\tau_{2a}$	Aqueous	73.79	68.90	69.50	N/A	21.08
BULK 2, $N\tau_{3a}$	Aqueous	399.97	404.70	258.33	N/A	114.25
f	Aqueous	0.01	0.16	0.15	N/A	0.12
F	Aqueous	0.03	0.78	0.42	N/A	0.53
APM MRT	Aqueous	251.45	256.48	242.79	N/A	149.10
Nucleonic MRT	Aqueous	268	314	284	N/A	178
INLET, τ_{1o}	Organic	144.97	255.29	78.00	165.98	113.37
BULK 1, $N\tau_{2o}$	Organic	42.73	67.00	34.62	38.49	50.81
BULK 2, $N\tau_{3o}$	Organic	400.55	122.08	250.00	450.00	120.64
f	Organic	0.12	0.20	0.05	0.12	0.59
F	Organic	0.99	0.16	0.31	1.28	0.81
APM MRT	Organic	229.93	333.31	123.39	252.47	205.72
Nucleonic MRT	Organic	142	347	162	253	173
Nucleonic MRT/TT	Aqueous	2.44	1.65	1.10	N/A	1.11
Nucleonic MRT/TT	Organic	0.74	1.24	1.35	1.18	3.20
VOLUMES						
Total Vessel Volume (m3)		N/A	N/A	50.98	50.98	17.72
Model Vessel Volume (m3)		53.37	44.12	49.84	N/A	15.81
Model CSTR Volume (m3)		35.37	31.10	30.17	N/A	10.76
Fractional Mixed Volume, D		0.66	0.71	0.61	N/A	0.68

TABLE 5.4: BP KINNEIL MODELLING SUMMARY						
Run Number		1	2	3	4	5
RESIDENCE TIMES IN SECONDS	INJECTION TYPE					
Gas Flow (m3/s)		1.57	2.36	1.79	3.06	2.18
Combined Liquid Flow (m3/s)		0.14	0.23	0.19	0.26	0.17
Transit Time (s)	Organic	322	196	237	173	266
APM PARAMETERS						
INLET, τ_{10}	Organic	273.00	160.44	208.03	112.18	247.54
BULK 1, $N\tau_{20}$	Organic	66.00	47.56	40.50	28.46	29.98
BULK 2, $N\tau_{30}$	Organic	66.00	47.56	784.05	576.17	63.97
f	Organic	0	0	0.02	0.03	0.32
F	Organic	0	0	0.33	0.52	0.37
APM MRT	Organic	339.00	208.00	261.71	155.52	288.56
Nucleonic MRT	Organic	300.00	198.00	240.00	130.00	269.00
MRT/TT	Organic	1.05	1.06	1.10	0.90	1.09
VOLUMES						
CSTR Vol from APM (m3)		38.22	36.90	39.53	29.17	42.08
Total Vol from APM (m3)		47.46	47.84	49.73	40.44	49.05
Actual CSTR Vol (m3)		6.21	6.21	6.21	6.21	6.21
Actual Total Vol (m3)		44.85	44.85	44.85	44.85	44.85
Fractional Mixed Volume, D	expt	0.81	0.77	0.79	0.72	0.86
Fractional Mixed Volume, D	calc	0.14	0.14	0.14	0.14	0.14

TABLE 5.5: BP MAGNUS MODELLING SUMMARY			
Run Number	INJECTION TYPE	1	2
Oil Flow (m3/s)		0.107	0.109
Water Flow (m3/s)		0.064	0.062
Water Cut (vol %)		37.43	36.26
Transit Time (s)	Aqueous	186	200
Transit Time (s)	Organic	122	115
APM PARAMETERS			
INLET, τ_{1a}	Aqueous	126.4	136.3
BULK 1, $N\tau_{2a}$	Aqueous	84.4	105.5
BULK 2, $N\tau_{3a}$	Aqueous	131.3	118.7
f	Aqueous	0.59	0.20
F	Aqueous	0.33	0.03
APM MRT	Aqueous	226	242.1
Nucleonic MRT	Aqueous	194	191
INLET, τ_{1o}	Organic	146.2	169.7
BULK 1, $N\tau_{2o}$	Organic	85.3	59.2
BULK 2, $N\tau_{3o}$	Organic	0.0	0.0
f	Organic	0.0	0.0
F	Organic	0.0	0.0
APM MRT	Organic	231.5	229.0
Nucleonic MRT	Organic	191	191
Nucleonic MRT/TT	Aqueous	1.04	0.97
Nucleonic MRT/TT	Organic	1.57	1.66
VOLUMES			
Total Vessel Volume (m3)		N/A	N/A
Model Vessel Volume (m3)		39.3	40.0
Model CSTR Volume (m3)		23.7	27.0
Fractional Mixed Volume, D		0.60	0.67

Chapter 6

MEASUREMENT OF RESIDENCE TIME DISTRIBUTIONS IN A PILOT SCALE LIQUID-LIQUID SEPARATOR

6.1 INTRODUCTION

The Residence Time Distribution data obtained by BP Exploration from existing field separators is very useful but limited in quantity due to operational restrictions upon the range and frequency of the experiments. In order to develop a good understanding of the fluid dynamics of a primary separator, a 1/5th scale model of a primary separator was constructed and Residence Time Distributions were obtained for a range of flow conditions and tank internal configurations.

The choice of internal configurations to be examined was dictated by the existing types of additional equipment employed within field separators. However, rather than try to produce any particular internals as there can be a wide variation of detail, simple representative types were selected. Internals can act to accelerate the fluid, by either diverting or restricting the flow path. This occurs for example in any structured packing or wave plates. Alternatively, internals can cause quiescent zones, for example side baffles or weirs. Two types of internal which have been chosen to be examined in these studies are side baffles and dip type baffles which extend into the liquid pool. The details of the flow facility and the specifications of the tank and internals are described in section 3.2.3.

In order to measure the Residence Time Distribution in the vessel, a dye injection technique was used in conjunction with a Jenway 6300 on-line spectrophotometer. The dyes chosen were either oil or water soluble, depending on which phase was to be investigated.

6.2 EXPERIMENTAL

Details of the experiments performed on the separator vessel are listed below, together with calibrations for the orifice plates and Residence Time Distribution

6.2.1 Flow Measurement

The flow rates of the liquid phases were metered by orifice plates, as described in Chapter 3. Plates of different orifice sizes were employed according to the flow rates to be measured.

6.2.2 Residence Time Distribution Measurement Technique

In order to measure the Residence Time Distribution of the separator tank it is necessary to choose a tracer that can be added at the tank inlet and whose progress can be monitored at the respective tank outlet. Radiotracers as used in industry were deemed unsuitable due to the hazard of radiation build-up in a closed loop system. Particulate tracers were considered too difficult to remove from the flow loop at the tank exits and were likely to intersperse between the phases. Addition of salt and monitoring conductivity was considered but this technique is only applicable to the aqueous phase. Therefore the best option appeared to be a colorimetry based technique where an oil or water soluble dye would be injected at the inlet and then the dye concentration at the respective outlet would be monitored. The instrument chosen to measure the outlet dye concentration was a Jenway 6300 spectrophotometer, which could be connected directly to an IBM compatible PC to

allow on-line measurement. The sampling system is described in greater detail in Section 3.2.3.

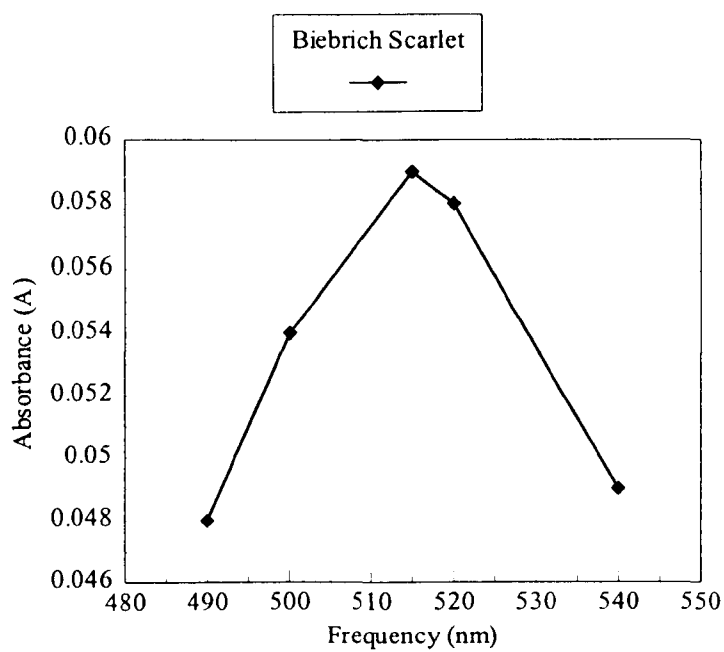


Figure 6.1: Frequency Scan for Biebrich Scarlet

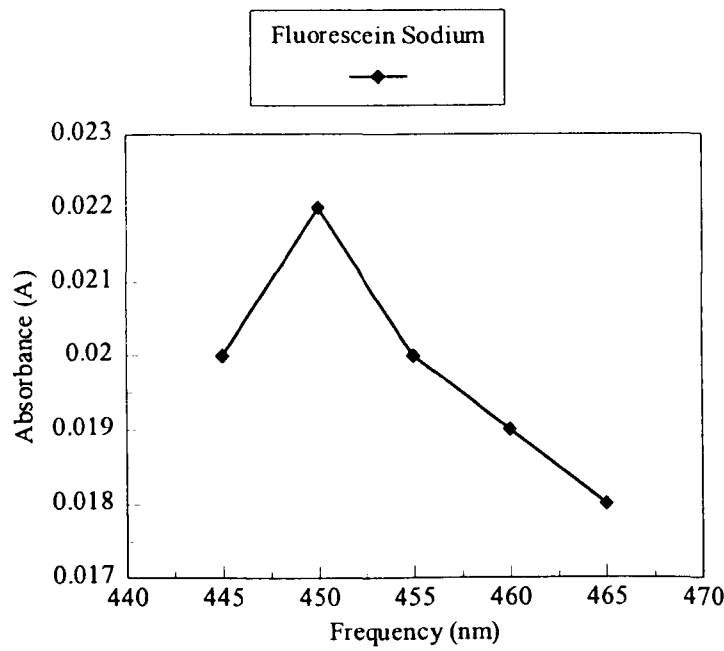


Figure 6.2:Frequency Scan for Fluorescein Sodium

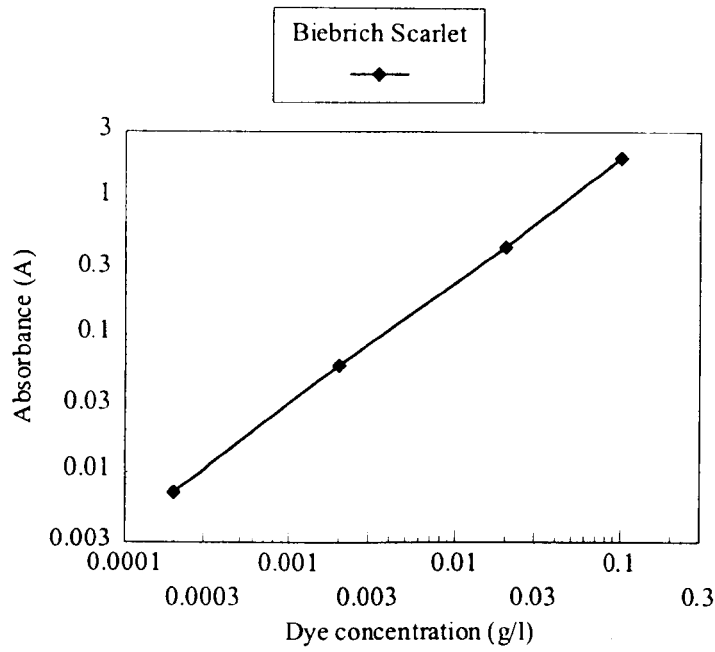


Figure 6.3: Calibration of Instrument for Organic Tracer

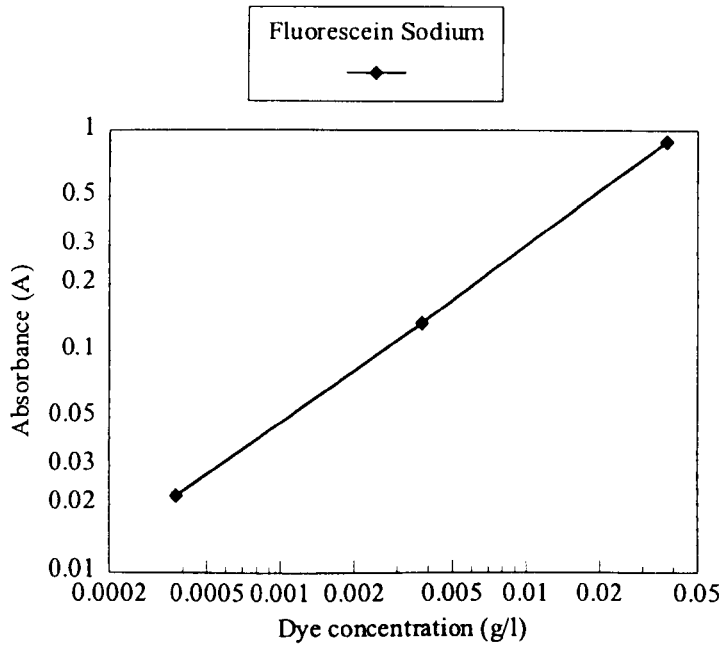


Figure 6.4: Calibration of Instrument for Aqueous Tracer

The choice of which dyes could be used as tracers was dictated by two requirements. The dyes had to be soluble in one phase only and must not stain any of the materials of construction in the flow loop. In order to test for this, concentrated solutions of

several oil and water soluble dyes were produced and samples of different types of plastics used in the loop, namely acrylic resin and PVC, were soaked in the solutions for a fortnight. A small amount of kerosene was added to the water soluble dye samples and vice-versa to check for any cross-solubility. The dyes found most suitable for the tracers on the basis of these tests were Biebrich Scarlet R for the organic phase and Fluorescein Sodium for the aqueous phase. A trial solution of each of these dyes was then tested in the spectrophotometer and the frequency range was scanned in order to obtain the greatest sensitivity. The results of the frequency scans can be seen in Figures 6.3 and 6.4 below. The peak frequencies were found to be 515nm for the organic tracer and 450nm for the aqueous tracer. The instrument was then calibrated for different concentrations of each dye (Figures 6.5 and 6.6).

The calibration curves show that the response of the instrument with concentration is linear and hence obeys Beers' law. Applying linear fits to both these curves yields the following result:

$$c_o = 0.0516 A \quad (5.1)$$

$$c_a = 0.0421 A \quad (5.2)$$

Where c is the concentration of tracer in g/l and A is the Absorbance. The constant of proportionality is equal to the constant due to the light wavelength multiplied by the path length of the flow cell. This calibration allows a mass balance to be performed on the tracer curves, which provides a useful check on the measurement technique.

In order to have confidence that the Residence Time Distribution obtained from the spectrophotometer was a true representation of the system, the volume of the flow system was calculated in an attempt to gauge any delay in the response of the instrument. The flow cells used had a total volume of 0.5 cm^3 each and the length of tubing from the sample point to the flow cell was 30 cm, of a diameter of approximately 2mm. In order to sample every second, it is necessary to sample at a flow rate above $0.5 \text{ cm}^3/\text{s}$ in order to refresh the cell every second. This will result in an instrument lag of about 1.5s, which can be considered as practically instantaneous when dealing with a tank of mean residence times of the order of 50-60 seconds. The flow rate through the cell was monitored throughout the measurement procedure and measured at the beginning and end of each set of runs.

The experimental Residence Time Distribution will require deconvolution with the inlet pulse of tracer unless the inlet pulse is of short enough duration to be considered as a perfect delta function. The spectrophotometer was installed at the inlet section and the Residence Time Distribution of the inlet pulses were recorded for a number of different flow rates of aqueous phase or organic phase separately, due to the difficulty of sampling from a two-phase dispersion. The width of the inlet pulses was compared with the outlet pulses and a FORTRAN convolution program was developed to determine whether or not the Residence Time Distribution data from the tank would need further processing.

6.2.3 Test Conditions

Residence Time Distributions were obtained for the range of flow conditions and internal configurations shown in Table 6.1 below. In addition to the dip and side

baffles, two different weir heights and positions of the oil-water interface were used. Both organic and aqueous Residence Time Distribution's were obtained for each run. The flow rates of oil and water were chosen on the basis of either keeping the total flow rate of oil and water constant and varying the fractional flow of each phase, or keeping the flow rate of one phase constant and varying the other. The total number of runs that could be performed was limited by the build-up of dye in the flow loop. The concentration of tracer injected in later runs was therefore increased and this seemed to compensate adequately for the build up.

Table 6.1: Flow Conditions and Tank Configurations

Run No	Oil Flow	Water Flow	Water Cut	Weir Ht.	Liq-Liq Interface	Perf. Plate	Baffles
	Rate (kg/s)	Rate (kg/s)	(Vol %)	H=0.3 m	H=0.23 m	S=20 mm holes	N=no baffles
				L=0.22 m	L=0.17 m	L=50 mm holes	S=Side baffles
							D=Dip baffle
1.1	2.1	1.5	0.36	L	L	L	N
1.2	2.1	2.5	0.49	L	L	L	N
1.3	2.1	3.5	0.57	L	L	L	N
1.4	2.1	3.9	0.60	L	L	L	N
2.1	3.34	1.5	0.26	L	L	L	N
2.2	3.34	2.5	0.37	L	L	L	N
2.3	3.34	3.5	0.46	L	L	L	N
2.4	3.34	3.9	0.48	L	L	L	N
3.1	1.5	2.5	0.57	L	L	L	N
3.2	2.5	1.5	0.32	L	L	L	N
3.3	3	1	0.21	L	L	L	N
4.1	2.1	3.9	0.60	L	L	L	N
4.2	3	3	0.44	L	L	L	N
4.3	4	2	0.29	L	L	L	N
5.1	2.1	3.9	0.60	L	L	L	S
5.2	3	3	0.44	L	L	L	S
5.3	4	2	0.29	L	L	L	S
6.1	1.5	2.5	0.57	L	L	L	S
6.2	2.5	1.5	0.32	L	L	L	S
6.3	3	1	0.21	L	L	L	S

Run No	Oil Flow	Water Flow	Water Cut	Weir Ht.	Liq-Liq Interface	Perf. Plate	Baffles
7.1	2.1	3.9	0.60	H	H	L	S
7.2	3	3	0.44	H	H	L	S
7.3	4	2	0.29	H	H	L	S
8.1	1.5	2.5	0.57	H	H	L	S
8.2	2.5	1.5	0.32	H	H	L	S
8.3	3	1	0.21	H	H	L	S
9.1	2.1	3.9	0.60	H	L	L	S
9.2	3	3	0.44	H	L	L	S
9.3	4	2	0.29	H	L	L	S
10.1	1.5	2.5	0.57	H	L	L	S
10.2	2.5	1.5	0.32	H	L	L	S
10.3	3	1	0.21	H	L	L	S
11.1	2.1	1.5	0.36	L	L	S	N
11.2	2.1	3.9	0.60	L	L	S	N
11.3	3	3	0.44	L	L	S	N
11.4	1.5	2.5	0.57	L	L	S	N
11.5	3	1	0.21	L	L	S	N
12.1	2.1	1.5	0.36	H	L	S	N
12.2	2.1	3.9	0.60	H	L	S	N
12.3	3	3	0.44	H	L	S	N
12.4	1.5	2.5	0.57	H	L	S	N
12.5	3	1	0.21	H	L	S	N
13.1	2.1	1.5	0.36	H	H	S	N
13.2	2.1	3.9	0.60	H	H	S	N
13.3	3	3	0.44	H	H	S	N
13.4	1.5	2.5	0.57	H	H	S	N
13.5	3	1	0.21	H	H	S	N
14.1	2.1	1.5	0.36	L	L	S	D
14.2	2.1	3.9	0.60	L	L	S	D
14.3	3	3	0.44	L	L	S	D
14.4	1.5	2.5	0.57	L	L	S	D
14.5	3	1	0.21	L	L	S	D
15.1	2.1	1.5	0.36	H	H	S	D
15.2	2.1	3.9	0.60	H	H	S	D
15.3	3	3	0.44	H	H	S	D
15.4	1.5	2.5	0.57	H	H	S	D
15.5	3	1	0.21	H	H	S	D
16.1	2.1	1.5	0.36	H	L	S	D
16.2	2.1	3.9	0.60	H	L	S	D
16.3	3	3	0.44	H	L	S	D
16.4	1.5	2.5	0.57	H	L	S	D
16.5	3	1	0.21	H	L	S	D

6.2.4 Experimental Error

The error in the experimental data can be defined as the difference between the true value and the observed value for a single observation, Kline & McClintock (1953). The errors to be considered here are the error in the flow rate measurements, as already discussed in Chapter 4 and tabulated in Table 6.2 below, and the error in the colorimetric measurement technique.

Table 6.2: Uncertainty in Liquid Flow Rates

Kerosene Flow (kg/s)	Uncertainty (%)	Water Flow (kg/s)	Uncertainty (%)
1.5	4.0	1.0	6.6
2.1	2.0	1.5	2.9
2.5	1.4	2.0	1.6
3.0	0.9	2.5	1.0
3.3	0.7	3.0	0.6
4	0.5	3.5	0.5
		3.9	0.3

The error in the colorimetric technique comes from two sources, the resolution of the instrument and the changes in the background reading due to the presence of haze and the build up of dye in the flow loop. The resolution of the instrument is $\pm 0.001A$, which is a small proportion of the error when the haze is considered. The errors in the mass balance are indicative of the effect of the background haze, as the instrument was calibrated using clean liquids. However, the background appeared to be more or less constant through each run. The instrument was left recording until the level of dye was the same before injection or had been constant for 30 seconds. The deviation between the start value and the end value was never more than $0.003A$, and the peak value obtained at the outlet was of the order of $0.05A$. Errors due to the background and the mass balance do not however affect the analysis of the Residence Time Distribution curves as the effect is simply one that compresses or

stretches concentration readings. Upon analysing the curves, the area under the curve is normalised to convert the result to a true Residence Time Distribution and satisfy Equation 2.45. The errors are therefore eliminated from the analysis.

6.3 RESULTS AND DISCUSSION

Measurements of the inlet pulse of dye were made for two water flow rates and one kerosene flow rate in order to verify the speed of response of the measurement technique and to determine whether any deconvolution of the outlet data would be required. The inlet pulses were found to be very sharp and repeatable at all three flow conditions tested and the width of the pulses was found to be no greater than 10-12 seconds at the base (Figures 6.5-6.7). These results were compared against theoretical output from a FORTRAN program, "Convolute", listed in Appendix A6. Convolute allows insertion of an inlet pulse as either a square wave or normal distribution, of which a normal distribution is the most suitable for this system. Figure 6.9 shows an outlet pulse as typical for run 1.4 convoluted with a normal distribution inlet pulse of standard deviation 2 seconds. This pulse is somewhat wider than the actual inlet pulses obtained as shown in Figure 6.8. The difference between the output Residence Time Distributions is negligible, so the data obtained at the tank outlets by the Jenway instrument may be definitely considered as the true Residence Time Distribution and no further processing other than normalising is required.

Tables 5.3 and 5.4 summarise the mean and peak residence times obtained from the Residence Time Distribution curves, together with details of mass balances performed on the tracer injected. The error in the mass balance is seen to differ on

most runs by $\pm 35\%$, which is a very significant discrepancy. In most cases the mass balance indicates that more tracer was detected than actually was injected. This can be explained by the presence of haze in the phase being measured. Haze is very fine droplets of one fluid dispersed in the other and causes the light passing through the flow cell to be obscured and hence the readings over predict the amount of tracer present. Haze was also thought to be responsible for the small amounts of baseline drifting which were noticed on some runs. This problem is unavoidable in such a flow system. It can also be noted, however, that on some runs, less tracer appeared to exit than was injected. This is of more concern and there are two possible explanations for this. Either the Residence Time Distribution was truncated, or some of one phase is carried along with the other and exits through the wrong outlet. At high water rates, it was noticed that the aqueous phase did not coalesce well and there was a thick layer of dispersion between the phases. This layer contained substantial amounts of oil and some was seen to exit through the water outlet. This agrees with the results of the mass balance where less organic tracer is seen to exit at the highest liquid flow rate. It is most likely that the mass balance inconsistencies are due to the effects of haze or carry over, as great care was taken to ensure that the Residence Time Distribution measurements were taken for a sufficient time to ensure that the baseline returned to the level previous to the tracer injection. It is also possible that the build up of tracer in the system may alter the constants in Equations 5.1 and 5.2, but without being able to calibrate the cells on-line, it is not possible to ascertain this.

A selection of the Residence Time Distribution curves measured are shown in Figures 6.10 to 6.27 and show the effect of different internal configurations and flow

rates. The effect of increasing water flow rate at a constant oil flow rate is shown for an empty tank on Figures 6.10 and 6.11. The aqueous Residence Time Distribution curves are shifted to the left upon increasing the water flow. As the flow areas are kept constant, the local flow velocity increases with flow rate and hence the mean residence time (MRT) is reduced. Another noticeable feature is that the curves tend to bunch together at high water flows and there is little difference between the curve obtained for 3.5 and 3.94 kg/s. Conversely, the Residence Time Distribution curves of the organic phase are seen to be shifted to the right with increasing water flow. This is strange behaviour as one would expect the organic phase residence time to be fairly constant. An explanation for this could be that the turbulence in the vessel increases with increasing flow and hence the oil disengages later from the water. As the water occupies more volume than the oil and travels more slowly, the oil residence time will increase.

Figures 6.12 and 6.13 show the behaviour of the Residence Time Distribution curves with changing water cut at a constant total flow rate of 6 kg/s. Use of constant total flow means that the effective Reynolds number in the tank, and hence the fluid dynamics should be similar. Again, the aqueous phase Residence Time Distribution curves shift to the left with increasing water cut which is as expected. However, the organic phase curves shift to the right with increasing water cut, i.e. increasing the water flow rate increases the residence time and the behaviour observed in the previous case (Figure 6.11) is reversed. This suggests that the anomalous behaviour is most likely due to the explanation proposed above of increased transit of oil due to mixing in the water at higher water flow rates.

Similar trends to Figures 6.12 and 6.13 are seen in Figures 6.14 to 6.17, which show the effect of changing water cut at a total flow of 4 kg/s upon the Residence Time Distribution when the tank is equipped with side or dip baffles. Another feature of these curves, which was also observed at 4 kg/s when the tank had no baffles, was the presence of a secondary peak at low water cuts. There is evidence that the settling of oil droplets towards the oil-water interface causes local acceleration which means that the liquid near the interface travels faster than the bulk flow, Davies (1998). This sets up a recirculation in the bulk aqueous phase and explains the presence of a secondary peak. The effect is most likely to be observed when the aqueous phase is travelling most slowly, as the water and organic phases are most distinct and the flow is least turbulent and indeed this is the case.

In addition to different types of baffle, the effect of changing weir and liquid-liquid interface heights was investigated. Figures 6.18 and 6.19 compare the Residence Time Distributions produced by keeping the liquid-liquid interface position constant, but varying the weir height. As expected, the aqueous phase Residence Time Distribution was not greatly affected by this change. The organic phase Residence Time Distribution was seen to shift to the right indicating a longer residence time of oil due to the increased flow area at the higher weir height. In Figures 6.18 to 6.27, the flow condition was a constant flow rate of 4 kg/s.

The effect of moving both the oil-water interface and weir height are illustrated in Figures 6.20 and 6.21. A small shift in the aqueous phase Residence Time Distribution is observed, the most interesting effect being the increase in secondary peak, or recirculation effect, when the liquid-liquid interface is moved upwards. This

is consistent with an increase in dead volume as the total volume occupied by the aqueous phase is increased. The organic phase takes longer to exit at the higher weir height which is again due to increased flow area. Again this effect is most noticeable at the lowest flow rates.

The inclusion of side baffles would be also be expected to increase the dead volume in the tank and this would have the effect of increasing secondary peaks and lengthening residence time. The shape of the baffles means that most of the obstruction to flow will occur in the volume occupied by the organic phase and this is discussed in greater detail in Chapter 7. The effect of side baffles is shown in Figures 6.22 and 6.23 and not much difference in the Residence Time Distribution is observed for the aqueous phase. The organic phase curve is seen to change significantly in shape and have a much longer tail, which is consistent with the above predictions. These observations are also present at other flow conditions although less pronounced.

The effect of the dip baffle would be expected to cause a local acceleration as it acts to constrict the flow area at the point it dips into the liquid pool. This will disrupt any global flow streamlines through the tank and possibly disturb the recirculation effects in the vessel. Figures 6.24 to 6.27 show that the secondary peak on the Residence Time Distribution is altered significantly and the curves are slightly shifted to the left. More investigation is obviously required and all the phenomena presented in this Chapter will be investigated further in Chapter 7, when the mathematical model of the separator described in Chapter 5 is applied to the experimental data.

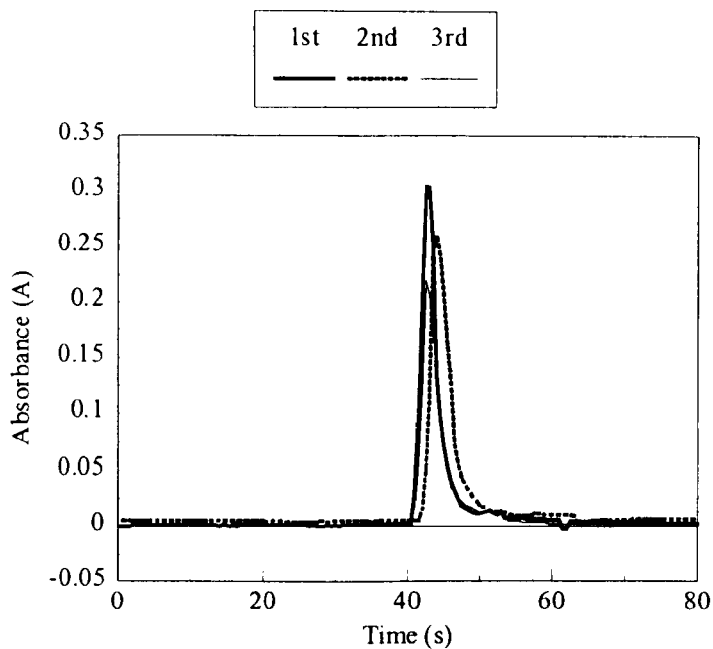


Figure 6.5: Inlet Impulse 1.5 kg/s water

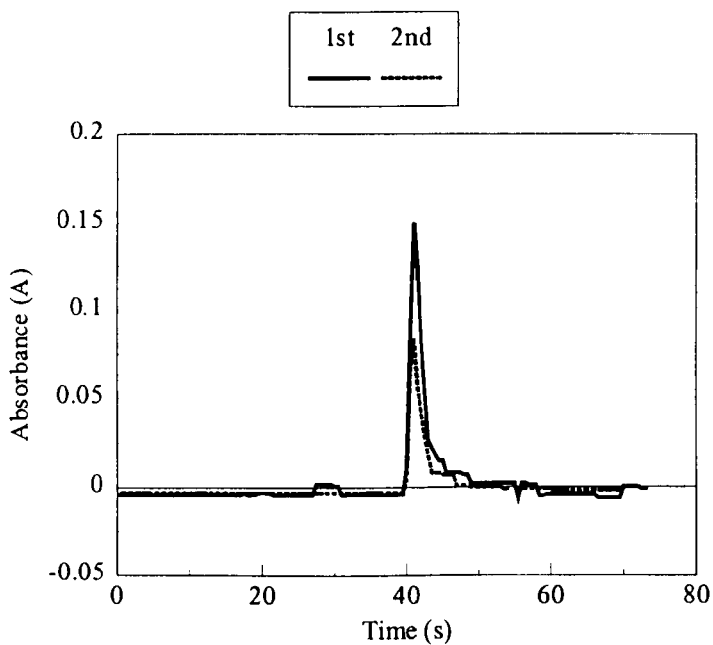


Figure 6.6: Inlet Impulse 4 kg/s water

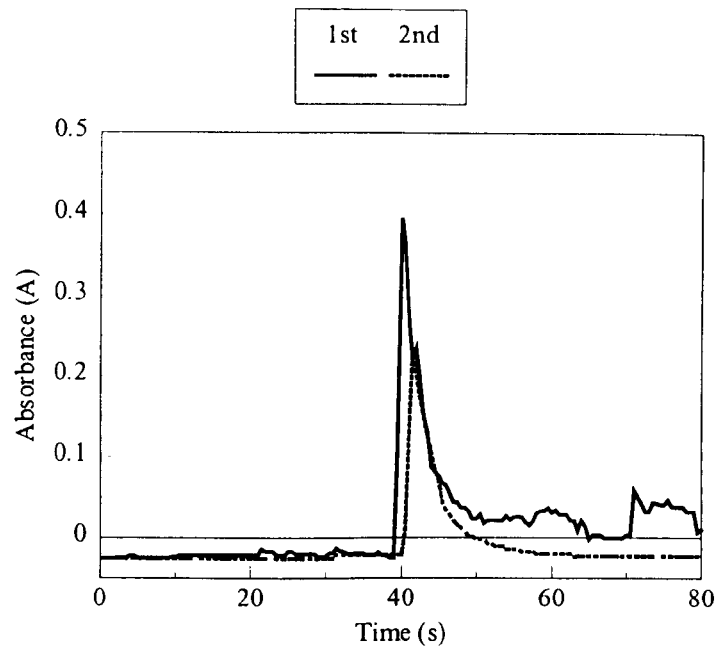


Figure 6.7: Impulse Response 2.1 kg/s oil

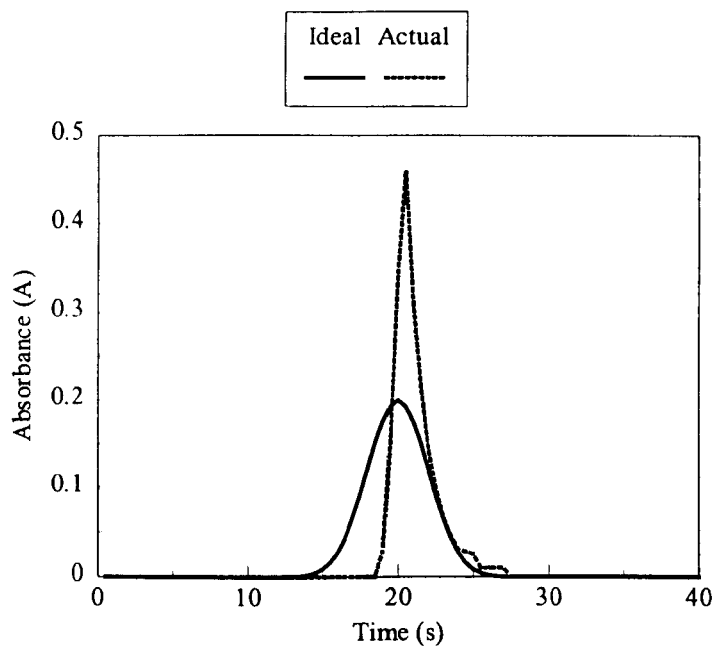


Figure 6.8: Comparing actual input impulse with simulated

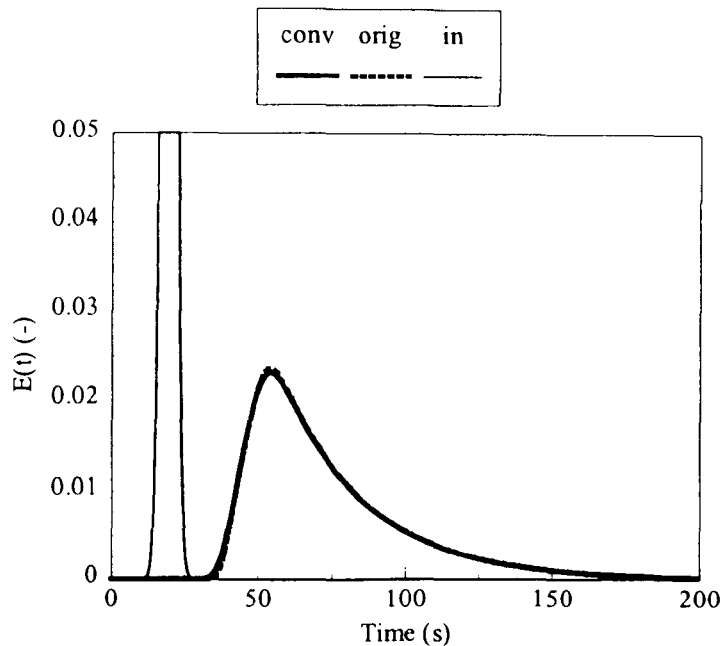


Figure 6.9: Convolution of a Normal Impulse with a Typical Residence Time Distribution

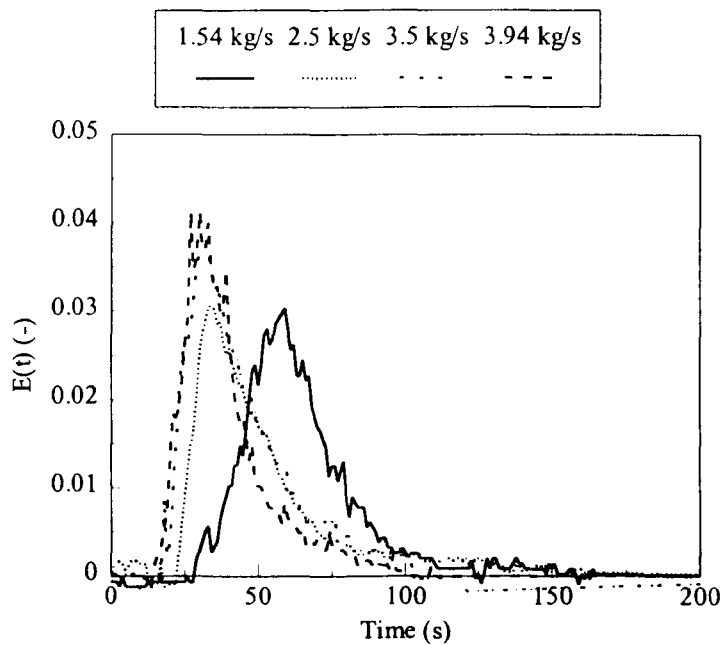


Figure 6.10: Run 1 Empty Tank: Effect of Water Flow Rate on Aqueous Phase Residence Time Distribution

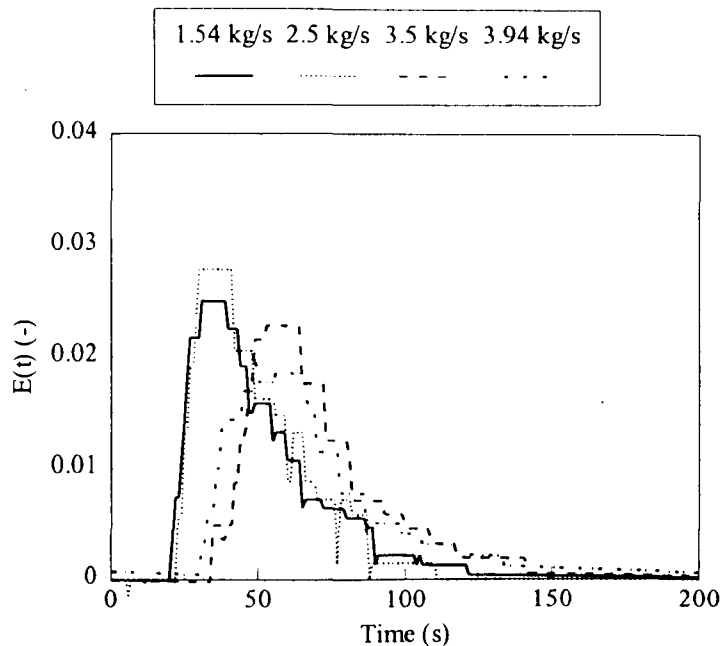


Figure 6.11: Run 1 Empty Tank: Effect of Water Flow Rate on Organic Phase

Residence Time Distribution

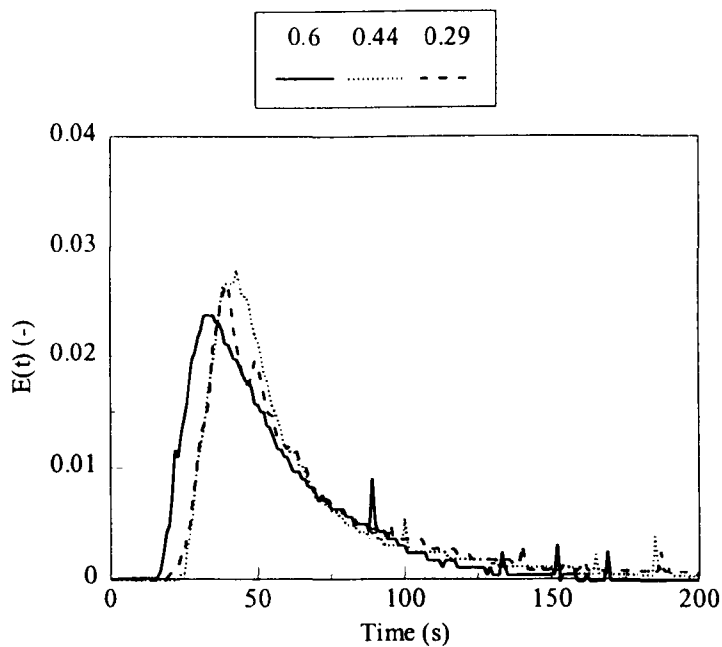


Figure 6.12: Run 4 Empty Tank: Effect of Water Cut on Aqueous Phase Residence

Time Distribution

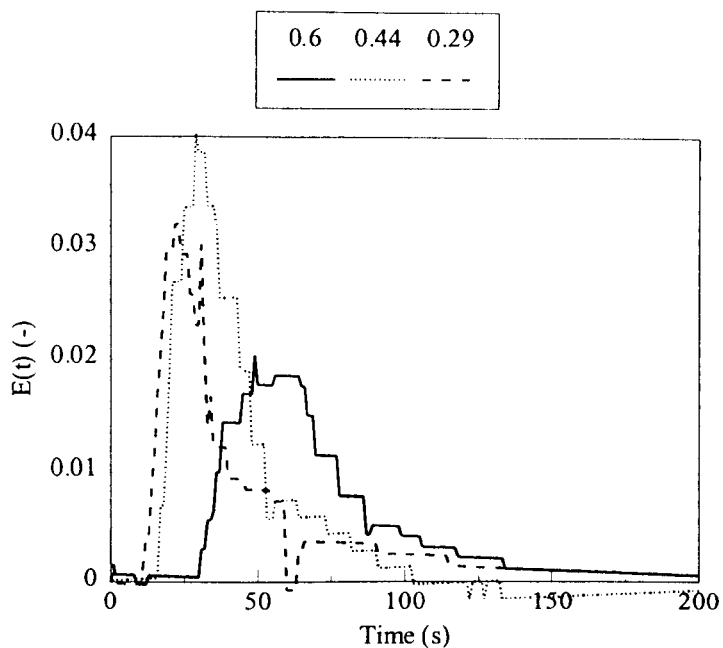


Figure 6.13: Run 4 Empty Tank: Effect of Water Cut on Organic Phase Residence

Time Distribution

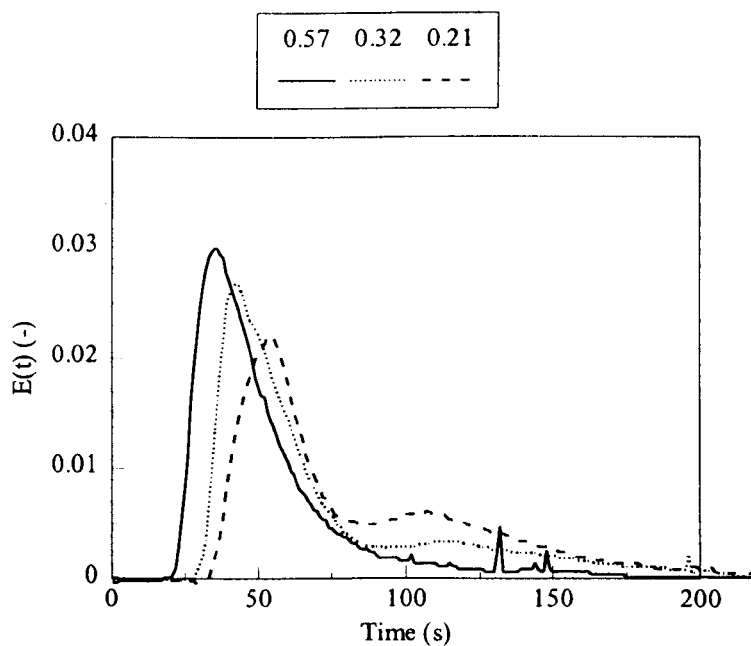


Figure 6.14: Run 6 Side Baffles: Effect of Water Cut on Aqueous Phase Residence

Time Distribution

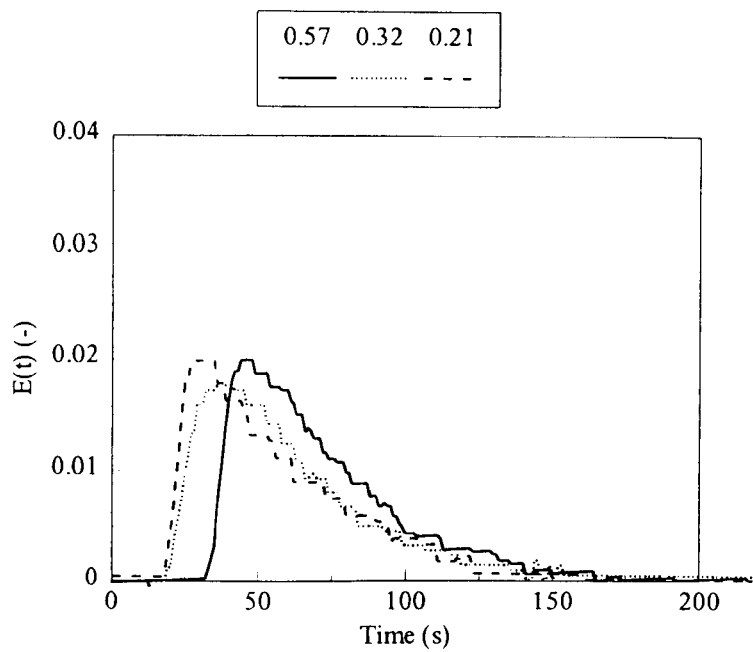


Figure 6.15: Run 6 Side Baffles: Effect of Water Cut on Organic Phase Residence

Time Distribution

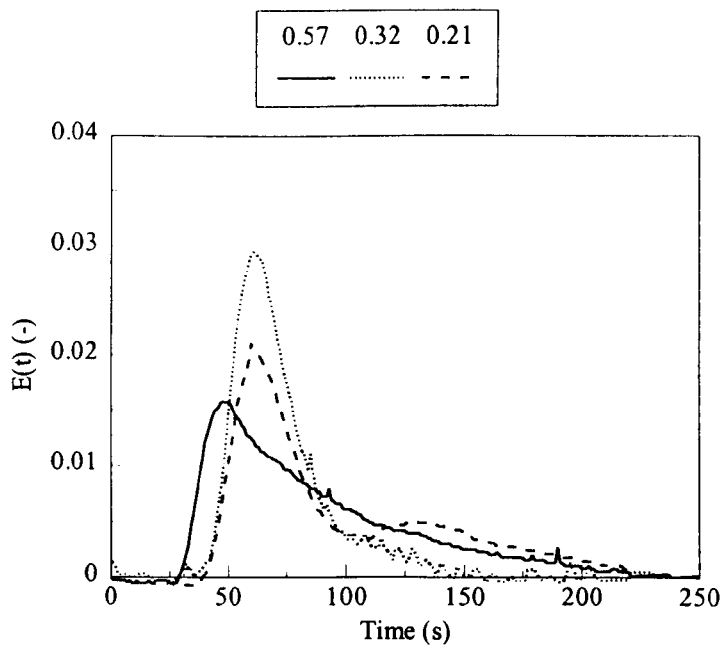


Figure 6.16: Run 14 Dip Baffles: Effect of Water Cut on Aqueous Phase Residence

Time Distribution

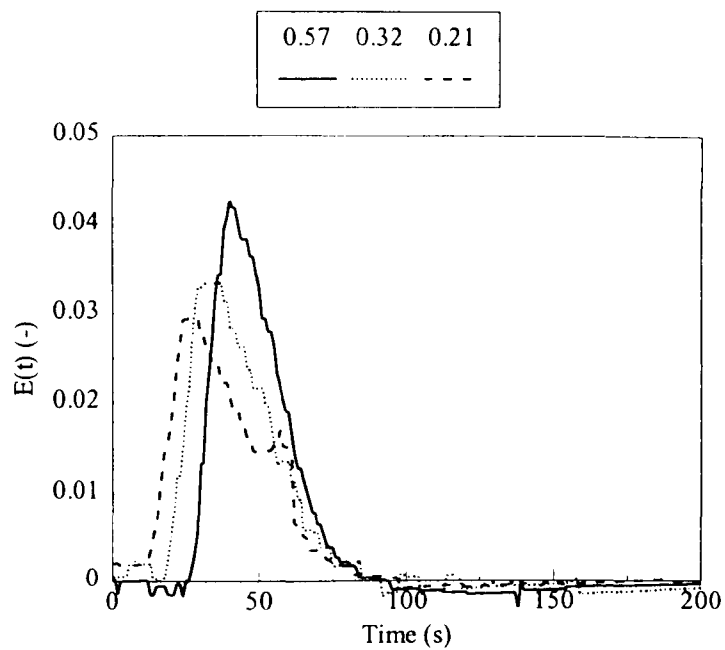


Figure 6.17: Run 14 Dip Baffles: Effect of Water Cut on Organic Phase Residence

Time Distribution

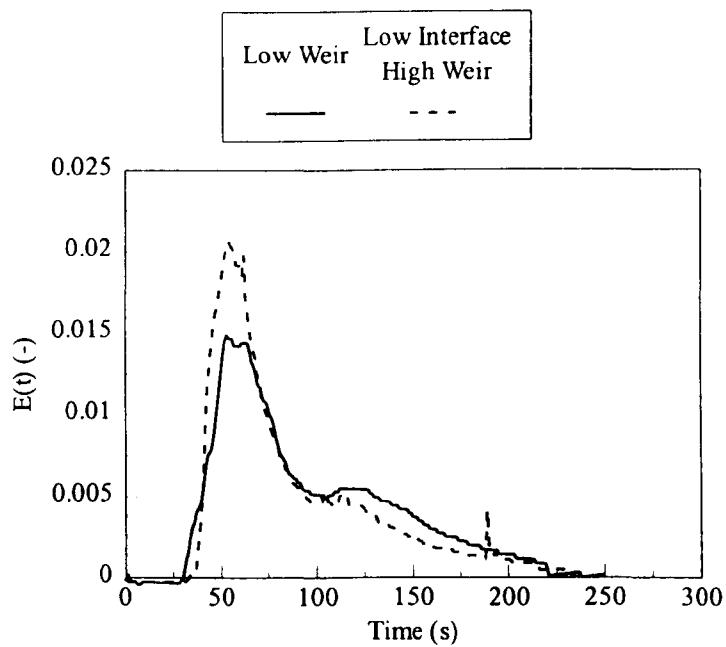


Figure 6.18: Run 11.5: Effect of Changing Weir Height on Aqueous Phase

Residence Time Distribution

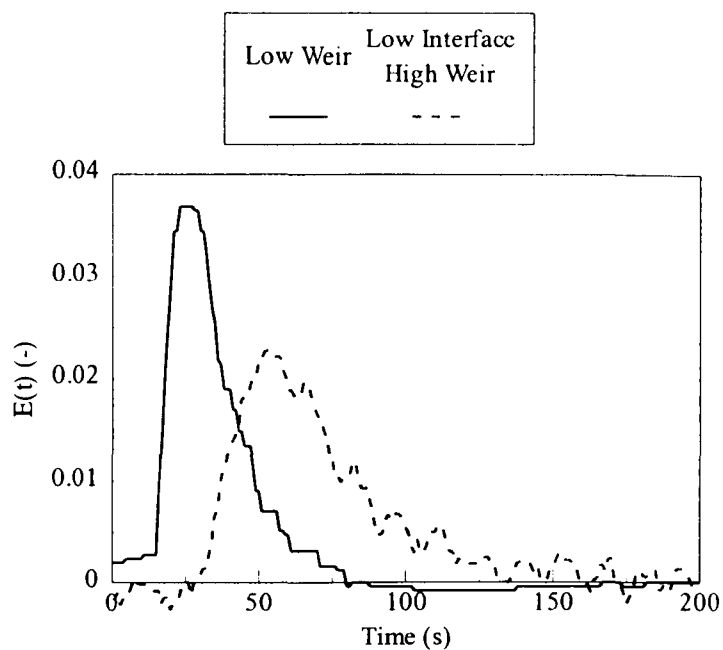


Figure 6.19: Run 11.5: Effect of Changing Weir Height on Organic Phase Residence

Time Distribution

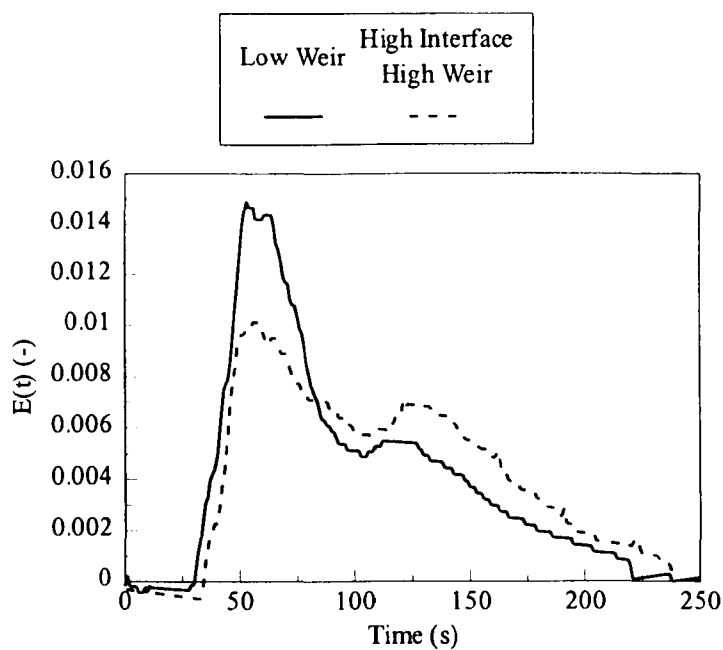


Figure 6.20: Run 11.5: Effect of Changing Weir Height on Aqueous Phase

Residence Time Distribution

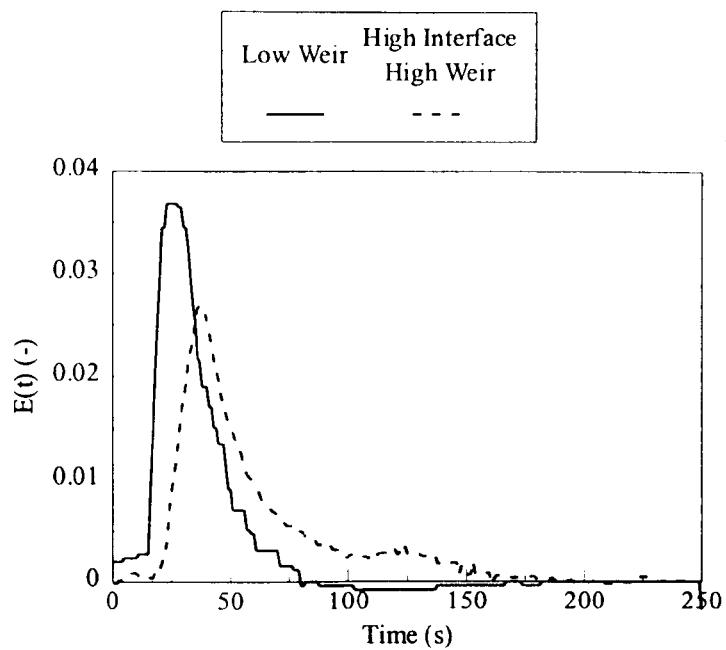


Figure 6.21: Run 11.5: Effect of Changing Weir Height on Organic Phase Residence

Time Distribution

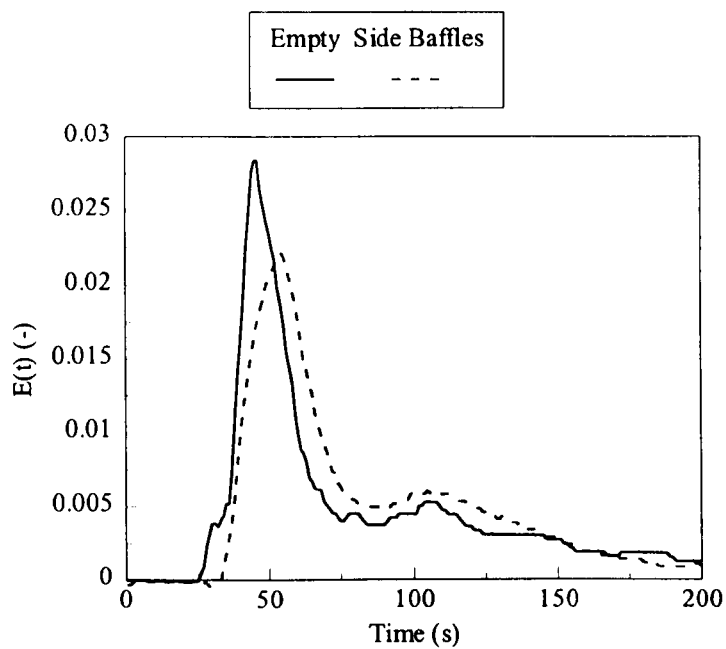


Figure 6.22: Run 3.3: Effect of Side Baffles on Aqueous Phase Residence Time

Distribution

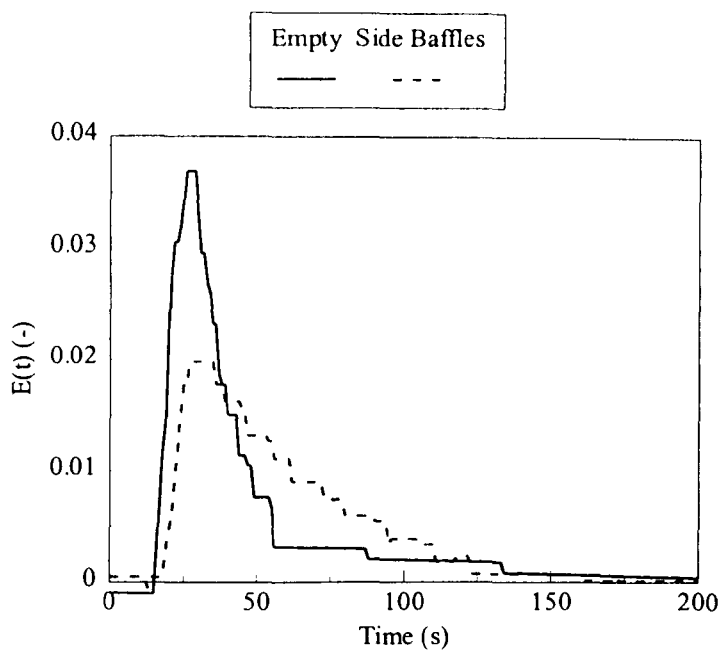


Figure 6.23: Run 3.3: Effect of Side Baffles on Organic Phase Residence Time Distribution

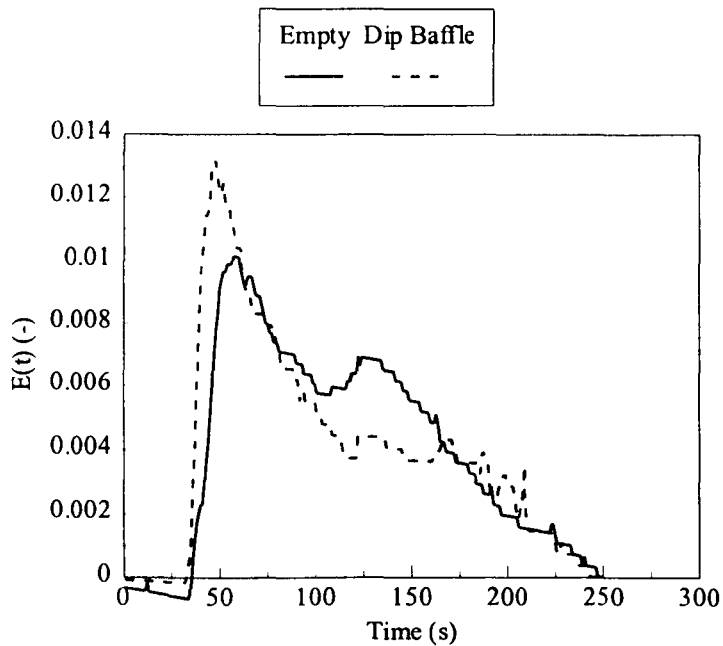


Figure 6.24: Run 13.5: Effect of Dip Baffle on Aqueous Phase Residence Time Distribution

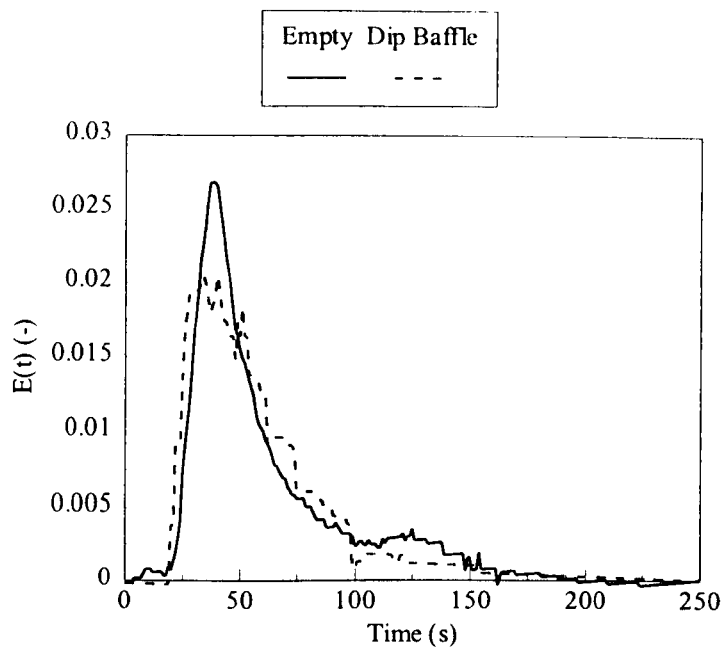


Figure 6.25: Run 13.5: Effect of Dip Baffle on Organic Phase Residence Time Distribution

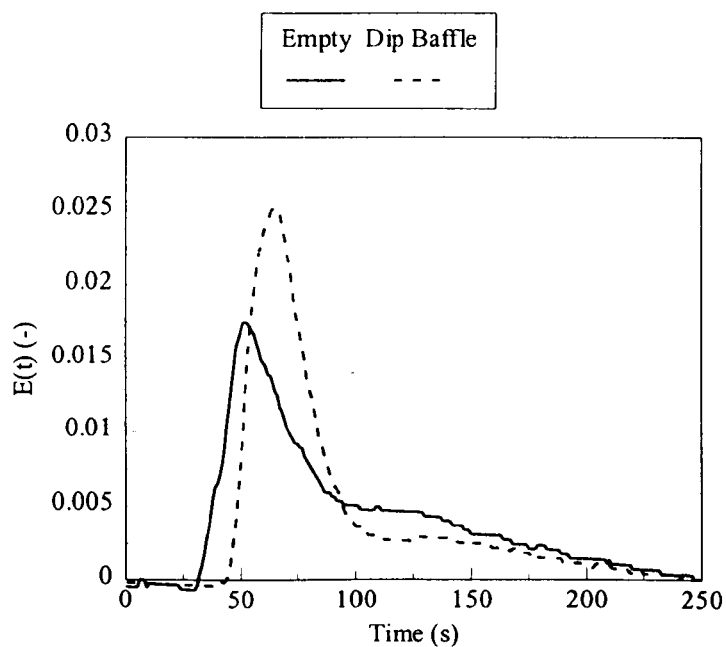


Figure 6.26: Run 13.1: Effect of Dip Baffle on Aqueous Phase Residence Time Distribution

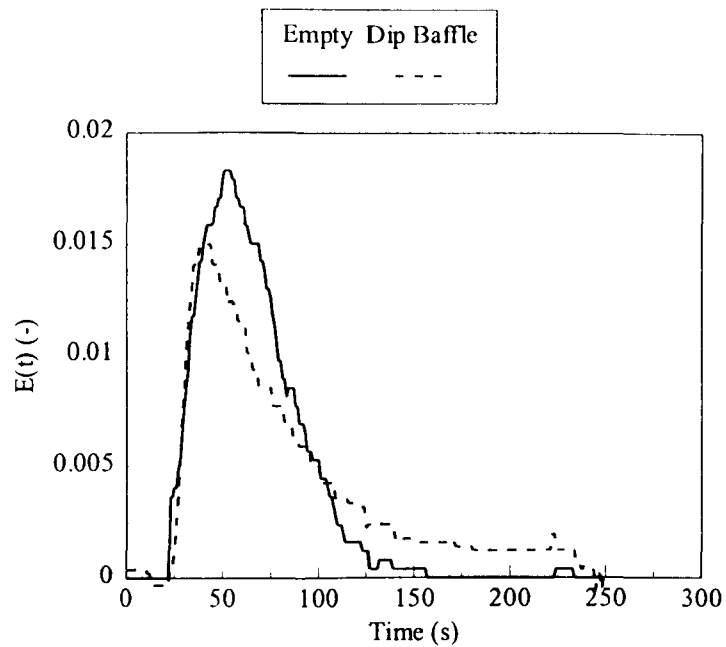


Figure 6.27: Run 13.1: Effect of Dip Baffle on Organic Phase Residence Time Distribution

6.4 CONCLUSIONS

A colorimetric measurement technique has been tested and used to measure Residence Time Distributions of the pilot scale separator tank. The inlet pulses of tracer were found to be sufficiently sharp and repeatable that deconvolution of the outlet pulses was not required. Error on the tracer mass balances were rather high ($\pm 35\%$), due to background haze and dye build up. However, the background appeared to be fairly constant for individual runs so upon normalising the data, the effect of this error is greatly diminished.

Residence Time Distributions were obtained for a range of flow rates and different internal configurations of the separator tank. Mean Residence Time was found to drop with increasing flow rate but the decrease was not as much as expected from the change in flow rate. This suggests the presence of dead zones in the tank. There is evidence from the secondary peaks on the Residence Time Distribution that recirculation zones can be set up in the vessel. These become more pronounced at the high weir height which is consistent with more dead volume in the vessel. This is discussed in greater detail in Chapter 7.

The presence of side baffles did not appear to greatly alter the MRT, but the oil-water interface looked cleaner with the baffles in place, although this could have been a local wall effect due to the quiescent zones caused by the baffles. The dip baffle caused an area of local acceleration, although once again the effect on the MRT was not consistent. Chapter 7 details mathematical modelling and further analysis of these effects.

Table 6.3: Summary of Experimental Data-Aqueous Tracer

Run No	File Code	Oil Flow	Water Flow	Water Cut	Tracer Injected	Tracer mass RTD	Error	MRT	PRT	Standard Deviation	Nominal Residence Time
		(kg/s)	(kg/s)	(by vol)	(g)	(g)	(%)	(S)	(s)	(s)	(s)
1.1	k6w14	2.1	1.5	0.36	0.120	0.115	-4.17	66.2	59	24.92	94.34
1.2	k6w38	2.1	2.5	0.49	0.250	0.296	18.40	55.2	34	33.65	58.11
1.3	k6w77	2.1	3.5	0.57	0.130	0.098	-24.62	43.9	32	17.59	41.51
1.4	k6w100	2.1	3.9	0.60	0.250	0.278	11.20	39.5	30	15.54	36.87
2.1	k15w14	3.34	1.5	0.26	0.250	0.159	-36.40	76.7	51	38.52	94.34
2.2	k15w38	3.34	2.5	0.37	0.250	0.208	-16.80	60.1	43	30.13	58.11
2.3	k15w77	3.34	3.5	0.46	0.250	0.311	24.40	47.6	30	23.63	41.51
2.4	k15w100	3.34	3.9	0.48	0.250	0.298	19.20	42.7	40	12.77	36.87
3.1	k3w38	1.5	2.5	0.57	0.250	0.291	16.40	60.1	34	33.21	58.11
3.2	k8w14	2.5	1.5	0.32	0.250	0.216	-13.60	77.8	60	37.8	94.34
3.3	k12w6	3	1	0.21	0.250	0.158	-36.80	84.2	45	49.6	142.43
4.1	k6w100	2.1	3.9	0.60	0.250	0.245	-2.00	53.6	35	26.5	36.87
4.2	k12w56	3	3	0.44	0.250	0.217	-13.20	63.8	43	36.15	48.27
4.3	k21w24	4	2	0.29	0.250	0.192	-23.20	66.8	40	38.45	72.64
5.1	k6w100b	2.1	3.9	0.60	0.350	0.442	26.29	33.5	26	13.42	36.87
5.2	k12w56b	3	3	0.44	0.350	0.366	4.57	48.1	37	23.4	48.27
5.3	k21w24b	4	2	0.29	0.350	0.300	-14.29	65.5	40	37.86	72.64
6.1	k3w38b	1.5	2.5	0.57	0.350	0.386	10.29	54.9	36	33.05	58.11
6.2	k8w14b	2.5	1.5	0.32	0.350	0.264	-24.57	73.0	43	41.17	94.34
6.3	k12w6b	3	1	0.21	0.350	0.194	-44.57	85.3	54	41.97	142.43

Run No	File Code	Oil Flow	Water Flow	Water Cut	Tracer Injected	Tracer mass RTD	Error	MRT	PRT	Standard Deviation	Nominal Residence Time
		(kg/s)	(kg/s)	(by vol)	(g)	(g)	(%)	(S)	(s)	(s)	(s)
7.1	k6w100hb	2.1	3.9	0.60	0.350	0.503	43.71	41.0	24	26.84	55.83
7.2	k12w56hb	3	3	0.44	0.350	0.309	-11.71	77.0	56	34.91	73.08
7.3	k21w24hb	4	2	0.29	0.350	0.262	-25.14	85.0	51	38.88	109.90
8.1	k3w38hb	1.5	2.5	0.57	0.350	0.382	9.14	87.6	60	42.54	87.98
8.2	k8w14hb	2.5	1.5	0.32	0.350	0.255	-27.14	91.0	58	42.23	142.83
8.3	k12w6hb	3	1	0.21	0.350	0.191	-45.43	97.9	61	44.7	215.65
9.1	k6w100lb	2.1	3.9	0.60	0.350	0.459	31.14	33.5	24	19.14	36.87
9.2	k12w56lb	3	3	0.44	0.350	0.321	-8.29	79.0	53	36.78	48.27
9.3	k21w24lb	4	2	0.29	0.350	0.322	-8.00	67.2	44	33.28	72.64
10.1	k3w38lb	1.5	2.5	0.57	0.350	0.398	13.71	56.9	35	36.48	58.11
10.2	k8w14lb	2.5	1.5	0.32	0.350	0.341	-2.57	87.1	53	42.95	94.34
10.3	k12w6lb	3	1	0.21	0.350	0.262	-25.14	93.1	55	44.93	142.43
11.4	k3w38s	1.5	2.5	0.57	0.350	0.592	69.14	49.8	39	20.92	58.11
11.1	k6w14s	2.1	1.5	0.36	0.350	0.497	42.00	86.9	58	41.88	94.34
11.2	k6w100s	2.1	3.9	0.60	0.350	0.377	7.71	48.2	49	31.67	36.87
11.5	k12w6s	3	1	0.21	0.350	0.483	38.00	96.6	53	46.05	142.43
11.3	k12w56s	3	3	0.44	0.350	0.193	-44.86	47.1	33	22.32	48.27
12.4	k3w38ls	1.5	2.5	0.57	0.350	0.660	88.57	77.4	30	46.69	58.11
12.1	k6w14ls	2.1	1.5	0.36	0.350	0.562	60.57	86.5	57	42.88	94.34
12.2	k6w100ls	2.1	3.9	0.60	0.350	0.277	-20.86	55.7	39	31.21	36.87
12.5	k12w6ls	3	1	0.21	0.350	0.494	41.14	87.9	54	43.56	142.43
12.3	k12w56ls	3	3	0.44	0.350	0.217	-38.00	57.2	42	25.01	48.27

Run No	File Code	Oil Flow	Water Flow	Water Cut	Tracer Injected	Tracer mass RTD	Error	MRT	PRT	Standard Deviation	Nominal Residence Time
		(kg/s)	(kg/s)	(by vol)	(g)	(g)	(%)	(S)	(s)	(s)	(s)
13.4	k3w38hs	1.5	2.5	0.57	0.350	0.491	40.29	79.2	32	46.33	87.98
13.1	k6w14hs	2.1	1.5	0.36	0.350	0.479	36.86	94.0	51	47.16	142.83
13.2	k6w100hs	2.1	3.9	0.60	0.350	0.214	-38.86	48.7	36	22.7	55.83
13.5	k12w6hs	3	1	0.21	0.350	0.387	10.57	111.9	56	48.48	215.65
13.3	k12w56hs	3	3	0.44	0.350	0.186	-46.86	68.2	48	31.52	73.08
15.4	k3w38d	1.5	2.5	0.57	0.350	0.612	74.86	87.7	48	42.41	58.11
15.1	k6w14d	2.1	1.5	0.36	0.350	0.511	46.00	72.9	61	23.33	94.34
15.2	k6w100d	2.1	3.9	0.60	0.350	0.251	-28.29	44.4	32	23.65	36.87
15.5	k12w6d	3	1	0.21	0.350	0.405	15.71	98.7	60	45.27	142.43
15.3	k12w56d	3	3	0.44	0.350	0.204	-41.71	63.7	63	24.18	48.27
16.5	k3w38dh	1.5	2.5	0.57	0.350	0.526	50.29	87.4	44	45.44	87.98
16.1	k6w14dh	2.1	1.5	0.36	0.350	0.468	33.71	90.2	64	40.03	142.83
16.2	k6w100dh	2.1	3.9	0.60	0.350	0.260	-25.71	60.8	31	38.79	55.83
16.4	k12w6dh	3	1	0.21	0.350	0.309	-11.71	104.3	47	53.52	215.65
16.3	k12w56dh	3	3	0.44	0.350	0.251	-28.29	99.9	34	59.03	73.08
17.4	k3w38dl	1.5	2.5	0.57	0.350	0.647	84.86	79.7	46	36	58.11
17.1	k6w14dl	2.1	1.5	0.36	0.350	0.677	93.43	86.3	57	40.1	94.34
17.2	k6w100dl	2.1	3.9	0.60	0.350	0.296	-15.43	73.3	32	50.78	36.87
17.5	k12w6dl	3	1	0.21	0.350	0.594	69.71	90.5	62	38.77	142.43
17.3	k12w56dl	3	3	0.44	0.350	0.279	-20.29	71.1	37	48.99	48.27

Table 6.4: Summary of Experimental Data-Organic Tracer

Run No	File Code	Oil Flow	Water Flow	Water Cut	Tracer Injected	Tracer mass RTD	Error	MRT	PRT	Standard Deviation	Nominal Residence Time
		(kg/s)	(kg/s)	(by vol)	(g)	(g)	(%)	(s)	(s)	(s)	(s)
1.1	k6w14	2.1	1.5	0.36	0.125	0.162	29.60	53.8	34	29.46	36.45
1.2	k6w38	2.1	2.5	0.49	0.125	0.093	-25.60	49.2	37	18.25	36.45
1.3	k6w77	2.1	3.5	0.57	0.125	0.104	-16.80	74.1	59	30.31	36.45
1.4	k6w100	2.1	3.9	0.60	0.175	0.155	-11.43	74.3	61	38.50	36.45
2.1	k15w14	3.34	1.5	0.26	0.175	0.206	17.71	46.5	37	18.54	24.00
2.2	k15w38	3.34	2.5	0.37	0.175	0.245	40.00	80.0	31	52.54	24.00
2.3	k15w77	3.34	3.5	0.46	0.175	0.251	43.43	77.5	38	40.93	24.00
2.4	k15w100	3.34	3.9	0.48	0.175	0.255	45.71	65.8	34	45.94	24.00
3.1	k3w38	1.5	2.5	0.57	0.175	0.134	-23.43	63.0	59	13.58	53.45
3.2	k8w14	2.5	1.5	0.32	0.175	0.199	13.71	53.6	31	41.26	32.86
3.3	k12w6	3	1	0.21	0.175	0.210	20.00	60.9	24	51.73	26.82
4.1	k6w100	2.1	3.9	0.60	0.175	0.155	-11.43	74.3	61	38.50	36.45
4.2	k12w56	3	3	0.44	0.175	0.129	-26.29	40.5	29	17.61	26.82
4.3	k21w24	4	2	0.29	0.175	0.269	53.71	53.6	25	46.10	20.25
5.1	k6w100b	2.1	3.9	0.60	0.175	0.236	34.86	78.4	60	27.96	36.45
5.2	k12w56b	3	3	0.44	0.175	0.182	4.00	47.2	40	15.37	26.82
5.3	k21w24b	4	2	0.29	0.175	0.254	45.14	39.2	33	14.40	20.25
6.1	k3w38b	1.5	2.5	0.57	0.175	0.268	53.14	73.4	48	33.16	53.45
6.2	k8w14b	2.5	1.5	0.32	0.175	0.340	94.29	65.2	41	38.22	32.86
6.3	k12w6b	3	1	0.21	0.188	0.355	88.83	58.0	34	31.71	26.82

Run No	File Code	Oil Flow	Water Flow	Water Cut	Tracer Injected	Tracer mass RTD	Error	MRT	PRT	Standard Deviation	Nominal Residence Time
		(kg/s)	(kg/s)	(by vol)	(g)	(g)	(%)	(s)	(s)	(s)	(s)
7.1	k6w100hb	2.1	3.9	0.60	0.263	0.292	11.24	80.2	64	28.26	47.60
7.2	k12w56hb	3	3	0.44	0.263	0.390	48.57	62.5	55	27.58	35.02
7.3	k21w24hb	4	2	0.29	0.263	0.400	52.38	47.7	25	29.1	26.44
8.1	k3w38hb	1.5	2.5	0.57	0.263	0.311	18.48	83.4	73	32.44	69.81
8.2	k8w14hb	2.5	1.5	0.32	0.250	0.358	43.20	84.6	30	51.86	42.92
8.3	k12w6hb	3	1	0.21	0.250	0.190	-24.00	40.3	24	28.46	35.02
9.1	k6w100lb	2.1	3.9	0.60	0.263	0.210	-20.15	93.9	68	30.88	74.65
9.2	k12w56lb	3	3	0.44	0.263	0.276	4.94	71.7	72	31.76	54.93
9.3	k21w24lb	4	2	0.29	0.263	0.420	59.70	62.1	31	35.61	41.47
10.1	k3w38lb	1.5	2.5	0.57	0.250	0.170	-32.00	88.4	75	20.87	109.50
10.2	k8w14lb	2.5	1.5	0.32	0.250	0.334	33.60	72.8	62	36.81	67.31
10.3	k12w6lb	3	1	0.21	0.250	0.238	-4.80	52.7	42	21.24	54.93
11.4	k3w38s	1.5	2.5	0.57	0.250	0.310	24.00	57.4	37	39.14	53.45
11.1	k6w14s	2.1	1.5	0.36	0.250	0.236	-5.60	50.6	41	26.27	36.45
11.2	k6w100s	2.1	3.9	0.60	0.375	0.154	-58.93	76.8	54	31.93	36.45
11.5	k12w6s	3	1	0.21	0.375	0.513	36.80	46.1	27	40.4	26.82
11.3	k12w56s	3	3	0.44	0.375	0.561	49.60	84.6	36	49.99	26.82
12.4	k3w38ls	1.5	2.5	0.57	0.250	0.235	-6.00	79.2	63	33.19	109.50
12.1	k6w14ls	2.1	1.5	0.36	0.250	0.211	-15.60	72.4	64	34.61	74.65
12.2	k6w100ls	2.1	3.9	0.60	0.250	0.178	-28.80	75.5	76	31.66	74.65
12.5	k12w6ls	3	1	0.21	0.250	0.318	27.20	72.3	54	30.53	54.93

Run No	File Code	Oil Flow	Water Flow	Water Cut	Tracer Injected	Tracer mass RTD	Error	MRT	PRT	Standard Deviation	Nominal Residence Time
		(kg/s)	(kg/s)	(by vol)	(g)	(g)	(%)	(s)	(s)	(s)	(s)
12.3	k12w56ls	3	3	0.44	0.250	0.312	24.80	66.2	36	44.41	54.93
13.4	k3w38hs	1.5	2.5	0.57	0.250	0.393	57.20	88.0	65	43.93	69.81
13.1	k6w14hs	2.1	1.5	0.36	0.250	0.332	32.80	60.4	52	18.58	47.60
13.2	k6w100hs	2.1	3.9	0.60	0.250	0.132	-47.20	98.5	85	26.21	47.60
13.5	k12w6hs	3	1	0.21	0.250	0.650	160.00	60.1	37	33.76	35.02
13.3	k12w56hs	3	3	0.44	0.250	0.296	18.40	70.3	31	58.1	35.02
15.4	k3w38d	1.5	2.5	0.57	0.375	0.408	8.80	48.1	42	10.32	53.45
15.1	k6w14d	2.1	1.5	0.36	0.375	0.298	-20.53	42.2	37	12.14	36.45
15.2	k6w100d	2.1	3.9	0.60	0.375	0.217	-42.13	59.7	51	15.98	36.45
15.5	k12w6d	3	1	0.21	0.375	0.601	60.27	39.3	57	16.49	26.82
15.3	k12w56d	3	3	0.44	0.375	0.471	25.60	48.5	25	36.8	26.82
16.5	k3w38dh	1.5	2.5	0.57	0.375	0.190	-49.33	48.8	35	22.95	69.81
16.1	k6w14dh	2.1	1.5	0.36	0.375	n/a	n/a	83.8	42	50.11	47.60
16.2	k6w100dh	2.1	3.9	0.60	0.375	0.236	-37.07	78.7	74	22.8	47.60
16.4	k12w6dh	3	1	0.21	0.375	0.382	1.87	59.1	39	33.57	35.02
16.3	k12w56dh	3	3	0.44	0.375	n/a	n/a	79.6	28	47.82	47.82
17.4	k3w38dl	1.5	2.5	0.57	0.375	0.263	-29.87	65.2	39	39.13	109.50
17.1	k6w14dl	2.1	1.5	0.36	0.375	0.435	16.00	73.3	57	32.34	74.65
17.2	k6w100dl	2.1	3.9	0.60	0.375	0.350	-6.67	96.9	79	24.45	74.65
17.5	k12w6dl	3	1	0.21	0.375	0.485	29.33	61.1	42	25.29	54.93
17.3	k12w56dl	3	3	0.44	0.375	n/a	n/a	41.5	34	13.33	54.93

PERFORMANCE CHARACTERISATION AND MATHEMATICAL MODELLING OF A PILOT SCALE SEPARATOR

7.1 INTRODUCTION

The data from field separators that has been modelled using the transfer function approach described in Chapter 5 cover a wide range of vessel sizes and different internal configurations. This data, which was supplied by BP Exploration, covers vessels with and without perforated baffles and several contain some form of inlet flowstreaming devices or structured packing. These vessels are also operating with fluids of different physical properties which can possibly vary over time.

A much more systematic set of data have been obtained using the pilot scale separator described in Chapter 3. Different weir heights and liquid-liquid interface positions have been employed to vary the volume occupied by the phases. In addition, dip or side baffles have been used to form either zones of acceleration or stagnation. The data obtained have been analysed using the Alternative Path Model to determine parameters such as Mean Residence Time, “F number” and “Fractional Mixed Volume”, which are all defined in Chapter 5. These will be examined in order to devise relationships which can be used to maximise the efficiency of the separator.

In this Chapter, the mathematical model will be applied to the pilot scale separator, and the results obtained will be compared and contrasted with the parameters obtained from the modelling of the BP Exploration data. In addition, some operating guidelines will be suggested in order to maximise the performance of existing separators and perhaps suggest improvements which can be implemented in future separator designs and retrofits.

7.2 INTERPRETATION OF DATA FROM PILOT SCALE SEPARATOR

The Alternative Path Model as described in Section 5.2.3 has been applied to all the Residence Time Distribution curves obtained and presented in Chapter 6. Additional parameters have also been calculated in light of the changing internal configurations and observations of the liquids flowing in the pilot scale separator. The side baffles obscured some of the flow area available to the liquids and it is necessary to understand the effect this may have had on the Residence Time Distribution. Additionally, it was noticed from visual inspection that the well-mixed liquids at the inlet of the vessel formed a coalescing wedge as they began to settle and so an analysis for the prediction of the length of this wedge is presented.

7.2.1 Flow Obstruction Caused by Side Baffles

Installation of side baffles cause some of the flow area to be obstructed, and because of the shape of the baffles as shown in Figure 7.1, this blocking effect is larger for the organic phase than the aqueous phase.

Table 7.1: Flow Area Obscured by Side Baffles (% Area)

	Low Weir (L)	High Weir, Low Interface (HL)	High Weir, High Interface (HH)
Organic phase	47.4	48.6	49.7
Aqueous phase	28.7	28.7	34.8

Table 7.1 shows that 47.4% of the flow area of the organic phase is obstructed compared with 28.7% for the aqueous phase at the same low weir height. Therefore the reduction in flow area for the organic phase is 1.7 times that for the aqueous phase. The ratio is similar when using the high weir at the low interface position but falls to a value of 1.4 for the high weir at the high interface position. It would therefore be expected that the side baffles would have a more profound effect on the Residence Time Distribution of the organic phase than the aqueous phase. This will be examined more closely later.

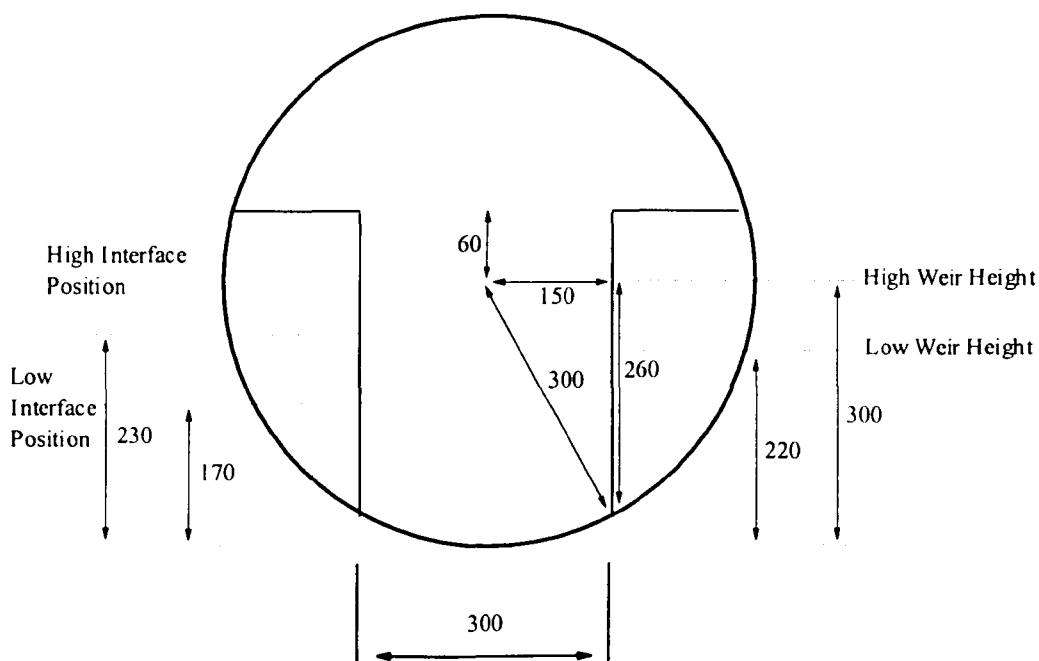


Figure 7.1: Detail of Side Baffles

7.2.2 Coalescing Zones

As the oil and aqueous phases settle out and coalesce after entering the vessel, a two-phase zone was seen to extend past the perforated baffle towards the outlets. The shape of this zone is important because the quality of the oil-water separation will be

affected if this two-phase mixture ever reaches the vessel outlets. Two possibilities are illustrated in Figure 7.2 below.

If it is considered that the mixing zone occupies the total volume of the vessel up to a certain point, after which there is a distinct water-oil interface (Type 1), then it can be simply derived that:

$$l_{mix} = D.l \tag{7.1}$$

Where l_{mix} is the length of the mixing zone, D is the Fractional Mixed Volume and l is the active length of the vessel. Observation of the flows within the vessel suggest that in reality, a more wedge shaped mixing zone is observed, the most extreme of which is Type 2 as illustrated in Figure 7.2. In this case a more complex geometrical relationship is required due to the cylindrical cross-section of the vessel.

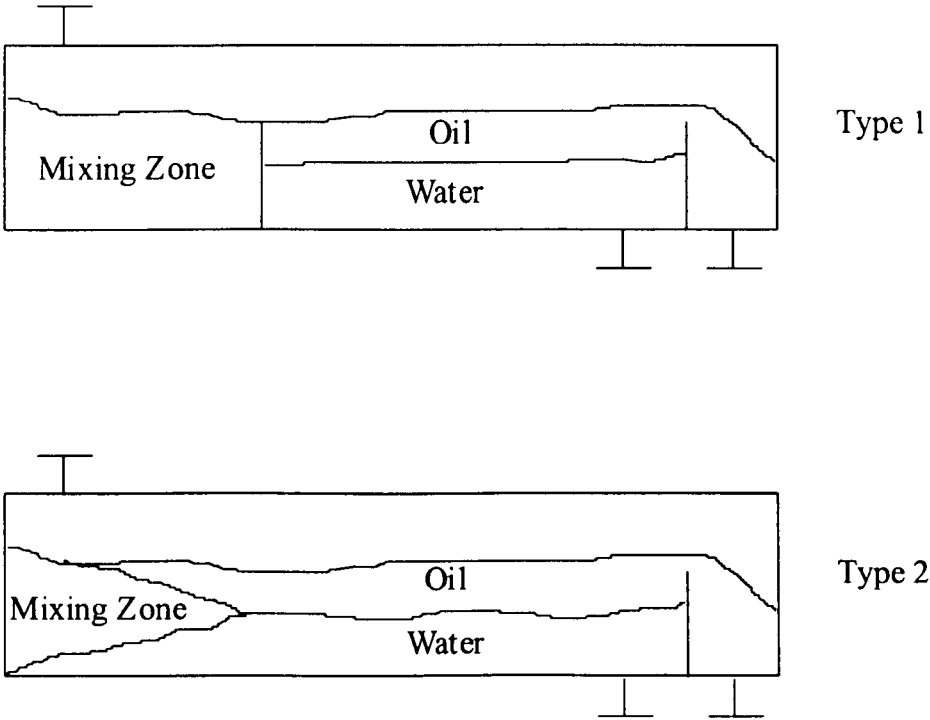


Figure 7.2: Types of Mixing Zone

The coalescing wedge can be split into two sections by extending a horizontal plane at the same height as the liquid-liquid interface. The lower section can then be defined as the zone where the coalescence settles up to the liquid-liquid interface, past which there is a clean aqueous phase. In the upper section, the drops coalesce downwards to the interface and beyond this zone there is a clean organic phase. The analysis to calculate the volume of both sections is similar, but the boundary conditions are different. One proceeds by considering the cross sectional area of the tank, as illustrated in Figure 7.3.

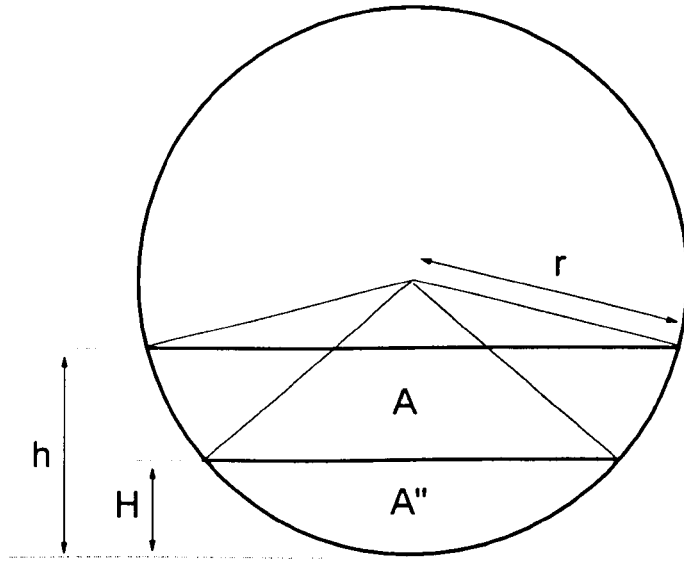


Figure 7.3: Coalescing Wedges

The areas of the segments corresponding to H and h (A and A'' respectively) can be derived as below.

$$A = r^2 \cos^{-1} \frac{r-H}{r} - (r-H)\sqrt{2rH-H^2} \quad (7.2)$$

$$A'' = r^2 \cos^{-1} \frac{r-h}{r} - (r-h)\sqrt{2rh-h^2} \quad (7.3)$$

Where H is the height of the liquid-liquid interface. The volume of either upper or lower coalescing wedge can now be obtained from:

$$V = \int_0^{l_{mix}} (A - A'') dz \quad (7.4)$$

A relationship now needs to be obtained between z and h and this will be different for the upper and lower sections. For the lower section, when $z=0$, $h=0$ and when $z=l_{mix}$, $h=H$. Hence

$$\frac{h}{H} = \frac{z}{l_{mix}} \quad (7.5)$$

Differentiation leads to the result below

$$\frac{dz}{l_{mix}} = \frac{dh}{H} \quad (7.6)$$

Substituting this result into Equation 7.4 the following expression is obtained

$$V_L = \int_0^H (A - A'') \frac{l_{mix}}{H} dh \quad (7.7)$$

After some manipulation, this expression can be reduced to

$$V_L = \frac{l_{mix}}{H} \int_0^H A'' dh - A l_{mix} \quad (7.8)$$

A similar expression can be written for the upper coalescing wedge, but this time at $z=0$, $h=h'$ and at $z=l_{mix}$, $h=H$, where h' is the height of the gas-oil interface. This leads to the expression below

$$h = \left(\frac{H - h'}{l_{mix}} \right) z + h' \quad (7.9)$$

Differentiation of this expression and substitution in Equation 7.4 as done previously gives, after some algebraic manipulation, the following result for the volume of the upper wedge.

$$V_U = \frac{l_{mix}}{H - h'} \int_{h'}^H A'' dh - \frac{AHl_{mix}}{H - h'} + \frac{Ah'l_{mix}}{H - h'} \quad (7.10)$$

Therefore the total volume, V_{mix} , of the coalescing wedge is equal to the sum of V_L and V_U and can also be found from the definition of Fractional Mixed Volume (Equation 5.19). These two expressions can then be used to calculate the length of the coalescing wedge for each run performed.

7.2.3 Nominal Residence Times

The Nominal Residence Time (NRT) of each phase is the theoretical residence time defined in Equation 7.11 below.

$$NRT = \frac{V_i}{Q_i} \quad (7.11)$$

Where NRT is the Nominal Residence Time, V_i is the volume occupied and Q_i is the volumetric flow rate of phase i . The calculation of V_i is simply obtained from equations 7.2 and 7.3 and the active vessel length, l . This is an interesting parameter to calculate because the Nominal Residence Times and Mean Residence Times rarely agree. The ratio of MRT/NRT therefore provides a measure of this agreement.

It is important when calculating the height of oil to take into account the extra height of liquid above the weir. It was found that for all flow conditions used on the test tank, the actual level of oil in the vessel was about 3 cm above the height of the weir.

This is a very significant proportion of the flow area, particularly at the low weir height and was included when calculating the oil Nominal Residence Time.

The above analysis has been applied to all of the experimental data obtained from the pilot scale separator as described in Chapter 6.

7.3 DISCUSSION OF RESULTS

The results of the modelling have been analysed to compare and contrast the parameters obtained at different flow rates with different internal configurations. Tables of all the calculated parameters appear in Appendix A7. Variation of the results with changing weir height and installation of side or dip baffles are discussed below and are compared with the results obtained from the modelling of the field data as described in Chapter 5. It is also hypothesised how the parameters should vary in the case of poor separation performance, for example in the case of blocked internal packings or sand clogging.

7.3.1 Effect of Changing Weir Height

The weir height was changed between 0.22 to 0.3m in order to observe the effect on the interaction of the phases and the quality of the separation. Additionally, two different liquid-liquid interface positions were used. The positions were chosen to keep the thickness of either water or oil constant at two combinations of weir height and interface level. For example, both the low weir position (L) together with the high weir-low interface (HL) position kept the height of water in the vessel constant, while the low weir position together with the high weir-high interface (HH) position kept the thickness of the oil layer more or less the same. It was chosen to keep the same thicknesses on the basis of the studying the effect on the gravity settling and

coalescence of the drops. . In particular, it was found that the extra volume of liquid in the tank at the high weir positions seemed to improve at least qualitatively the phase separation, as the Nominal Residence Time of the vessel was increased. The aqueous phase was noticeably cleaner and the coalescing layer was smaller than for the low weir position.

The effect of changing the weir height and interface positions on the various experimental and model parameters are detailed in Figures 7.5-7.8. The variation of the Mean Residence Time for the organic phase with changing thickness of the oil layer is illustrated on Figure 7.5a, and the Mean Residence Time is greater at the HL position for 4 kg/s total flow. However at 6 kg/s the difference is less marked. Values of F number are lower at the HL position at 6 kg/s (Figure 7.8c) and this has the effect of causing the Mean Residence Time to be lower than the other runs which have more distinguishable secondary peaks. The presence of secondary peaks appears to occur at extremes of water cut and when the oil layer is thin and therefore travelling faster. As already mentioned in Section 6.3, the presence of a faster travelling organic phase plus the settling of the oil droplets from the aqueous phase can modify the velocity profile through the tank, setting up a recirculating zone in the aqueous phase. If some oil droplets become trapped in this recirculation, their Nominal Residence Time through the tank will be increased and hence a secondary peak will also appear in the oil Residence Time Distribution. This effect is illustrated in Figure 7.4 and is an important argument in explaining the trends in the various parameters. It would be expected from this that the values of F number would be higher at the HH and L positions and this is the case for both oil and aqueous phases as shown in Figure 7.8. Additionally, the thickness of the oil layer at

the HL position would mean that any oil trapped in a water recirculating zone would be a smaller proportion of the exiting flow.

The trend of aqueous Mean Residence Time with varying water layer thickness is illustrated on Figure 7.5b and as expected, the values are higher at the HH position than for the HL position. However for both the oil and aqueous phases, the variation of Mean Residence Time is less than expected if one compares the Nominal Residence Times. The values of MRT/NRT are greater than expected at the 6 kg/s flow conditions (Figures 7.6-7.7). This is consistent behaviour for a vessel with a large dead zone, as the increasing flow rate reduces the size of the dead zone but increases the active flow area. As the two phenomena are opposite, the Mean Residence Time does not change much. This indicates the vessel is behaving in a manner closer to plug flow, and indeed the values of Fractional Mixed Volume are less at the 6 kg/s flow (Figure 7.9) condition but do not show much trend with weir height or interface position.

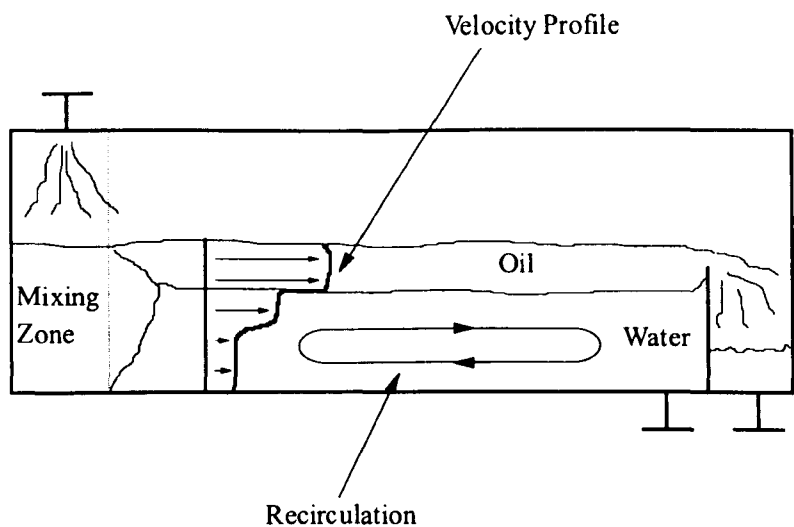


Figure 7.4: Recirculation Effects in the Separator

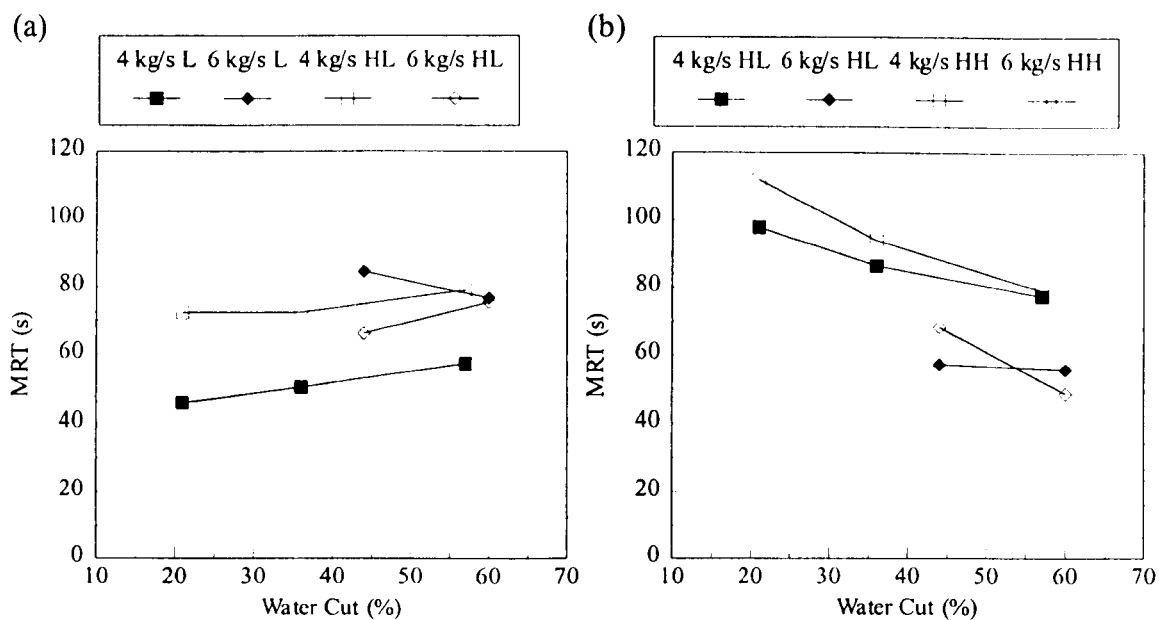


Figure 7.5: Variation of Mean Residence Time with Weir Height for (a) Organic phase and (b) Aqueous phase

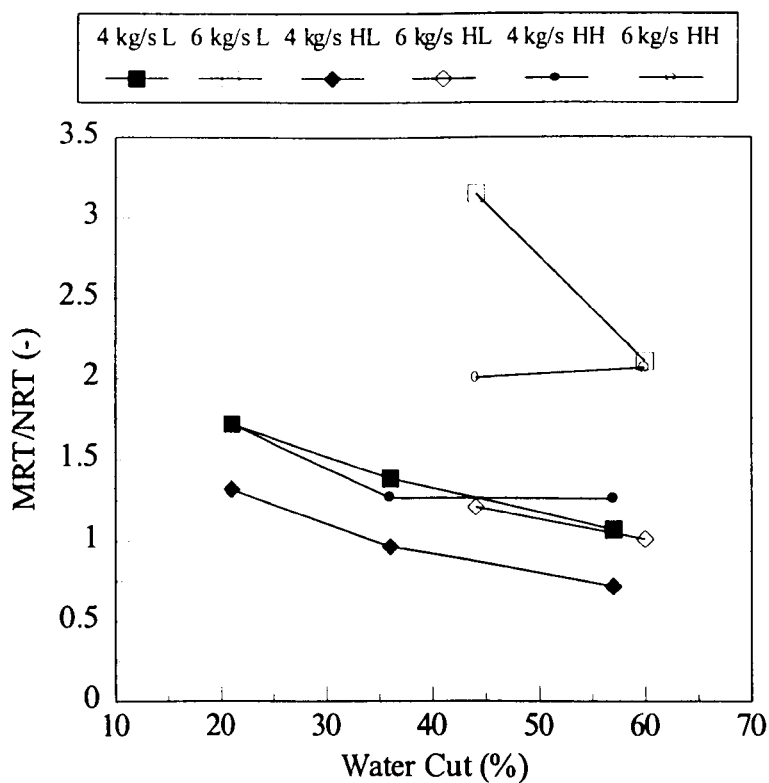


Figure 7.6: Variation of MRT/NRT with Weir Height-Organic phase

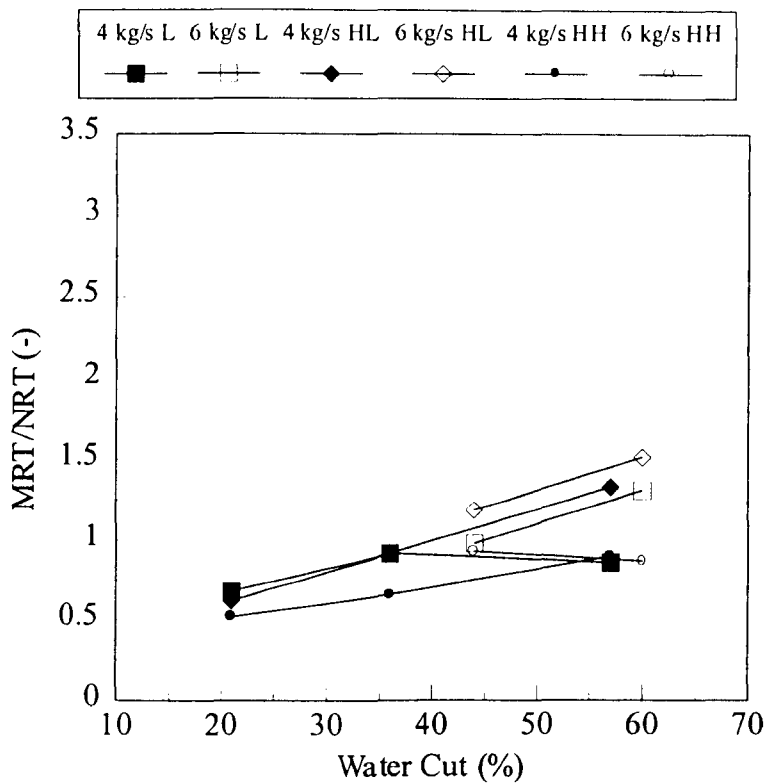
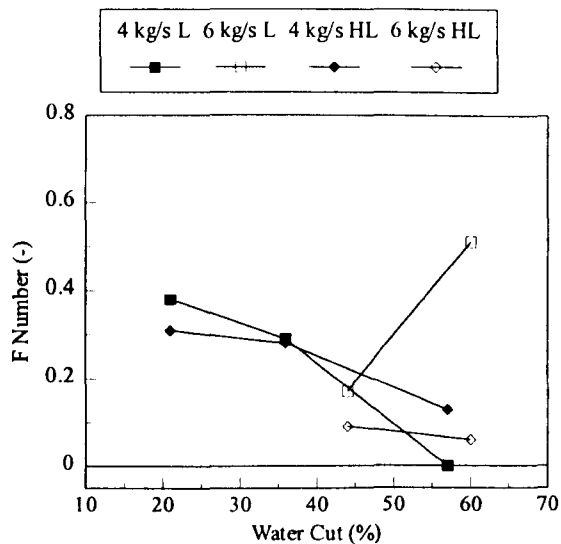
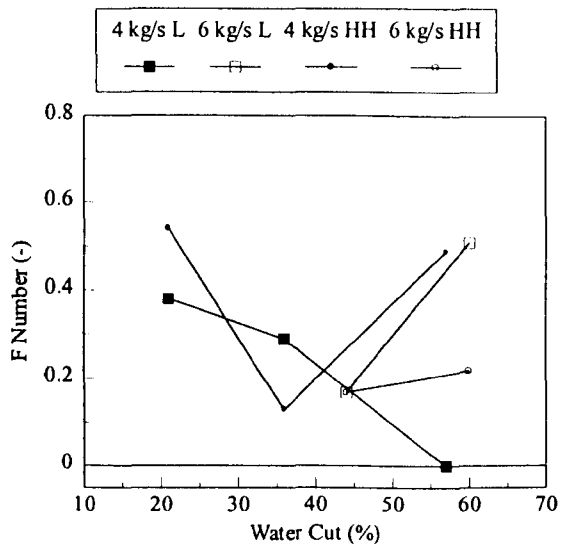


Figure 7.7: Variation of MRT/NRT with Weir Height-Aqueous Phase

(a)



(b)



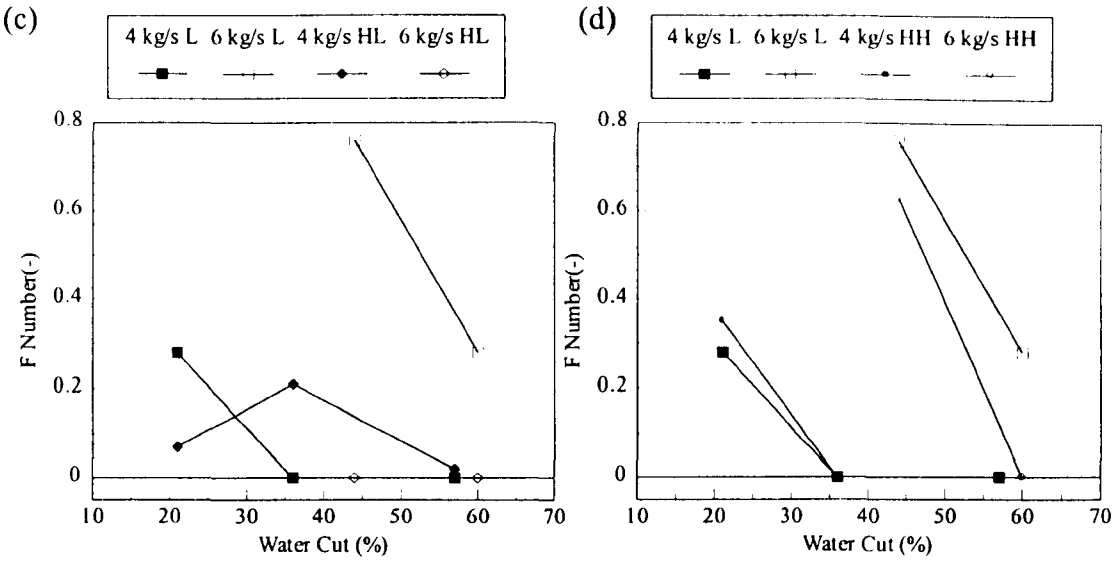


Figure 7.8: Variation of F number with Different Weir and Interface Heights for (a and b) Organic phase and (c and d) Aqueous phase

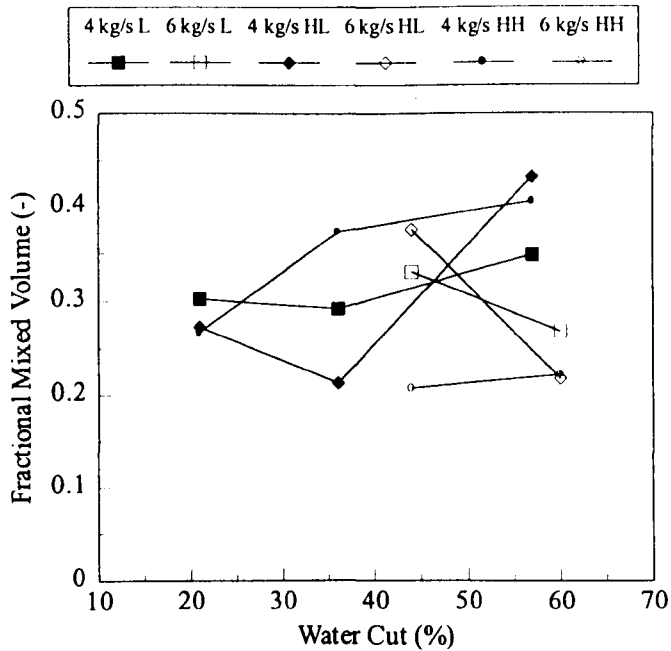


Figure 7.9: Variation of Fractional Mixed Volume with Weir Height

7.3.2 Effect of Side Baffles

The inclusion of side baffles in the rig would be expected to cause quiescent zones in the tank. Their presence might also upset the recirculating mechanism described in Figure 7.4. The Nominal Residence Times of the phases when the side baffles were installed were calculated on the basis of the open area between the baffles acting as the effective flow area. The bulk of the liquid would therefore be expected to exit more quickly and the values of MRT/NRT will reflect this hypothesis. Some liquid is likely to pool around the baffles and this is likely to act as a smoothing effect on the separation of the oil and aqueous phases, and increase the tail on the Residence Time Distribution curve. Less turbulence was observed when the side baffles were in place, particularly at higher flow rates. The first set of baffles from the inlet seemed to act as momentum breakers on the turbulent mixed liquids and the interface seemed to form earlier than when the tank was empty.

The Mean Residence Time of the organic phase was seen to change only slightly upon installation of the side baffles (Figure 7.10). At the slower flow condition, 4 kg/s, the values dropped slightly while at the higher condition of 6 kg/s, the values rose slightly. At both flow conditions the aqueous phase Mean Residence Time dropped by a small amount with the baffles in place.

The aqueous values of MRT/NRT were hardly affected by the presence of the side baffles (Figure 7.11) but the values for the organic phase increased significantly. It would be expected that the phases would exit the tank more quickly with the side baffles in place due to the smaller active flow area, but this did not occur for the organic phase and the aqueous phase accelerated only slightly. The fact that the

baffles did not greatly affect the Mean Residence Time of either phase suggests again that the vessel suffers from large dead or recirculatory zones.

The values of Fractional Mixed Volume are not significantly changed due to the baffles (Figure 7.13). At the high flow condition, there is a small drop in the value with the baffles, while at the low flow condition, there is a larger increase. This is at odds with the observations of a cleaner oil-water interface, but it is possible that the observation of the cleaner interface is a wall effect due to the presence of baffles. If the wedge lengths in Tables 7.4 and 7.5 are taken into consideration, it becomes clear that the coalescing zone may extend further down the vessel, even though this cannot be seen at the vessel wall.

A similar trend is seen for F number of the aqueous phase (Figure 7.12). At the low flow condition there is an increase of F number with side baffles, while at the high flow condition, the values drop. The similar variations of F number and Fractional Mixed Volume agree because at low flows, an increased secondary peak would suggest more mixing and recirculation so the Fractional Mixed Volume goes up, and vice versa. The reason for the reverse in the behaviour is less clear, but may be due to the increased flow rate sweeping away the dead areas in the centre completely. Then F would drop and Fractional Mixed Volume would increase providing that there was sufficiently fast interchange of liquid in the dead zones between the baffles. The F number of the organic phase is reduced by the presence of the side baffles to zero which may suggest most of the recirculation now occurs in small packets so that no oil is released late enough to cause a secondary peak.

Figure 7.14 illustrates the calculated wedge length as obtained from the Fractional Mixed Volume and assuming that the side baffles reduce the flow area as shown in Table 7.1. The wedge length is made dimensionless by dividing by the active length of the vessel. If it is assumed that the flow volume is reduced by the presence of the side baffles and that the liquid pooling to the sides is stagnant, then the length of the wedge is calculated to be longer than the active length of the vessel. This would suggest poor separator performance due to carry over of the two-phase region into the vessel outlets. There was no visual evidence from the side of the tank that this was occurring however and it seems that calculating the length of the wedge in this way is an extreme case. Examining the Fractional Wedge Lengths as shown in Table A4.4 in Appendix A7 shows that the values range between 0.28-0.97, with most values in the range 0.4-0.6. These values are greater than the values of Fractional Mixed Volume as can be deduced visually from Figure 7.2 but are all less than unity suggesting that the liquids do settle out by the time they reach the outlet. In reality, the coalescing zone appears to be of a shape somewhere in between types 1 and 2, but it is the differences between different runs which is of interest, rather than absolute values.

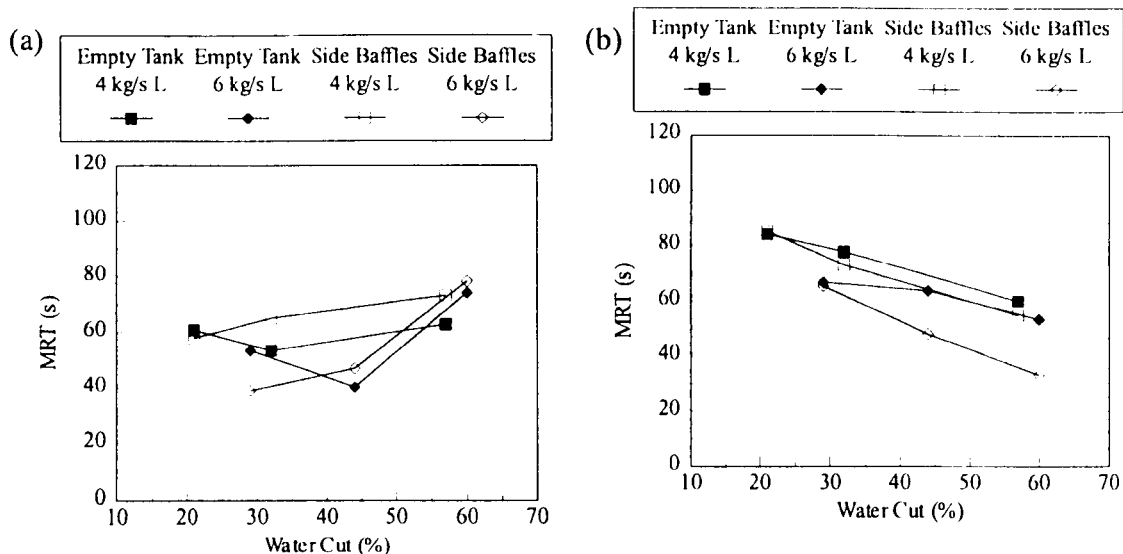


Figure 7.10: Variation of Mean Residence Time with Side Baffles, (a) Organic phase, (b) Aqueous phase

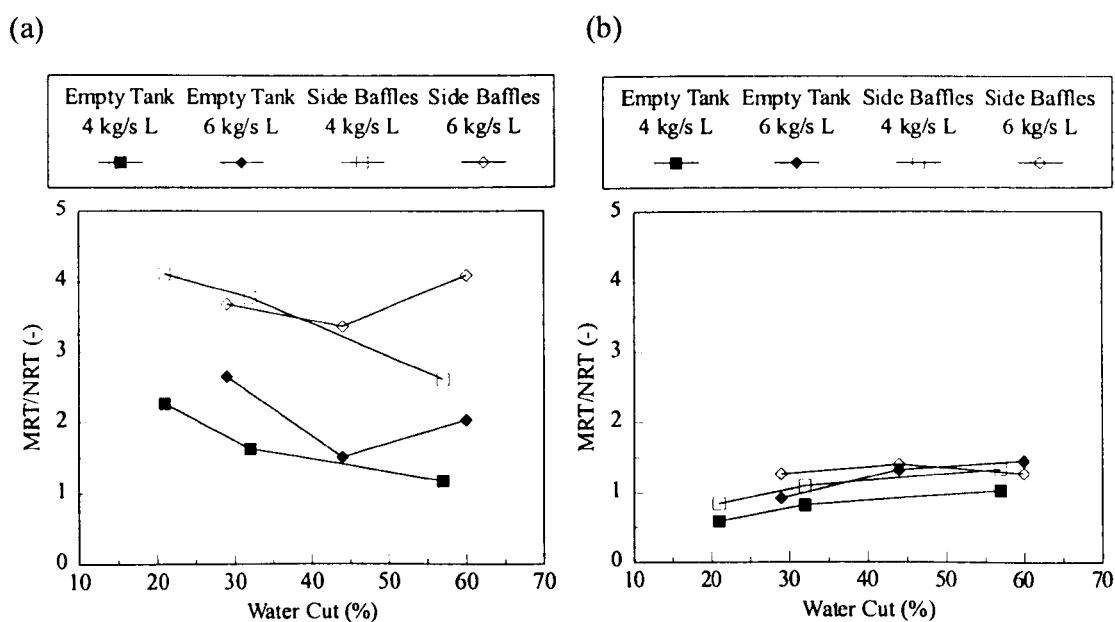


Figure 7.11: Variation of MRT/NRT with Side Baffles, (a) Organic phase, (b) Aqueous phase

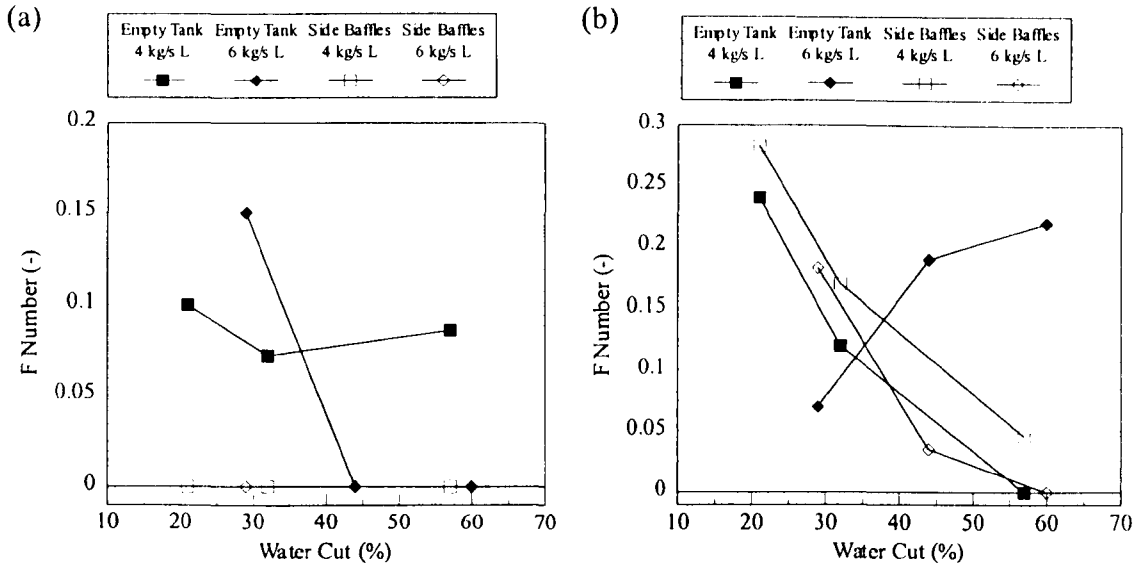


Figure 7.12: Variation of F Number with Side Baffles, (a) Organic phase, (b) Aqueous phase

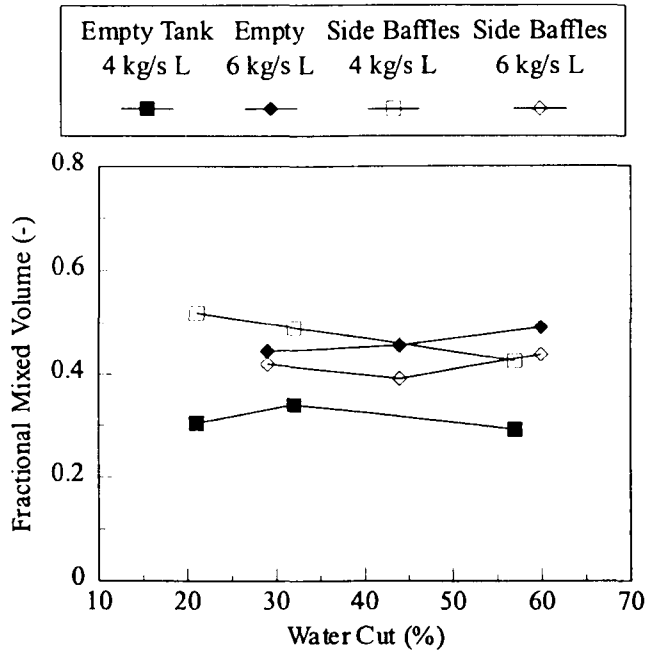


Figure 7.13: Variation of Fractional Mixed Volume with Side Baffles

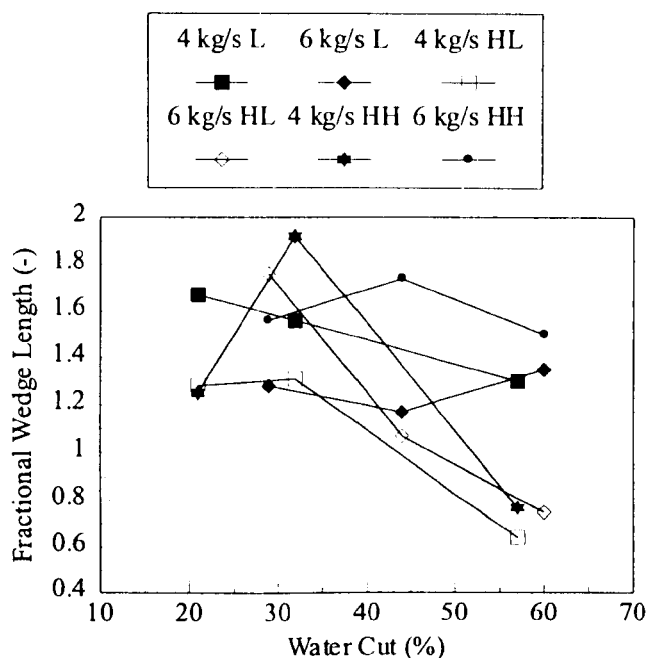


Figure 7.14: Variation of Fractional Wedge Length with Side Baffles

7.3.3 Effect of Dip Baffle

The dip baffle would be expected to act as a zone of local flow acceleration as it obscures part of the flow area at one point in the flow. At position HH, the baffle was designed to extend below the depth of the oil layer and enter the aqueous phase. When the vessel was operating in this mode, the aqueous phase was substantially depressed so that a layer of oil could pass under the baffle. A large amount of eddying was observed just downstream of the baffle.

The variation of Mean Residence Time of the organic phase with the dip baffle present is illustrated on Figure 7.17. No significant difference was found for the aqueous phase which visually was relatively undisturbed apart from the condition described in the above paragraph. The dip baffle caused the Mean Residence Time to drop at weir position L but at positions HL and HH the value appears to go through a maximum. Values of MRT/NRT again show the same elevated values at

the 6 kg/s flow condition (Figure 7.15) but the presence of the dip baffle appears to change this effect, particularly the trend. The values of MRT/NRT for the aqueous phase are again not significantly affected, apart from a slight rise in values for flows of 6 kg/s at positions HL and HH. The presence of the dip baffle appears to be altering the interactions between the phases at these high weir heights, possibly due to recirculation and eddying around the baffle.

The values of F number are significantly reduced by the presence of the dip baffle for either phase if the depth of the water or oil layer is small (Figure 7.16). The weir and interface positions when the depth of the phase layers are large correspond to the aqueous phase at position HH and the organic phase at position HL. In these cases the values of F number are not reduced and are sometimes increased. It seems that the acceleration past the baffle causes some recirculation in one phase if it is sufficiently thick but the trends in Mean Residence Time are rather unpredictable and may explain the rather random values of Fractional Mixed Volume obtained when the dip baffle was in place.

The dip baffle seems to produce rather random trends in some parameters, particularly Fractional Mixed Volume (Figure 7.18) but the changes in F number described above are very interesting. When the tank was empty, similar variations in F number occurred but the values of MRT/NRT and Fractional Mixed Volume followed a more obvious trend. It is possible that a zone of acceleration, or blockage in the tank can be identified by random variations in these variables, but that the extra recirculations caused mean that F number stays the same or increases.

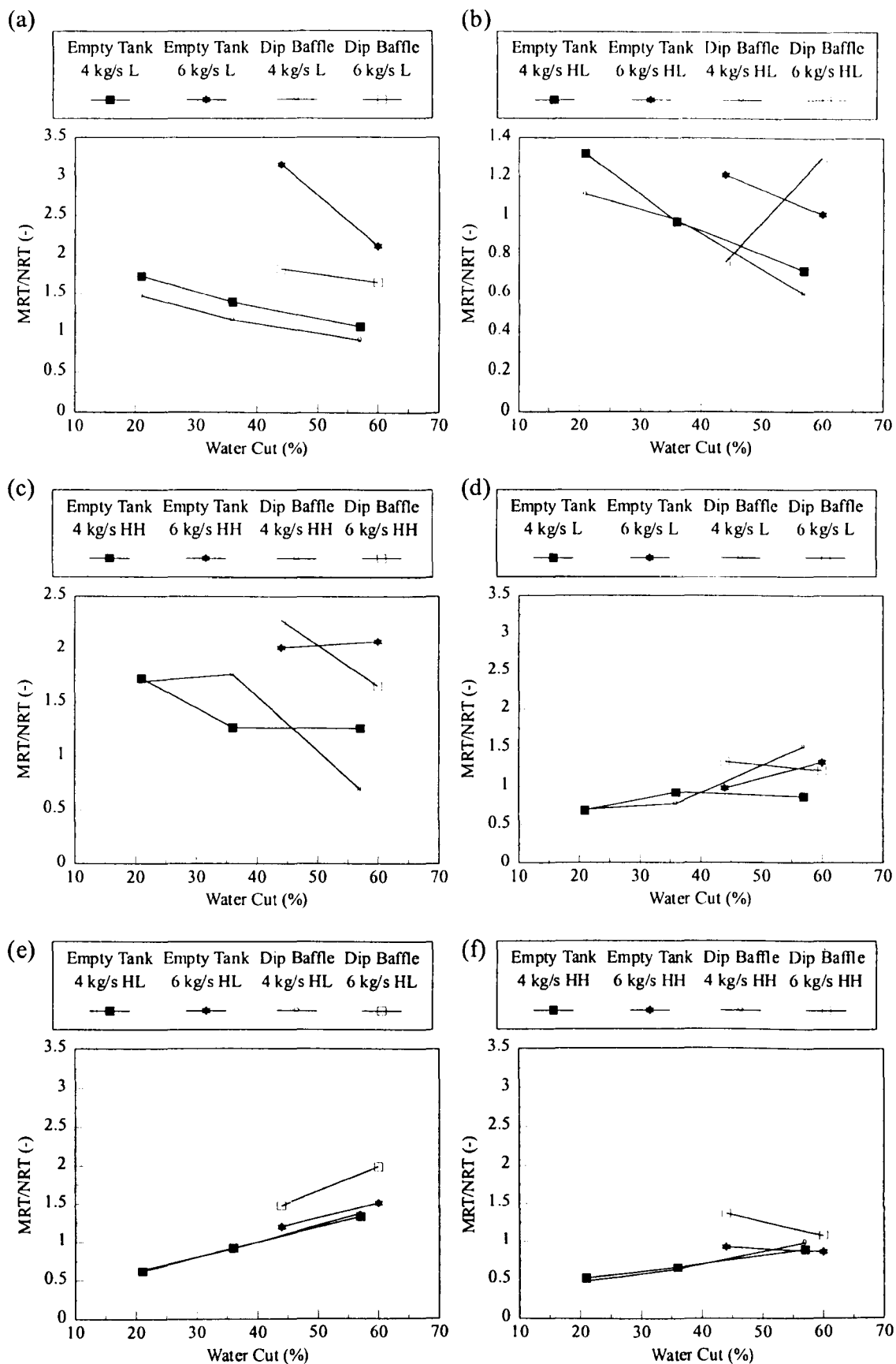


Figure 7.15: Variation of MRT/NRT with Dip Baffles at Different Weir Heights, Organic phase (a-c) and Aqueous phase (d-f)

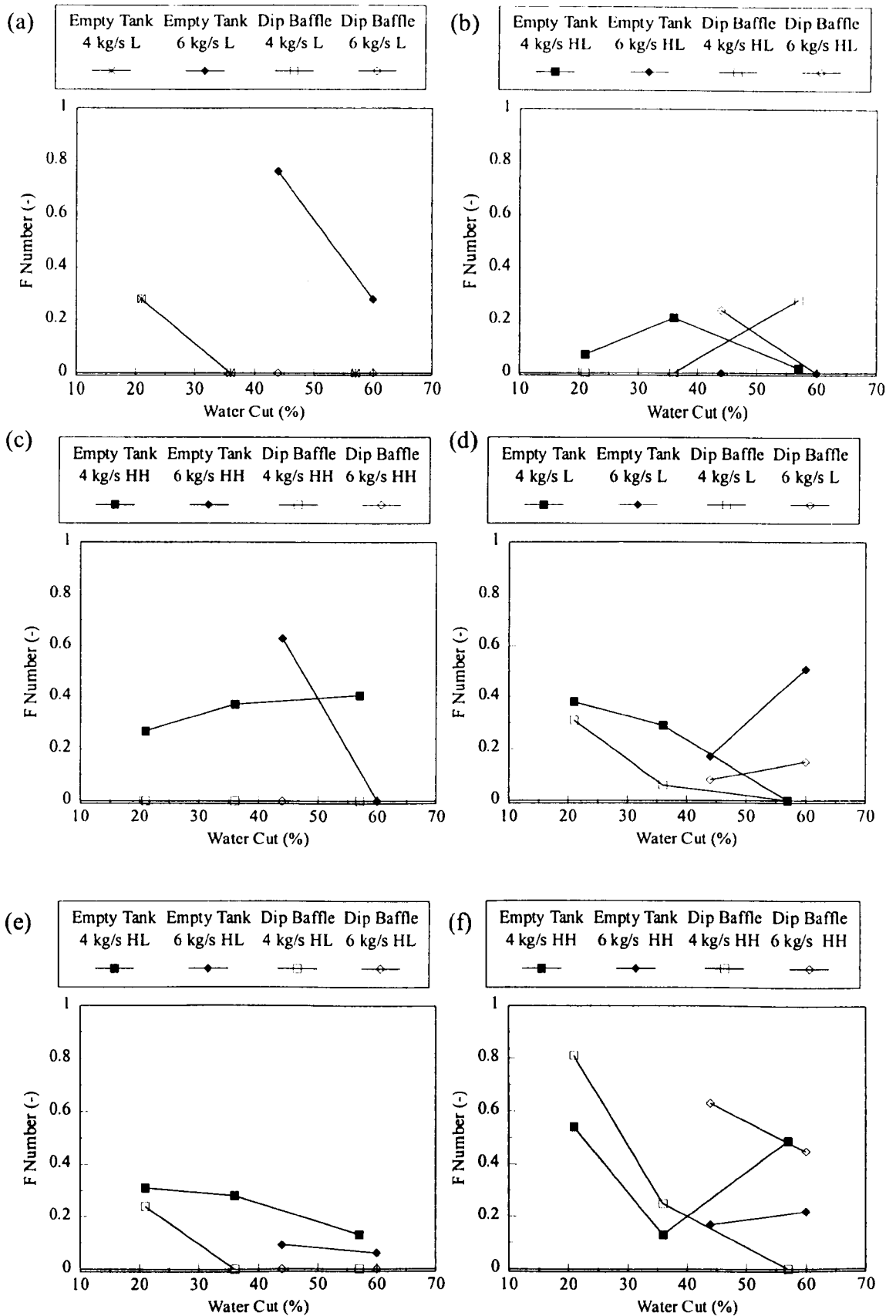


Figure 7.16: Variation of F Number with Dip Baffle at Different Weir Heights, (a-c) Organic phase and (d-f) Aqueous phase

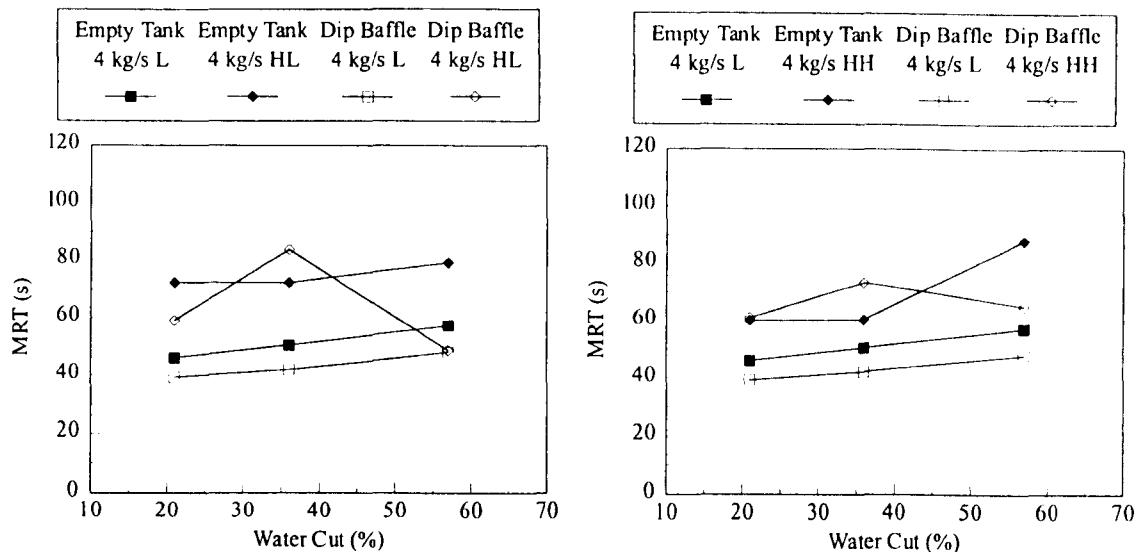


Figure 7.17: Variation of Mean Residence Time of Organic phase with Dip Baffle at different interface heights

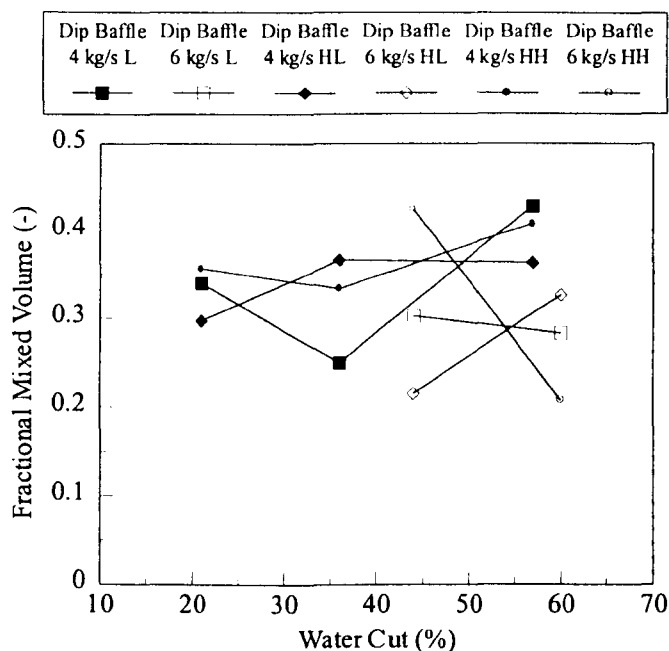


Figure 7.18: Variation of Fractional Mixed Volume with Dip Baffle

7.3.4 Comparisons with Field Data

The trends in the model parameters generated for the BP data, as described in Chapter 5, were compared with the results obtained on the pilot scale separator in order to investigate any correlations or contradictions.

As mentioned in Chapter 6, the secondary peaks seem most dominant when there is the largest differences in velocity between the phases. This too occurs for the test separator and the effect can be exacerbated by the presence of internals, for example, secondary peaks are present for the aqueous phase at position HH and they become bigger when the dip baffle is installed.

Fractional Mixed Volume was found from the field data to be linked more closely to the vessel configuration than any flow rate parameters. The values for the test separator were found to fluctuate with flow rate and were also affected by internal configuration, although the trend was not always predictable. Comparing values of MRT/NRT show that the values lie in a similar range to the data from the test separator but there is considerable fluctuation, particularly for the Milne separator where there are only very small changes in water cut (Figures 7.19-7.20).

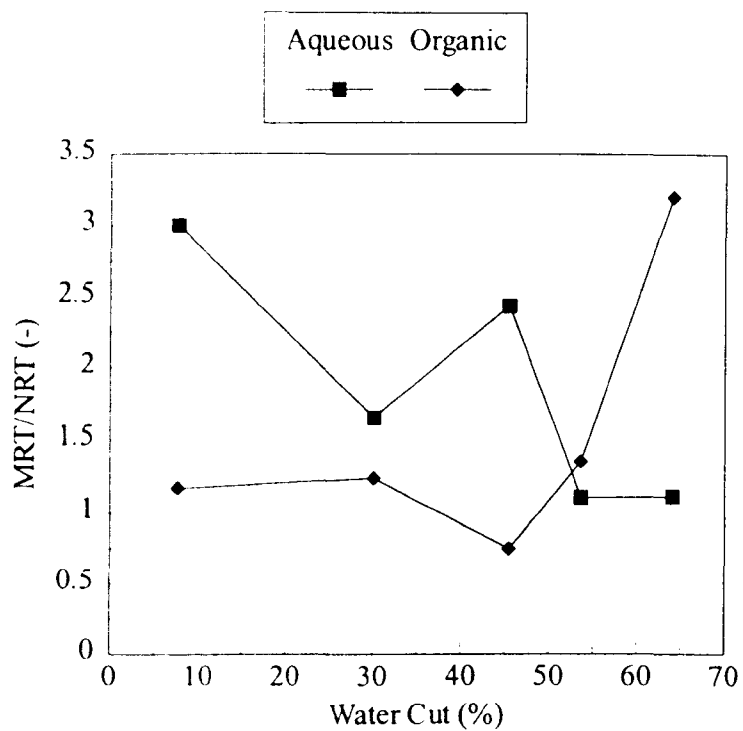


Figure 7.19: Variation of MRT/NRT for Ula Separator

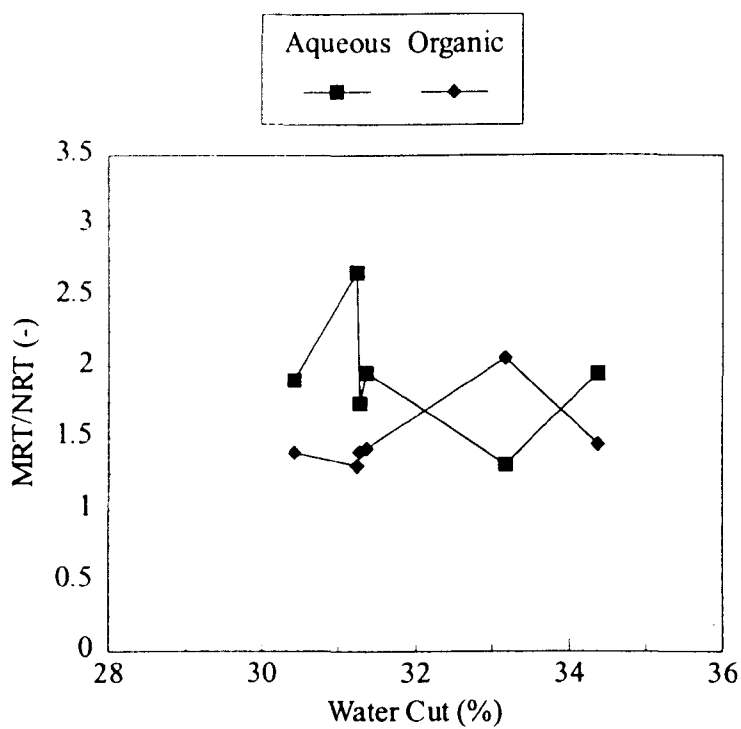


Figure 7.20: Variation of MRT/NRT for Milne Point Separator

7.4 CONCLUSIONS

The Alternative Path Model has been applied to the experimental data obtained for different configurations of the separator tank as described in Chapter 5. The effects upon the parameters of the model and Mean Residence Time of changing weir height and insertion of dip and side baffles have been examined.

The experimental data and flow observations point to the existence of recirculatory zones in the aqueous phase, and possibly the organic phase in the case of the dip baffle. The recirculatory zones cause the presence of secondary peaks and changing the weir height shows that the effect is greatest when the differential velocities between the phases is largest due either to flow rate or oil/water layer thickness.

The side baffles cause quiescent zones in the separator tank and superficially the interface appears cleaner. However this is possibly just a wall effect caused by the baffles. The values of Mean Residence Time were not significantly affected by the side baffles which again suggests large dead zones within the vessel. The side baffles appear to increase recirculation at low flows, perhaps due to extra pooling at the vessel walls, but seem to decrease it at high flows. This may be due to the faster travelling liquid down the centre of the vessel sweeping away the central dead zone completely.

The most important consideration in using this model to characterise performance is to examine differences. Therefore a set of parameters needs to be obtained when the vessel is working well, and then these can be compared with values obtained when the vessel is working badly. For example, the dip baffle appears to aid recirculation

which is shown by an increase in F number, if a secondary peak is already present. It also causes some strange variations in Mean Residence Time. An extreme of a dip baffle would be blocked internals and it is possible that these could be identified by unpredictable Mean Residence Time and an increase in F number. Unpredictable Mean Residence Time and an increase in F number would suggest a blockage causing local acceleration while behaviour similar to inclusion of the side baffles would suggest extra quiescent zones.

Fractional Mixed Volume was found to be quite different between baffled and unbaffled field separators but did not vary as consistently for the test separator, which always had a perforated baffle installed. Values of Fractional Mixed Volume ranged from 0.4-0.6, which is consistent with the BP baffled vessels. If Fractional Mixed Volume was found to change greatly on an existing separator, this would suggest that there was major internal failure of either the inlet diverter or spreading baffle causing greatly increased turbulence. The Residence Time Distribution would also be noticeably less sharp.

Chapter 8

CONCLUSIONS AND FUTURE WORK

Primary separators perform a vital role in providing the first stage separation of oil and mixtures obtained from oil wells. However their bulky size means that they are expensive items to construct and install, particularly on offshore platforms. There has therefore been considerable industrial motivation to reduce size and improve performance of the vessels.

There are several factors to consider when examining which variables will affect separator performance. The flow pattern and drop sizes of any dispersions present will have ramifications for the gravity settling process taking place. Inclusion of internals such as baffles or packing is a more recent development and packing manufacturers claim performance increases. The physical properties of the fluids and flow rates are obviously very important for design. Most current design methods use as their basis gravity settling. Some CFD work has been performed but is limited in its application. The Residence Time Distribution (RTD) of field separators has been measured using a nucleonic technique by BP Exploration as a performance characterisation and diagnostic technique.

In light of these observations, a programme of work which involved measuring drop sizes and flow patterns in pipe flow (Chapter 4) and residence time distributions in a pilot scale separator was performed (Chapter 6). A mathematical transfer function model, the Alternative Path Model, was developed and tested against some field data

from BP Exploration (Chapter 5) and the residence time distributions from the pilot scale separator (Chapter 7).

8.1 DROP SIZES AND FLOW PATTERNS IN LIQUID-LIQUID PIPE FLOWS

Drop size distributions were obtained for dispersions of aqueous potassium carbonate solution in kerosene for a range of flow rates at both horizontal and vertical orientations in a 0.063m pipe. Two drop size measurement techniques were employed, a laser diffraction technique using a Malvern 2600 instrument and a back-scatter technique using a Par-Tec 300C. The back-scatter technique produced distributions of chords rather than diameters, so a mathematical method, the FEM, was proposed and tested against theoretical distributions and some experimental data (Appendix A2). All the data obtained from the Par-Tec was processed using this algorithm.

It was discovered that the instruments were limited to different concentration ranges. The theory of Fraunhofer diffraction, which governs the analysis of the light patterns of the scattered drops from the Malvern, assumes that the light is only scattered by one drop at a time. At high dispersed phase concentrations, multiple scattering of the laser beam occurs and hence the results from the instrument are no longer meaningful. The measurements taken by the Malvern were therefore limited to dispersed phase concentrations below 3% by volume. Conversely, the Par-Tec only gave repeatable results above a concentration of 5%.

The drop size distributions obtained were characterised by use of the Sauter Mean Diameter and little variation was seen with different measurement positions for vertical upflow suggesting that the flow was reasonably homogeneous. However,

stratification at low flow rates for the horizontal configuration caused large variations with position (Appendix A1). Sauter Mean diameters in the range 170-400 μ m were obtained using the Malvern and 250-500 μ m using the Par-Tec. The reason for the discrepancy is likely due to the effects of concentration of the dispersed phase and the coarseness of measurement of the Par-Tec at high size bands.

In order to try to identify any measurement differences which may have been due to measurement technique, both instruments were used to simultaneously measure the size of glass beads suspended in water in a test cell. Good agreement was obtained although the distribution produced by the Par-Tec was slightly wider, particularly at large size bands. The distribution of glass beads measured was however significantly narrower than those obtained from the pipe flow. A systematic study of different distributions and materials, together with perhaps different combinations of sieve cuts forming bimodal distributions would be useful in the future. This work was curtailed in this study due to malfunction of the Par-Tec instrument.

The flow patterns obtained by high speed videography were found to agree reasonably well with the flow pattern map of Brauner and Moalem Maron (1992a,1992b). Scatter present is likely due to the short length of the test section, although the height of the liquid-liquid interface was predicted quite well by the analysis of Taitel and Dukler (1976).

8.2 MATHEMATICAL MODEL OF A PRIMARY SEPARATOR

The Alternative Path Model was developed using a transfer function approach to model the Residence Time Distributions obtained from primary separators. The model was developed and tested against field data supplied by BP Exploration. The

Alternative Path Model was constructed by splitting the separator into a series of zones. At the vessel inlet, the flow was assumed to be well mixed, followed by plug flow behaviour, with some dispersion, in the bulk of the vessel. To allow for short circuiting or dead zones, which can be indicated by secondary peaks in the Residence Time Distribution curves, two parallel paths were put into the bulk flow region, and the time constants could be altered separately. These paths were modelled by the “N stirred tanks in series” approach and the value of N was set to 50.

The fits obtained from the field data were found to be excellent. Other parameters were also developed to characterise the fluid behaviour in the vessels. A “Fractional Mixed Volume” was defined which is the ratio of the volume occupied by the inlet mixing zone to the total vessel volume. It was found that vessels which had a perforated or spreading baffle installed near the inlet had lower values of this parameter. An “F number” was also defined as a measure of presence of secondary peaks on the Residence Time Distribution curve and this parameter was greatest at high oil flows and low water flows. This is consistent with recirculatory zones being set up in the water phase due to a velocity gradient between the water and oil phases.

8.3 RESIDENCE TIME MEASUREMENT AND MODELLING OF A PILOT SCALE SEPARATOR

A colorimetric measurement technique was developed to obtain residence time distributions from a pilot scale separator tank as described in Chapter 3. The technique was found to be repeatable and the inlet pulses, injected by compressed air, were sufficiently fast to be considered as perfect delta functions. Mass balances were performed as a check and the error was found to be quite high due to background haze and dye build up. However, the background was fairly constant for

each run so this error was unimportant after normalising of the data. Overall, the technique was successful and easy to perform due to the on-line recording of the outlet dye concentration using the Jenway 6300 spectrophotometer.

Residence Time Distributions were obtained for different flow conditions for a number of different internal configurations. A different weir height as well as the effect of adding side or dip baffles was tested. Changing the weir height showed that the presence of secondary peaks was greatest when the thickness of the oil layer was a minimum and the thickness of the water layer was maximum. This meant the differential velocities between the phases was a maximum and appeared to create larger recirculatory effects.

The introduction of side baffles did not have the expected effect of decreasing the Mean Residence Time which again suggests the presence of large dead zones in the tank. The baffles would be expected to cause quiescent zones in the tank and indeed the oil –water interface appeared cleaner and more settled close to the tank wall. The baffles appeared to increase recirculation at low flow rates, but decrease it at higher flows. Perhaps this is due to the faster liquid travelling down the centre of the vessel sweeping the dead zones away.

The dip baffle appeared to have the effect of increasing the secondary peak of the oil phase if the oil layer was at a maximum thickness. Inspecting the tank visually showed that there was a lot of pooling and eddying around the baffles which could explain this effect. It appears from the analysis that the most important consideration to be made in using this model to characterise performance is to examine differences

in values of the parameters, rather than the absolute values. It is necessary to obtain a Residence Time Distribution for a vessel when it is working satisfactorily, then compare this with the result when problems occur. For example, a situation which can occur in field vessels is blockage of internals by sand or asphalt. This can be considered as an extreme of a dip baffle as this will cause local phase acceleration. It would be expected in this case that F number would increase due to pooling and eddying past the blockage, but the trend of Mean Residence Time would change, as indeed it did for the dip baffle. Variations in Fractional Mixed Volume tend to occur due to inlet configurations, so a sudden increase in the value of this parameter would be most likely due to mechanical failure or blockage of the inlet diverter or spreading baffles. The shape of the peak of the Residence Time Distribution would also be expected to be less sharp in this case.

8.4 FUTURE WORK

Future work on the pilot scale separator should involve a quantitative measure of separator performance. This could involve isokinetic sampling of the outlet liquids followed by centrifuging to determine the fractions of dispersed phase at different flow rates with different bafflings. This could then perhaps be linked to parameters in the model. Installation of internals such as packings or plates could also be attempted. Installation of different mixers to measure the effect of altering the flow pattern at the inlet would also be a study of interest. It is expected that a dispersed phase would separate less easily than one which is already partially separated, as in the case of stratified or slug flow.

Future work studying the change of drop distribution at different distances from the mixer would be a useful aid to the understanding of flow development. Most of the published work on liquid-liquid systems refers to mixers and there is a dearth of information on flow development of concentrated systems. A systematic study of flow development in different diameter pipes would add greatly to the current knowledge.

A comparative study of the Par-Tec and Malvern instruments with glass beads of different sieve cuts and distribution widths, possibly together with bimodal distributions would be useful in determining which parameters of the measurement are artefacts of the technique. The effect of bead materials of different refractive indices would also be beneficial. The FEM chord to diameter conversion could also be made more robust for rapidly changing distributions by modifying the algorithm.

Bibliography

- Ade-John, A.O. and Jeffreys, G.V. (1978). Flow Visualisation and Residence Time Studies in a Spray Drier, *Trans. IChemE.*, **56**, 36-42
- Al-Deen, M.F.N., Hamad, F.A. and Bruun, H.H. (1998). Kerosene-Water Two-Phase Flow in Vertical and Inclined Pipes, *Third International Conf. on Multiphase Flow, Lyon, France June 8-12 1998*
- Allen, T and Davies, R. (1988) An Evaluation of the Lab-Tec 100 Particle Size Analyser, *Particle Size Analysis*, 33-34, 1988
- Andreas, J.M., Hauser, E.A. and Tucker, W.B. (1938). Boundary Tension by Pendant Drops, *15th Colloid Symposium, Cambridge, Massachusetts*, June 9-11 1938, 1001-1019
- Arnold, K.G. and Koszela, P.J. (1990). Droplet settling versus retention time theories for sizing an oil/water separator, *SPE Production Engineering*, **5** (1), 59-64
- Azzopardi, B.J. (1997). Drops in Annular Two-Phase Flow, *Int. J. Multiphase Flow*, **23** (S), 1-53
- Azzopardi, B.J. and Hervieu, E. (1994). Phase Separation at T-Junctions, *Multiphase Science and Technology*, **8**, 645-714
- Azzopardi, B.J., Freeman, G. and King, D.J. (1980). Drop Sizes and Deposition in Annular Two-Phase Flow. *UKAEA Report AERE R9634*
- Azzopardi, B.J., Zaidi, S.H. and Sudlow, C.A. (1996). The Effect of Inclination on Drop Sizes in Annular Gas-Liquid Flow, *European Two-Phase Flow group Meeting, Grenoble, 2-5 June 1996*
- Azzopardi, B.J., Sudlow, C.A. & James, P.W. (1999) The effect of a ball valve on liquid /liquid flows. In preparation.
- Bailes, P.J. (1995). An Electrical Model for Coalescers that Employ Pulsed DC Fields, *Trans IChemE*, **73**, 559-566
- Bailes, P.J. and Larkai, S.K.L. (1981). An Experimental Investigation into the Use of High Voltage D.C. Fields for Liquid Phase Separation, *Trans IChemE*, **59**, 229-237
- Bailes, P.J. and Larkai, S.K.L. (1981). Liquid Phase Separation in Pulsed DC Fields, *Trans IChemE*, **59**, 115-121
- Bochangel, J. (1986). Design of Liquid / Liquid Gravity Separators, *Chemical Engineering*, **93** (4), 133-135
- Bodden, M. and Mewes, D. (1995). Two-Phase Flow Inside the Upper Plenum of a PWR, *European Two-Phase Flow Group Meeting, 1995, Netherlands*, 1-17
- Bon, L. and Alhassani, G. (1982). How to Check the Capacity of Existing Separators, *World Oil*, **194** (7), 253
- Brauner, N. and Moalem Maron D. (1992). Flow Pattern Transitions in Two-Phase Liquid-Liquid Flow in Horizontal Tubes, *Int. J. Multiphase Flow*, **18** (1), 123-140

- Brauner, N. and Moalem Maron D. (1992). Stability Analysis of Stratified Liquid-Liquid Flow, *Int. J. Multiphase Flow*, **18** (1), 103-121
- Breman, B.B. Beenackers A.A.C.M. and Bouma M.J. (1995). Flow Regimes, Gas Hold Up and Axial Gas Mixing in the Gas/Liquid Multistage Agitated Contactor, *Chem. Engng. Sci.*, **50** (18), p 2963
- Broussard, G.L., Meldrum, N. and Choi, M.S. (1992). Case History: Design, Implementation and Results of Separator Retrofits, *Society of Petroleum Engineers*, 425-433
- Calderbank, P.H. (1958). Physical Rate Processes in Industrial Fermentations; Part I: The Interfacial Area in Gas-Liquid Contacting with Mechanical Agitation, *Tran. Inst. Chem. Eng.*, **36**, 443-463
- Charles, M.E., Govier, G.W. and Hodgson, G.W. (1961). The Horizontal Flow of Equal Density Oil-Water Mixtures, *Can. J. Chem. Eng.*, 27-36, February 1961
- Clark, N.N. and Turton, R. (1988). Chord Length Distributions Related to Bubble Size Distributions in Multiphase Flow, *Int. J. of Multiphase Flow*, **14** (4), 413-424
- Clark, N.N., Liu, W. and Turton, R. (1996). Data Interpretation Techniques for inferring Bubble Size Distribution from Probe Signals in Fluidized Systems, *J. Powder Technology*, **88**, 179-188
- Clarke, A. and Issa, R.I. (1997) A Numerical Model of Slug Flow in Vertical Tubes, *Computers & Fluids*, **26** (4), 395-415
- Coker, A.K., (1993). Computer Program Enhances Guidelines for Gas/Liquid Separator Designs, *Oil & Gas J.*, **91** (19), 55-62
- Colenbrander, G.W. (1991). CFD in Research for the Petrochemical Industry, *Applied Scientific Research*, **48**, 211-245
- Davies, G.A. (1992). Mixing and Coalescence Phenomena in Liquid-Liquid Systems, *Science and Practice of Liquid-Liquid Extraction*, **1**, 245-342, Clarendon Press
- Davies, G.A., Personal Communication (1998)
- Dovas, S., Kostoglou, M. and Karabelas, A.J. (1996). A New Method for Computing the Steady State Size Distribution of Dispersions in Breakage Processes, *European Two-Phase Flow Group Meeting, Grenoble*, June3-5, 1996
- Druzhinin, O.A. and Elghobashi, S.E. (1998) DNS of Bubble Laden Turbulent Flows using the Two-Fluid Formulation, *Third Int. Conf. on Multiphase Flow, Lyon France, June 8-12 1998*
- Elghobashi, S.E. (1994) On Predicting Particle-Laden Turbulent Flows, *App. Sci. Res.*, **52**, 309-321
- ✓ El-Hamouz, A.M. and Stewart, A.C. (1996). On-line drop size distribution measurement of oil-water dispersion using a Par-Tec M300 laser back-scatter instrument, *SPE International*, 36672:1-14

- ★ El-Hamouz, A.M., Stewart, A.C. and Davies, G.A. (1995). A Study of Kerosene-Water Dispersions in Shear Flow Through Pipes and Fittings, *Two-Phase Flow Modelling and Experimentation*, 987-997
- Farrar, B. and Bruun, H.H. (1996). A Computer Based Hot-Film Technique used for Flow Measurements in a Vertical Kerosene-Water Pipe Flow, *Int. J. Multiphase Flow*, **22** (4), 733-751
- Fewel, J.R and Kean J.A. (1992). Computer Modelling Aids Separator Retrofit, *Oil & Gas J.*, **90** (27), 76-80
- Franca, F. and Lahey, R.T., (1992). The Use of Drift-Flux Techniques for the Analysis of Horizontal Two-Phase Flows, *Int. J. Multiphase Flow*, **18** (6), 787-801
- Fujii, T., Junichi, O. Takeshi, N. and Morimoto, O. (1994). The Behaviour of an Immiscible Equal-Density Liquid-Liquid Two-Phase flow in a Horizontal Tube, *JSME International Journal*, **B37** (1), 22-29
- Gerunda, A. (1981). How to Size Vapour Liquid Separators", *Chem. Engng.*, **88** (9), 81-84
- Godfrey, J.C., Obi, I.N. and Reeve, N. (1987). Measurement of Drop Size in Continuous Liquid-Liquid Mixers, *Fluid Mixing III, Inst. Chem. Engng. Symp. Ser. No. 108*, 123-180, Instn. Chem. Engng., Rugby, UK
- ★ Godfrey, J.C., Obi, I.N. and Reeve, N. (1989). Measuring Drop Size in Continuous Liquid-Liquid Mixers, *Chemical Engineering Progress*, December 1989, 61-69
- Gosman, A.D., Lekakou, C. and Politis, (1992) Multidimensional Modelling of Turbulent Two-Phase Flows in Stirred Vessels, *AIChE J.*, **38** (12), 1946-1956
- Grabmuller, H. and Schadlich, H.K., (1983). Residence Time of a Plug Flow in a Finite Packed Bed Chemical Reactor, *Chem. Eng. Sci.*, **38** (9), 1543-1553
- Guzhov, A., Grishin, A.D., Medredev, V.F. and Medredeva, O.P. (1973). Emulsion Formation During the Flow of Two Immiscible Liquids, *Neft. Choz* (in Russian), **8**, 58-61
- Hadjiev, D and Kuychonkov, G., A. (1989). Separator for Liquid/Liquid Dispersions, *Chemical Engineering Journal*, **41**, 113-116
- Hafskjold, B and Morrow, T.B. (1994). Drop Drop Coalescence in Oil Water Separation, *Proceedings-SPE Annual Technical Conference and Exhibition*, **2**, 203-212
- Hafskjold, B. and Dodge, F. (1989). An Improved Design Method for Horizontal Gas/Oil and Oil/Water Separators, *64th Annual Technical Conference and Exhibition of the Society of Petroleum Engineers, 1989, San Antonio*
- Hansen, E. W. M., Celius, H.K. and Hafskjold, B. (1995). Fluid Flow and Separation Mechanisms in Offshore Separation Equipment, *Two Phase Flow Modelling and Experimentation*, 999-1004
- Hansen, E. W. M., Heitmann, H. Laksa, B. and Loes, M., (1994). Numerical Simulation of Fluid Flow Behaviour Inside and Redesign of a Field Separator, *Two Phase Flow Modelling and Experimentation*, 117-128

- Hansen, E. W. M., Heitmann, H. Laksa, B., Ellingsen, A., Ostby, O., Morrow, T.B. and Dodge, F.T. (1991). Fluid Flow Modelling of Gravity Separators, *5th International Conference on Multiphase Production, 1991 Cannes*, A.P Burns (Ed), 364-381
- Herm-Stapelberg, H. and Mewes, D. (1994). Pressure Drop Calculation in Three-Phase Slug Flow of Water, Oil and Air. *International Chemical Engineering*, **34** (3), 295-314
- Herm-Stapleberg, H. and Mewes, D. (1992). Calculation of Pressure Drop in Ternary Slug Flow of Oil, Water and Air, *Chemie Ingenieur Technik*, **64** (2), 155-171
- Herringe, R.A., and Davis, M.R. (1976). Structural development of gas –liquid mixture flows, *J. Fluid Mechs*, **73** (1), 97-123
- Hesketh, P., Russell, T.W.F and Etchells, A.W. (1987). Bubble Size in Horizontal Pipelines, *AIChE Journal*, **33**, 289-295
- Hinze, O. (1955). Fundamentals of the Hydrodynamic Mechanism of Splitting in Dispersion processes, *AIChE Journal*, **1**, 289-295
- Hirt, C.W. and Nichols, B.D. (1981). Volume of Fluid (VOF) Model for the Dynamics of Free Boundaries, *Journal of Computational Physics*, **39**, 201-225
- Hobbel, E.F., Davies, R., Rennie, F.W., Allen, T., Butler, L.E., Waters, E.R., Smith, J.T. and Sylvester, R.W. (1991). Modern Methods of On-line Size Analysis for Particulate Process Streams, *Part. Part. Syst. Charact.*, **8**, 29-34
- Issa, R.I. and Oliveira, P.J. (1994). Numerical Prediction of Phase Separation in two-phase Flow Through T-Junctions, *Computers Fluids*, **23** (2), 347-372
- James, P.W., Azzopardi, B.J., Graham, D.I. & Sudlow, C.A. (1999) The effect of a bend on droplet size distribution in two-phase flow. *Submitted to Int.J.Multiphase Flow*
- Karabelas, A.J. (1978). Droplet Size Spectra Generated in Turbulent Pipe Flow of Dilute Liquid/Liquid Dispersions, *AIChE J*, **24** (2), 170-180
- Kline, S.J. and McClintock, F.A. (1953). Describing the Uncertainties in Single-Sample Experiments, *Mechanical Engineering*, **75**, p3-8
- Kostoglou, M. and Karabelas, A.J. (1998). On the Attainment of Steady State in Turbulent Pipe Flow of Dilute Dispersions, *Chem. Eng. Sci.*, **53** (3), 505-513
- Kostoglou, M. and Karabelas, A.J. (1998). On the Evolution of Droplet Size Distribution in Turbulent Flow of Dilute Dispersions, *Third Int. Conf. on Multiphase Flow, Lyon, France, June 8-12 1998*
- Kostoglou, M., Dovas, S. and Karabelas, A.J. (1997). On the Steady State Size Distribution of Dispersions in Breakage Processes, *Chem. Eng. Sci.*, **52** (8), 1285-1299
- Kubie, J. and Gardner, G.C. (1977). Drop Sizes and Drop Dispersion in Straight Horizontal Tubes and in Helical Coils, *Chem. Eng. Sci.*, **32**, 195-202
- Kurban, A.P.A., Angeli, P.A., Mendes-Tassis, M.A. and Hewitt, G.F. (1995). Stratified and Dispersed Oil-Water Flows in Horizontal Pipes, *7th International Conference on Multiphase Production, Cannes, France*, 277-289

- Lahey, R.T. and Drew D.A. (1992). On the Development of Multidimensional Two Fluid Models for Vapour-Liquid Two Phase Flows, *Chem. Eng Comm.*, **118**, 125-139
- Lahey, R.T. and Drew, D.A., (1992) On the development of Multidimensional Two-Fluid Models for Vapour/Liquid Two Phase Flows, *Chem. Engng. Communications*, **118**, 125-139
- Langston P. A., Heyes D. M., Tüzün U. (1995). Discrete Element Simulation of Granular Flow in 2D and 3D Hoppers : Dependence of Discharge Rate and Wall Stress on Particle Interactions. *Chem. Eng. Sci.*, **50**, 967.
- Launder, B.E. and Spalding, D.B. (1972) Lectures in Mathematical Modelling of Turbulence, *London Academic Press*
- Levenspiel, Chemical Reaction Engineering, 2nd Edition, *John Wiley and Sons*.
- Liu, W., Clark, N.N. and Karamavruc, A.I. (1998). Relationship Between Bubble Size Distributions and Chord Length Distribution in Heterogeneously Bubbling Systems, *Chem. Eng. Sci.*, **53** (6), 1267-1276
- Lockhart, R.W. and Martinelli, R.C. (1949). Proposed Correlation of Data for Isothermal, Two-Phase, Two-Component Flow in Pipes, *Chem. Eng. Prog.*, **45**, 39-48
- Lun, I., Calay, R.K. and Holdo, A.E. (1996). Modelling Two-Phase Flows using CFD, *Applied Energy*, **53** (3), 299-314
- Luyben, W.L. (1990) Process Modelling, Simulation and Control for Chemical Engineers, 2nd Edition, *McGraw-Hill International Publications*
- Markatos, N.C. (1993). Mathematical Modelling of Single Phase and Two-Phase Flow in the Process Industries, *Revue de L'Institute Francais du Petrole*, **48** (6), 631-662
- Meon, W., Rommel, W. and Blass, E. (1993). Plate Separators For Dispersed Liquid/Liquid Systems: Hydrodynamic Coalescence Model, *Chem Eng Sci*, **48** (1), 159-168
- Milne Point Unit Slug-Catcher/Separator Tests (1997), *BP Internal Report No. SPR/TRT/020/97*
- Mohamad Nor, M.I. and Wilkinson D. (1998). Experimental and CFD Studies to Improve Oil-Water Separation in Horizontal Separators, *1998 IChemE Research Event, Newcastle, England*
- Mohamad Nor, M.I. and Wilkinson D. (1998). Oil-Water Separation in Horizontal Separators, *1998 IChemE Research Event, Newcastle, England*
- Morud, K.E. and Hjertager, B.H. (1996). LDA Measurements and CFD Modelling of Gas-Liquid Flow in a Stirred Vessel, *Chem. Eng. Sci.*, **51** (2), 233-249
- Nadler, M. and Mewes, D. (1997). Flow Induced Emulsification in the Flow of Two Immiscible Liquids in Horizontal Pipes, *Int. J. Multiphase Flow*, **23** (1), 55-68
- Netto, R.F.N., Mendes de Moura, L.F. and Alves, N.A. (1995) Bubble and Slug Vertical Flow Numerical Simulation Using an Eulerian-Lagrangian Description, *7th International Conference on Multiphase Production, Cannes, France: 7-9 June 1995*
- Oglesby, K.D. (1979). An Experimental Study on the Effects of Oil Viscosity, Mixture Velocity and Water Fraction on Horizontal Oil-Water Flow, *MSc Thesis, University of Tulsa*

- Pacek, A.W. and Nienow, A.W (1997). Breakage of Oil Drops in a Kenics Mixer, *BHR Group 1997 Process Internsification*, 165-174
- Pacek, A.W. and Nienow, A.W. (1995). A Problem for the Description of Turbulent Dispersed Liquid-Liquid Systems, *Int. J. Multiphase Flow*, **21** (2), 323-328
- Pacek, A.W. Nienow, A.W. and Moore I.P.T, (1994). On the Structure of Turbulent Liquid-Liquid Dispersed Flows in an Agitated Vessel, *Chem. Eng. Sci.*, **49** (20), 3485-3498
- Patrick, R.H., Klindera T., Crynes L.L., Cerro R.L., Abraham_MA (1995). Residence Time Distribution in a 3 Phase Monolith Reactor, *AIChE J.*, **41** (3), 649-657
- Performance Trials on F801 Separator, BP Kinneil, Grangemouth (1997), *BP Internal Report No. 10/EC97/149*
- Peyret, R. (1996) Handbook of Computational Fluid Dynamics, *London Academic Press*
- Radioisotope Studies of C1001, C2001 & C2002 Separators, BP Magnus Platform, *BP Internal Report No. EC96/083*
- Robertson, D.S. Lawson, P.N.E. and Little L.M., Developments in Separator Design, Methods and Hardware, BPX, Sunbury-on-Thames, UK
- Rommel, W., Blass, E and Meon, W. (1992) Plate Separators For Dispersed Liquid/Liquid Systems: Multiphase Flow, Droplet Coalescence, Separator Performance and Design, *Chem. Eng. Sci.*, **47** (3), 555-564
- Rowley, M.E. and Davies, G., (1988) The Design of Plate Separators for the Separation of Oil/Water Dispersions, *Chem. Eng. Res. Des.*, **66** (4), 313-322
- Russell, T.W. F., Hodgeson, G.W. and Govier, G.W. (1959). Horizontal Pipeline Flow of Mixtures of Oil and Water, *Can. J. Chem. Eng.*, 9-17, February 1959
- Seville JPK, Tüzün U, Clift R. (1997). Processing of Particulate Solids, *Blackie Academic & Professional*. ISBN 0 7514 0376 8
- Shemagin, I.A. (1985) Wave Flow of a Liquid Film in a Horizontal Separator, *Fluid Dynamics*, **20** (2), 316-318
- Simmons, M.J.H., Azzopardi, B.J. and Zaidi, S.H., (1998), Measurement of Drop Sizes and Flow Patterns in Liquid-Liquid Pipe Flow, *3rd Int. Conf. On Multiphase Flow, Lyon France, June 8-12 1998*
- Simmons, M.J.H., Azzopardi, B.J., Lester, E. and Zaidi, S.H. (1998). Drop Size Measurements and Flow Patterns in Liquid-Liquid Pipe Flows, *1998 IChemE Research Event, Newcastle, April 1998*
- Simmons, M.J.H., Langston, P.A. and Burbidge, A.S., (1998). Particle and Drop size Analysis from Chord Distributions, *Powder Technology* (in print)
- Smalley, C. Investigating the Performance of Separators Using Radioisotopes, *ICI Tracerco Report*
- Sparks, R.G. and Dobbs C.L. (1993) The Use of Laser Backscatter Instrumentation for the On-Line Measurement of the Particle Size Distribution of Emulsions, *Part. Part. Syst. Charact.*, **10**, 279-289

- Svrcek, W.Y. & Monnery, W. D. (1993). Design Two Phase Separators within the Right Limits, *Chem. Eng. Prog.*, **89** (10), 53-60
- Swanborn, R.A. (1995). New Separator Internals Cut Revamping Costs, *Journal of Petroleum Technology*, **47** (8) 688-693
- Swithenbank, J., Beer, J.M., Taylor, D.S., Abbot, D. and McCreath, G.C. (1976). A Laser Diagnostic for the Measurement of Droplet and Particle Size Distributions, *Prog. Astronaut. Aeronaut.*, **1**, 421-447
- Taitel, Y. and Dukler, A.E. (1976). A Model for Predicting Flow Regime Transitions in Horizontal and Near Horizontal Gas-Liquid Flow, *AIChE J.*, **22** (1), 47-55
- Talavera, G., (1990). Selecting Gas / Liquid Separators, *Hydrocarbon Processing*, **69**, 81-84
- Trallero, J.L., Sarica, C. and Brill, J.P. (1997). A Study of Oil-Water Flow Patterns in Horizontal Pipes. *SPE Production and Facilities*, August 1997, 165-172
- Ula Separators-Trials on HP and Test Separators (1995), *BP Internal Report No. XFE/014/95*
- Viles, J.C., (1993), Predicting Liquid Reentrainment in Horizontal Separators, *Journal of Petroleum Technology*, **45** (5), 405-409
- Wendt, J.F. (Ed.) (1996) Computational Fluid Dynamics-An Introduction, *A Von Karman Institute Book*
- Wicks, M. and Dukler, A.E. (1966). In-Situ Measurements of Drop Size Distribution in Two-Phase Flow- A New Method for Electrically Conducting Liquids, *AIChE-Proc. Third International Heat Transfer Conf.*, 39-49
- Wilkinson, D., and Waldie, B. (1994). CFD and Experimental Studies of Fluid and Particle Flow in a Horizontal Primary Separator, *Trans. IChemE*, **72** (A), 189-196
- Winsky, S.G. (1994). New Advanced Solids/Oil/Water Separator, *Proceedings of the Permian Basin Oil and Gas Recovery Conference*
- Wu, F.H. (1984). Drum Separator Design-a New Approach, *Chem. Engng.*, **91** (7), 74-80
- Zienkiewicz, O.C., and Taylor, R.L. (1989). The Finite Element Method, 4th Ed.

Nomenclature

Variables

\dot{m}	mass flux	(kg/m ² s)
A	absorbance	(A)
a	parameter of upper-limit log-normal distribution	(-)
c(t)	concentration at time t	(kg/m ³)
C _d	drag coefficient	(-)
D	fractional mixed volume	(-)
D	tube diameter	(m)
d ₃₂	Sauter Mean Diameter	(m)
d ₉₅	drop diameter at 95%	(m)
d _{max}	maximum drop diameter	(m)
η	dynamic viscosity	(kg/ms)
E(t)	residence time distribution at time t	(-)
Eo _D	Eotvos number	(-)
F	F number	(-)
f	friction factor	(-)
F(t)	cumulative age distribution at time t	(-)
F _b	buoyancy force	(N)
F _d	drag force	(N)
F _g	gravity force	(N)
g	acceleration due to gravity	(m/s ²)
h	interface height	(m)
j	phase superficial velocity	(m/s)
ν	kinematic viscosity	(m ² /s)

l	characteristic length	(m)
χ	Lockhart Martinelli parameter	(-)
m_{IE}	mass flux of entrained drops	(kg/m ² s)
p	pressure	(N/m ²)
P	wetted perimeter	(m)
δ	parameter of upper-limit log-normal distribution	(-)
Q	volumetric flow rate	(m ³ /s)
R	radius	(m)
Re	Reynolds Number	(-)
s	complex parameter	(-)
S	surface flow area	(m ²)
σ	surface tension	(N/m)
t	time	(s)
τ	time constant (mean residence time)	(s)
t_m	mean residence time	(s)
u	phase velocity	(m/s)
u_t	terminal velocity	(m/s)
V	volume	(m ³)
ϕ	volume fraction of dispersed phase	(-)
We	Weber Number	(-)
X	diameter ratio, d/d_{32}	(-)
z	axial length along a tube	(m)
T_t	shear stress	(N/m ²)
ρ	density	(kg/m ³)

Subscripts

- c continuous phase
- d dispersed phase
- g gas
- l liquid
- s superficial

Appendix A1

CALCULATION OF LIQUID PHYSICAL PROPERTIES

1.1 DENSITY MEASUREMENTS

The density of the kerosene and potassium carbonate solution was obtained by use of a 25 cm³ density bottle. An average of 3 measurements was taken for each fluid at 22°C.

Table A1.1: Density Measurements

Measurements	Kerosene	Potassium carbonate solution
1	797.44	1165.80
2	797.11	1165.70
3	797.20	1166.45
Average	797.25	1166.00

1.2 DYNAMIC VISCOSITY MEASUREMENTS

The viscosity of the liquids was measured using an Ostwald viscometer, calibrated using water at 22°C. The viscosity of water is $9.572 \cdot 10^{-4}$ kg/ms at 22°C. The time for the liquid to fall through the viscometer was taken as an average of 3 readings. Now

$$\frac{\mu_l}{\mu_w} = \frac{\rho_l t_l}{\rho_w t_w} \quad (\text{A1.1})$$

Table 1.2: Viscosity Measurements

Times	Water	Kerosene	K ₂ CO ₃ Solution
1	89.56	210.39	126.42
2	89.65	210.79	125.85
3	89.33	210.06	125.32
Average	89.51	210.41	125.86
10 ⁻³ .Viscosity (kg/ms)	0.957	1.798	1.5734

1.3 INTERFACIAL TENSION

This was measured by the ring method but proved to be somewhat troublesome. It is possible that this is due to the presence of surfactants in the oil phase. A range of values was obtained where the interfacial tension of kerosene and potassium carbonate ranged from 0.011 to 0.016 N/m

A pendant drop method as described by Andreas *et al.* (1938) was also tried where a drop of potassium carbonate was suspended in kerosene from a narrow bore hollow glass rod. Again there was a range in the values obtained of 0.008-0.011 N/m. It was therefore decided to use a value of 0.01 N/m.

Appendix A2

TECHNIQUES FOR CONVERTING CHORD DISTRIBUTIONS TO DIAMETER DISTRIBUTIONS

(To be Published in Powder Technology, in Print)

A2.1 INTRODUCTION

An advantage of the majority of the techniques that have been employed to measure droplet sizes is that diameter is either directly measured or easily derived. However, these methods can only obtain useful data from dilute systems. The Par-Tec 300C instrument used in the particle sizing studies in Chapter 4 can obtain data at higher concentrations of dispersed phase, but present the data in the form of chord length. It is necessary to convert this data to an equivalent diameter distribution in order to compare the results with other techniques.

Herringe and Davis (1976) presented probabilistic techniques to solve a similar problem which arises with the use of needle conductance probes, but the output is very dependent upon the shape of the particles and can suffer problems with very irregular distributions. Clark and Turton (1988) proposed transforms to generate size distributions from chord measurements for a variety of different shaped bubbles. Hobbel *et al.* (1991) described a method of calculating diameter distributions from chord distributions assuming random sphere cuts. Most recently, Liu *et al.* (1998) have considered the probability relationships in obtaining representative overall bubble size distributions from local bubble chord measurements in heterogeneous bubbling systems, such as fluidised beds.

This appendix details two methods which have been developed to obtain diameter distributions from chord data: a probability apportioning method and a finite element method. Both methods are applied to three separate sets of chord data, one generated from simple geometry, one from the Par-Tec probe and one developed from an existing particle flow model (Langston *et al.* 1995) to simulate the Par-Tec instrument. The results were examined to see how well the original diameter distributions could be deconvoluted using each technique.

A2.2 GENERATION OF CHORD DISTRIBUTIONS

The generation of chord size distributions from known diameter distributions is necessary in order to test the effectiveness of the methods. Three methods of obtaining sets of data have been used, the first “ideal” data developed by calculating a chord distribution from an assumed diameter distribution using the methods in Section 4.2.2. The second is true experimental data from the Par-Tec probe. The third method is a pseudo-experimental model that takes into account the sampling characteristics of the Par-Tec measurement and is described in greater detail below. The choice of three independent data sets gives greater freedom to test the robustness of the estimation methods.

A2.2.1 Distinct Element Model (DEM) of Par-Tec Instrument

A simulation of the Par-Tec instrument has been developed using a modified DEM simulation (Langston *et al.* (1995)). The simulation was originally developed to model the flow of granular materials in hoppers and silos. This models spheres falling into a silo coming to rest at the bottom and then discharging when the orifice at the base is opened. With appropriate data this has been used to replicate chord

size detection by the Par-Tec instrument. The simulation is run for the initial stages of filling the silo. The particles constitute a very lean phase falling in mid-air, so there is no packing and organisation of structure that would affect the independent nature of the chord measurements. The simulation is “frozen” with the particles suspended and the position and diameter of the particles is recorded. There are 5000 particles of diameters between 0.2 and 0.5 and the silo diameter is 30 and height 80. The chord detection is then simulated by passing a circle of radius r up the hopper to form a cylinder (Figure A2.1).

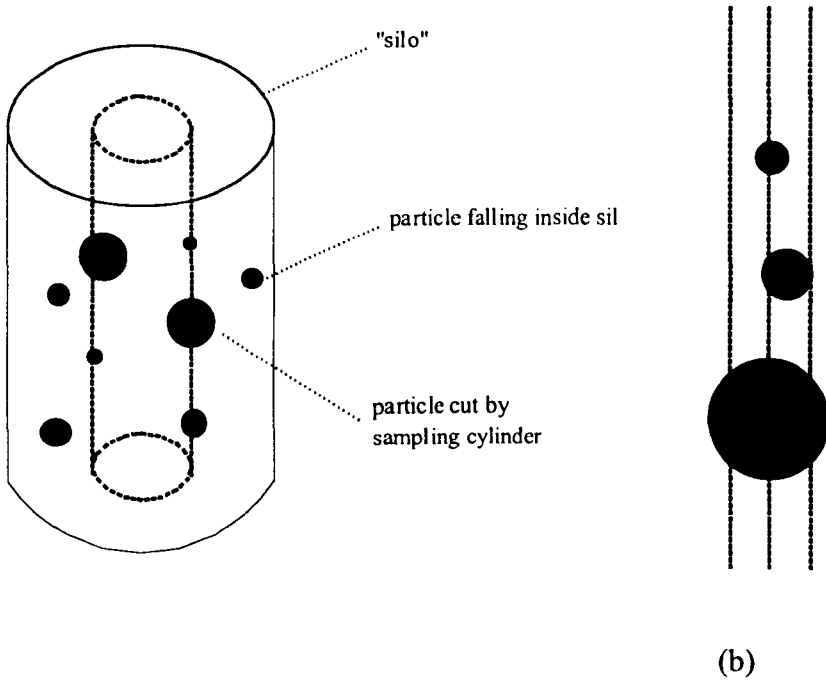


Figure A2.1: Schematic of PAM/DEM simulation chord size sampling (a) showing probability of ‘hitting’ a particle is proportional to its diameter (b)

Where the cylinder intersects a particle, the maximum horizontal cut length and diameter are noted. The number of particles detected is therefore time independent in the simulation. In reality the absolute number of particles detected by the Par-Tec sensor is obviously a linear function of velocity for the same particle concentration

and detection period, but the effect in terms of the chord size distribution generated from a dilute assembly of spheres is considered to be the same.

The main benefit of this analysis is that a chord size distribution is obtained where the actual sphere diameter distribution is known. Therefore, a direct measure of the effectiveness of the methods used to generate the diameter distribution can be made. It can also be shown how good the sample is at representing the overall population. A comparison of the distribution obtained from cutting a percentage of the 5000 particles can be made to the original distribution. It also allows the robustness of the diameter deconvolution methods to be evaluated when the probability distributions are not ideal.

The total sample size is an important parameter when determining the minimum percentage cut which can be representative of the entire system. It is important to have a statistically significant sample size when determining the diameter distribution and this in turn depends upon the dispersion of droplet diameter. Data has been presented from photographic based measurement techniques where the sample size is of the order of 250-500 particles (Karabelas (1978)). This small sample size is due to the rather tedious analysis procedures of such techniques but this is very small when compared to samples of the order of thousands that can be obtained very quickly from either conductance probes or the Par-Tec instrument. To obtain confidence that the sample size is adequate, comparison of samples obtained at the same conditions should be made to show they are repeatable.

A2.3 CONVERSION METHODS FOR INTERPRETATION OF CHORD DATA

The best method currently available would seem to be that due to Hobbel *et al.* (1991). The authors describe a method of calculating diameter distributions from chord distributions assuming random sphere cuts. This is basically a “peeling” method where the largest chord size is assumed to be the largest diameter, and the chord distribution from this diameter is subtracted from the total chord size distribution. This is repeated for successively smaller diameters. As noted in the reference this method is sensitive to “noise” in the population of the largest sizes. The two methods developed below do not suffer from this problem, although each has its own virtues and disadvantages which will become apparent later. Presented below are two alternative methods which can be used to convert the chord distributions to diameter distributions.

A2.3.1 Probability Apportioning Method (PAM)

This method assumes that the diameter bands are known, then back-calculates the diameter distribution from the chord data using equation 4.7. Each chord size detected is taken and then the probability P_i that the particle has diameter d_i , is calculated. Here d_i is the representative of the i th diameter “bin” in the diameter distribution. Again it is assumed that each particle detection is independent of all others and that each particle is randomly cut. Figure 2 shows probability distributions for six diameters between 0.2 and 0.5 in bands of 0.01, e.g. the probability that a random cut on a particle of diameter 0.225 will give a chord length between 0.09 and 0.1 is about 0.022. (NB this method uses arbitrary particle diameters except for the Par-Tec measurements, which are in microns.)

P_i is calculated from equation 4.7 for each diameter band d_i . Obviously P_i will be zero if the chord length is greater than d_i . If information on the particle diameters is known, the values of d_i can be chosen to reflect this, otherwise a set of trial values can be used. The probabilities from each cut are summed and the distribution for d_i is thus accumulated. This distribution is then re-scaled because the probability of a particle being hit is proportional to its diameter as shown by Hobbel *et al.* (1991) and as already illustrated in Figure A2.1. That is P_i is divided by d_i and then normalised so that $\sum P_i=1.0$.

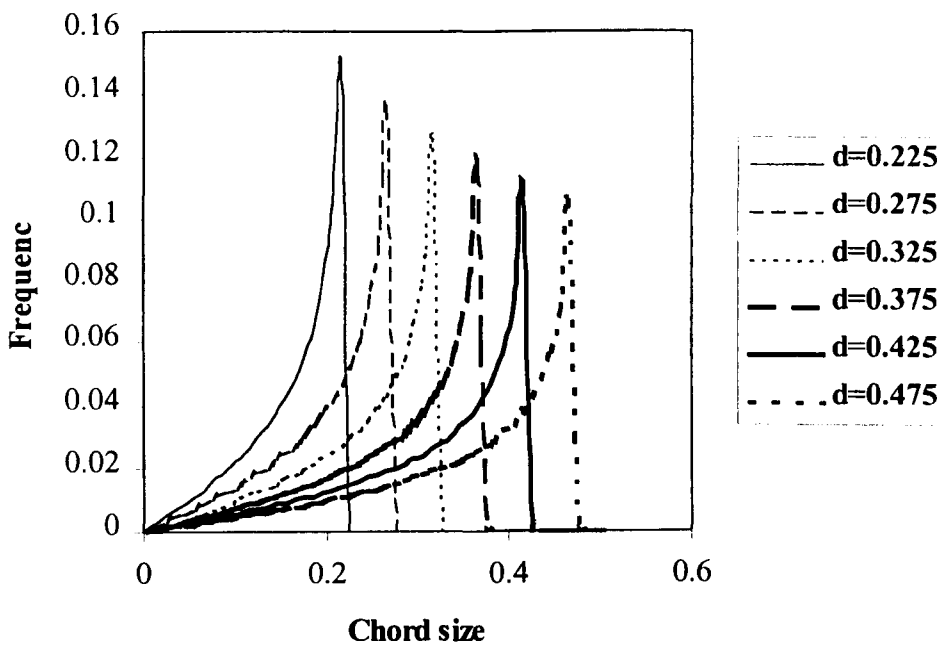


Figure A2.2: Chord Probability Distributions for Random Sphere Cuts- six diameters between 0.2 and 0.5

This method is inherently simple and stable. It assumes that each particle-detection is independent of all others. It does not give more weighting to the detection of the larger particles as the “peeling” method described previously. However, each item

of data is used in isolation, and thus does not utilise the collective information from the overall set, unlike the FEM described below.

A2.3.2 Finite Element Method (FEM)

This method uses a Galerkin finite element technique (Zienkiewicz and Taylor (1997)) to solve simultaneously the equations relating the chord data to the diameter distribution. This method also addresses cumulative error problems associated with the “peeling off” method. As the method also considers the collective information from the entire data set, rather than each particle size individually, it is more robust than the PAM.

In order to develop this method, Equation 4.7 from section 4.2.2 can be modified to include a bandwidth, $2w$. If we assume the probability of chord size detection at size x from a particle within true diameter band k is given by:

$$P_k(x) = \frac{\sqrt{D_k^2 - (x - w)^2} - \sqrt{D_k^2 - (x + w)^2}}{D_k} \quad (\text{A2.1})$$

where D_k = diameter of particle band k and w is half the width of the diameter band.

If a polydisperse dilute particle mixture is considered, the total number of chords measured at size x , $\hat{n}(x)$, can be obtained by summing the contributions from all the particles for every diameter of particle in the mixture.

$$\hat{n}(x) = \sum_{k=1}^K n_k P_k(x) \quad (\text{A2.2})$$

where n_k is the number of particles in the k^{th} diameter band of the system. The diameter bands can be set arbitrarily equal to the size of the chord bands, or set by experience if some other parameters for the mixture are known.

If $n(x)$ is the true number of counts at chord size x , then a measure of the quality of the discretised estimate, i.e. the residual, at point x can be given by

$$R(x) = n(x) - \hat{n}(x) = n(x) - \sum_{k=0}^K n_k P_k(x) \quad (\text{A2.3})$$

This can be integrated over all values of x with an arbitrary weighting function over the range of chord sizes to give us the total weighted residual of the discrete system.

Now we wish to solve for n_k , so we seek the set of n_k that will minimise this weighted residual, i.e. the best fit. The weighting function for the Galerkin finite element method is as follows, ensuring that the total residual is minimised with respect to variations of n_k at all true diameter bands.

$$R_i = \int_0^x \frac{\partial \hat{n}(x)}{\partial n_i(x)} (n(x) - \hat{n}(x)) dx \quad (\text{A2.4})$$

Hence we have the same number of equations as true diameter bands. This is a closed system as the number of equations is the same as the number of degrees of freedom.

Since, by differentiation of equation A2.2

$$\frac{\partial \hat{n}(x)}{\partial n_i(x)} = P_i(x) \quad (\text{A2.5})$$

and substituting into equation A2.4

$$R_i = \int_0^x P_i(x) [n(x) - \hat{n}(x)] dx = 0 \quad (\text{A2.6})$$

and then substituting from equation A2.2, we obtain the result.

$$R_i = \int_0^x P_i(x) \left[n(x) - \sum_{k=0}^K P_k(x) n_k(x) \right] dx = 0 \quad (\text{A2.7})$$

where $n(x)$ are the experimentally measured points, and n_k are the estimates to the true diameter distribution. Rearranging the above, we can form a linear system of equations in n_k as follows.

$$[A]\{x\} = \{b\} \quad (\text{A2.8})$$

and

$$[A]_{i,j} = \int_0^x P_i(x) P_j(x) \quad (\text{A2.9})$$

where

$$\{x\}_i = n_i \text{ (the solution vector)}$$

and

$$\{b\}_i = \int_0^x P_i(x) n(x)$$

Integration can be analytical or numerical. Here it is numerical and by the trapezium rule. Note that for a normal finite element system the shape functions P_i do not overlap and hence $[A]$ is a diagonally dominant sparse matrix. This is not true here and so $[A]$ is not sparse. This means that the method used here is computationally more expensive than traditional FEM solutions.

A2.4 RESULTS

A2.4.1 Analysis of ideal data

Comparison of the results from both the PAM and FEM for the ideal data is shown for a unimodal distribution on Figure A2.3. Choice of diameter bands is shown to greatly affect the results from the PAM. If only one diameter band is chosen, then obviously the PAM will give the correct answer. However, if ten are chosen, the results are very smeared and the PAM predicts particles of a smaller diameter than exist in the system. This is a statistical limitation of the method which is discussed later. The FEM, used with 10 diameter bands, gives a much better prediction, although the resulting distribution becomes negative just before the peak at $d=1$. This is due to the numerical method and there may be an insufficiently small step size near the actual diameter bands, where the rate of change of number fraction is high.

The same problems occur for ideal bimodal distributions in Figure A2.4, where the FEM gives approximately the correct proportion of each diameter for each case, but the output signal is somewhat smeared. The method is therefore more useful to illustrate the relative proportions of the particles rather than absolute values. Choice of a mesh that adjusts with the rate of change of number fraction may help to improve this situation. In any case, the diameter distributions employed by the simulation are not smooth and hence have discontinuous derivatives. This presents a problem for the finite element method and leads to instabilities in the solution. Similar phenomena can occur in stress analyses close to sharp corners. The FEM is likely to perform better for real distributions, where the discontinuities are less severe and the number of size bands is usually larger. This will be examined later using the Par-Tec data.

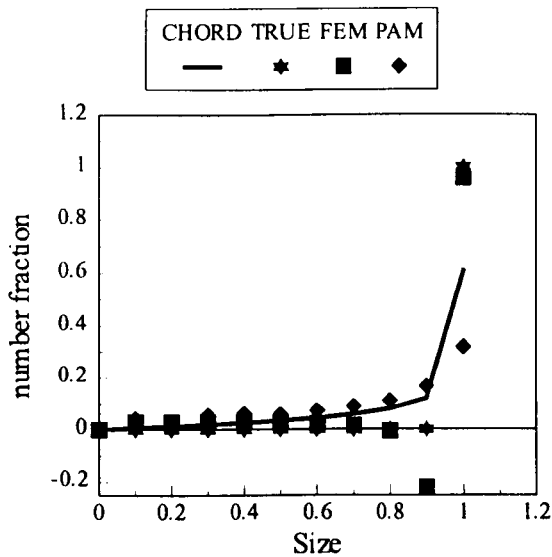


Figure A2.3: Comparison of Chord Conversion Methods for an Ideal Unimodal Distribution.

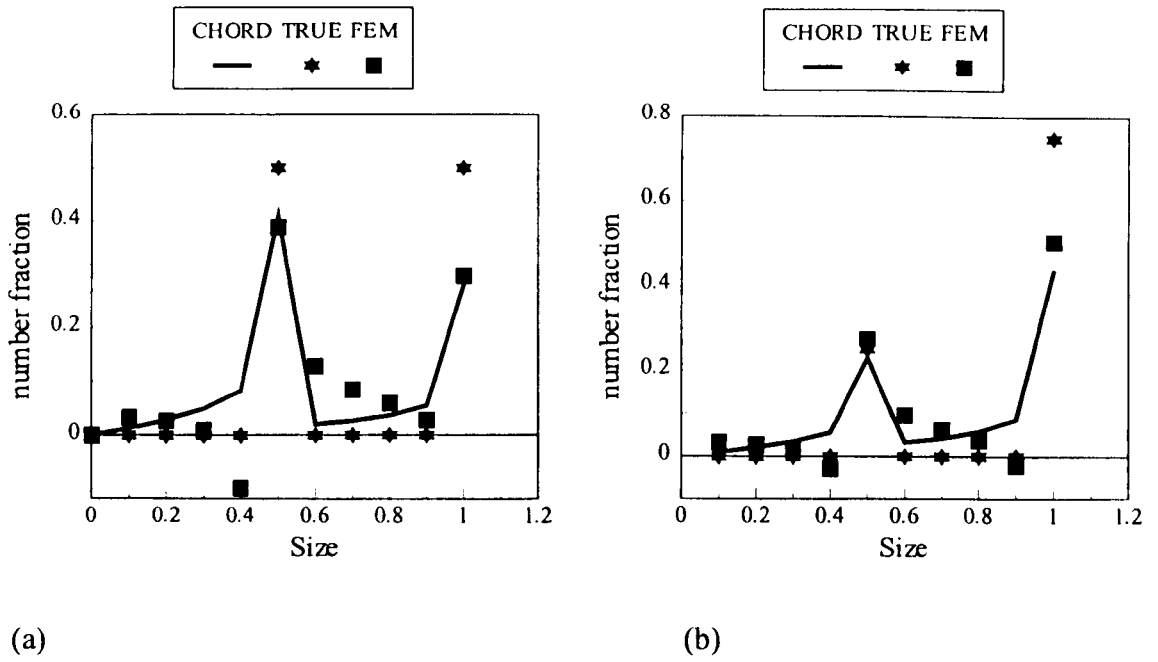


Figure 2.4: Validation of the FEM for (a) 50:50 Bimodal Distribution, (b) 25:75 Bimodal Distribution

A2.4.2 Analysis of DEM data

An overall summary of the DEM simulation and PAM analysis is shown in Tables A2.1-A2.2. Here d_i are the representative diameters chosen; $n_{i\%}$ the percentage of particles with diameter d_i in the simulation; $n_{s\%}$ the sample distribution accounting for probability of hit; $n_{c\%}$ the calculated diameter distribution from the sampled distribution using the PAM. The tables also show the radii r of the sampling cylinders projected upward through the silo and the number of particles cut, n_{cut} .

The effect of population sampling by the DEM method is shown in Table A2.1. The first case considered was for particle diameters randomly assigned between 0.2 and 0.5. 5000 particles were “dropped” into the hopper. Six representative d_i values

were selected (six equal sized “bins”). Two samples were taken and analysed, each one using three cylinders projected through the hopper to cut the particles.

The first point to note is that in cutting about 10% of the population we obtain a reasonable sample of the population. The error here is in fact greater than that in the subsequent analysis. The calculated diameter distribution looks quite reasonable for both samples in this case. To investigate how the method performs when the distribution is not uniform, different bimodal distributions were chosen for investigation.

The next scenario considers a bimodal distribution where the diameters of the particles are either 0.2 or 0.5, but the population of each is unknown. The results are shown in Table A2.2. The first case shows the limit of 0/100 split. Obviously all the sample is of diameter 0.5 but the PAM estimates about 20% of the population has a diameter of 0.2. This problem has been previously illustrated in Figure A2.3 and is clearly the most difficult scenario for the model to handle. In simple terms small chord cuts on the large particles may come from small particles. The second case shows a 20/80 split that is predicted slightly more accurately. The third case with the 50/50 split and the fourth with 80/20 are reasonably predicted with sample sizes of 5 to 10%.

Having analysed the PAM results, it is of interest to compare the performance of both FEM and PAM in different situations. The methods are compared for the DEM data on Figure A2.5. It is noteworthy that the PAM analysis has been shown in the previous section to give poor results when the diameter bands are not known.

The results for a 0/100 split produced by the DEM simulation is shown in Figure A2.5a, all of diameter 0.5. As shown previously, the PAM predicts an 80:20 split of particles of diameter 0.5 and 0.2, when in fact no particles of diameter 0.2 are present. The FEM only gives a significant number fraction at a diameter of 0.5. All the number fractions at the other size bands are reduced close to zero. The FEM is therefore more accurate in this situation.

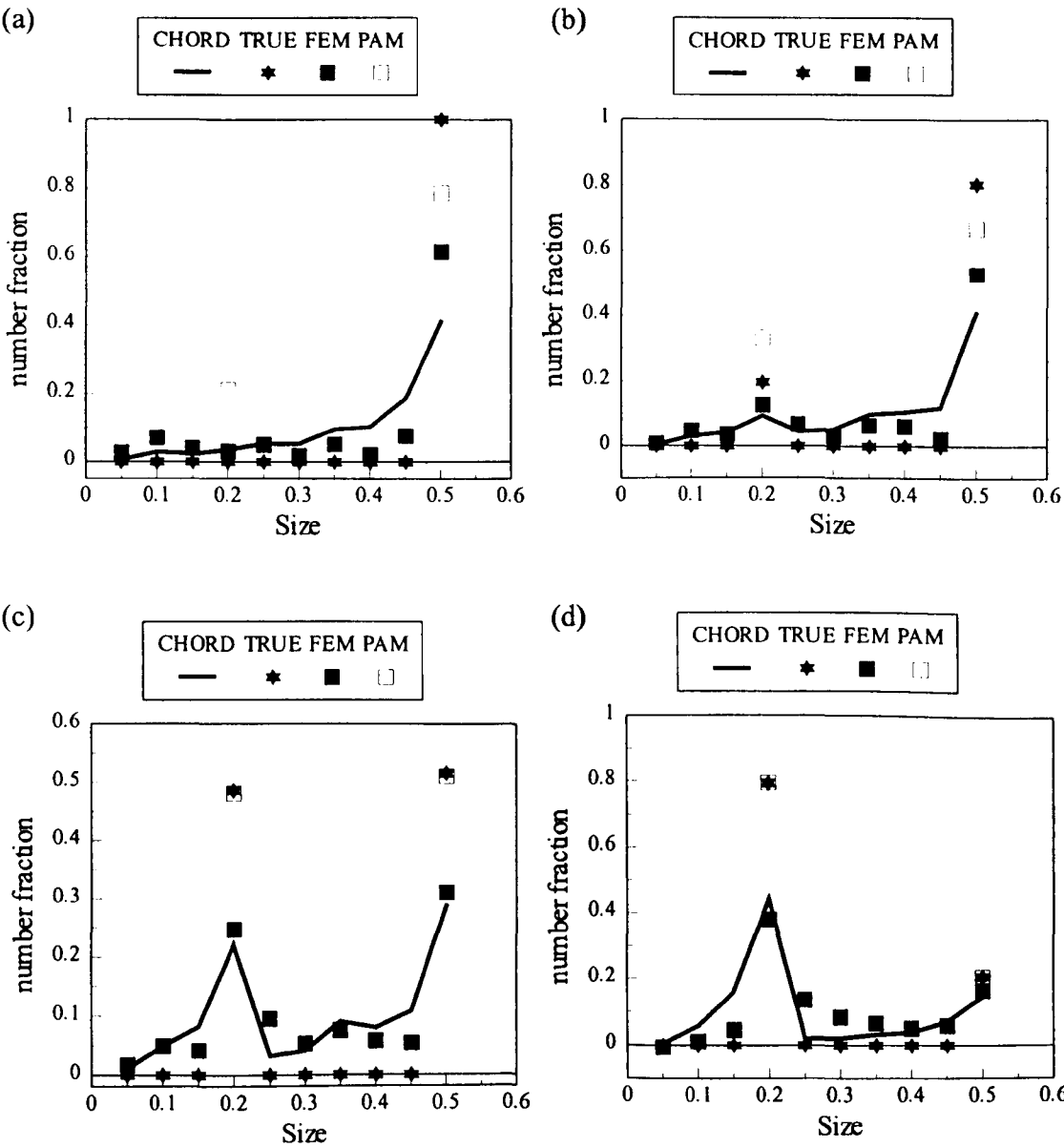


Figure A2.5: Comparison of Chord Conversion Methods for Bimodal Distributions:
 (a) 0:100 split, (b) 20:80 split, (c) 50:50 Split and (d) 80:20 split

For a 20/80 split as shown in Figure A2.5b, the ratio of peaks from the chord data is 4.42. The ratio from the FEM is approximately the same, giving an effective 18.5/81.5% split. This is a significantly better prediction than that given by the PAM for the same case.

The split predicted by the FEM for a 50/50 mixture, as shown in Figure A2.5c is 42/58, which is worse than the PAM prediction. Again, the FEM is overcompensating and hence the peaks from the FEM are lopsided. As already mentioned, this is a consequence of the discontinuity of the derivatives and would therefore be expected to be less of a problem when working with real particle size distributions.

For an 80/20 mix (Figure A2.5d) the peak ratio is 2.2, i.e. a 60/30 split. The FEM seems to consistently over-predict the number of larger particles. This could perhaps be improved by choosing an adjustable mesh.

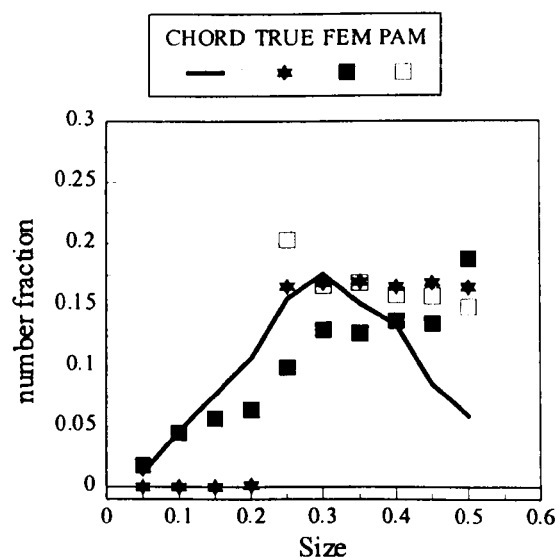


Figure A2.6: Comparison of Chord Conversion Methods for a Uniform Distribution

The results for a uniform diameter distribution of between 0.2 and 0.5 are shown on Figure A2.6. The DEM simulation results show that the chord distribution produced by the probe is almost symmetrical. The PAM results are quite accurate for this case where the upper and lower limits on particle size have been specified. The FEM technique takes the lower limit as zero, hence the comparison is biased against the FEM, which requires a large number of diameter bands to work effectively. A fairer test would be to restrict the range from 0.2-0.5 only as this would remove the discontinuity in the derivative.

A2.4.3 Conversion of experimental data

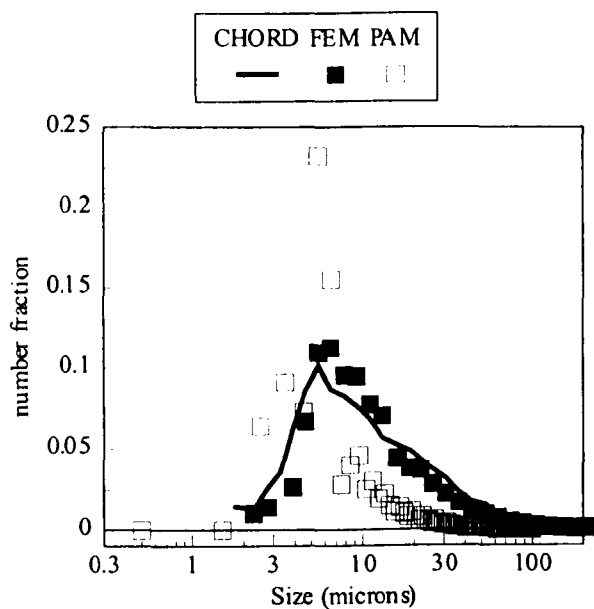


Figure A2.7:Chord Conversion of Par-Tec data

The FEM has been applied to a set of data from the Par-Tec instrument and this is shown in Figure A2.7. The converted distribution is seen to shift to the right and become slightly sharper which is as would be expected. The value of mean diameter before and after conversion is seen to shift by a factor of 1.11. Application of the PAM to the same data set produces a much sharper peak, but curiously the peak is

not shifted. One would expect the curve to be shifted to the right when converting to a diameter distribution so this brings the PAM into question and is probably due to the fact that the method does not utilise the collective information from the data set.

A2.5 CONCLUSIONS

The Distinct Element simulation has been shown to be a useful tool in evaluating mathematical techniques for estimating diameter distributions from chord sizes. It also shows that a representative population of particles can be found by only sampling 10% of the 5000 particles present. This gives confidence that the data from the Par-Tec instrument is a true representation of the system, as a typical measurement sample from the instrument is of the order of 3000-6000. The Probability Apportioning Method is robust providing the particle diameters in the sample are known and gives equal weighting to all measurements. It does not lead to negative particle populations as is possible with the “peeling” method. The FEM has limitations where large discontinuities occur in the input data but it can estimate the size and proportion of particles in samples of unknown size. The method is more efficient with a larger number of particles and size bands. In these situations the FEM produces a better estimate, and is more applicable to engineering situations, where the actual particle sizes are usually unknown.

In general the FEM correctly estimates the sizes of the particle diameters as peaks in the output, even though the output itself may be “noisy”. This could also be due to the inevitable noise on the input signal, caused by the random apportioning used in the DEM simulation and problems with “non-smooth” data.

Further work is required to investigate a wider range of distributions using the DE simulation, perhaps with a log-normal distribution set up. Other statistical techniques should be evaluated especially when the particle packing or droplet flow is dense phase and the assumption of independent measurements is no longer valid.

A2.6 NOMENCLATURE FOR APPENDIX A2

$\hat{n}(x)$	cumulative number of chord counts at size x
D	particle diameter
d_i	diameter of particle band i
n	number of particles in the simulation
$n_{c\%}$	the percentage of particles i calculated in simulation
n_{cut}	the number of particles cut in simulation
$n_{i\%}$	the percentage of particles i in simulation
n_k	number of counts in k^{th} diameter band
$n_{s\%}$	the percentage of particles i sampled in simulation
$P()$	probability distribution of chord size
r	radius of sampling cylinder in DE simulation
R_i	i th residual
w	half width of diameter band
x	chord size

Table A2.1: PAM Analysis of Uniform Particle Size Distribution

n=5000		Sample A r=7,10,13 ncut=457		sample B r=5,8,11 ncut=386	
d _i	n _i %	n _s %	n _c %	n _s %	n _c %
0.225	16.3	21.9	20.9	17.5	18.7
0.275	16.9	14.7	17.4	14.7	15.4
0.325	16.9	16.3	17.6	16.9	16.3
0.375	16.3	16.7	15.6	13.9	17.2
0.425	16.8	15.7	14.5	16.4	15.3
0.475	16.7	14.6	14	20.5	17.1

Table A2.2: PAM Analysis of Binary Particle Size Distribution with known D

Case 1 n=5000		Sample A r=6,10,14 ncut=658	
d _i	n _i %	n _s %	n _c %
0.2	0	0	21.2
0.5	100	100	78.8

Case 2 n=5000		Sample A r=12 ncut=215		sample B r=8 ncut=180		sample C r=6,10,14 ncut=590		n
d _i	n _i %	n _s %	n _c %	n _s %	n _c %	n _s %		
0.2	19.6	24	34.4	16.3	30.7	20.8		
0.5	80.4	76	65.6	83.7	69.3	79.2		

Case 3 n=5000		Sample A r=6,10,14 ncut=466		sample B r=8,12 ncut=344	
d _i	n _i %	n _s %	n _c %	n _s %	n _c %
0.2	48.5	51	55.3	44.7	49.3
0.5	51.5	49	44.7	53.3	50.7

Case 4 n=5000		Sample A r=6,10,14 ncut=332		sample B r=8,12 ncut=251	
d _i	n _i %	n _s %	n _c %	n _s %	n _c %
0.2	79.2	81.5	79.4	75.6	74.4
0.5	20.8	18.5	20.6	24.4	25.6

Appendix A3

IMAGE ANALYSIS OF VIDEO FOOTAGE

Photographs of the flow of the liquids in the 0.063m pipe were taken for both vertical and horizontal orientations. At dilute concentrations, it was found that reasonable quality images of the drops were obtained for vertical upflow. These droplets were sized by a technique which involved the use of the Optimas 5.1 image analysis package.

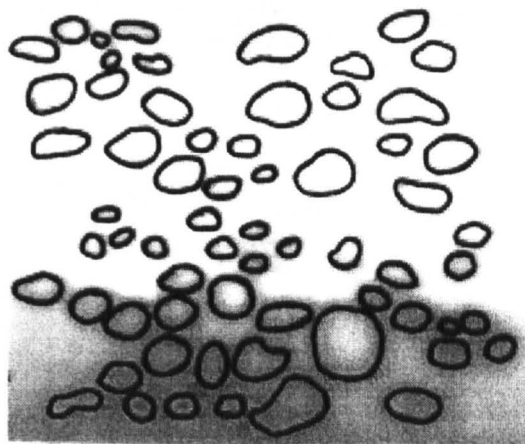


Figure A3.1: Tracing of droplets from video footage

Printouts of the video footage were obtained and the outlines of the drops were drawn around by hand by use of tracing paper as shown in Figure A3.1. The final tracing was then transferred to computer using an image grabber. The image was then processed using the software to remove any light gray colours and shadowing from the image and then the colours were inverted (Figure A3.2).

The “fill” function on the software was then used to shade the inside of the drop outlines as shown in Figure A3.3. The “erode” function was then applied to separate

any touching drops. The software then discriminates between the areas of black and white and calculates the co-ordinates of the edges of the drops. The drops are then scaled and sized using this data. At each flow condition, a minimum sample size of approx. 150 drops was taken. The total number of drops analysed was limited by the number of good quality images and the time-consuming tracing of the drops.

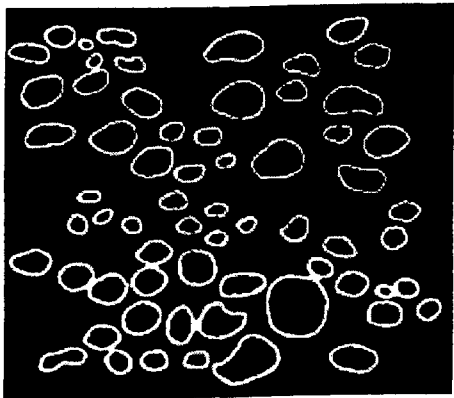


Figure A3.2: Inverted image

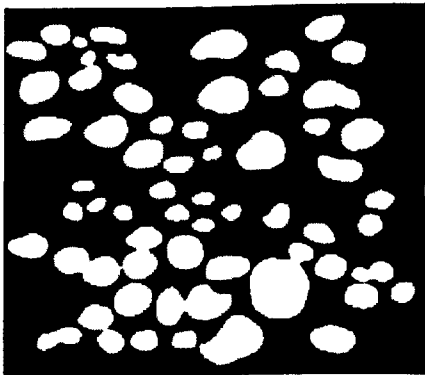


Figure A3.3: Filled image

Appendix A4

DROP SIZE DISTRIBUTIONS

A4.1 DROP SIZE DISTRIBUTIONS FROM PAR-TEC INSTRUMENT

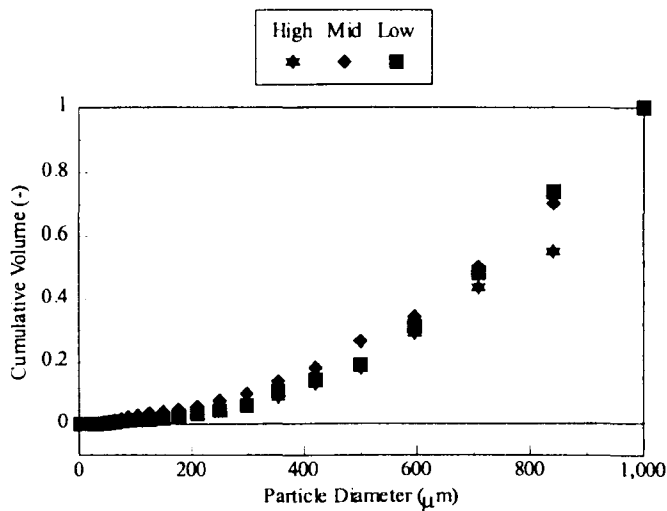


Figure A 4.1: Results from Partec on Vertical Section $u_{\text{mix}}=1.00$ m/s

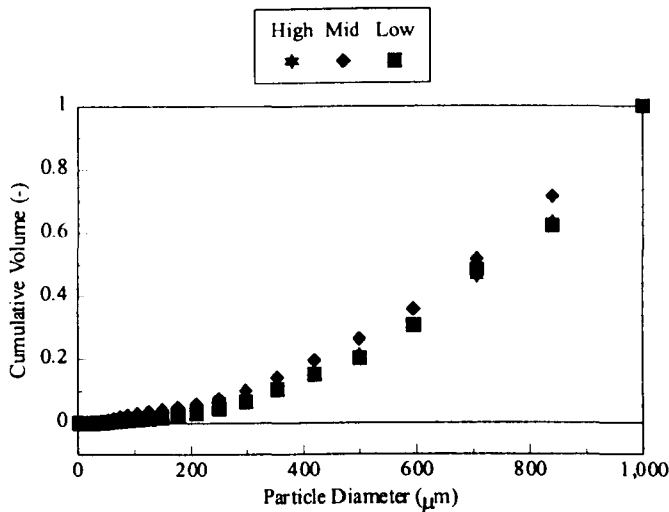


Figure A 4.2: Results from Partec on Vertical Section $u_{\text{mix}}=1.15$ m/s

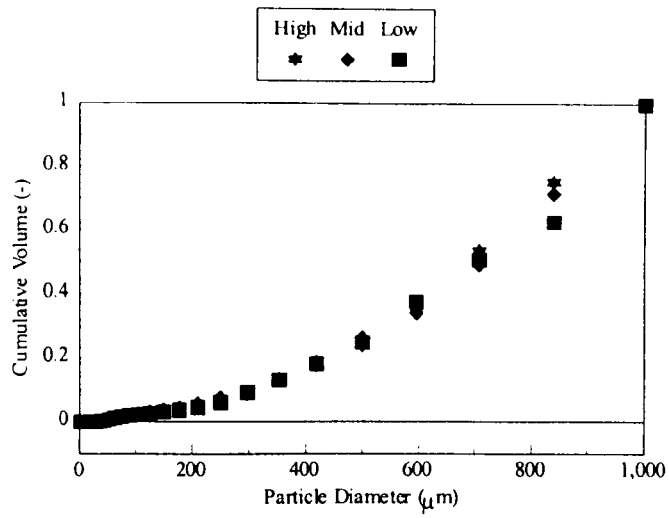


Figure A 4.3: Results from Partec on Vertical Section $u_{\text{mix}}=1.33$ m/s

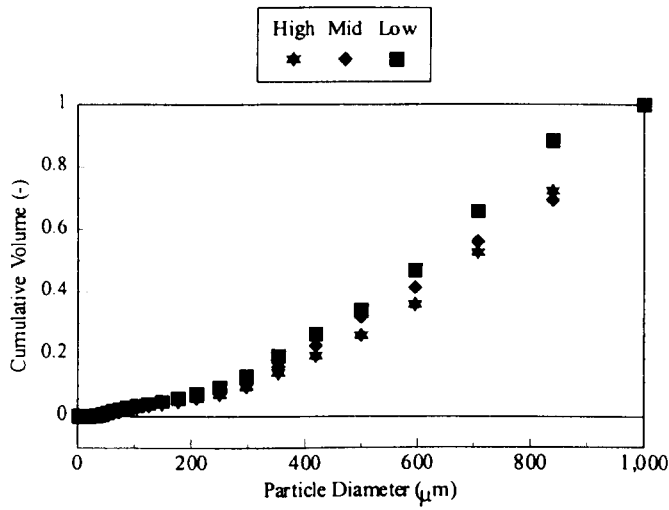


Figure A 4.4: Results from Partec on Vertical Section $u_{\text{mix}}=1.45$ m/s

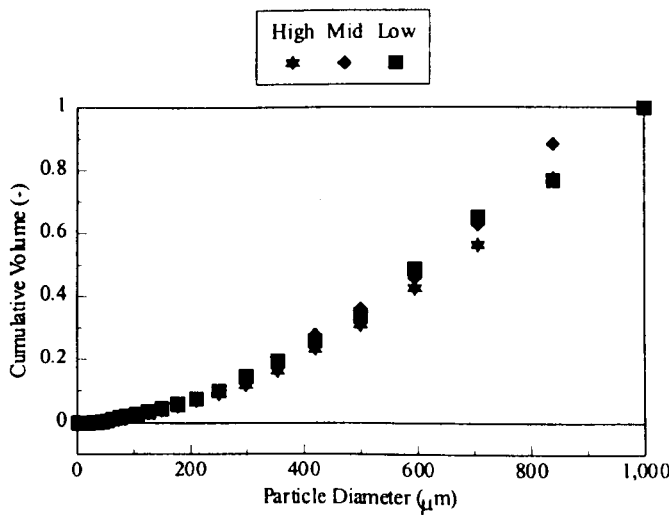


Figure A 4.5: Results from Partec on Vertical Section $u_{\text{mix}}=1.65$ m/s

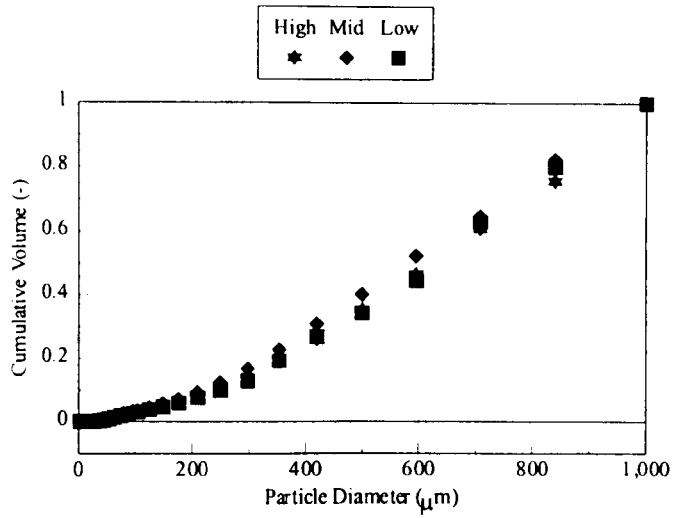


Figure A 4.6: Results from Partec on Vertical Section $u_{\text{mix}}=1.81 \text{ m/s}$

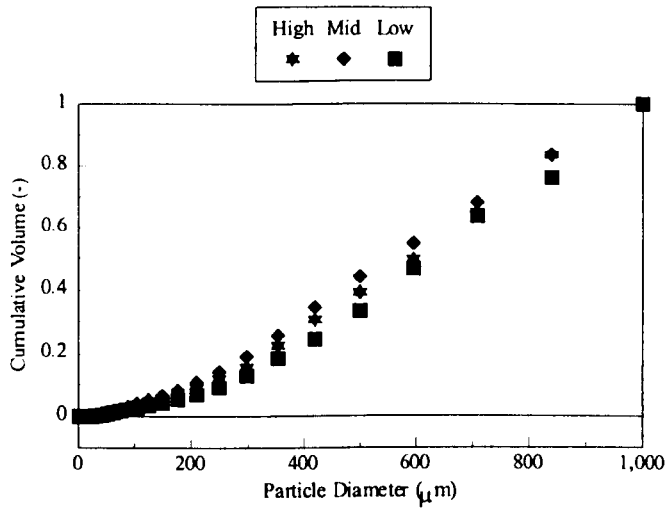


Figure A 4.7: Results from Partec on Vertical Section $u_{\text{mix}}=1.98 \text{ m/s}$

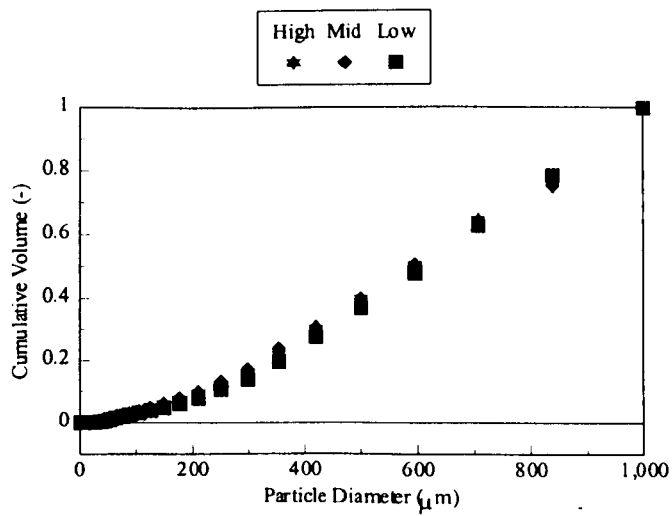


Figure A 4.8: Results from Partec on Vertical Section $u_{\text{mix}}=2.10 \text{ m/s}$

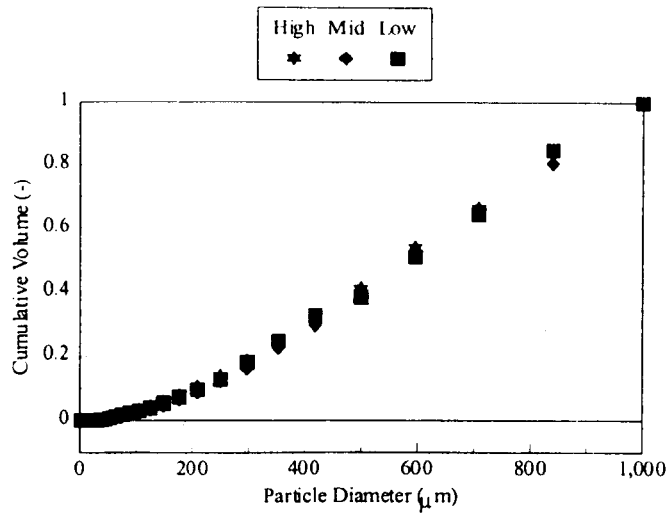


Figure A 4.9: Results from Partec on Vertical Section $u_{\text{mix}} = 2.55 \text{ m/s}$

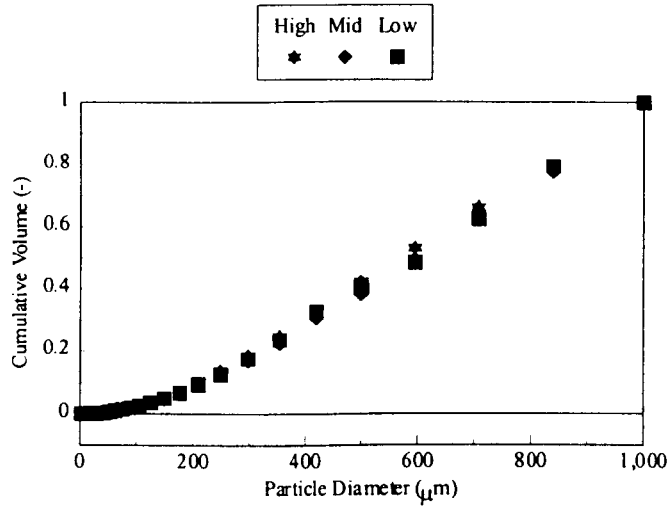


Figure A 4.10: Results from Partec on Vertical Section $u_{\text{mix}} = 2.71 \text{ m/s}$

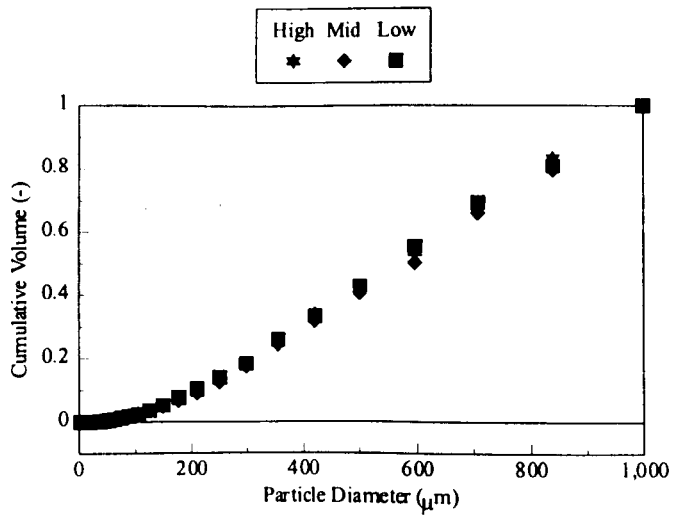


Figure A 4.11: Results from Partec on Vertical Section $u_{\text{mix}} = 2.88 \text{ m/s}$

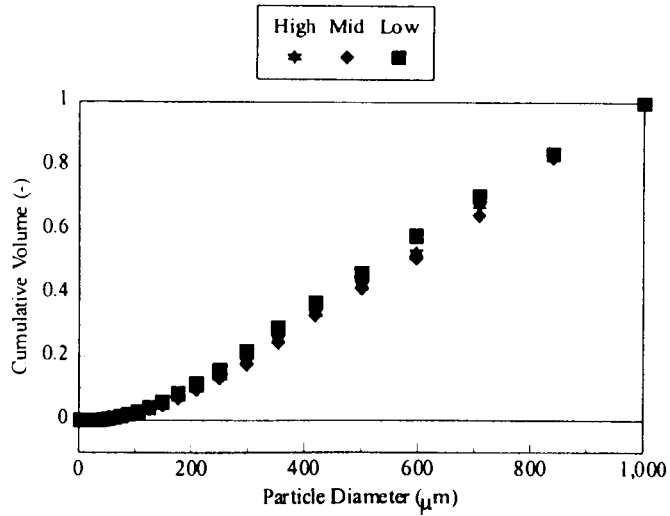


Figure A 4.12: Results from Partec on Vertical Section $u_{\text{mix}} = 3.01 \text{ m/s}$

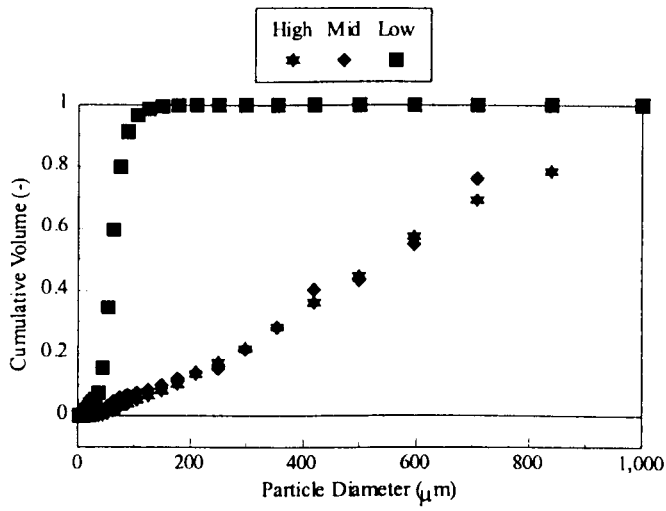


Figure A 4.13: Results from Partec on Horizontal Section $u_{\text{mix}} = 1.00 \text{ m/s}$

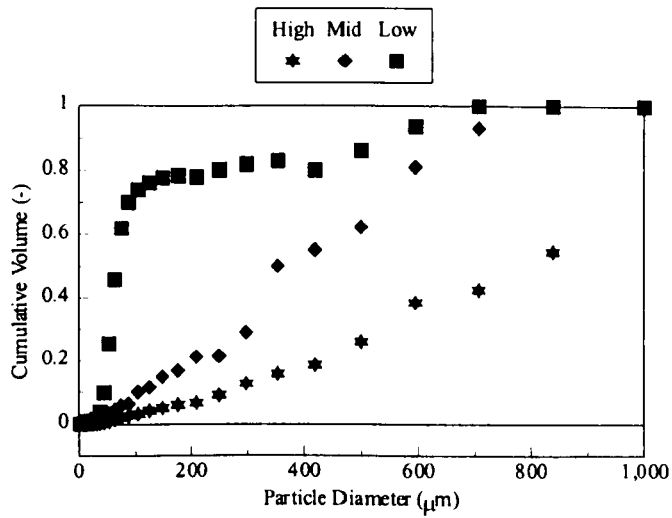


Figure A 4.14: Results from Partec on Horizontal Section $u_{\text{mix}} = 1.15 \text{ m/s}$

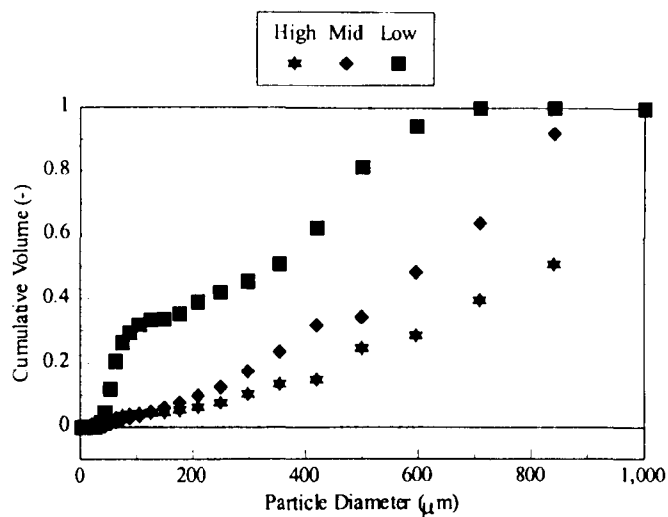


Figure A 4.15: Results from Partec on Horizontal Section $u_{\text{mix}} = 1.33 \text{ m/s}$

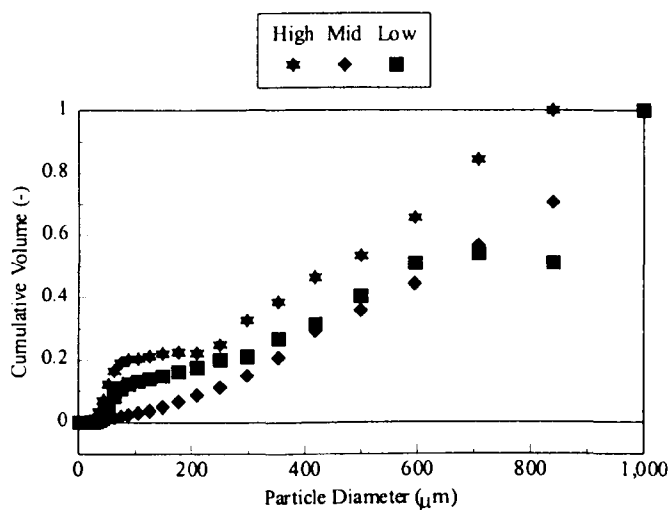


Figure A 4.16: Results from Partec on Horizontal Section $u_{\text{mix}} = 1.45 \text{ m/s}$

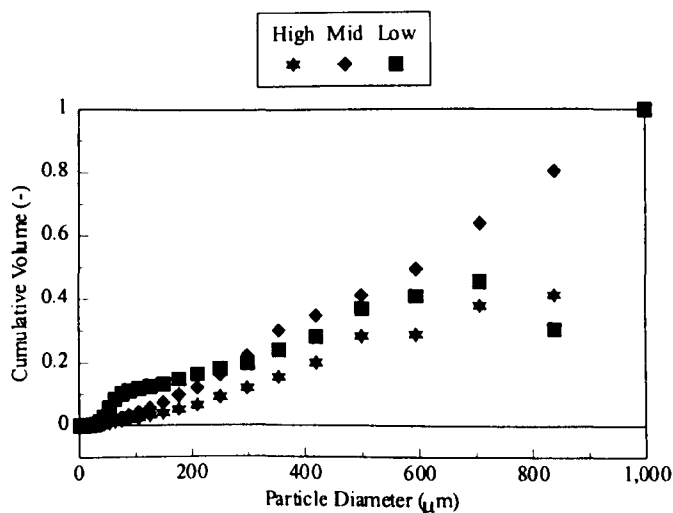


Figure A 4.17: Results from Partec on Horizontal Section $u_{\text{mix}} = 1.65 \text{ m/s}$

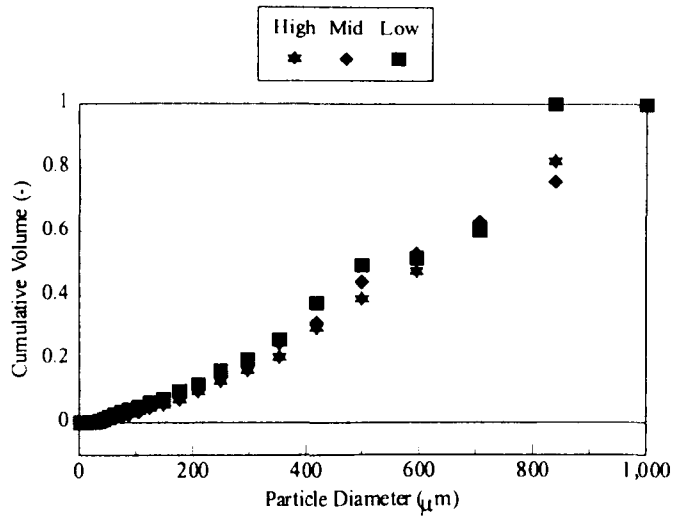


Figure A 4.18: Results from Partec on Horizontal Section $u_{\text{mix}}=1.81$ m/s

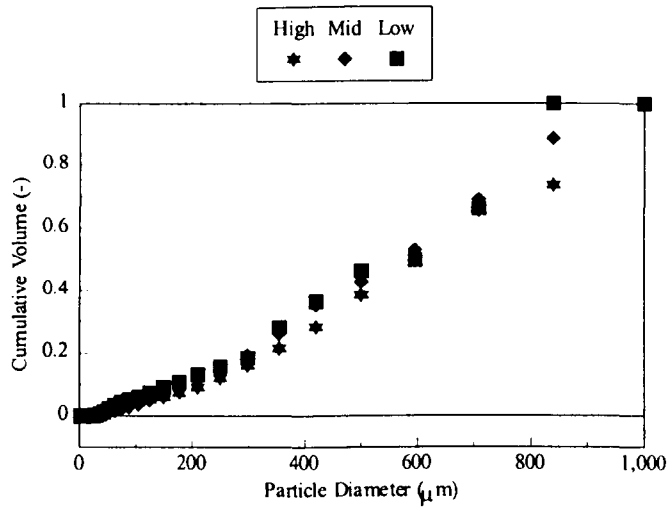


Figure A 4.19: Results from Partec on Horizontal Section $u_{\text{mix}}=1.98$ m/s

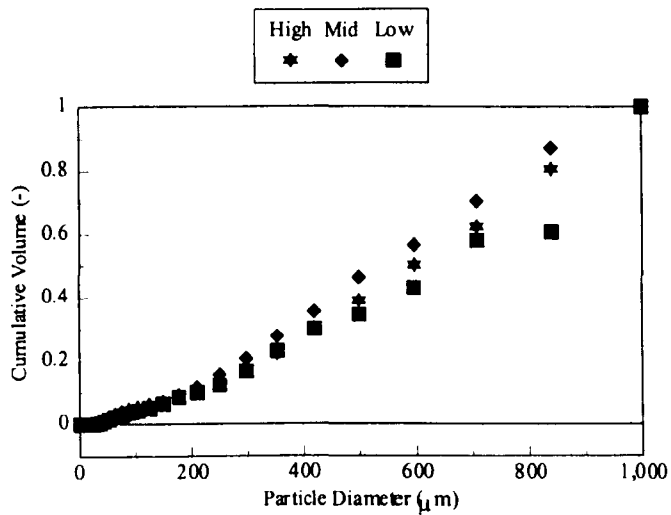


Figure A 4.20: Results from Partec on Horizontal Section $u_{\text{mix}}=2.10$ m/s

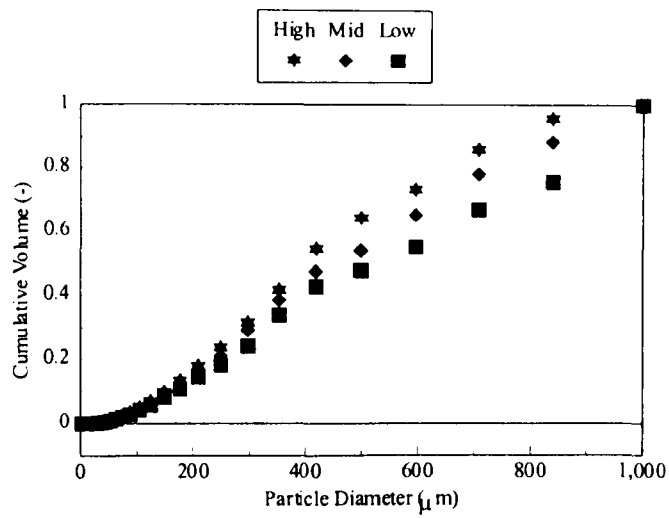


Figure A 4.21: Results from Partec on Horizontal Section $u_{\text{mix}}=2.55$ m/s

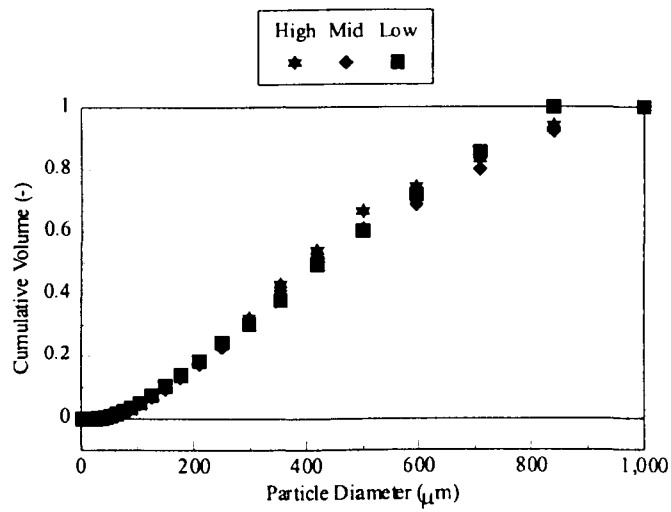


Figure A 4.22: Results from Partec on Horizontal Section $u_{\text{mix}}=2.71$ m/s

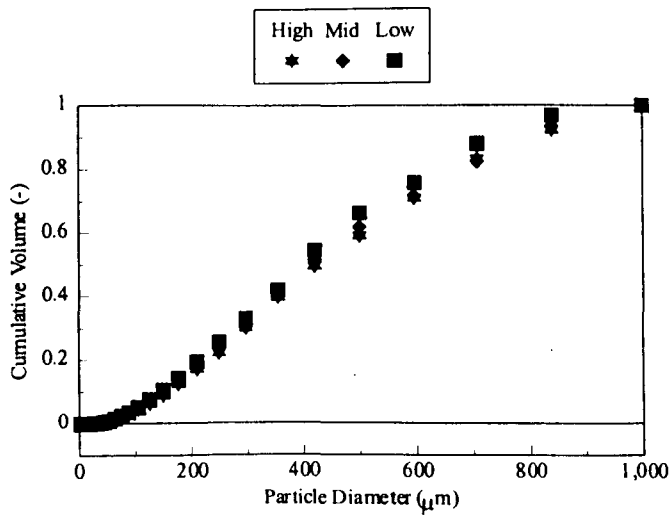


Figure A 4.23: Results from Partec on Horizontal Section $u_{\text{mix}}=2.88$ m/s

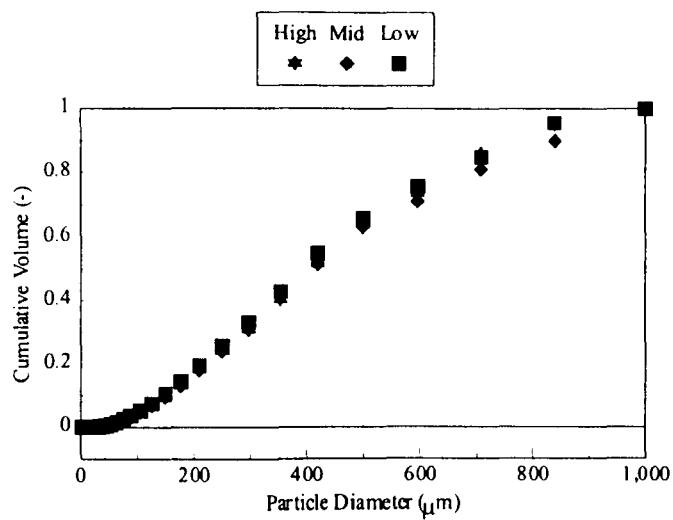


Figure A 4.24: Results from Partec on Horizontal Section $u_{\text{mix}}=3.01$ m/s

Appendix A5

FLOW PATTERN MAPS

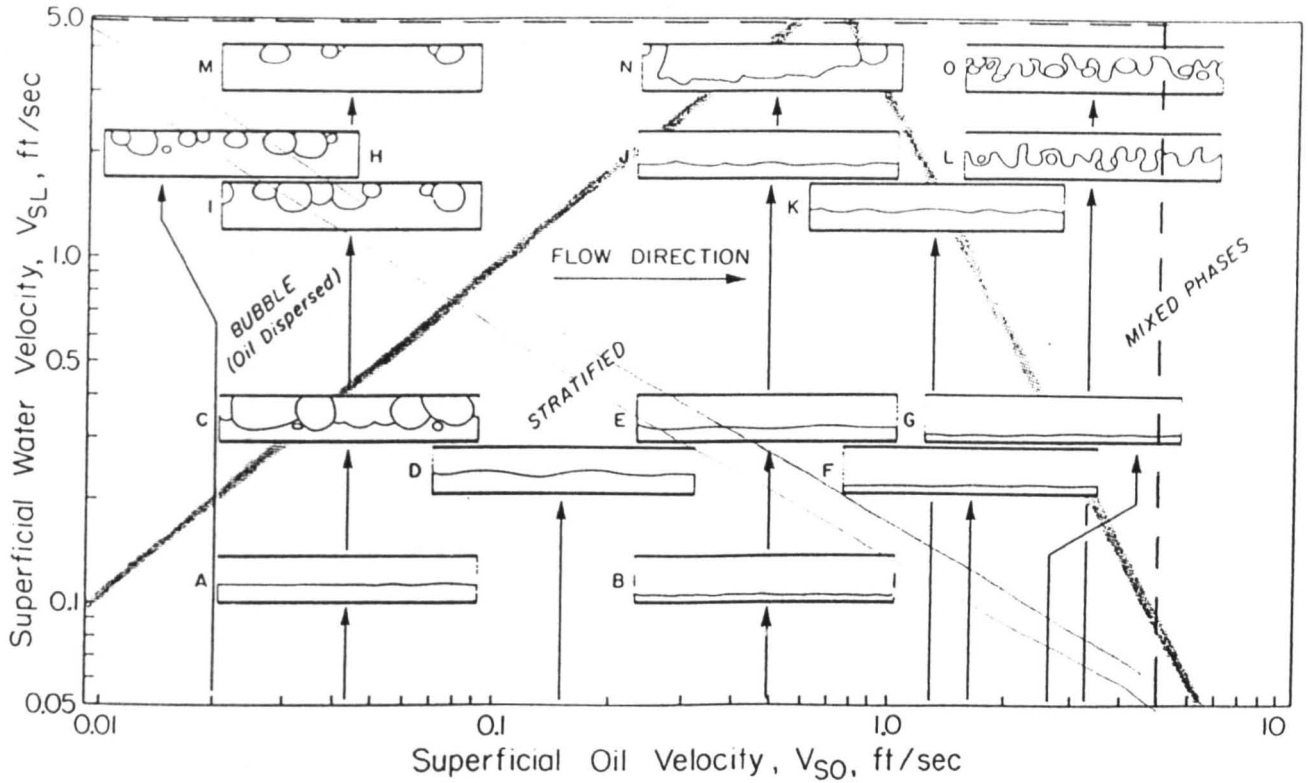


Figure A5.1: Oil-Water Flow Regime Map of Russel *et al.* (1959)

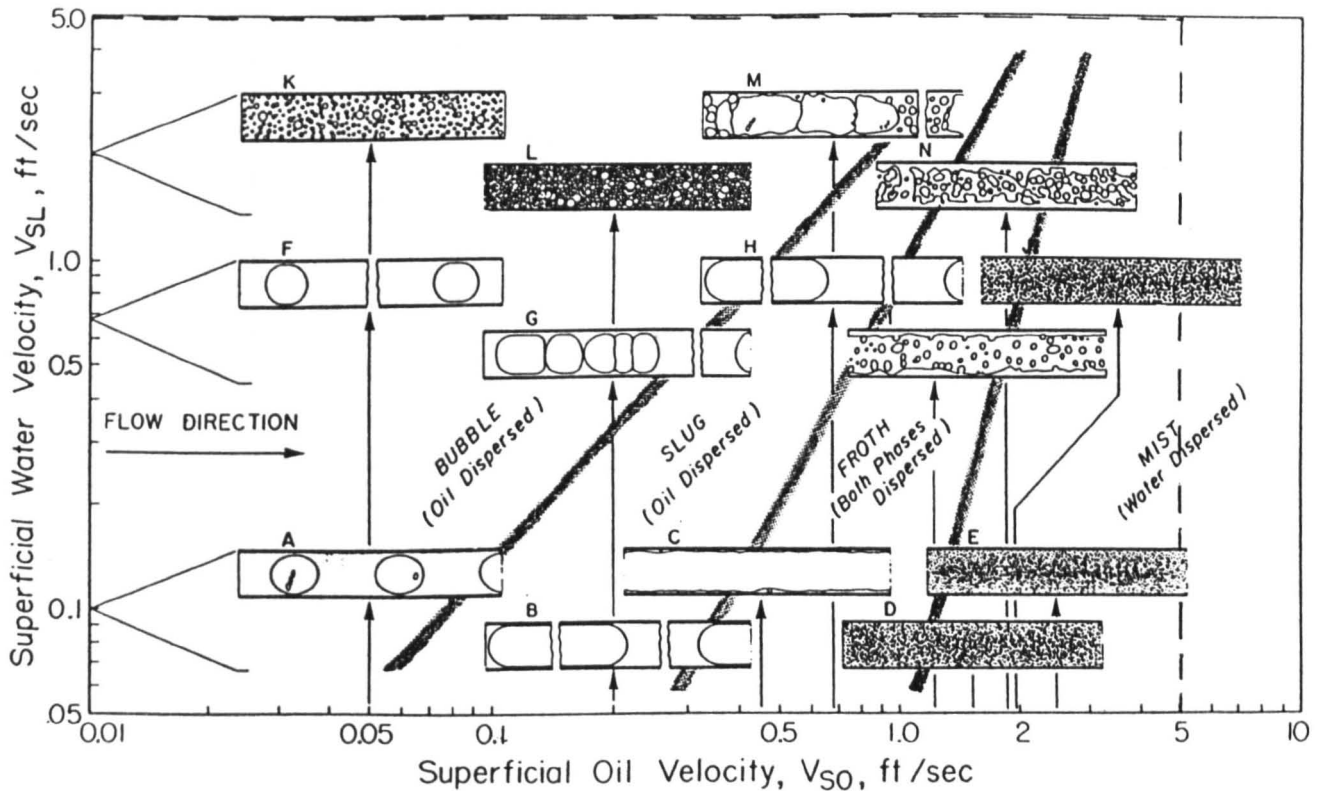


Figure A5.2: Oil-Water Flow Regime Map of Charles *et al.* (1961)

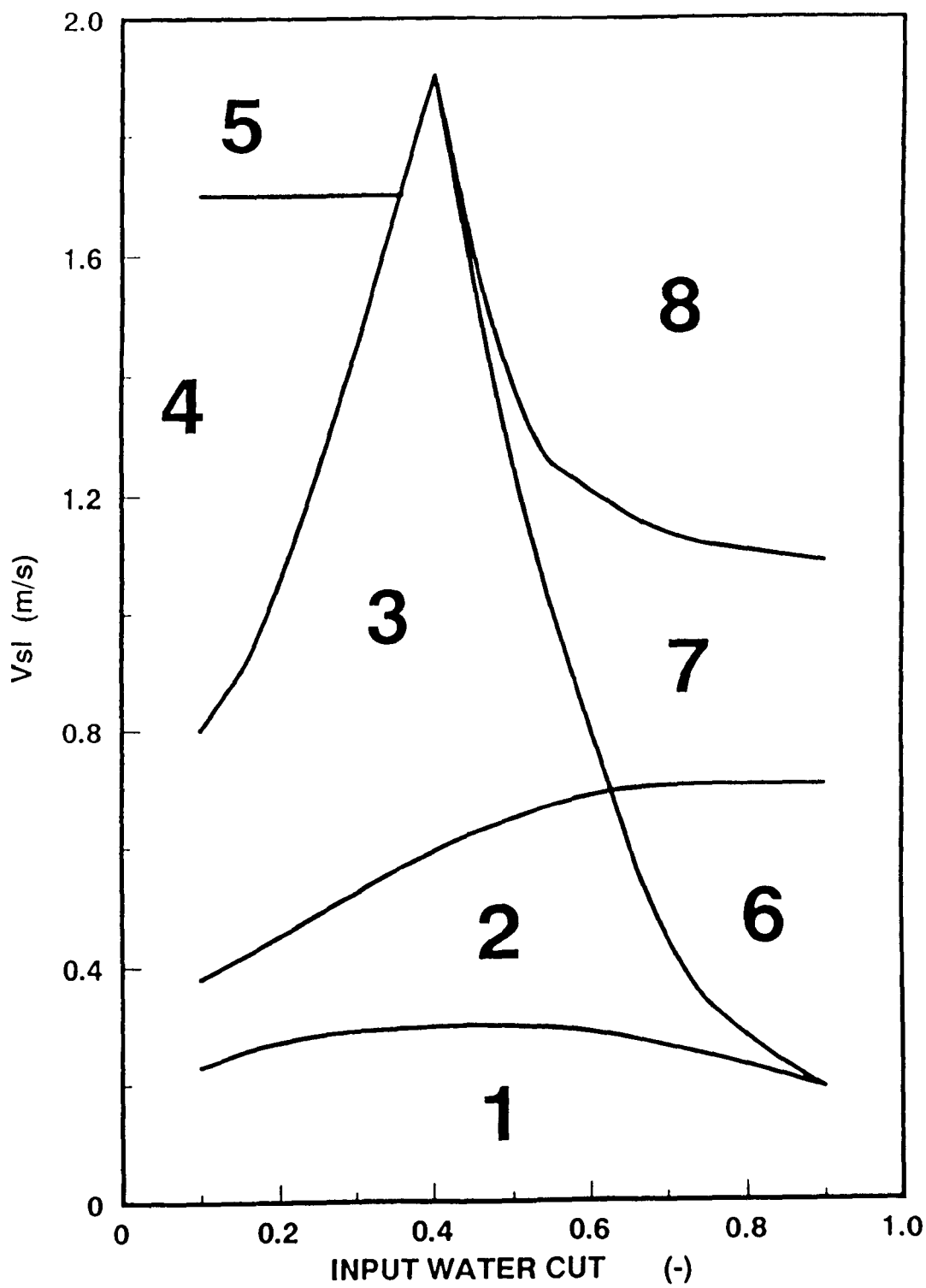


Figure A5.3: Oil-Water Flow Regime Map of Guzhev *et al* (1973)

OIL-WATER FLOW REGIME BY GUZHOV ET AL (1973)	
CODE	DESCRIPTION
1	Stratified Flow
2	Stratified flow with dense layer of emulsion at the interface (lower layer = water)
3	Stratified flow with dense layer of emulsion at the interface (lower layer = dilute oil-in-water emulsion)
4	Emulsion of water-in-oil and oil-in-water
5	Emulsion of water-in-oil
6	Dense emulsion of oil-in-water and water
7	Dense emulsion of oil-in-water and dispersed emulsion of oil-in-water
8	Emulsion of oil-in-water

Figure A5.4: Flow Regime Classification of Guzhov *et al.* (1973)

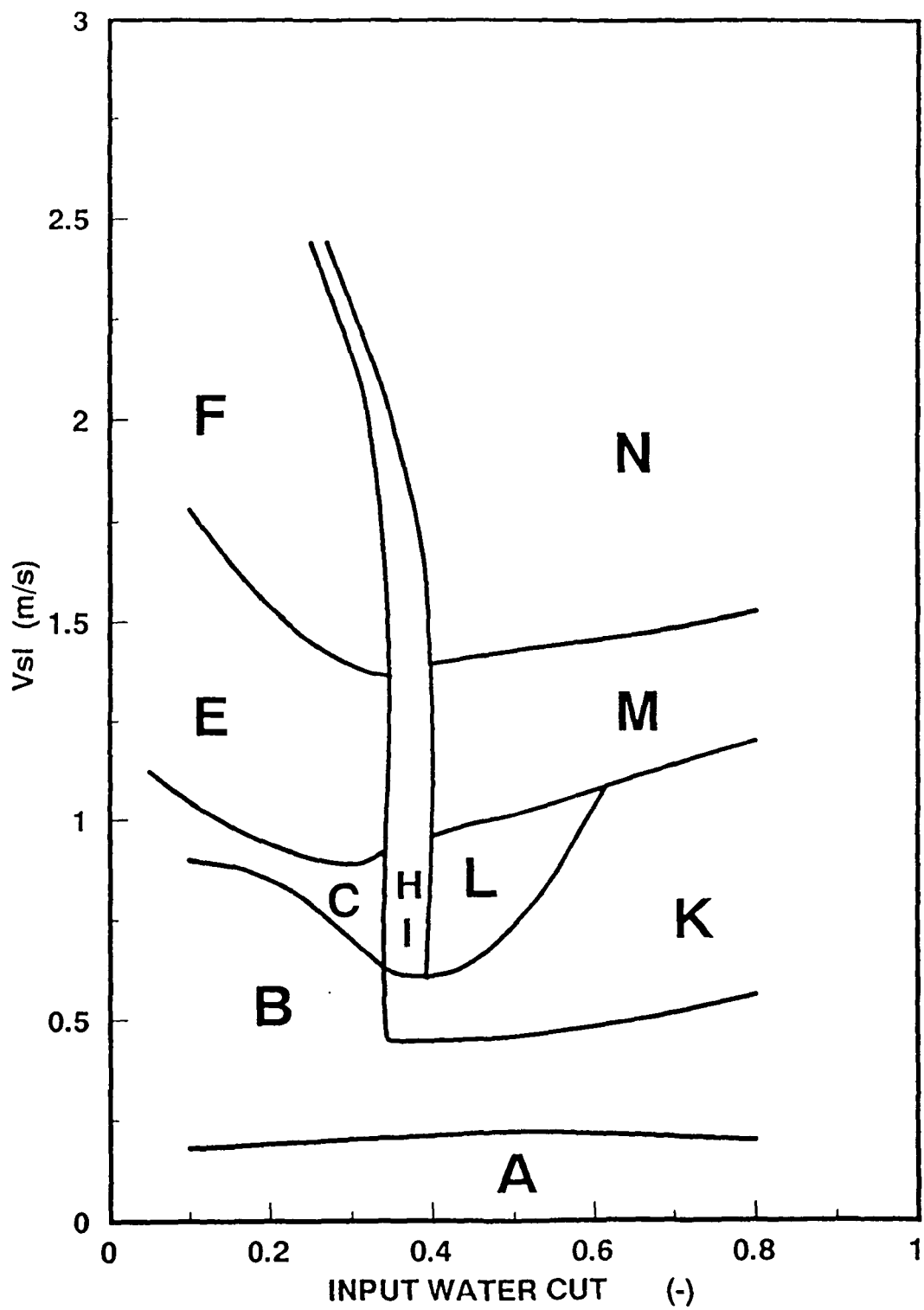


Figure A5.5: Oil-Water Flow Regime Map for 32cP Oil, Oglesby (1979)

FLOW PATTERN CODE

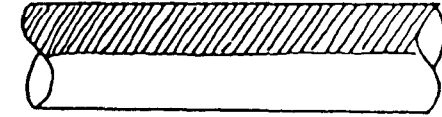
<u>Oil Dominant</u>	<u>Water Dominant</u>
-------------------------	---------------------------

Description

Sketch

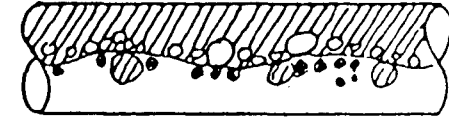
A

Segregated - no mixing at the interface.



B

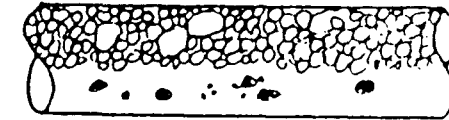
Semi-segregated - some mixing at the interface.



C

K

Semi-mixed - segregated flow of a dispersion and "free" phase. Bubbly interface. Dispersion volume less than $\frac{1}{2}$ the total pipe volume.

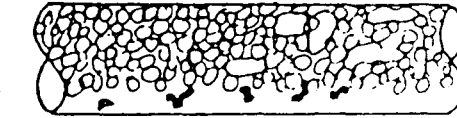


Example: water-in-oil dispersion with a "free" water phase

D

L

Mixed - same as the above coding but with the dispersion occupying more than $\frac{1}{2}$ the pipe volume.



Example: water-in-oil dispersion with a "free" water phase

Figure A5.6a: Flow Regime Classification of Oglesby (1979)

FLOW PATTERN CODE


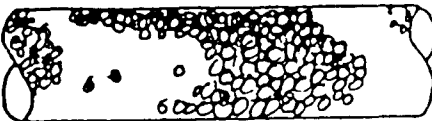
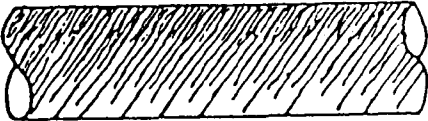
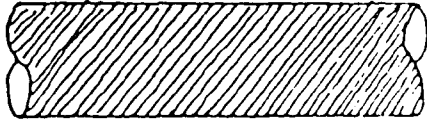
<u>Oil Dominant</u>	<u>Water Dominant</u>	<u>Description</u>	<u>Sketch</u>
G	J	Annular or concentric - core of one phase within the other phase.	 <p>Example: water-core in an oil layer</p>
H	I	Slug - phases alternately occupying the pipe volume as a free phase or as a dispersion.	
E	M	Semi-dispersed - some vertical gradient of fluid concentrations in the mixture.	
F	N	Fully dispersed homogeneous flow.	

Figure A5.6b: Flow Regime Classification of Oglesby (1979)

Appendix A6

PROGRAM LISTINGS

This Appendix contains the following FORTRAN and MATLAB programs employed in this study.

- 1) Taitel-Dukler Model: Tait1.for
- 2) Chord-Diameter Conversion Program: Zeroord.m
- 3) Frequency Response Program: Milmw1.m
- 4) Convolution Program (APM): Convolut.for

6.1 TAITEL-DUKLER MODEL (FORTRAN)

```
$debug
C
C      PROGRAM TAIT
C
C      *****
C      *
C      * This program will calculate how liquid height varies
C      *           with both liquid and gas velocities
C      *
C      * NEW VERSION ..... MJS 5/8/96
C      * TO CALCULATE LIQUID HEIGHT IN LIQ/LIQ STRAT. FLOW *
C      *****
C
C      The next section states the variables that are going to be
used
C
C
C      DIMENSION WGT(10)
C      OPEN (UNIT=6, FILE='F:\FORTRAN\TAITOUT.DAT', STATUS='OLD'
&)
C      OPEN (UNIT=5, FILE='F:\FORTRAN\TAITIN.DAT', STATUS='OLD')
c      1 D')
C
C      The following DO loop will step through values of WGS
C
C      READ(5,*) WGT(1),WGT(2)
```

```

DO 100 I=1,3
WGS=WGT(I)
C
C   The value of any constants are calculated here
C
RHOG=797.25
RHOL=1000
DIA=0.063
PIE=3.141592654
VISL=1.0e-3
VISG=1.798e-3
C
C   The following DO loop will step through values of ehl
C
EHL=0
10 EHL=EHL+0.05
IF(EHL.GT.1.0)GO TO 200
DO 200 Ehl=0.01,0.51,0.05
C
C   Determining the gas superficial velocity, UGS
C
AREA=PIE*(DIA**2)/4
UGS=WGS/(RHOG*AREA)
C
C   Next, the variables required to calculate ULS are determined
C
S=PIE/4
SG=0.25*(ACOS(2*ehl-1)-(2*ehl-1)*(1-(2*ehl-1)**2)**0.5)
SL=0.25*(PIE-ACOS(2*ehl-1)+(2*ehl-1)*(1-(2*ehl-1)**2)**0.5)
UG=S/SG
UL=S/SL
PL=PIE-ACOS(2*ehl-1)
PI=(1-(2*ehl-1)**2)**0.5
PG=ACOS(2*ehl-1)
DL=4*SL/PL
DG=4*SG/(PG+PI)
REL=RHOL*UL*DL/VISL
REG=RHOG*UG*DG/VISG
IF (REL.GT.2000) THEN
EN=0.2
CL=0.046
ELSE
EN=1.0
CL=16
ENDIF
IF (REG.GT.2000) THEN
EM=0.2
CG=0.046
ELSE
EM=1
CG=16
ENDIF
X2=(UG*DG)**(-EM)*((PG/SG)+(PI/SG)+(PI/SL))*SL/
1(((UL*DL)**(-EN))*(UL**2)*PL)
C
C   In order to calculate ULS, FLS and FGS are required
C
ULS=UL
500 RELS=RHOL*ULS*DIA/VISL
REGS=RHOG*UGS*DIA/VISG

```

```

IF (RELS.GT.2000) THEN
  ENS=0.2
  CLS=0.046
ELSE
  ENS=1.0
  CLS=16
ENDIF
IF (REGS.GT.2000) THEN
  EMS=0.2
  CGS=0.046
ELSE
  EMS=1.0
  CGS=16
ENDIF
FLS=CLS*((RHOL*ULS*DIA/VISL)**(-ENS))
FGS=CGS*((RHOG*UGS*DIA/VISG)**(-EMS))
ULS1=((X2*(UGS**2)*RHOG*FGS)/(RHOL*FLS))**0.5
IF (ABS(1-(ULS1/ULS)).LT.0.0001) THEN
  GO TO 400
ELSE
  ULS=ULS1
  GO TO 500
ENDIF
C
C   Calculating the liquid mass velocity
C
400 WLS=ULS1*RHOL*AREA
    eh1A=eh1*DIA
    ELM=((ULS**2)*RHOL*FLS/((UGS**2)*RHOG*FGS))
C
C   The following statement writes the output to an out file
C
C
WRITE(*,300)WGS,WLS,eh1A,ELM,eh1
WRITE(6,700)WGS,WLS,eh1A,ELM,eh1,sg,sl
300 FORMAT (1X,'Gas mass flowrate (kg/s) = ',F9.4/,1X,
1'Liquid mass flowrate (kg/s) = ',F9.4/,1X,
1'Liquid height (m) = ',F9.4/,1X,'Lockhart-Martinelli
parameter
1 = ',F9.4/,1X,'HL/D= ',F9.4/,)
700 format(7f9.4)
    GO TO 10
200 CONTINUE
C   GO TO 5
100 CONTINUE
    STOP
    END

```

6.2 CHORD-DIAMETER CONVERSION PROGRAM (MATLAB)

```

%-----Galerkin Chord-Diameter Conversion Program
%-----MJS/ASB March 1998
clear

%
% Open files for I/O
%
fidd=fopen('norm.txt','wt')
fidd=fopen('newout.txt','wt')
fid=fopen('input.mat')

```

```

%
% set loop for multiple runs
%

for files=1:1

%
% set number of size bands from input file
%

nbands=fscanf(fid,'%lg',[1,1])

%
% read in data values, y and corresponding band maxima,x
%

x=zeros(nbands,1);
y=zeros(nbands,1);
x=fscanf(fid,'%lg',[nbands,1]);
y=fscanf(fid,'%lg',[nbands,1]);

%
% Calculate midpoints of each band,m and bandwidth,2w
%
m=zeros(nbands,1);
w=zeros(nbands,1);
m(1)=x(1)/2;
w(1)=x(1)/2;
for i=1:nbands-1

m(i+1)=(x(i)+x(i+1))/2;
w(i+1)=(x(i+1)-x(i))/2;
end

%
% initialise variables and matrices
% d=diameter bands corresponding to chord bands, set the same for
now
a=zeros(nbands,nbands);
b=zeros(nbands,1);
d=x
X=nbands
pix=0
pkx=0
%delta=(d(2)-d(1))/2
delta=0.001
%
% CALCULATING MATRICES
%

%
% Sum term, pix 1st order integration
%

for i=1:X
for k=i:X
for j=1:X
pix=real((((d(i)^2-(m(j)-delta)^2)^0.5-(d(i)^2-
(m(j)+delta)^2)^0.5)*2*w(i))/d(i));

```

```

pkx=real((((d(k)^2-(m(j)-delta)^2)^0.5-(d(k)^2-
(m(j)+delta)^2)^0.5)*2*w(k))/d(k));
a(i,k)=a(i,k)+pix*pkx*2*w(j);
end
end
end

for i=1:X
for j=1:i
pix=real((((d(i)^2-(m(j)-delta)^2)^0.5-(d(i)^2-
(m(j)+delta)^2)^0.5)*2*w(i))/d(i));
b(i,1)=b(i,1)+pix*(y(j)/x(j))*2*w(j);
end
end
diam=a\b
sum=0
for n=1:X
sum=sum+diam(n)
end
for n=1:X
diamn(n)=diam(n)/sum
end
out=sprintf('%12.8f\t',diam)
outl=sprintf('%12.8f\t',diamn)
fprintf(fid,'%c',out)
fprintf(fid,' end of data')
fprintf(fid,'\n')
fprintf(fiddd,'%c',outl)
fprintf(fiddd,' end of data')
fprintf(fiddd,'\n')

end
fclose(fid)
fclose(fidd)
fclose(fiddd)

```

6.3 FREQUENCY RESPONSE PROGRAM (MATLAB)

% m-file milmw1.m (C) J A Wilson, M Simmons-----5 May 1998

```
clear
```

```

%----Open files for I/O
fid=fopen('milnela.txt','rt')
out=fopen('outlala.txt','wt')
colnum=6
%----Set number of rows in matrix to a power of 2
ni=512,ni2=ni/2

```

```

%----Set loop for multiple runs
for files=1:1

```

```

%----Program data analysis parameters
    samplerate=10
    tau=.1
    taul=20; tau2=10
    Adead=10

```



```

%----Set number of matrix rows from input file
nrows=fscanf(fid,'%lg',[1,1])

%----Read in matrix, 1st column x, 2nd y1 etc
[A]=zeros(ni,7);
[DATA,c]=fscanf(fid,'%lg',[7,nrows]);
[DATA]=[DATA]';

%----Removing background
DATA(:,4)=DATA(:,4)-DATA(:,5);
DATA(:,6)=DATA(:,6)-DATA(:,7);

%----Sampling system:Reducing number of data points
newrows=nrows/samplerate
m=0
for n=1:samplerate:nrows
m=m+1;
B(m,:)=DATA(n,:);
end

%----pad matrix with zeros to create ni elements
for i=1:newrows;
A(i,:)=B(i,:);
end

%----setting correct time coordinates
T=A(2,1)-A(1,1);
B=A;
for i=1:ni;
B(i,1)=(i-1)*T;
end

%----Fast fourier transform of impulse response
C=fft(B(:,colnum));
M=abs(C);
P=angle(C);
%P=unwrap(P);

%----scale magnitude against 'DC' value (zero frequency)
z=M(1);
M=M/z;

%----calculate frequency co-ordinates
w=zeros(1,ni2);
for i=2:ni2
w(i)=2*pi*(i-1)/(ni*T);
end

%----calculate exact frequency response data
D=zeros(ni,2);

for i=1:ni2
s=sqrt(-1)*w(i);
D(i,2)=exp(-Adead*s)/((taul*s+1)*(tau2*s+1));
end

```

```

Mc=abs(D(1:ni2,2));
Pc=angle(D(1:ni2,2));
%Pc=unwrap(Pc);

%----Creating plots
t=B(:,1);
Mp=M(1:ni2);
Pp=P(1:ni2);
wp=w;wp(1)=10^(floor(log10(2*pi/(ni*T))));
%----for plotting lowest frequency point is next lowest decade
%----to avoid negative log(w)

subplot(2,2,1);plot(log10(wp),20*log10(Mp))
title('magnitude')
xlabel('log w')
ylabel('db=20log10M')

subplot(2,2,2);plot(log10(wp),Pp*180/pi)
title('phase angle')
xlabel('log w')
ylabel('phase angle (deg)')

subplot(2,2,3);plot(DATA(:,1),DATA(:,colnum))
title('input data')
xlabel('t')
ylabel('impulse output')

%subplot(2,2,4);plot(B(:,1))

%----Outputting input data
XOUTT=zeros(ni,2);
XOUTT(:,1)=B(:,1);
XOUTT(:,2)=B(:,colnum);

for i=1:newrows
output=sprintf('%12.8f\t',XOUTT(i,:));
fprintf(out,'%c',output);
fprintf(out,'\n');
end

%----Outputting frequency, magnitude and phase
XOUTW=zeros(ni2,3);
XOUTW(:,1)=w';
XOUTW(:,2)=20*log10(Mp);
XOUTW(:,3)=(Pp*180/pi);

for i=1:ni2
output=sprintf('%12.8f\t',XOUTW(i,:));
fprintf(out,'%c',output);
fprintf(out,'\n');
end

%fprintf(fiddd,' end of data')
%fprintf(fiddd,'\n')

end
fclose(fid)
fclose(out)

```

6.4 CONVOLUTION PROGRAM AND ALTERNATIVE PATH MODEL (FORTRAN)

```
C
C
C   Program Convolute
C
C   A program to convolute input pulses to an outlet tracer
C   Also can generate own input and output distributions
C   Includes APM Curve Generator
C   (C) M J SIMMONS 1998
C

      PROGRAM CONVOLUTE
      IMPLICIT REAL*8(A-H,O-Z)
      DIMENSION T(800),Y(800),YIN(800),YC(800),Y1(800),Y2(800)

      COMMON /CONSTANTS/ PI,TOL

C
C   Values of constants
C

      PI=3.141592654

C
C   Open files for I/O
C

      OPEN(UNIT=1, FILE='TRACEIN.TXT', STATUS='OLD')
      OPEN(UNIT=2, FILE='TRACEOUT.TXT', STATUS='UNKNOWN')
      OPEN(UNIT=3, FILE='DEBUG.TXT', STATUS='UNKNOWN')

C
C   Input data
C

      READ(1,*)INPUT,OUTPUT,NUM
      IF(INPUT.EQ.1)THEN
      READ(1,*)SDEV
      ENDIF
      IF(OUTPUT.EQ.1) THEN
      DO 10 I=1,NUM
      READ(1,*) T(I),Y(I)
10    CONTINUE
      ENDIF
      IF(OUTPUT.EQ.2) THEN
      READ(1,*)TAU1,TAU2,TAU3,FB,N
      READ(1,*)TSTART,TEND
      STEP=(TEND-TSTART)/NUM
      DO 15 J=1,NUM
      T(J)=TSTART+(J-1)*STEP
15    CONTINUE
      C
C   Generate output curve from alternative path model
C

      CALL NSTIS(NUM,N,TAU1,TAU2,Y1,T)
      CALL NSTIS(NUM,N,TAU1,TAU3,Y2,T)
      DO 16 J=1,NUM
      Y(J)=FB*Y1(J)+(1-FB)*Y2(J)
16    CONTINUE
      ENDIF

C
```

```

C      CALCULATE AREA UNDER TRACER OUTPUT CURVE
C
      AREA0=0.
      DO 20 I=1,NUM-1
      AREA0=AREA0+(Y(I+1)+Y(I))/2*(T(I+1)-T(I))
20    CONTINUE
      WRITE(*,*)AREA0

C
C      GENERATE INPUT CURVE
C
C      IF(INPUT.EQ.1) THEN
C
C      NORMAL DISTRIBUTION
C
      RMEAN=T(40)

      DO 30 I=1,NUM
      YIN(I)=1/(SDEV*(2*PI)**0.5)*EXP(-0.5*((T(I)-RMEAN)/SDEV)**2)
C      IF(T(I).GT.4*SDEV) YIN(I)=0.
30    CONTINUE
      ELSE

C
C      SQUARE-WAVE
C
      RSTART=T(40)
      RFINISH=T(120)
      WRITE(*,*)RSTART,RFINISH
      TDIFF=T(120)-T(40)
      PHEIGHT=1/TDIFF
      DO 35 I=1,NUM
      IF((I.GE.RSTART/STEP).AND.(I.LE.RFINISH/STEP)) THEN
      YIN(I)=PHEIGHT
      ELSE
      YIN(I)=0.
      ENDIF
35    CONTINUE
      ENDIF

C
C      CONVOLUTING DISTRIBUTION
C
C
      DO 40 I=1,NUM-1
      I=1
      AREAI=(YIN(I+1)+YIN(I))/2*(T(I+1)-T(I))
      AREAI=10
      WRITE(*,*)T(I),AREAI
      PAUSE
      DO 50 J=1,NUM-I
      YC(J+I)=Y(J)*AREAI+YC(J+I)

50    CONTINUE
40    CONTINUE

C
C      OUTPUTTING TO FILE
C
C
      DO 60 I=1,NUM
      WRITE(2,100)T(I),YC(I),Y(I),YIN(I)

```

```
100  FORMAT(2X,F10.4,3E10.4)
60   CONTINUE
```

```
END
```

```
C
C   SUBROUTINE NSTIS
C   CALCULATES OUTLET DISTRIBUTION FOR A DIRAC PULSE OF
C   N STIRRED TANKS IN SERIES PLUS INLET MIXING ZONE
C   TIME CONSTANTS TAU1 (MIXER) , TAU2 (EACH NTH TANK)
C
```

```
      SUBROUTINE NSTIS(NUM,N,TAU1,TAU2,Y,T)
      IMPLICIT REAL*8(A-H,O-Z)
      DIMENSION T(800),Y(800),TERM(800)
```

```
      DO 5 I=1,NUM
```

```
C
C      TERM 1 (INVOLVING EXP (-T/T1)
C
```

```
      TERM1=TAU1**(N-1)/((TAU1-TAU2)**N)*EXP(-T(I)/TAU1)
      IF(T(I).EQ.1) WRITE(*,*)TERM1,T(I),N,TAU1,TAU2
```

```
C
C      GENERAL TERMS (N OF THESE)
C
```

```
      DO 10 J=1,N
      TOP=TAU1**(N-J)*T(I)**(J-1)*EXP(-T(I)/TAU2)
      M=J-1
      BOTTOM=(TAU1-TAU2)**(N+1-J)*TAU2**(J-1)*FACT(M)
C      IF(M.EQ.10) WRITE(*,*)FACT(M)
      TERM(J)=TOP/BOTTOM
```

```
10  CONTINUE
```

```
C
C      SUMMING FOR Y
C
```

```
      Y(I)=TERM1
      DO 20 J=1,N
      Y(I)=Y(I)-TERM(J)
20  CONTINUE
      IF(T(I).EQ.1) WRITE(*,*)TERM(1),TERM(3),T(I),Y(I),FACT(M)
      5  CONTINUE
```

```
END
```

```
      FUNCTION FACT(M)
      IMPLICIT REAL*8(A-H,O-Z)
      FACT=1.0
      R=0
      DO 10 J=1,M
      R=R+1
      FACT=FACT*R
10  CONTINUE
      END
```

Appendix A7

MODELLING OF PILOT SCALE SEPARATOR-TABLES OF RESULTS

Table A7.1: Residence Time Summary-Aqueous Phase

Run No	Config	Oil Flow (kg/s)	Water Flow (kg/s)	MRT (s)	PRT (s)	STD DEV (s)	MRT/ PRT (-)	Transit Time (s)	MRT /TT (-)	PRT/ TT (-)
1.1	L	2.1	1.5	66.2	59	24.92	1.12	94.34	0.70	0.63
1.2	L	2.1	2.5	55.2	34	33.65	1.62	58.11	0.95	0.59
1.3	L	2.1	3.5	43.9	32	17.59	1.37	41.51	1.06	0.77
1.4	L	2.1	3.9	39.5	30	15.54	1.32	36.87	1.07	0.81
2.1	L	3.34	1.5	76.7	51	38.52	1.50	94.34	0.81	0.54
2.2	L	3.34	2.5	60.1	43	30.13	1.40	58.11	1.03	0.74
2.3	L	3.34	3.5	47.6	30	23.63	1.59	41.51	1.15	0.72
2.4	L	3.34	3.9	42.7	40	12.77	1.07	36.87	1.16	1.08
3.1	L	1.5	2.5	60.1	34	33.21	1.77	58.11	1.03	0.59
3.2	L	2.5	1.5	77.8	60	37.8	1.30	94.34	0.82	0.64
3.3	L	3	1	84.2	45	49.6	1.87	142.43	0.59	0.32
4.1	L	2.1	3.9	53.6	35	26.5	1.53	36.87	1.45	0.95
4.2	L	3	3	63.8	43	36.15	1.48	48.27	1.32	0.89
4.3	L	4	2	66.8	40	38.45	1.67	72.64	0.92	0.55
5.1	LS	2.1	3.9	33.5	26	13.42	1.29	26.3	1.27	0.99
5.2	LS	3	3	48.1	37	23.4	1.30	34.4	1.40	1.08
5.3	LS	4	2	65.5	40	37.86	1.64	51.8	1.26	0.77
6.1	LS	1.5	2.5	54.9	36	33.05	1.53	41.4	1.33	0.87
6.2	LS	2.5	1.5	73.0	43	41.17	1.70	67.3	1.09	0.64
6.3	LS	3	1	85.3	54	41.97	1.58	101.6	0.84	0.53
7.1	HHS	2.1	3.9	41.0	24	26.84	1.71	36.4	1.13	0.66
7.2	HHS	3	3	77.0	56	34.91	1.38	47.6	1.62	1.18
7.3	HHS	4	2	85.0	51	38.88	1.67	71.7	1.19	0.71
8.1	HHS	1.5	2.5	87.6	60	42.54	1.46	57.4	1.53	1.05
8.2	HHS	2.5	1.5	91.0	58	42.23	1.57	93.1	0.98	0.62
8.3	HHS	3	1	97.9	61	44.7	1.60	140.6	0.70	0.43
9.1	HLS	2.1	3.9	33.5	24	19.14	1.40	26.3	1.27	0.91
9.2	HLS	3	3	79.0	53	36.78	1.49	34.4	2.30	1.54
9.3	HLS	4	2	67.2	44	33.28	1.53	51.8	1.30	0.85
10.1	HLS	1.5	2.5	56.9	35	36.48	1.63	41.4	1.37	0.84
10.2	HLS	2.5	1.5	87.1	53	42.95	1.64	67.3	1.29	0.79
10.3	HLS	3	1	93.1	55	44.93	1.69	101.6	0.92	0.54

Run No	Config	Oil Flow (kg/s)	Water Flow (kg/s)	MRT (s)	PRT (s)	STD DEV (s)	MRT/ PRT (-)	Transit Time (s)	MRT /TT (-)	PRT/ TT (-)
11.4	PL	1.5	2.5	49.8	39	20.92	1.28	58.11	0.86	0.67
11.1	PL	2.1	1.5	86.9	58	41.88	1.50	94.34	0.92	0.61
11.2	PL	2.1	3.9	48.2	49	31.67	0.98	36.87	1.31	1.33
11.5	PL	3	1	96.6	53	46.05	1.82	142.43	0.68	0.37
11.3	PL	3	3	47.1	33	22.32	1.43	48.27	0.98	0.68
12.4	PHL	1.5	2.5	77.4	30	46.69	2.58	58.11	1.33	0.52
12.1	PHL	2.1	1.5	86.5	57	42.88	1.52	94.34	0.92	0.60
12.2	PHL	2.1	3.9	55.7	39	31.21	1.43	36.87	1.51	1.06
12.5	PHL	3	1	87.9	54	43.56	1.63	142.43	0.62	0.38
12.3	PHL	3	3	57.2	42	25.01	1.36	48.27	1.19	0.87
13.4	PHH	1.5	2.5	79.2	32	46.33	2.48	87.98	0.90	0.36
13.1	PHH	2.1	1.5	94.0	51	47.16	1.84	142.83	0.66	0.36
13.2	PHH	2.1	3.9	48.7	36	22.7	1.35	55.83	0.87	0.64
13.5	PHH	3	1	111.9	56	48.48	2.00	215.65	0.52	0.26
13.3	PHH	3	3	68.2	48	31.52	1.42	73.08	0.93	0.66
14.4	PLD	1.5	2.5	87.7	48	42.41	1.83	58.11	1.51	0.83
14.1	PLD	2.1	1.5	72.9	61	23.33	1.20	94.34	0.77	0.65
14.2	PLD	2.1	3.9	44.4	32	23.65	1.39	36.87	1.20	0.87
14.5	PLD	3	1	98.7	60	45.27	1.65	142.43	0.69	0.42
14.3	PLD	3	3	63.7	63	24.18	1.01	48.27	1.32	1.31
15.5	PHHD	1.5	2.5	87.4	44	45.44	1.99	87.98	0.99	0.50
15.1	PHHD	2.1	1.5	90.2	64	40.03	1.41	142.83	0.63	0.45
15.2	PHHD	2.1	3.9	60.8	31	38.79	1.96	55.83	1.09	0.56
15.4	PHHD	3	1	104.3	47	53.52	2.22	215.65	0.48	0.22
15.3	PHHD	3	3	99.9	34	59.03	2.94	73.08	1.37	0.47
16.4	PHLD	1.5	2.5	79.7	46	36	1.73	58.11	1.37	0.79
16.1	PHLD	2.1	1.5	86.3	57	40.1	1.51	94.34	0.91	0.60
16.2	PHLD	2.1	3.9	73.3	32	50.78	2.29	36.87	1.99	0.87
16.5	PHLD	3	1	90.5	62	38.77	1.46	142.43	0.64	0.44
16.3	PHLD	3	3	71.1	37	48.99	1.92	48.27	1.47	0.77

Table A7.2: Residence Time Summary-Organic Phase

Run No	Config	Oil Flow (kg/s)	Water Flow (kg/s)	MRT (s)	PRT (s)	STD DEV (s)	MRT/ PRT (-)	Transit Time (s)	MRT /TT (-)	PRT/ TT (-)
1.1	L	2.1	1.5	53.8	34	29.46	1.58	36.45	1.48	0.93
1.2	L	2.1	2.5	49.2	37	18.25	1.33	36.45	1.35	1.02
1.3	L	2.1	3.5	74.1	59	30.31	1.26	36.45	2.03	1.62
1.4	L	2.1	3.9					36.45	0.00	0.00
2.1	L	3.34	1.5	46.5	37	18.54	1.26	24.00	1.94	1.54
2.2	L	3.34	2.5	80.0	31	52.54	2.58	24.00	3.33	1.29
2.3	L	3.34	3.5	77.5	38	40.93	2.04	24.00	3.23	1.58
2.4	L	3.34	3.9	65.8	34	45.94	1.94	24.00	2.74	1.42
3.1	L	1.5	2.5	63.0	59	13.58	1.07	53.45	1.18	1.10
3.2	L	2.5	1.5	53.6	31	41.26	1.73	32.86	1.63	0.94
3.3	L	3	1	60.9	24	51.73	2.54	26.82	2.27	0.89
4.1	L	2.1	3.9	74.3	61	38.50	1.22	36.45	2.04	1.67
4.2	L	3	3	40.5	29	17.61	1.40	26.82	1.51	1.08
4.3	L	4	2	53.6	25	46.10	2.14	20.25	2.65	1.23
5.1	LS	2.1	3.9	78.4	60	27.96	1.31	19.17	4.09	3.13
5.2	LS	3	3	47.2	40	15.37	1.18	14.11	3.35	2.84
5.3	LS	4	2	39.2	33	14.40	1.19	10.65	3.68	3.10
6.1	LS	1.5	2.5	73.4	48	33.16	1.53	28.11	2.61	1.71
6.2	LS	2.5	1.5	65.2	41	38.22	1.59	17.28	3.77	2.37
6.3	LS	3	1	58.0	34	31.71	1.71	14.11	4.11	2.41
7.1	HHS	2.1	3.9	80.2	64	28.26	1.25	23.94	3.35	2.67
7.2	HHS	3	3	62.5	55	27.58	1.14	17.62	3.55	3.12
7.3	HHS	4	2	47.7	25	29.1	1.91	13.30	3.59	1.88
8.1	HHS	1.5	2.5	83.4	73	32.44	1.14	35.11	2.38	2.08
8.2	HHS	2.5	1.5	84.6	30	51.86	2.82	21.59	3.92	1.39
8.3	HHS	3	1	40.3	24	28.46	1.68	17.62	2.29	1.36
9.1	HLS	2.1	3.9	93.9	68	30.88	1.38	38.37	2.45	1.77
9.2	HLS	3	3	71.7	72	31.76	1.00	28.23	2.54	2.55
9.3	HLS	4	2	62.1	31	35.61	2.00	21.32	2.91	1.45
10.1	HLS	1.5	2.5	88.4	75	20.87	1.18	56.28	1.57	1.33
10.2	HLS	2.5	1.5	72.8	62	36.81	1.17	34.60	2.10	1.79
10.3	HLS	3	1	52.7	42	21.24	1.25	28.23	1.87	1.49
11.4	PL	1.5	2.5	57.4	37	39.14	1.55	53.45	1.07	0.69
11.1	PL	2.1	1.5	50.6	41	26.27	1.23	36.45	1.39	1.12
11.2	PL	2.1	3.9	76.8	54	31.93	1.42	36.45	2.11	1.48
11.5	PL	3	1	46.1	27	40.4	1.71	26.82	1.72	1.01
11.3	PL	3	3	84.6	36	49.99	2.35	26.82	3.15	1.34
12.4	PHL	1.5	2.5	79.2	63	33.19	1.26	109.50	0.72	0.58
12.1	PHL	2.1	1.5	72.4	64	34.61	1.13	74.65	0.97	0.86
12.2	PHL	2.1	3.9	75.5	76	31.66	0.99	74.65	1.01	1.02
12.5	PHL	3	1	72.3	54	30.53	1.34	54.93	1.32	0.98

Run No	Config	Oil Flow (kg/s)	Water Flow (kg/s)	MRT (s)	PRT (s)	STD DEV (s)	MRT/ PRT (-)	Transit Time (s)	MRT /TT (-)	PRT/ TT (-)
12.3	PHL	3	3	66.2	36	44.41	1.84	54.93	1.21	0.66
13.4	PHH	1.5	2.5	88.0	65	43.93	1.35	69.81	1.26	0.93
13.1	PHH	2.1	1.5	60.4	52	18.58	1.16	47.60	1.27	1.09
13.2	PHH	2.1	3.9	98.5	85	26.21	1.16	47.60	2.07	1.79
13.5	PHH	3	1	60.1	37	33.76	1.62	35.02	1.72	1.06
13.3	PHH	3	3	70.3	31	58.1	2.27	35.02	2.01	0.89
14.4	PLD	1.5	2.5	48.1	42	10.32	1.15	53.45	0.90	0.79
14.1	PLD	2.1	1.5	42.2	37	12.14	1.14	36.45	1.16	1.02
14.2	PLD	2.1	3.9	59.7	51	15.98	1.17	36.45	1.64	1.40
14.5	PLD	3	1	39.3	57	16.49	0.69	26.82	1.47	2.13
14.3	PLD	3	3	48.5	25	36.8	1.94	26.82	1.81	0.93
15.5	PHHD	1.5	2.5	48.8	35	22.95	1.39	69.81	0.70	0.50
15.1	PHHD	2.1	1.5	83.8	42	50.11	2.00	47.60	1.76	0.88
15.2	PHHD	2.1	3.9	78.7	74	22.8	1.06	47.60	1.65	1.55
15.4	PHHD	3	1	59.1	39	33.57	1.52	35.02	1.69	1.11
15.3	PHHD	3	3	79.6	28	47.82	2.84	35.02	2.27	0.80
16.4	PHLD	1.5	2.5	65.2	39	39.13	1.67	109.50	0.60	0.36
16.1	PHLD	2.1	1.5	73.3	57	32.34	1.29	74.65	0.98	0.76
16.2	PHLD	2.1	3.9	96.9	79	24.45	1.23	74.65	1.30	1.06
16.5	PHLD	3	1	61.1	42	25.29	1.45	54.93	1.11	0.76
16.3	PHLD	3	3	41.5	34	13.33	1.22	54.93	0.76	0.62

Table A7.3: APM Summary-Aqueous Phase Including Fractional Mixed Volume

Run No	Config	Oil Flow (kg/s)	Water Flow (kg/s)	τ_1 (s)	τ_2 (s)	τ_3 (s)	f (-)	Model MRT (s)	F (-)	D (-)
1.1	L	2.1	1.5	21.58	0.91	n/a	n/a	67.1	n/a	0.428
1.2	L	2.1	2.5	23.72	0.58	n/a	n/a	52.7	n/a	0.460
1.3	L	2.1	3.5	23.17	0.49	n/a	n/a	47.7	n/a	0.634
1.4	L	2.1	3.9	15.1	0.49	n/a	n/a	39.6	n/a	
2.1	L	3.34	1.5	25	0.8	2.4	0.05	29.8	0.100	0.552
2.2	L	3.34	2.5	24.53	0.65	2.4	0.083	32.4	0.223	0.738
2.3	L	3.34	3.5	23.96	0.53	n/a	n/a	50.5	n/a	0.605
2.4	L	3.34	3.9	16.84	0.595	n/a	n/a	46.6	n/a	0.549
3.1	L	1.5	2.5	22.86	0.62	n/a	n/a	53.9	n/a	0.29
3.2	L	2.5	1.5	17.74	0.94	2.47	0.12	73.9	0.195	0.34
3.3	L	3	1.0	12.99	0.81	2.1	0.24	69.0	0.382	0.30
4.1	L	2.1	3.9	29.54	0.42	0.58	0.58	55.2	0.221	0.49
4.2	L	3	3.0	23.9	0.56	0.69	0.83	57.3	0.193	0.46
4.3	L	4	2.0	30.71	0.58	0.63	0.86	61.9	0.074	0.45
5.1	LS	2.1	3.9	11.64	0.43	n/a	n/a	33.1	n/a	0.44
5.2	LS	3	3.0	15.96	0.59	2.13	0.035	48.2	0.091	0.39
5.3	LS	4	2.0	18.7	0.66	1.9	0.183	63.0	0.344	0.42
6.1	LS	1.5	2.5	21.01	0.57	2.57	0.046	54.1	0.161	0.43
6.2	LS	2.5	1.5	19.06	0.74	2.35	0.17	69.7	0.370	0.49
6.3	LS	3	1.0	19.23	0.88	2.17	0.283	81.5	0.415	0.52
7.1	HHS	2.1	3.9	22.18	0.37	n/a	n/a	40.7	n/a	0.47
7.2	HHS	3	3.0	19.88	0.59	2.19	0.212	66.3	0.575	0.53
7.3	HHS	4	2.0	21.36	0.85	2.19	0.238	79.8	0.375	0.48
8.1	HHS	1.5	2.5	17.19	1.04	2.54	0.235	86.8	0.339	0.30
8.2	HHS	2.5	1.5	15.1	1.05	2.45	0.277	87.0	0.369	0.57
8.3	HHS	3	1.0	13.11	1.05	2.33	0.381	90.0	0.464	0.41
9.1	HLS	2.1	3.9	11.85	0.39	1.31	0.063	34.2	0.149	0.29
9.2	HLS	3	3.0	21.89	0.88	2.37	0.203	81.0	0.344	0.37
9.3	HLS	4	2.0	11.49	0.79	1.88	0.241	64.1	0.333	0.53
10.1	HLS	1.5	2.5	15.42	0.61	2.21	0.105	54.3	0.275	0.27
10.2	HLS	2.5	1.5	17.69	0.93	2.34	0.275	83.6	0.417	0.43
10.3	HLS	3	1.0	30.37	0.94	2.25	0.244	93.4	0.340	0.42
11.4	PL	1.5	2.5	22.86	0.57	n/a	n/a	51.4	n/a	0.46
11.1	PL	2.1	1.5	29.68	0.914	2.55	0.162	88.6	0.290	0.38
11.2	PL	2.1	3.9	17.86	0.47	2.41	0.123	53.3	0.508	0.33
11.5	PL	3	1.0	36.09	0.91	2.39	0.234	98.9	0.381	0.40
11.3	PL	3	3.0	12.8	0.6	2.39	0.058	48.0	0.173	0.38
12.4	PHL	1.5	2.5	56.23	0.46	2.13	0.035	82.2	0.127	0.55
12.1	PHL	2.1	1.5	24.19	0.88	2.13	0.199	80.6	0.283	0.35
12.2	PHL	2.1	3.9	19.05	0.65	2.13	0.0245	53.4	0.056	0.31
12.5	PHL	3	1.0	24.95	0.91	2.36	0.197	84.7	0.314	0.39
12.3	PHL	3	3.0	17.79	0.72	2.38	0.041	57.2	0.095	0.48

Run No	Config	Oil Flow	Water Flow	τ_1	τ_2	τ_3	f	Model MRT	F	D
		(kg/s)	(kg/s)	(s)	(s)	(s)	(-)	(s)	(-)	(-)
13.4	PHH	1.5	2.5	40.49	0.52	1.9	0.184	79.2	0.488	0.51
13.1	PHH	2.1	1.5	48.9	0.83	2.19	0.078	95.7	0.128	0.50
13.2	PHH	2.1	3.9	18.3	0.58	2.19	0.078	53.6	0.217	0.31
13.5	PHH	3	1.0	47.31	0.92	2.31	0.359	118.3	0.542	0.38
13.3	PHH	3	3.0	20.24	0.81	2.31	0.09	67.5	0.167	0.29
14.4	PLD	1.5	2.5	53.35	0.76	n/a	n/a	91.4	n/a	0.50
14.1	PLD	2.1	1.5	17.16	1.07	3.28	0.027	73.6	0.056	0.35
14.2	PLD	2.1	3.9	16.44	0.5	3.31	0.026	45.1	0.146	0.35
14.5	PLD	3	1.0	26.42	1.04	2.6	0.204	94.3	0.306	0.44
14.3	PLD	3	3.0	17.51	0.88	1.9	0.073	65.2	0.085	0.37
15.5	PHHD	1.5	2.5	50.8	0.723	n/a	n/a	87.0	n/a	0.54
15.1	PHHD	2.1	1.5	17.86	1.12	3	0.1462	87.6	0.245	0.45
15.2	PHHD	2.1	3.9	25.61	0.51	2.5	0.115	62.6	0.449	0.30
15.4	PHHD	3	1.0	34.81	0.811	3	0.3	108.2	0.810	0.49
15.3	PHHD	3	3.0	34.7	0.7	2.4	0.261	91.9	0.634	0.50
16.4	PHLD	1.5	2.5	45.48	0.74	n/a	n/a	82.5	n/a	0.49
16.1	PHLD	2.1	1.5	27.09	0.97	n/a	n/a	75.6	n/a	0.49
16.2	PHLD	2.1	3.9	35.39	0.49	n/a	n/a	59.9	n/a	0.41
16.5	PHLD	3	1.0	12.58	1.18	2.7	0.19	86.0	0.245	0.42
16.3	PHLD	3	3.0	14.78	0.62	n/a	n/a	45.8	n/a	0.34

Table A7.4: APM Summary-Organic Including Length of Coalescing Wedge

Run No	Config	Oil Flow	Water Flow	τ_1	τ_2	τ_3	f	Model MRT	F	Fract. Wedge Length	Fract. Wedge Length
		(kg/s)	(kg/s)	(s)	(s)	(s)	(-)	(s)	(-)	Full Flow	Side Baffles
1.1	L	2.1	1.5	26.5	0.52	n/a	n/a	52.5	n/a	0.59	
1.2	L	2.1	2.5	24.3	0.55	n/a	n/a	51.8	n/a	0.65	
1.3	L	2.1	3.5	29.69	0.82	2.39	0.019	32.0	0.036	0.97	
1.4	L	2.1	3.9								
2.1	L	3.34	1.5	24.57	0.51	n/a	n/a	50.1	n/a	0.82	
2.2	L	3.34	2.5	25.76	0.44	2.4	0.1	35.4	0.307	1.15	
2.3	L	3.34	3.5	26.36	0.59	2.4	0.079	34.5	0.324	0.91	
2.4	L	3.34	3.9	33.91	0.47	2.42	0.108	47.0	0.448	0.81	
3.1	L	1.5	2.5	9.23	1.04	1.66	0.086	63.9	0.051	0.35	
3.2	L	2.5	1.5	19.67	0.45	1.85	0.072	47.2	0.224	0.44	
3.3	L	3	1.0	15.83	0.41	2.13	0.1	44.9	0.420	0.37	
4.1	L	2.1	3.9	34.2	0.86	n/a	n/a	77.2	n/a	0.71	
4.2	L	3	3.0	21.74	0.44	n/a	n/a	43.7	n/a	0.64	
4.3	L	4	2.0	19.5	0.33	1.73	0.15	46.5	0.636	0.63	
5.1	LS	2.1	3.9	43.57	0.92	n/a	n/a	89.6	n/a	0.61	1.35
5.2	LS	3	3.0	23.79	0.62	n/a	n/a	54.8	n/a	0.53	1.17
5.3	LS	4	2.0	22.43	0.47	n/a	n/a	45.9	n/a	0.58	1.28
6.1	LS	1.5	2.5	34.69	0.81	n/a	n/a	75.2	n/a	0.59	1.30
6.2	LS	2.5	1.5	40.81	0.55	n/a	n/a	68.3	n/a	0.71	1.56
6.3	LS	3	1.0	38.74	0.48	n/a	n/a	62.7	n/a	0.76	1.67
7.1	HHS	2.1	3.9	38.25	1.05	n/a	n/a	90.8	n/a	0.63	1.50
7.2	HHS	3	3.0	53.55	0.5	n/a	n/a	78.6	n/a	0.74	1.74
7.3	HHS	4	2.0	31.25	0.38	n/a	n/a	50.3	n/a	0.66	1.56
8.1	HHS	1.5	2.5	39.94	1.02	1.89	0.067	93.9	0.057	0.33	0.77
8.2	HHS	2.5	1.5	71.1	0.48	1.76	0.009	95.7	0.024	0.81	1.92
8.3	HHS	3	1.0	22.79	0.34	n/a	n/a	39.8	n/a	0.53	1.25
9.1	HLS	2.1	3.9	26.34	1.18	2.08	0.292	98.5	0.223	0.33	0.75
9.2	HLS	3	3.0	35.18	0.54	1.21	0.473	78.0	0.587	0.47	1.07
9.3	HLS	4	2.0	45.58	0.46	n/a	n/a	68.6	n/a	0.77	1.76
10.1	HLS	1.5	2.5	23.46	1.36	n/a	n/a	91.5	n/a	0.28	0.64
10.2	HLS	2.5	1.5	43.47	0.54	1.11	0.401	81.9	0.423	0.57	1.31
10.3	HLS	3	1.0	26.48	0.52	0.77	0.39	57.4	0.188	0.56	1.28
11.4	PL	1.5	2.5	25.07	0.57	n/a	n/a	53.6	n/a	0.64	
11.1	PL	2.1	1.5	24.17	0.68	n/a	n/a	58.2	n/a	0.50	
11.2	PL	2.1	3.9	25.73	0.87	2.08	0.2	81.3	0.278	0.41	
11.5	PL	3	1.0	17.84	0.39	2.14	0.062	42.8	0.278	0.54	
11.3	PL	3	3.0	36.82	0.54	2.19	0.248	84.3	0.758	0.51	
12.4	PHL	1.5	2.5	29.98	1.03	2.33	0.013	82.3	0.016	0.80	
12.1	PHL	2.1	1.5	27.06	0.73	1.26	0.288	71.2	0.209	0.43	
12.2	PHL	2.1	3.9	24.88	1.35	n/a	n/a	92.4	n/a	0.36	

Run No	Config	Oil Flow	Water Flow	τ_1	τ_2	τ_3	f	Model MRT	F	Fract. Wedge Length	Fract. Wedge Length
		(kg/s)	(kg/s)	(s)	(s)	(s)	(-)	(s)	(-)	Full Flow	Side Baffles
12.5	PHL	3	1.0	30.54	0.8	1.06	0.204	73.2	0.066	0.50	
12.3	PHL	3	3.0	36.66	0.47	n/a	n/a	60.2	n/a	0.67	
13.4	PHH	1.5	2.5	52.13	0.99	n/a	n/a	101.6	n/a	0.71	
13.1	PHH	2.1	1.5	34.98	0.73	n/a	n/a	71.5	n/a	0.68	
13.2	PHH	2.1	3.9	28.71	1.45	n/a	n/a	101.2	n/a	0.34	
13.5	PHH	3	1.0	23.78	0.58	2.2	0.127	63.1	0.355	0.48	
13.3	PHH	3	3.0	21.42	0.48	3.34	0.199	73.9	1.186	0.32	
14.4	PLD	1.5	2.5	16.6	0.72	1.9	0.001	52.7	0.002	0.73	
14.1	PLD	2.1	1.5	22	0.52	n/a	n/a	48.0	n/a	0.46	
14.2	PLD	2.1	3.9	21.81	0.83	n/a	n/a	63.3	n/a	0.46	
14.5	PLD	3	1.0	22.7	0.32	0.47	0.582	43.2	0.278	0.61	
14.3	PLD	3	3.0	20.42	0.4	n/a	n/a	40.4	n/a	0.49	
15.5	PHHD	1.5	2.5	21.07	0.53	n/a	n/a	47.6	n/a	0.76	
15.1	PHHD	2.1	1.5	49.25	0.63	n/a	n/a	80.8	n/a	0.60	
15.2	PHHD	2.1	3.9	13.18	1.31	n/a	n/a	78.7	n/a	0.32	
15.4	PHHD	3	1.0	31.48	0.46	n/a	n/a	54.5	n/a	0.67	
15.3	PHHD	3	3.0	45.7	0.55	n/a	n/a	73.2	n/a	0.69	
16.4	PHLD	1.5	2.5	24.98	0.63	3.07	0.072	65.3	0.279	0.69	
16.1	PHLD	2.1	1.5	45.74	0.7	n/a	n/a	80.7	n/a	0.70	
16.2	PHLD	2.1	3.9	22.66	1.41	n/a	n/a	93.2	n/a	0.55	
16.5	PHLD	3	1.0	33.98	0.63	n/a	n/a	65.5	n/a	0.57	
16.3	PHLD	3	3.0	17.71	0.51	0.73	0.56	49.3	0.239	0.42	